Order Number 9429619

The conformational dynamics and subunit equilibrium of *Escherichia coli* ribosomal protein L7/L12

Hamman, Brian David, Ph.D.

University of Hawaii, 1994

U·M·I

300 N. Zeeb Rd.
Ann Arbor, MI 48106

THE CONFORMATIONAL DYNAMICS AND SUBUNIT EQUILIBRIUM OF *ESCHERICHIA COLI* RIBOSOMAL PROTEIN L7/L12

A DISSERTATION SUBMITTED TO THE GRADUATE DIVISION OF THE UNIVERSITY OF HAWAI'I IN PARTIAL FULFILLMENT OF THE REQUIREMENTS FOR THE DEGREE OF

DOCTOR OF PHILOSOPHY

IN

BIOMEDICAL SCIENCES (BIOCHEMISTRY)

MAY 1994

By

Brian D. Hamman

Dissertation Committee:

David M. Jameson, Chairperson
Robert R. Traut
Nadhipuram V. Bhagavan
Richard J. Guillory
Robert S.-H. Liu

ACKNOWLEDGEMENTS

First and foremost, I must thank my advisor Dr. David Jameson for his elite scientific guidance and financial support throughout the last few years. Dave made working hard actually fun. Through Dave, I met several other excellent scientists who must be acknowledged for their contributions to this work including:

Dr. Robert Traut, who designed and financed the synthesis and initial characterizations of the various mutant forms of L7/L12 mentioned throughout this dissertation; Dr. Andrew Oleinikov, who did the initial characterizations of the various L7/L12 mutants and contributed important insight into the problems approached in this dissertation; Dr. George Jokhadze--it was George who did most of the molecular biology for the various phenotypes of L7/L12 mentioned in this dissertation; the rest of the Traut laboratory that has contributed in one way or another over the past couple of years. Again, I must thank the Traut laboratory for their generous and constant supply of the various L7/L12 cysteine mutants.

I am also very honored to have met and worked with the great Dr. Gregorio Weber. I shall refer you to the references section of this dissertation, where I have referenced 19 (only as first author) of Dr. Weber's publications, from 1952 to 1993. In addition to the published work of the professor, he has verbally contributed several pivotal points in my research. I would also like to acknowledge Dr. Kancheng Ruan and Dr. Leonardo Erijman for helpful assistance with the high-pressure instruments at the University of Illinois, Urbana; they also contributed with several important discussions.

Additionally, Dr. Enrico Gratton, Alex Rietveld, Dr. Theodore Hazlett, Dudley Williams, and Dr. Ed Voss have all contributed to this work with several important discussions. Dr. Voss supplied the author with generous amounts of various anti-fluorescein antibodies. I thank Dr. Neil Reimer for the use of his HPLC instrument and important advice on the technique; similarly, I thank Dr. Richard Guillory for my constant use of his SE-HPLC column. I would also like to thank the staff of the Department of Biochemistry and Biophysics for making sure I never had to go somewhere else for money during the initial two years of work towards my doctorate. Finally, I thank the National Science Foundation for financing our laboratory (via Dave) over the last few years.

I have not included a dedication page, but here I shall mention that this dissertation is dedicated to my wife and our newborn baby Natascha; I also dedicate this dissertation to my parents who have constantly and reasonably supported me throughout my life. I must also thank the rest of my family, past and present, for additional emotional (and sometimes financial) support throughout the past four and a half years.

ABSTRACT

L7/L12 is a dimeric 24 kD ribosomal protein. The structure and mobility of L7/L12 are highly conserved among eubacteria, archaebacteria, and eukaryotes as it plays an essential role in the binding of elongation factors, factor dependent hydrolysis of GTP, and proofreading of nascent peptides. L7/L12 function is putatively dependent on high mobility via its flexible hinge region, coupled with an ability to become elongated. A full understanding of the dynamics of L7/L12 free in solution is required before one can deduce detailed information about its dynamic function on the considerably more complex ribosome. Large discrepancies exist in the literature on the axial ratio of L7/L12, the stability of its dimeric form, the full quaternary structure of the dimer, and to a lesser extent, the dynamics conferred via its flexible hinge.

Since L7/L12 contains no tryptophans, tyrosines, or cysteines, site-directed mutagenesis was utilized to incorporate cysteine residues within the protein, which enabled subsequent site-specific attachment of fluorescent probes. Time-resolved fluorescence polarization studies verify the spherical structure of the globular C-terminal domains, the rigidity of a hinge-deletion mutant, and independent mobility of the dimeric N-terminal domain and monomeric C-terminal domains within hinge-intact L7/L12. Preliminary data suggests that similar mobility persists within ribosome-reconstituted, hinge-intact L7/L12. Furthermore, time-resolved polarization and resonance energy transfer studies demonstrate that the large axial ratios (up to 19:1) reported earlier for L7/L12 are unlikely and indicate a maximum value of 6.6:1.

The thermodynamic parameters of L7/L12 subunit association were deduced from studies with dilution, high-pressure, temperature, denaturants, and salt. The dimer to monomer dissocation constant is 38 nM indicating that the dimeric form dominates at biological concentrations (~μM). L7/L12 dimerization is solely dependent on interaction between the two N-terminal domains α-helices which form a putative coiled-coil as opposed to previous x-ray crystallography studies that indicated possible intersubunit C-terminal domain association.

Numerous recently developed or novel spectroscopic and chromatographic methods were used to characterize the unequivocal dynamic exchange between L7/L12 subunits. The rate of subunit exchange, more specifically, the time elapsing between one cycle of dissociation, translational diffusion, and reassociation, is about 100 milliseconds at 20°C. Preliminary data is presented suggesting at least half of the ribosome-reconstituted L7/L12 dimers undergo subunit exchange.

TABLE OF CONTENTS

LIST OF TABLES

LIST OF FIGURES

LIST OF ABBREVIATIONS

CTF = L7/L12 C-terminal fragment; amino acids 52-120

NTF = L7/L12 C-terminal fragment; amino acids 1-53

$\Delta 7$ or $\Delta 35\text{-}52$ = the hinge deletion mutant of L7/L12; amino acids 35-52 deleted

PMIA, FITC, 1,5-IAEDANS, TMRIA, 5-IAF, ANS bis-ANS, and CPM are all abbreviations for the various probes used in the present study and listed in Figure 9, page 40

τ = fluorescence or excited-state lifetime

ϕ = phase delay

S.S.P. or P = steady-state polarization

P_0 = limiting polarization

r = anisotropy

r_0 = limiting anisotropy

ρ = rotational relaxation time

$\varnothing$ = rotational correlation time

χ^2 = chi-square or degree of fit between calculated and measured values of various time-resolved fluorescence parameters

FRET = fluorescence resonance energy transfer

R = average distance between two probes undergoing FRET

R_0 = distance whereby two probes can transfer resonance energy with 50% efficiency

Note: all other symbols used in the present study for describing fluorescence are given in Chapter 3 of this dissertation.

Gu-HCl = guanidine HCl

PAGE = polyacrylamide gel electrophoresis

HPLC = high-performance liquid chromatography; RP = reverse phase; SE= size exclusion

Standard abbreviations are used for units of time, temperature, volume, pressure, molecular weight, concentration, etc.

CHAPTER 1:
GENERAL INTRODUCTION
BACKGROUND AND RESEARCH OBJECTIVES

THE RIBOSOME AND PROTEIN BIOSYNTHESIS: AN OVERVIEW

Ribosome Structure. The ribosome is a large complex of ribonucleic acids (RNA) and protein molecules that together catalyze protein biosynthesis in all organisms. Eucaryotic and procaryotic ribosomes are very similar in design and function. Each are composed of one large and one small subunit, which fit together to form a complex with a mass of several million daltons (Figure 1). The small subunit binds messenger RNAs (mRNA) and transfer RNAs (tRNA) and the large subunit catalyzes peptide bond formation during protein synthesis (vide infra).

More than half of the weight of the ribosome is RNA, and there is increasing evidence that the ribosomal RNA (rRNA) molecules play a central role in its catalytic activities (Noller et al, 1992 and references therein). Furthermore, the rRNA primary, secondary and tertiary structures are highly conserved among a diverse array of organisms (Noller and Woese, 1981; Gutel et al, 1985). In addition to the ribosomal proteins a variety of soluble non-ribosomal proteins, including initiation factors, elongation factors, and release factors, are essentially associated with the ribosome at various stages of protein biosynthesis (vide infra).

A variety of physical and chemical techniques including chemical modification of RNA, fluorescence spectroscopy, electron and immuno-electron microscopy, neutron diffraction, chemical crosslinking and affinity

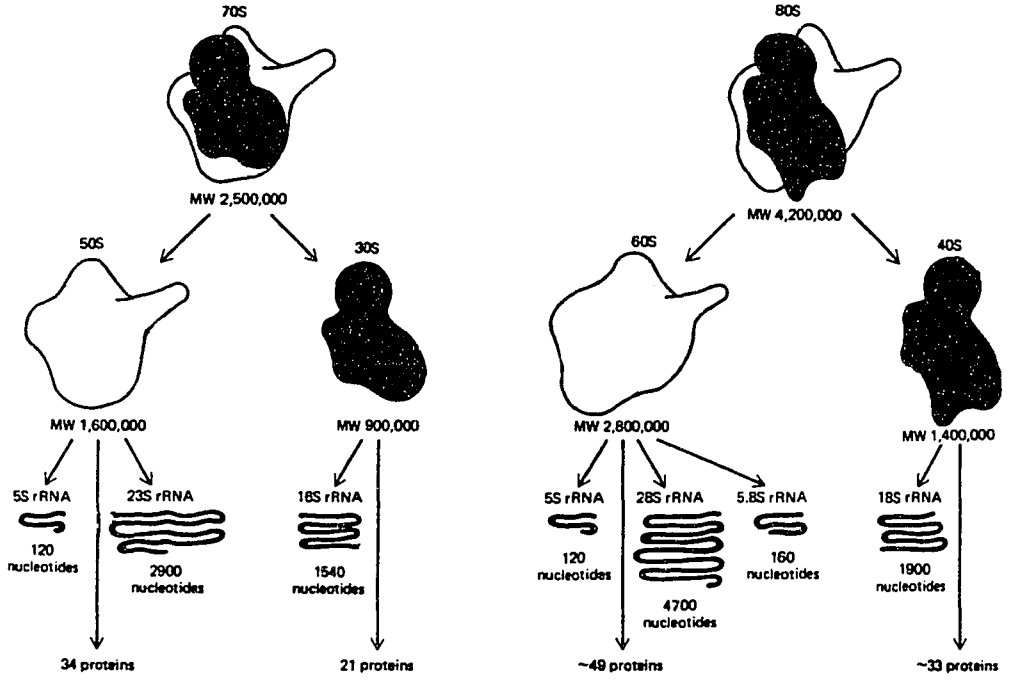

Procaryotic Ribsomes

Eucaryotic Ribosomes

Figure 1: A comparison of the structures of procaryotic and eucaryotic ribosomes. Ribosomal subunits are commonly designated by their "S" values, which indicate their rate of sedimentation in an ultracentrifuge (taken from Alberts et al, 1989). In *E. coli*, the 34 proteins of the large subunit are denoted L1-L34 and the 21 proteins of the small subunit are denoted S1-S21. In procaryotes, a series of 70S ribosomes simultaneously bind a single mRNA forming a polyribosome complex. In eucaryotes, the 80S ribosomes bind to an organelle called the endoplasmic reticulum.

labeling to both RNA and protein have all led to a present consensus model for the structure of the ribosome (Prince et al, 1983; Figure 2).

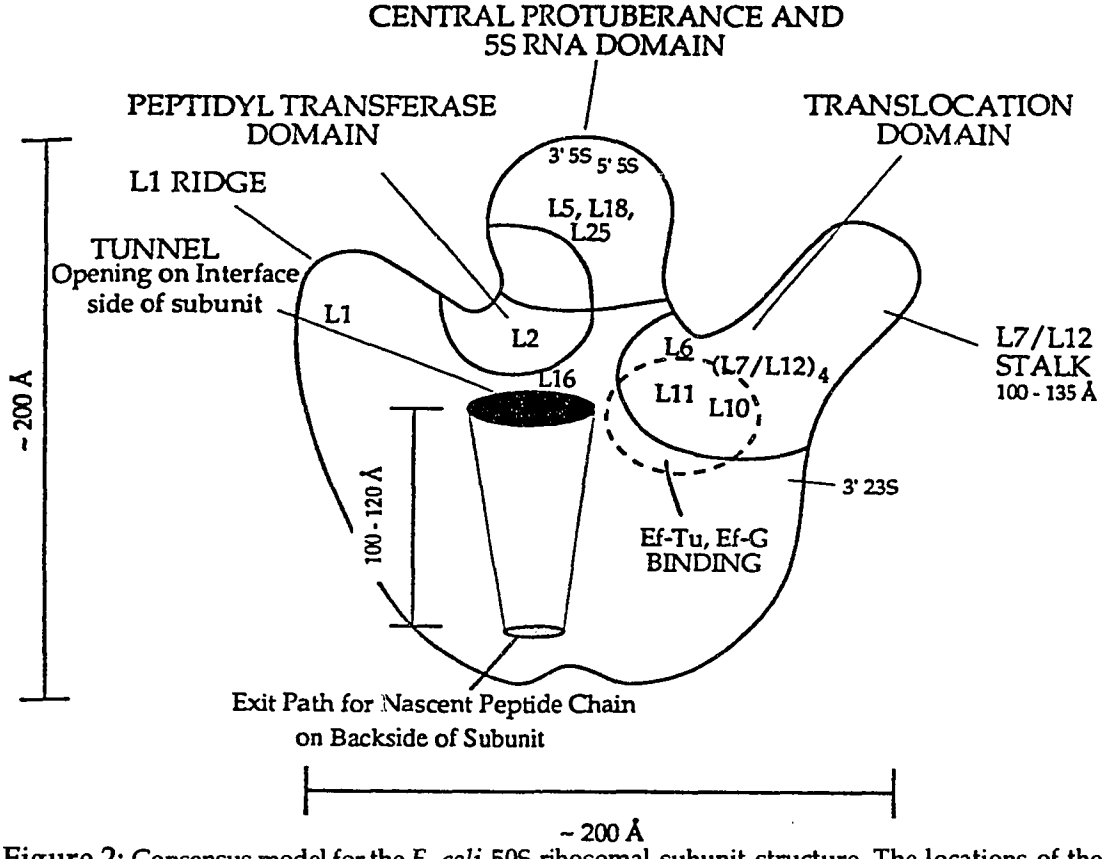

Figure 2: Consensus model for the *E. coli* 50S ribosomal subunit structure. The locations of the major structural and functional domains are depicted. A similar model is available for the 30S subunit that possesses the decoding site during protein biosynthesis . The opening of the tunnel is on the (30S) interface side of the 50S subunit (Zecherle, 1990).

Ribosome Mechanism and Protein Biosynthesis. Protein biosynthesis can be divided into three mechanistically distinct phases: initiation, elongation, and termination.

During initiation, a complex of initiation factors, initiator tRNA (containing the amino acid f-Met in procaryotes), and the small ribosomal subunit bind mRNA. The initiator tRNA anticodon binds the mRNA initiator codon and the initiation factors are subsequently released simultaneous to binding of the large ribosomal subunit to the small subunit; this event marks the end of the initiation phase.

The elongation phase of protein biosynthesis consists of three separate reactions: 1) binding of aatRNA; 2) peptide bond formation at the peptidyl transferase domain; and 3) translocation, which occurs at the translocation domain. The peptidyl transferase and translocation domains are depicted in Figure 2. A schematic of the *E. coli* ribosomal elongation phase is given in Figure 3 (Zecherle, 1990). At the end of the initiation phase, a second aminoacyl tRNA (aatRNA) is brought to the recognition (R-site) site of the ribosome via a ternary complex consisting of the aatRNA, an elongation factor (EF-Tu in procaryotes), and guanosine triphosphate (GTP). At the R-site, proofreading occurs until the correct aatRNA is bound and then transferred to the acceptor (A-site) site adjacent to the initiator tRNA already bound to the peptidyl (P-site) site. GTP is simultaneously cleaved and EF-TuGDP dissociates from the ribosome. The peptidyl transferase domain, consisting primarily of 23S rRNA (Barta et al, 1984) as well as L2 and L16 (Liljas, 1982), is responsible for subsequent peptide bond formation. Peptide bond formation occurs between the COOH-terminus of the nascent peptide chain at the P-site and the NH_2-terminus of the aatRNA in the A-site. The A-site, occupied by a peptidyl tRNA, is no longer able to accept delivery of aatRNA by the EF-Tu ternary complex and the peptidyl transferase step is complete. The last step of the elongation phase is the translocation step. The translocation domain on the ribosome includes the large subunit proteins L6, L10, L11, and L7/L12 as well as 23S rRNA (Liljas, 1991, and references therein). The translocation step is catalyzed by the action of an elongation factor (EF-G in procaryotes). Subsequent to the peptidyl transferase reaction, EF-G/GTP binds to the ribosome in the translocation domain. Binding of EF-G/GTP is followed by GTP hydrolysis and induction of a conformational change necessary for the movement of the ribosome relative to the mRNA:tRNA

complex (Kaziro, 1978; Burma et al, 1986). The ultimate result of this movement is the repositioning of the peptidyl-tRNA from the A-site to the P-site. The deacylated tRNA, previously in the P-site, moves to the exit (E-site) where it is putatively involved allosterically in the proofreading step associated with EF-Tu (vide supra). Upon binding of the cognate aatRNA to the A-site, the deacylated tRNA in the E-site is released (Nierhaus et al, 1986).

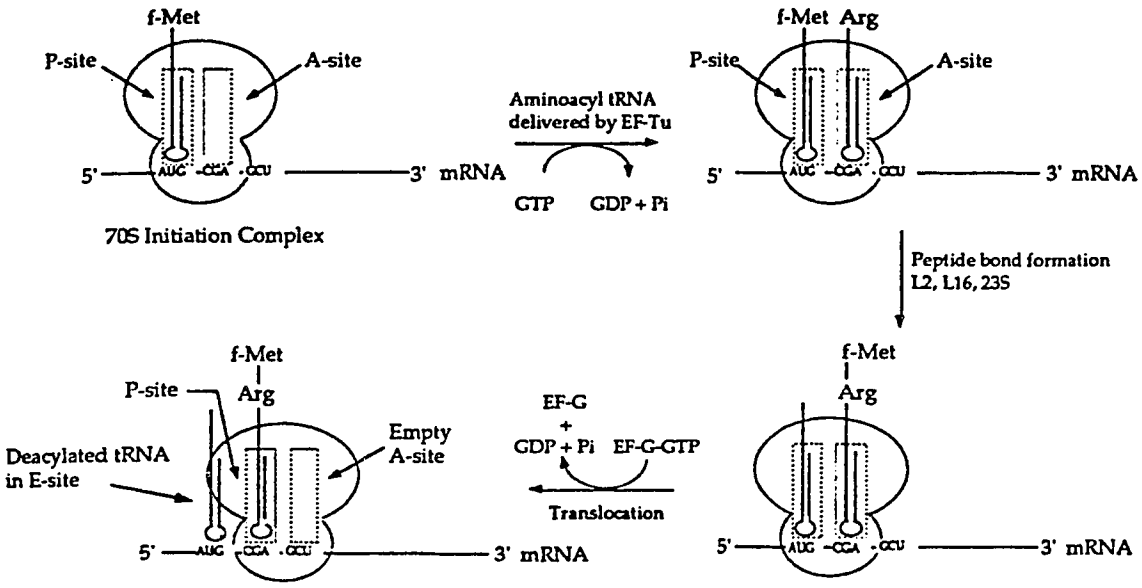

Figure 3: The ribosomal elongation phase (see text for explanation).

Finally, binding of release factor protein to a stop codon in the mRNA sequence marks the final, so-called termination phase of protein synthesis. The completed polypeptide is released and the ribosome subsequently dissociates into its large and small components.

ESCHERICHIA COLI RIBOSOMAL PROTEIN L7/L12

Genetics and Structure. L7/L12 is found in the large subunit of *E. coli* ribosomes (Möller et al, 1970) and is conserved along a diverse array of species (Matheson et al, 1980; Liljas, 1991) indicative of its essential role in protein

synthesis (vide infra). L7/L12, first characterized as the acidic, alanine rich ribosomal A-protein (Möller and Castleman, 1967), is the only multi-copy ribosomal protein; it is present in four copies, which are believed to form two dimers (Hardy, 1975; Subramanian, 1975). All four copies can be selectively removed from the ribosome and quantitatively reconstituted (Hamel et al, 1972).

In *E. coli*, the protein is the product of a single gene, *rpl* L, which codes directly for L12 (Goldberg et al, 1979). L7 is the N-terminally acetylated form of L12 (Terhorst et al, 1972). Acetylase deficient strains of E. coli contain only L12 and show no distinguishable phenotypic alteration (Isono and Isono, 1981). The amino acid sequences of L7 and L12 have been elucidated, revealing that, in their monomeric form, both contain 120 amino acids and have a molecular weight of 12200 daltons (Terhorst, Möller, et al 1973). L7 and L12 are highly acidic proteins possessing isoelectric points of 4.7 and 4.85, respectively (Möller et al, 1972).

The dimeric form of native L7/L12 (at micromolar concentrations) was verified by sedimentation equilibrium analysis (Möller et al 1972; Luer and Wong, 1979; Kar and Aune, 1981), low-angle X-ray scattering (Österberg et al, 1976), and sodium dodecylsulfate polyacrylamide gel electrophoresis (SDS-PAGE) analysis of crosslinked protein (Österberg et al, 1976; Oleinikov et al, 1993A and B). Interestingly, Kar and Aune proposed that dimeric L7/L12 exists in an equilibrium with tetrameric and monomeric forms; this suggestion is discussed in detail later in this dissertation (see Chapter 5). Further evidence for a tetrameric form of L7/L12 existing in fairly high salt is deduced from sedimentation equilibrium, light scattering, and low angle x-ray scattering studies (Georgalis et al, 1989); these studies suggested that the

tetramer, rather than the dimer, is the native form of L7/L12 and that it possesses a somewhat oblate ellipsoid shape.

Dimeric L7/L12 is putatively highly elongated, possessing axial ratios of revealed by sedimentation velocity and viscometry of 8:1 (Wong and Paradies, 1974) or 19:1 (Luer and Wong, 1979; 1980) and low-angle x-ray scattering of 15:1 (Österberg et al, 1976). Five proposed models for the quaternary structure of L7/L12 are seen in Figure 4 and this topic is discussed extensively in Chapter 4.

Experimental evidence for a parallel alignment of the L7/L12 subunits comes from zero-length cross-linking (Oleinikov et al, 1993B) and molecular dynamics simulations (Aqvist et al, 1985). But the question still remains whether this alignment is staggered (i.e., shifted in alignment) as indicated by 9 Å crosslinking studies (Maassen et al, 1981) or non-staggered as indicated by recent zero-length cross-linking studies (Oleinikov et al, 1993B) and proton nuclear magnetic resonance studies (Bushuev et al, 1984). Alternatively, Georgalis and co-workers have proposed a tetrameric L7/L12 that possesses subunits in an anti-parallel and non-staggered alignment. This problem is assessed in detail in subsequent chapters of the present text.

L7/L12 is composed of two major structural domains separated by a flexible hinge (Figure 4). The N-terminal domain forms a long α-helix and the C-terminal is globular (vide infra)--all together L7/L12 contains as much as 76% α-helix (Luer and Wong, 1979). The N-terminal domain and C-terminal domains are separated by a flexible, evolutionally conserved, and alanine rich hinge region, residues 37-52. This flexible hinge region was verified by proton nuclear magnetic resonance (Cowgill et al, 1984; Bushuev et al, 1989), X-ray crystallography (Leijonmarck and Liljas, 1987; Liljas and Gudkov, 1987), and disulfide crosslinking (Oleinikov et al, 1993B; Traut et al,

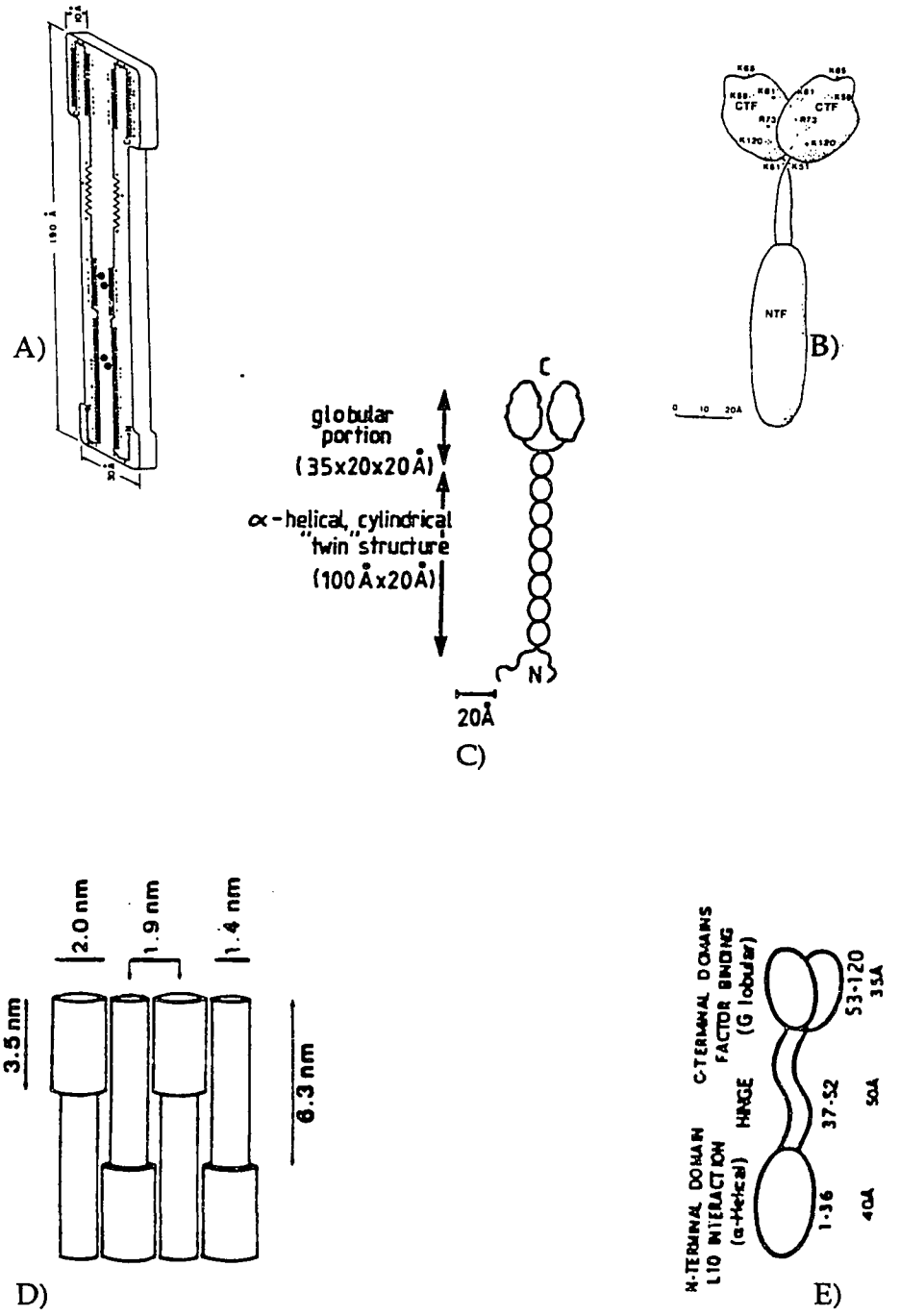

Figure 4: Five proposed quaternary structures for L7/L12 displaying the putative axial ratios, the C-terminal domains, the flexible hinge, and the N-terminal domains. Note the variation in hinge length. A) Model proposed by Luer and Wong, 1979; B) model proposed by Liljas, 1982; C) model proposed by Möller and Maassen, 1986; the frayed single-stranded N-terminal region proposed by Schop and Maassen, 1982; D) Georgalis et al, 1989; E) Traut, 1993 (personal communication). See text for more details.

1993). The essential role of this flexible hinge in protein biosynthesis is described in detail in subsequent subsections of this chapter.

Crystallization of L7/L12 results in cleavage at the flexible hinge producing an N-terminal fragment, amino acid residues 1-46, and a C-terminal fragment, residues 47-120. The x-ray structure of the C-terminal domain, residues 53-120, was elucidated at 1.7-Å resolution (Figure 5; Leijonmarck and Liljas, 1987). Amino acid residues 47-52, comprising part of the flexible hinge, cannot be identified in electron density maps of the C-terminal fragment. Hence, the x-ray data indicate that these residues can adopt multiple conformations or else they are highly mobile in the crystal (lacking discernible diffraction pattern). Interestingly, the N-terminal fragment crystals lack sufficient electron density for elucidation of their structure. Modern 3-D and 4-D nuclear magnetic resonance spectroscopy methods might prove fruitful in the elucidation of this intriguing N-terminal structure.

The N-terminal domains, residues 1-36, are putatively responsible for the dimerization of L7/L12 (Gudkov, 1977; Gudkov and Behlke, 1978), although X-ray crystallography studies (Leijonmarck et al, 1980; Leijonmarck and Liljas, 1987) have suggested the possibility of limited interaction between the two C-terminal domains (the results chapters 4, 5, 6, and 7 of this dissertation bear on this issue). Analysis of the N-terminal domain amino acid sequence suggests hydrophobic interactions as the primary dimerizing force (Luer and Wong, 1979) and one study suggests that the two α-helices might result from a coiled-coil structure (Tsurugi and Mitsui, 1991); this topic will be discussed further in Chapter 4. Interestingly, reversible oxidation of the three methionine residues located in the N-terminal domains of L7/L12 leads to monomerization (Caldwell et al, 1978; Gudkov et al, 1978A/B) and

subsequent loss of biological activity (i.e., *in vitro* poly-phenylalanine synthesis). The loss of activity is putatively a result of the inability of monomeric L7/L12 to rebind L7/L12 depleted 50S ribosomal subunits (Caldwell et al, 1978). The methionine sulfoxides are readily reversed to methionine by simple β-mercaptoethanol treatment and biological activity is subsequently restored.

As seen in Figure 5, the structure of a C-terminal domain from X-ray crystallography is rather plum-shaped with dimensions of 35x35x25 Å (Leijonmarck and Liljas, 1987). A set of three α-helices are alternated with three antiparallel β-sheets and each are separated by a flexible structureless loop. The amino acids found in the interior are hydrophobic and on the exterior, charged residues (15 acidic and 11 basic) produce a hydrophilic

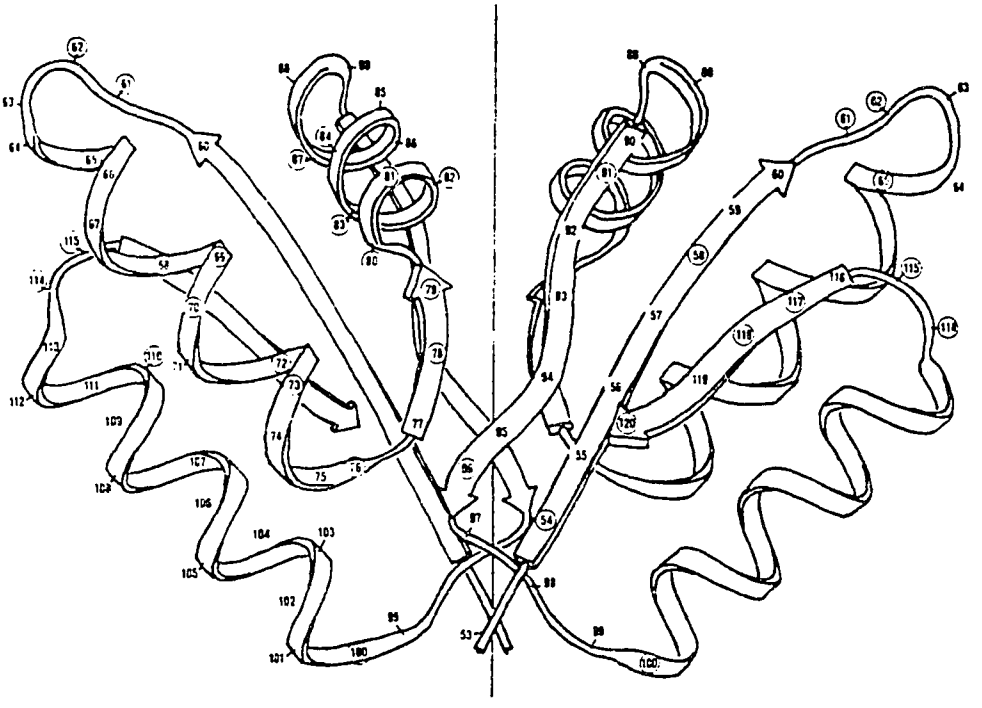

Figure 5: X-ray structure of the C-terminal domains of L7/L12, illustrating a putative twofold symmetry between the two subunits.

surface. Two patches on the external surface of a monomeric C-terminal domain of L7/L12 are hydrophobic. The first patch is located in an evolutionally conserved region putatively involved in factor binding during protein synthesis via a conjectural twofold axis of symmetry formed between two subunits (seen in Figure 5; Liljas, 1982). Furthermore, this region possesses a lysine residue attached to a sulfate characteristic of a typical nucleotide binding region. The second patch is in the interface of the putative C-terminal domain subunit interaction site seen in the crystal structure (Figure 5).

Finally, one region of the L7/L12 C-terminal domain contains a helix-turn-helix motif, spanning amino acid residues 69-87 and characteristic of DNA binding proteins (Rice and Steitz, 1989). The significance of this motif in L7/L12 is unclear but suggests interaction of L7/L12 with one of the RNA species involved in protein synthesis; alternatively, it might be the evolutionary result of gene duplication and mutation from a gene encoding a nucleic acid binding protein.

Location and Dynamics of L7/L12 on the Ribosome. The L7/L12 stalk was depicted earlier in Figure 2. Two dimers of L7/L12 attach via their N-terminal domains to the large ribosomal subunit protein L10 (Schrier et al, 1973; van Agthoven et al, 1975; Schop and Maassen, 1982) and are unable to bind to the ribosome in the absence of L10 (Stöffler et al, 1974). L7/L12 can be removed from the ribosome in the form of a pentameric complex consisting of two L7/L12 dimers and one L10 monomer (Österberg et al, 1976; Pettersson et al, 1976; Dijk et al, 1977). Furthermore, this pentameric complex can be formed in vitro from the separately purified proteins and is "stable" in 6M urea (Pettersson et al, 1976) being completely dissociated only by SDS or at low pH (see Chapters 5 and 6 of this dissertation).

The $(L7/L12)_4L10$ pentameric complex binds *in vitro* to the 5' one-third (nucleotides 1-1200) of 23S RNA (Dijk et al, 1977; Dijk et al, 1979; Beauclark et al, 1984), although L7/L12 alone binds very weakly and in a non-specific manner to rRNA (possibly the nucleic acid binding helix-turn-helix motif?). Under certain conditions only one L7/L12 dimer remains tightly bound in the $(L7/L12)_4L10$-23S rRNA complex, which suggesting that non-equivalent binding sites for L7/L12 exist on L10 (Dijk et al, 1979; Lee et al, 1981). The existence of two non-equivalent binding sites is supported by studies of L7/L12 treated with urea (Möller et al, 1983) or purified in the absence of reducing agents (Zantema et al, 1982a); in both cases, centrifugation through a sucrose cushion subsequent to L7/L12 ribosome reconstitution led to the selective release of a single dimer. Furthermore, a single dimer of L7/L12 is released from the ribosome upon binding of a monoclonal antibody specific for the N-terminal amino acid residues 1-73 of L7/L12 (Traut et al, 1986; Nag et al, 1987). Hence, these results all suggest a strong and weak binding site of L7/L12 to the 50S ribosome via L10.

Interestingly, initial immunoelectron microscopy studies using monoclonal antibodies specific to L7/L12 indicated that L7/L12 was located in the central protuberance of the 50S ribosomal subunit (see Figure 2) (Tischendorf et al, 1975) rather than what is now called the L7/L12 stalk. In contrast, a second group using the same method found that L7/L12-depleted ribosomes lacked the two side protuberances (Boublik et al, 1976). Finally, a third group, using essentially the same methods, found what is now the commonly accepted location of L7/L12 on the ribosome, the L7/L12 stalk (Strycharz et al, 1978). The investigators of this latter study did not, however, rule out the possibility of L7/L12 being located at another position on the ribosome. Furthermore, this latter model was supported by another study (Tokimatsu et

al, 1981) in which four polyclonal antibodies against L7/L12 were observed bound to the tip of the L7/L12 stalk, also suggesting that both dimers were bound to the stalk.

Why then, did the earlier studies claim to have observed L7/L12 at regions distant to the L7/L12 stalk? As Traut and co-workers reported in 1983, L7/L12 could chemically crosslink to a large number of 50S ribosomal proteins up to 70 Å away from the L7/L12 stalk (Figure 6A). This result alone suggested that L7/L12 possesses large flexibility via its hinge and in combination with its elongated structure, is able to bend towards and react with regions on the ribosome distant to the stalk. Finally, the selective release of one L7/L12 dimer via a monoclonal antibody specific to the N-terminal of L7/L12 leads to the disappearance of the L7/L12 stalk as visualized by electron microscopy (Tewari et al, 1986). A subsequent study found that the C-terminal domains of the other dimer are located in the body of the 50S ribosomal subunit (Olsen et al, 1986). Several more recent studies support the theory that L7/L12 can bend via its flexible hinge enabling it to interact with distant regions on the 50 S ribosomal subunit (Zecherle, 1992A/B); Oleinikov et al, 1993A). A present model is given in Figure 6B.

As mentioned earlier, L7/L12 possesses an alanine rich, low secondary structure hinge region similar in characteristics to that of the muscle protein myosin. Proton nuclear magnetic resonance studies indicate that L7/L12 intact 80S ribosomes exhibit very broad signals (>1KHz wide) as expected for large, slowly rotating samples. Superimposed on these broad lines are some very sharp resonances uncharacteristic of rRNA and therefore presumably due to ribosomal proteins (Gudkov et al, 1982; Cowgill et al, 1984). When L7/L12 is removed from the ribosome these sharp resonances disappear from the ribosome and are only regained upon L7/L12 reconstitution suggesting

that L7/L12 is the most mobile component of the ribosome (or that some other elements of the ribosome become highly mobile upon addition of L7/L12). These same sharp resonances are observed in ribosomes of such evo-

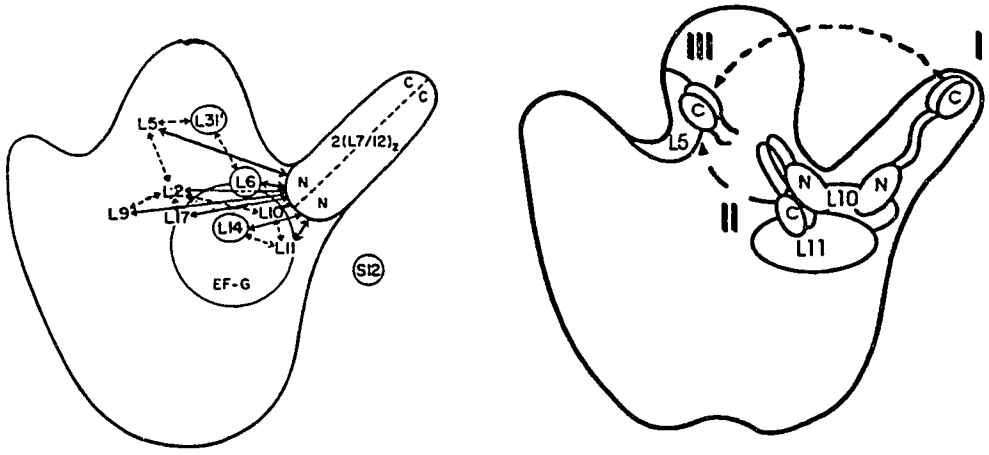

A) B)

Figure 6: A) Results of crosslinking studies in which circled proteins crosslink EF-G and solid arrows represent proteins that can crosslink to L7/L12 (Traut et al, 1986); B) Present model for the conformations of the two dimers of L7/L12 within the 50 S ribosomal subunit as well as their interactions (Traut et al, 1993).

lutionally distant organisms as yeast, brine shrimp, and rat liver suggesting existence of highly mobile L7/L12 equivalent proteins. Further studies indicated that these sharp resonances arise in pure L7/L12 (Bushuev et al, 1989) and are abolished or attenuated upon specific amino acid deletions in the hinge region.

The significance of this highly mobile region in protein biosynthesis has been investigated by a number of scientists and, as described above, appears essential for interaction of L7/L12 with distant regions on the ribosome. Furthermore, this flexibility of L7/L12 via its hinge appears necessary for function as described in the next subsection.

Functional Role of L7/L12 in Protein Biosynthesis. The components and mechanism of protein biosynthesis were described earlier in this text. Purified ribosomes are able to support the hydrolysis of GTP in the presence of only EF-G (i.e., without any other components of the translational machinery) (Kuruki et al, 1970). Treatment of ribosomes with 0.5 M NH_4Cl, and 50% EtOH at 0°C causes selective release of L7/L12 and subsequent loss of EF-G dependent GTPase activity (Hamel et al, 1972). Furthermore, polyphenyl-alanine synthesis is abolished. Both activities are completely restored upon reconstitution with L7/L12.

L7/L12 interacts with a number of factors involved in protein synthesis as well as the ribosomal proteins seen in Figure 6A. In the absence of a fully intact L7/L12, EF-G dependent GTPase activity is almost completely inhibited (van Agthoven et al, 1975). In this study, the lysine residues of L7/L12 were blocked by citriconylation and addition of trypsin led to subsequent cleavage at the sole arginine residue producing an N-terminal fragment, residues 1-73, and a C-terminal fragment, residues 74-120. Addition of the N-terminal peptide to L7/L12 depleted ribosomes completely blocked binding of native L7/L12 as well as EF-G dependent GTPase activity. This result proved that the N-terminal fragment of L7/L12 was responsible for ribosome binding but that the C-terminal fragment was necessary for interaction with EF-G.

The involvement of the C-terminal domains in L7/L12 function was also demonstrated by Kirsebom and colleagues (1986) who found that point mutations of two amino acids in the conserved region of the C-terminal domains led to decreased ribosomal proofreading. Similarly, certain monoclonal antibodies specific for the C-terminal domains inhibit binding of EF-G to the ribosome (Sommer et al, 1985). Furthermore, interaction between L7/L12 and EF-G on the ribosome was recently shown to induce

conformational changes in the latter protein (Gudkov and Gongadze, 1984; Gudkov and Bubunenko, 1989).

The number of copies of L7/L12 required to reconstitute polyphenylalanine synthesis and EF-G GTPase activity has been studied (Möller et al, 1983). These studies demonstrated that a single dimer of L7/L12 is sufficient in promoting EF-G GTPase activity while*two* dimers are necessary for complete restoration of poly-phenylalanine synthesis.

Some studies, such as chemical crosslinking (San Jose et al, 1976) and proteolysis (Gudkov and Bubunenko, 1989) have suggested the interaction of L7/L12 with EF-Tu; conversely, others suggest functional independence of EF-Tu from L7/L12 (Langer et al, 1984). One study verified that binding of a polyclonal antibody specific to the C-terminal fragment of L7/L12 led to inhibition of EF-Tu binding to the ribosome although peptidyl transferase activity was unaffected (Nag et al, 1987). Similarly, researchers have verified that a specific antibody to the C-terminal domain of L7/L12 inhibited interaction of release factors with the ribosome (Tate et al, 1990).

L7/L12 is essential for factor dependent GTPase activity and poly-phenylalanine synthesis via interactions with factor binding sites known to be distant on the ribosome from the L7/L12 stalk. As explained in the previous subsection, this L7/L12 functionality is most likely accomplished via bending of its flexible hinge, and by the ability of L7/L12 to extend to distances greater than 100 Å allowing its C-terminal domains to interact with various other ribosomal components.

Direct evidence for the requirement of L7/L12 flexibility via its hinge has come from a number of studies. Point mutations in the flexible hinge of L7/L12 lead to decreased growth rate of *E. coli* caused by a decreased elongation rate of protein synthesis (Kirsebom et al, 1986) as well as errors in

ribosomal proofreading (Kirsebom and Isaksson, L.A., 1985). Furthermore, point mutations in the hinge region of L7/L12 were shown by proton NMR to result in decreased hinge mobility (Bushuev et al, 1989).

Two laboratories have found that genetic deletion of various sections of the L7/L12 hinge result in partial to nearly complete abolition of poly-phenylalanine synthesis (Gudkov et al, 1991; Traut et al, 1993 and Oleinikov et al, 1993B). The Traut group found that incomplete ribosome binding occurred when amino acid residues 35-41 were deleted indicating their involvement in ribosome binding of L7/L12. Deletion of residues 42-52, however, had little if any effect on ribosome binding. Furthermore, the C-terminal conformation was apparently not effected by the hinge deletions nor was the dimeric structure of L7/L12, as judged by electrophoretic methods. The Traut group found in another study that conformational changes in the N-terminal region of the hinge are necessary for L7/L12 binding to the ribosome since an intersubunit disulfide bridge between cysteines substituted at amino acid position 33 results in absence of ribosome binding (our results bear on this issue, see Chapter 6). Requirement for a dynamic L7/L12 in protein biosynthesis was reviewed again recently by Möller (1990) who postulated that L7/L12 drives rotational movement of tRNA–like a ribosomal bicep contraction. Conversely, the fluorescence results of Lee et al (1981B) suggest little if any interaction of L7/L12 with tRNA on the ribosome.

FLUORESCENCE SPECTROSCOPY AS A TOOL FOR EQUILIBRIUM PROTEIN DYNAMICS RESEARCH

Fluorescence Spectroscopy: An Introduction. The details of the methodology and instrumentation for fluorescence studies are described extensively in the next chapter. In this section, we shall briefly review the uses of the method.

Fluorescence spectroscopy is a method of revealing a broad spectrum of information in the physical, chemical, biological, and medical sciences:

1) It allows scientists to study biological systems from millimolar down to picomolar concentrations essentially covering the concentration range of most biomolecules found in nature. This extremely high sensitivity has enabled fluorescence methods to replace radioisotope methods in many chemical assays;

2) It provides us with a molecular stopwatch monitoring microscopic and submicroscopic events from the microsecond to the picoseconds range which is ideal for many different biochemical and/or biological events as depicted in Table 1;

3) Fluorescence resonance energy transfer provides us with estimations of approximate distances between different locations in a particular system (i.e., as Stryer put it, a "molecular ruler", 1978);

4) It allows measurements under equilibrium conditions (i.e., separation of components is not required and there is no need for harsh chemical or physical treatments prior to measurements). Furthermore, the system's chemical conditions can be changed rapidly with stop-flow mixing devices (~ a millisecond) or its physical conditions such as temperature and pressure using respectively, a thermal circulator or pressure pump (see Chapter Two).

More specifically, fluorescence parameters such as spectral shifts, quantum yields, polarizations, time-resolved properties (all described in detail in the next chapter) allow us to study processes such as rotational motions of proteins, average shapes of proteins, internal and flexible motions of proteins, dynamic equilibria, determination of distances between specific molecules or macromolecules, diffusion and transport of molecules or

macromolecules (e.g., through membranes), etc. There are numerous excellent review chapters and books on the use of this technique in the fields listed above (i.e., Jameson, 1984; Jameson and Reinhart, 1989; Jameson and Hazlett, 1991; Lakowicz, 1991).

Table 1: Time Scale of Significant Events in Globular Proteins (Careri et al, 1979).

Protein surface	
Tightly bound water relaxation	10^{-9}
Loosely bound water relaxation	10^{-11}
Side chains rotational correlation	10^{-10}
Proton transfer reaction of ionizable side chains	$10^{-7}-10^{-9}$
Protein conformation	
Local motion	$10^{-8}-10^{-9}$
Isomerization process	$10^{-2}-10^{-7}$
Folding–unfolding transition	10^{+2} -1
Enzyme-substrate complex in solution	
Encounter rate	(diffusion controlled)
Estimated lifetime of the transition state in covalent reactions	$<10^{-10}$
Change in metal ion coordination sphere in metalloenzymes	$10^{-6}-10^{-9}$
Enzyme-substrate local conformational motion	10^{-9}
Covalent enzyme-substrate intermediate lifetime	$10^{-3}-10^{-4}$
Enzyme-substrate complex conformational isomerization	$10^{-2}-10^{-4}$
Enzyme-substrate complex unfolding transition	10^{+2} -1

*Representative values in seconds. For further details see text.

This text deals with the application of fluorescence spectroscopy to a protein, L7/L12. Fluorescence properties of a protein can be studied via an intrinsic or extrinsic fluorophore. Intrinsic protein fluorescence can be accomplished via the deep ultraviolet (UV) electromagnetic excitation of the amino acids tryptophan, tyrosine, and phenylalanine. In most cases tryptophan is the amino acid of choice due to its relatively high quantum yield (the ratio of photons emitted to the number of photons absorbed). If no

tryptophans exist then tyrosine, if present, is the next best amino acid to study. In extremely rare cases, like that of L7/L12, neither tryptophan or tyrosine exist, only two phenylalanines. Since phenylalanine's quantum yield is so low and its absorption maximum is deep in the UV, excitation sources such as synchrotron radiation with good intensity at 260 nm, are required. The possibility of undesirable and destructive photochemical reactions in such studies must always be considered. A simpler route in this latter case is to use an extrinsic fluorophore, that is, one that can bind at a specific region (non-covalently) or specific amino acid side chain (covalently) and possesses more ideal spectral properties. The difficulties that arise in the use of an extrinsic fluorophore are specificity and possible alteration in protein conformation and/or biological activity. One must also choose a fluorophore which possesses spectral properties that would best characterize their system (see Valeur, 1991 and Chen and Scott, 1985 for a review of fluorescent probe spectral properties; also, Molecular Probes, Inc. 1993 Catalogue).

In many cases, such as elucidation of protein denaturation and dissociation properties (i.e., Paladini and Weber, 1981B; Silva et al, 1986; Xu and Weber, 1982; Ruan and Weber, 1988; Panda et al, 1992; Silva et al, 1992A/B; Erijman et al, 1993), specificity is unnecessary. Equally important, these equilibrium studies were virtually unaffected by the extrinsic fluorophore used when compared to the intrinsic tryptophan fluorescence. In the above cases, an amine specific isothiocyanate, sulfonyl chloride, or succinimidyl ester derived fluorophore was used. Since most proteins have more than one basic amino acid such as lysine, arginine, and histidine, an amine specific probe binds at usually more than one site. Specificity is required in the case of distance determination via fluorescence resonance energy transfer. Although specific labeling of two lysine residues in L7/L12

(which contains thirteen lysines and one arginine) has been accomplished via tedious chemical modification procedures (Zantema et al, 1982A/B; Maassen et al, 1983; Thielen et al, 1984), simpler methods exist (vide infra).

Specificity via a natural ligand can also greatly simplify interpretations of fluorescence detected hydrodynamics results (Johnson et al, 1978; Johnson et al, 1982; Abrahamson et al, 1985; Jameson et al, 1987; Hazlett et al, 1989; Watson et al, 1992). In these studies, natural active sites on proteins provided the fluorescence spectroscopist with another solution for specificity. For example, the hydrodynamics of the ternary complex of aminoacyl tRNA/EF-Tu/GTP was studied subsequent to reaction of iodoacetamidyl fluorescein with Phe-tRNA^{phe}. The iodoacetamide moiety was covalently bound to a specific thiouridine residue located on this tRNA (see Watson et al, 1992).

Iodoacetamidyl and maleimidyl derived fluorophores are highly specific for sulfhydryls and proteins containing cysteines or preferably a single cysteine (Allen, 1981; Molecular Probes, Inc. '93 Catalogue). The procedures used for specific sulfhydryl labeling with the above probes are well characterized and described in the next chapter. Under unusual conditions such as high pH, specificity is altered (Lee et al, 1981A).

Obviously, verification of particular amino acid modification is required when one desires specificity. A number of methods exist which include: 1) trypsin digestion of a protein labeled with a radiolabeled fluorescent probe followed by two-dimensional electrophoresis and subsequent autoradiography; 2) trypsin digestion of the fluorophore labeled protein, followed by peptide fragment separation via reverse-phase high-performance liquid chromatography (RP-HPLC), and amino acid sequencing of the fragment (s) possessing fluorescence; 3) finally, trypsin fragmentation

and RP-HPLC, followed by mass spectrometry of the desired fragment. The latter two methods are the most reliable (see next chapter).

Site-directed mutagenesis provides the fluorescence spectroscopist with a tool for simplifying the problem of specificity. If more than one cysteine exists in the protein one of the cysteines can be simply deleted or substituted by another amino acid (i.e., James et al, 1992). In the present studies of *L7/L12*, in which the *wild type contains no cysteine*, a number of single cysteine containing mutants were produced (e.g., Zecherle et al, 1992 A and B; Oleinikov et al, 1993 A and B; Traut et al, 1993; present study). In these cases, verification of probe specificity is provided by simple comparison of the extent of labeling of the mutant in comparison to that of the wild type (which contains no cysteines, see next chapter).

Finally, after a particular protein is fluorescently labeled it is desirable to check if conformation, dynamic equilibrium (i.e., state of aggregation), and function are maintained. In most cases, if function is maintained then one assumes that the conformation and/or subunit (if any) dynamic equilibrium were not effected. Functional assays are possible for most proteins. Conformation and state of aggregation should always be checked nonetheless, and are usually checked by size-exclusion HPLC (SE-HPLC; discussed in subsequent chapters) or analytical ultracentrifugation.

Protein Dynamics: A Brief Overview. It is essential to realize, as Linderstrom-Lang and Schellman pointed out in 1959, that proteins are *dynamic* as opposed to the very *static* (crystallized) impressions one obtains with x-ray crystallography structures. Dr. Gregorio Weber has characterized proteins as "screaming" and "kicking" (Weber, 1975). Excellent reviews of the experimental evidence exist (Careri et al, 1979; Karplus and McCammon, 1981; Weber, 1992A; Weber, 1992B). An enormous variety of protein motions have

been revealed by fluorescence spectroscopy, nuclear magnetic resonance spectroscopy, hydrogen exchange, and raman scattering (recall Table 1).

Proteins can assume an enormous number of nearly isoenergetic conformations (conformational substates; e.g. see Frauenfelder, Sligar, and Wolynes, 1991). This perspective is supported by numerous studies (for rotations of amino acid side chains, see Gratton et al, 1986A and references therein; Gratton et al, 1986B; Careri et al, 1979; reviewed in respect to protein folding and function relation by Jaenicke, 1991 and Ptitsyn and Semisotnov, 1991; Weber, 1992A). Furthermore, a plethora of literature exists on the functionally essential rotational and conformational hydrodynamics of immunoglobulins and muscle proteins (see introduction to Chapter 4 of this text for review) as well as L7/L12 in protein biosynthesis (see Chapter 4 results). Similarly, protein oligomers undergo conformational drift upon dissociation (i.e., Xu and Weber, 1982; Weber, 1986; King and Weber, 1986A/B; Ruan and Weber, 1989; Silva et al, 1989; Erijman, L. and Weber, G., 1991A/B; Silva et al, 1992; Ruan and Weber, 1993). The concept of protein conformational drift (as Weber first described in 1986) states subsequent to dissociation of an oligomeric protein, by dilution or physical or chemical methods, the isolated subunit undergoes conformational changes (Xu and Weber, 1982). Essentially, the more time the subunit spends in the dissociated state, the more time it has to change conformation and therefore become energetically less able to reassociate. The phenomenon of conformational drift was further elucidated via fluorescence spectroscopy investigations on oligomers dissociated by high pressure and/or temperature modifications and both methods are described in detail in Chapter 5.

A wealth of evidence using electrophoresis and fluorescence spectroscopy verifies the subunits of oligomeric proteins are in a dynamic

equilibrium (i.e., Hermann et al, 1982 and references therein; King and Weber, 1986A/B; Saad et al, 1986; Jaenicke and Rudolph, 1989; Erijman and Weber, 1991 A/B, Erijman and Weber, 1993; Ruan and Weber, 1993; the present study, Chapter 6), alternating through cycles of dissociation and reassociation (AD cycles as Weber first put it, 1986). AD cycles essentially allow protein subunits to exchange in solution and the rate of exchange is hence dependent exclusively on the rate of dissociation (see Chapter 6 for details). What then determines the rate of dissociation? As Weber describes (1992A), dissociation of an oligomer into subunits requires diffusion of the separated subunits a minimum distance, dx, such as they become independent and are essentially separated by a layer of water which is approximately 5 Å. From the Einstein diffusion equation:

$$\langle dx^2 \rangle = 2D\,dt \qquad (1)$$

A *translational* diffusion coefficient D of ~8×10^{-7} $cm^2 \cdot sec^{-1}$ as that expected for a spherical 35 kD particle in water at 25°C would predict a time for separation, dt, of ~one nanosecond. Hence, the dissociating state must last longer than one nanosecond. A good candidate as seen in Table 1 (page 19), is a fluctuation of charge such as the half-life of a protonated carboxyl group which is a few microseconds (also, see Weber, 1986; Cheng et al, 1993). Clearly, a very rapid subunit dissociation and reassociation cycle (subunit exchange) is feasible and has recently been observed at the sub-second level for a dimeric protein (Wendt et al, 1993; Chapter 6, this study). In the case of larger protein aggregates, where the aggregated state is dependent on a multitude of conformational substates and energetics, subunit exchange can occur at tremendously slower rates (i.e., references given in previous paragraph; these concepts will be described extensively in Chapters 5 and 6).

Previous knowledge on the *functional* requirement for conformational and rotational dynamics of L7/L12 was already reviewed in the second section of this chapter. In fact, we will find in Chapters 4, 5, and 6 of the present text as Österberg (published in Möller and Maassen, 1986) putatively discovered using a distributional analysis of low-angle x-ray scattering data--the elongated conformation of L7/L12 is, in fact, very transient. Further characterization of L7/L12 dynamics is a goal of subsequent chapters of this text. Furthermore, the possibility of L7/L12 dimers undergoing a dynamic exchange of subunits *free in solution and on the ribosome* is explored in Chapter 6 of this dissertation.

THESIS OUTLINE

Fluorescence spectroscopy, utilizing extrinsic fluorophores labeled at specific amino acids was the primary method used to study various site-directed cysteine mutants of L7/L12 as well as wild type L7/L12 and the goals of this research were as follows:

1) To label various site-directed cysteine mutants, deletion mutants, and wild type L7/L12 with different fluorescent probes.

2) To characterize the rotational modalities and conformational substates of L7/L12 using contemporary time-resolved fluorescence techniques; SE-HPLC is used for the separation of any heterogenous oligomeric states of L7/L12 prior to quantitative time-resolved fluorescence measurements. Furthermore, to obtain preliminary time-resolved fluorescence results on the hydrodynamics of various ribosome-reconstituted L7/L12 cysteine mutants.

3) To utilize steady-state and time-resolved fluorescence spectroscopy, absorption spectroscopy, and SE-HPLC to determine the dimer/monomer dissociation constant and secondary/tertiary stabilities of various wild type

and mutated forms of L7/L12. Furthermore, to characterize the forces involved in the dimerization process.

4) To determine and characterize L7/L12 subunit dynamics (i.e., L7/L12 subunit exchange in solution) and to obtain preliminary results on the subunit dynamics of L7/L12 bound to the ribosome.

CHAPTER TWO:
MATERIALS AND METHODS

BASIC BUFFERS USED

TMN buffer: unless otherwise indicated contains 50 mM Tris (hydroxy-aminomethane)-HCl (Tris-HCl, pH 7.4), 10 mM magnesium chloride ($MgCl_2$), 100 mM ammonium chloride (NH_4Cl); TMND buffer: same as TMN but containing 3 mM dithiothreitol (DTT) unless otherwise indicated; TMNB buffer: same as TMN but containing 8 mM β-mercaptoethanol; 70N buffer: 100 mM NH_4Cl, 10 mM Tris-HCl (pH7.2), 10 mM $MgCl_2$, and 0.5 mM ethylenediaminetetraacetic acid (EDTA -- chelates metals essential for proteases). Other buffers are listed later in specific protocols.

MOLECULAR BIOLOGY TECHNIQUES

Oligonucleotide Site-directed Mutagenesis. This method was performed in the laboratory of Dr. Robert Traut at the University of California, Davis. Cysteine residues do not exist in L7/L12 and therefore cysteines were introduced at specific sites on L7/L12 to determine its topography, conformation, and interactions. The various L7/L12 mutants that have presently been produced are shown in their protein form in Figure 7. The genetic constructions for substitution of Ser-89 by Cys-89 and Ala-63 by Cys-63 have already been described (Zecherle et al, 1992B; Oleinikov et al, 1993A), as well as for the various hinge deletions (Traut et al, 1993; Oleinikov et al, 1993A). The Ser-33 to Cys-33 substitution was generated using the site-specific oligonucleotide-directed in vitro mutagenesis system from Amersham (Oleinikov et al, 1993B). Furthermore, the unpublished Ser-99 substitution by Cys-99, Ala-12 by Cys-12, N-terminal tails (residues 1-53), and Cys-89 C-terminal domain heads were all constructed using the same Amersham

system (with the primers possessing the appropriate restriction sites enabling subsequent insertion into a restriction-site with appropriately modified pT7-6 plasmid), the engineering details of which go beyond the scope of this text. Verification of successful site-mutations is accomplished via DNA sequencing using the Sequenase T7 system from United States Biochemicals.

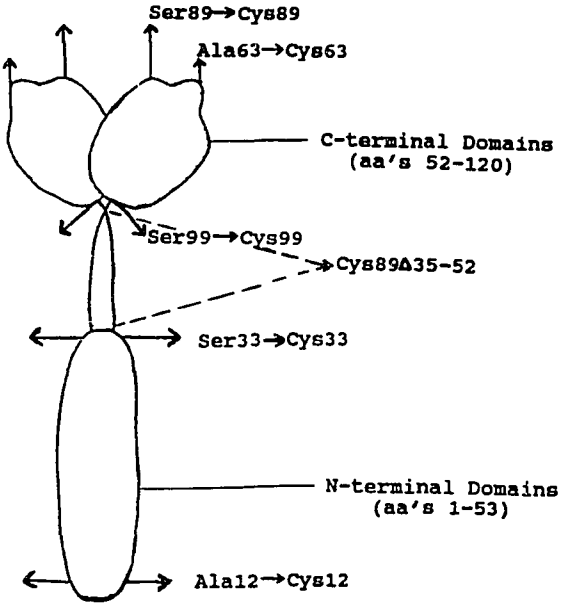

Figure 7: Various protein L7/L12 mutants produced in the laboratory of Dr. Robert Traut at the California, Davis and used in the present study.

Transformation of Competent Escherichia coli with L7/L12 Plasmid Constructs via the Calcium Chloride Method. The basic method of $CaCl_2$ transformation of *E. coli* is well established (see Sambrook et al, 1991). The strain of *E. coli* used for the transformation of various L7/L12 site-directed plasmid constructs is called DH5-α, which intrinsically possesses a thermosensitive helper plasmid pGP1-2 (shown in Figure 8). The procedure is as follows: 1) a single colony of *E. coli* cells is inoculated into 50 ml LB medium (in 1 liter, 10 g tryptone, 5 g yeast extract, 10 g NaCl, pH 7.5; bacto-agar

added to 1.5%) and grown overnight at 37°C with moderate shaking (250 rpm); 2) inoculate 4 ml of the culture into 400 ml LB medium in a sterile flask. Grow at 37°C, shaking (250 rpm), to an OD_{590} of 0.375; 3) aliquot culture into eight 50 ml prechilled, sterile polypropylene tubes and leave the tubes on ice 5 to 10 min.; 4) centrifuge cells 7 min at 3000 rpm (1600xg), 4°C. Allow centrifuge to decelerate without brake; 5) pour off supernatant and gently resuspend each pellet in 10 ml ice-cold $CaCl_2$ solution on ice; 6) centrifuge cells 5 min at 2500 rpm (1100xg), 4°C. Discard supernatant and resuspend each pellet in 10 ml cold $CaCl_2$ solution. Keep resuspended cells on ice 30 min.; 7) centrifuge cells 5 min. at 2500 rpm (1100xg), 4°C. Discard supernatant and resuspend each pellet in 2 ml of ice cold $CaCl_2$ solution. This suspension may be left on ice for several days; 8) dispense cells into prechilled, sterile polypropylene tubes. Freeze immediately at -70°C; 9) aliquot 10 ng of DNA in a volume of 10 to 25 µl into a 15-ml sterile, round-bottom test tube and place on ice; 10) rapidly thaw competent cells by warming between hands and dispense 100 µl immediately into test tubes containing DNA. Gently swirl tubes to mix, then place on ice for 10 mins. Competent cells should be used immediately; 11) heat shock cells by placing tubes into a 42°C water bath for 2 min; 12) add 1 ml LB medium to each tube. Place each tube on a roller drum at 250 rpm for 1 hr at 37°C; 13) plate aliquots of transformation culture on LB containing 60 µg/ml each of ampicillin *and* kanamycin antibiotics (see rationale for two antibiotics in Figure 8); 14) plates are either grown at 37°C (30°C for the mutant L7/L12 constructs--see next section) for 12 to 16 hours prior to expression or stored at 4°C for subsequent use.

Expression of the Mutant L7/L12 Constructs. As shown in Figure 8, pGP1-2 contains the gene for T7 RNA polymerase under the control of the λ_{pL} promoter that is repressed by a temperature-sensitive repressor (cI857). pGP1-2

contains a p15A origin of replication that is compatible with the ColE1 origin of replication on the expression vector pT7-6. The two plasmids are maintained in the same cell by selection with kanamycin (pGP1-2) and ampicillin (pT7-6 expression vector). The advantages of using this system are: 1) the T7 RNA polymerase synthesizes RNA at a rate several times faster than that of the *E. coli* RNA polymerase and 2) furthermore, is highly specific for initiation at its own promoter sequences and does not initiate any sequences on *E. coli* DNA which together usually results in nearly all transcription under the control of the T7 RNA polymerase. The protocol for induction of expression of the L7/L12 mutant genes is as follows (slightly modified from Ausubel et al, 1992): 1) Subclone the fragment containing the gene to be expressed into pT7-6 (as described in Site-directed...section) and transform an *E. coli* DH1-α strain already containing the pGP1-2 thermosensitive T7 RNA polymerase plasmid with the vector containing the mutant L7/L12 gene to be expressed under the control of the p_{T7} promoter (transformation already described in previous subsection); 2) plate the transformants (containing both plasmids) on LB/kanamycin/ ampicillin antibiotic plates and grow overnight at 30°C; *at 30°C the T7 RNA polymerase inhibitor promoter is activated, subsequently preventing promotion of the T7 RNA polymerase gene and therefore the T7 RNA polymerase dependent promoter on the expression vector;* 3) pick a single colony that contains the two plasmids with sterile toothpick or pipet. Inoculate it into 5 ml 2xYT (in 1 liter, add 16 g tryptone, 10 g yeast extract, 5 g NaCl, pH 7.0)/kanamycin/ampicillin (60 μg/ml of each antibiotic as usual) medium and grow overnight at 30°C; 4) dilute the overnight culture of cells 1:40 into fresh 2xYT/ampicillin/kanamycin medium and grow for several hours at 30°C to an OD_{590} of ~0.4; 5) induce the

gene for T7 RNA polymerase by rapidly raising the temperature to 42°C (thereby preventing transcription of the T7 RNA polymerase inhibitor prom-

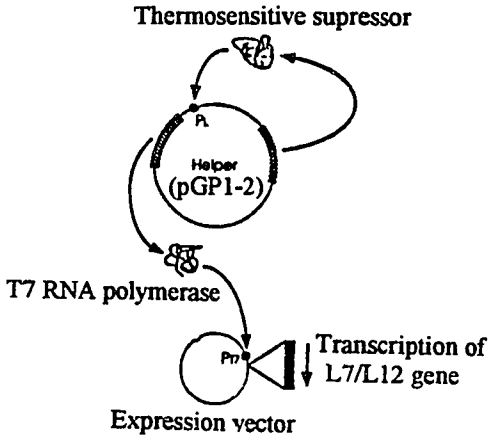

Figure 8 (Ausubel, et al, 1992) Schematic of the two-plasmid T7 RNA polymerase/promoter system used for expression of the various mutant L7/L12 constructs. The combination of the antibiotics kanamycin and ampicillin allows selection of colonies possessing both pGP1-2 and the expression vector (pT7-6), respectively.

otor) for 30 min., which in turn induces the genes under control of the T7 promoter (p_{T7}), i.e., the L7/L12 mutant genes; 6) reduce temperature to 37°C and grow cells an additional 90 min. with shaking; to analyze the induced proteins by SDS-PAGE, resuspend a 1 ml centrifuged pellet of the bacteria into 100 µl cell cracking SDS loading buffer. The purity of recombinant L7/L12 is already ~50-70% at this stage; 7) harvest the cells by centrifuging and discarding supernatant. For greater than 100-ml cultures, centrifuge 10 min in a Sorvall GS-3 rotor at 5000 rpm (4000xg), 4°C; the pellet is rinsed with 70 N buffer and recentrifuged. The pellet is rapidly frozen at -70°C for later purification.

Purification of Overexpressed L7/L12 Cysteine Mutants (protocol used in the laboratory of Dr. Robert Traut). 1) Thaw cells and add 80 µl/g cells of 10 mg/ml stock of lysozyme (freshly prepared) and mix gently; 2) set on ice for 30 minutes, then centrifuge for 15 mins at 5000 rpm; freeze pellet in liquid nitrogen; 3) weigh out 2.5 times cell pellet weight of alumina; grind cells 5 times 1 min at 4°C and then suspend in 10 ml 70 N buffer and place in sorvall tube; rinse mortar and pestle with 10 ml 70 N buffer, and combine with other 10 ml; 4) add 2µl DNase (RNase free). Wait 15 mins still at 4°C; 5) centrifuge in sorvall at 8000 rpm at 4°C for 15 minutes; 6) collect the supernatant into a Ti60 centrifuge tube and place on ice; 7) resuspend the alumina pellet in 10 ml 70N buffer and centrifuge again in sorvall at 8000 rpm, 15mins, and 4°C; discard pellet; pool the supernatant into the Ti60 tube and centrifuge at 33000 rpm for 30 minutes at 4°C; 8) transfer the supernatant into a clean Ti60 centrifuge tube and discard the pellet; 9) centrifuge the supernatant at 58000 and 4°C for two hours; 10) collect the supernatant and dialyze against 80 mM NH_4OAc, pH 5.7, and 7 mM β-ME. A white precipitate should form; centrifuge to remove the precipitate and run on SDS-PAGE a small amount of both the supernatant and the precipitate.

Since some contaminating nucleic acids and possibly some $(L7/L12)_4L10$ pentameric complex might still exist, further purification and character-ization is done via DEAE-HPLC and SE-HPLC as described in the next section. The purity of recombinant L7/L12 following SE-HPLC is ≥ 99% as judged by SDS-PAGE and Coomassie blue staining or immunoblotting as described in the next section.

BASIC BIOCHEMICAL TECHNIQUES

This section excludes fluorescence methodologies/instrumentation (next chapter) and all novel procedures described in chapters four through six of

this dissertation.

Diethylaminoethane (DEAE-HPLC) High-performance Liquid Chromatography Purification of Overexpressed L7/L12 Variants (Oleinikov, 1993). Recombinant L7/L12 from the supernatant of the NH_4OAc step (up to 25 mgs of total protein) was added to a Pharmacia Resource Q (DEAE-TSK analog) 1 ml volume column equilibrated with 80 mM NH_4OAC (pH 5.7) and 7 mM β-ME. The column was then rinsed with 80 mM NH_4OAc (pH 5.0) and 7 mM β-ME. Finally, 300-400 μl fractions of L7/L12 were collected upon elution with a buffer containing a gradient of up to 1 M NH_4OAC (pH 5.0) and 7 mM β–ME. Some nucleic acids elute from the column several minutes later than the L7/L12. For overexpressed cysteine mutants of L7/L12, possible intersubunit disulfide bonds were reduced with 1.0% β-ME for 30-60 mins at 37°C prior to addition to the DEAE-HPLC. The purity of the eluted fractions of L7/L12 is checked by SDS-PAGE prior to addition to SE-HPLC. Concentration with a Centricon-10 microconcentrator (10kD MW cut-off from Amicon) is usually desirable prior to SE-HPLC otherwise protein was usually stored at -70°C.

Size-exclusion High-performance Liquid Chromatography (SE-HPLC). SE-HPLC of L7/L12 was either performed on 1) the Hewlett-Packard diode-array detector instrument at University of Hawaii using a Toso-Haas, G2000SW, 30 cm x 7.8 mm (ID); else, on the Toso-Haas instrument at the University of California, Davis using a Toso-Haas, G3000-SWXL, 30 cm x 7.8 mm (ID) column. The size of the silica packing particles and pore sizes were 5 μM and 250 Å, respectively for the $G3000SW_{XL}$ column; and similarly, 10 μM and 125 Å for the G2000SW column. Unless otherwise indicated the usual buffer used for equilibration of SE-HPLC columns was TMN. Individual uses of the SE-HPLC system are described throughout the text. Protein was always added in greater than 5.0 μM dimeric concentration. The state of aggregation of

L7/L12 was verified by comparison on a semi-logarithmic plot to a number of molecular weight standards (MW 0.1k-1500kDaltons). Dimeric L7/L12 runs at approximately same rate expected for a spherical ~40 kilodalton protein (see Chapter 4 for extensive details). The fractions of L7/L12 were usually concentrated with a Centricon 10 (10,000 daltons MW cutoff) microconcentrator (Amicon) and stored at -70°C until later use.

Sodium Dodecylsulfate Polyacrylamide Gel Electrophoresis (SDS-PAGE). Verification of the purity of L7/L12 variants was carried out with the Pharmacia PhastGel systems in gels containing 20% acrylamide followed by transfer to nitrocellulose and immunoblotting of the proteins with a monoclonal antiL7/L12 antibody as described (Zecherle et al, 1992A). In comparison to molecular weight standards, monomeric L7/L12 runs at ~12-13kD.

Measurement of L7/L12 Protein Concentrations. The protein concentrations of L7/L12 were determined by the Coomassie Plus assay from Pierce or Bio-rad using initially a BSA standard. Greater accuracy (20%) with the Coomassie method was obtained in comparison to the traditional Coomassie assay as judged from comparisons to the protein concentrations of L7/L12 obtained from the gravimetric method of simple extensive dialysis against ddH_2O to remove all salts followed by lyopholization and weighing. Gravimetrically quantified L7/L12 was used as a standard for more recent Coomassie assays. The Coomassie method is then the choice method for subsequent protein concentration determinations of L7/L12 due to its accuracy and rapidity. *All L7/L12 protein concentrations are calculated and given for the dimeric form. All optical density readings were acquired with a Perkin-Elmer spectrophotometer.*

Monomerization of L7/L12 via Methionine Oxidation. Methionines of L7/L12 were oxidized by any one of the following three methods (as indicated in subsequent chapters): 1) 1-3 mgs/ml of L7/L12 is dialyzed (or exchanged into via Biospin-6 column--see section below titled Labeling Procedures) into TMN buffer; 50% acetic acid containing hydrogen peroxide (0.7-1.0 mg/ml) is added and incubation is overnight at 4°C followed by exchange of buffer to desired one (Gudkov, 1977); this was the original procedure for L7/L12 methionine oxidation but two separate, less harsh, and simpler methods are available; 2) add to a 500 μl solution containing 1-2 mgs/ml of L7/L12 in 20 mM Tris, 1N $HClO_4$ so that the pH is brought down to 2.2; raise temperature to 30°C and add up to 2% hydrogen peroxide and incubate at 30°C for 2 hours followed exchange to appropriate buffer (Neumann, 1967; Caldwell et al, 1978); 3) a much simpler method yet was communicated to the author from Dr. Oleinikov (1993C) at UC, Davis: simply add 1% hydrogen peroxide to 1-2 mgs/ml L7/L12 in TMN buffer and incubate at 90°C for 30 mins! This method works probably with less specificity (i.e., oxidation of other residues might occur) but specificity is not usually a factor if one only desires L7/L12 monomerization. L7/L12 cysteine mutants can be oxidized by this latter method (Oleinikov) subsequent to labeling of the cysteine residues.

Finally, the methionine sulfoxides (as opposed to methionine sulfones) which are always formed in the above oxidations are readily reversible by reduction for 4 hours at 37°C with 10 mM DTT (personal observation) or by reduction for 12 hours with 1% β-mercaptoethanol at 30°C (Caldwell et al, 1978). Verification is accomplished by SE-HPLC or dimethylsuberimidate crosslinking followed by SDS-PAGE (monomers do not crosslink--see Oleinikov, 1993A).

L7/L12 Cysteine Mutant Intrasubunit Zero-length Disulfide Crosslinking (Makarov et al, 1993 and references therein). Disulfide formation reactions between cysteine residues were carried out using ambient O_2 as the oxidizing agent with the redox catalyst 500 μM Cu (II) (1,10 phenanthroline)$_3$ at room temperature for 30-60 mins (TMN buffer is ok). Analysis with SDS-PAGE (no β-ME) typically verified greater than 98% crosslinked dimers as a ~29kD L7/L12 dimer appears. SE-HPLC in TMN buffer verified that intrasubunit crosslinking occurred as opposed to intersubunit crosslinking which would have led to larger molecular weight products.

Glutaraldehyde Crosslinking of L7/L12. This procedure is essentially performed in a phosphate buffer (PBS) since glutaraldeyde crosslinks amino groups. Crosslinking is performed by simply adding 0.5% glutaraldehyde to L7/L12 (~0.1-1.0 mgs/ml) and incubated at room temperature ~30mins. Usually the yield of crosslinked dimers is about 50% as verified by SDS-PAGE and most of the rest is larger crosslinked product.

Trypsin Digestions of Modified L7/L12 Variants. 200 μg lyopholized protein was resuspended in 75 μl 0.2 M N-ethylmorpholino acetate, pH 8.0. TPCK-trypsin (Worthington) was added to a final concentration of trypsin of 2% (w/w) and incubated 2 hours at 37°C. The peptides were frozen, lyophilized and resuspended either 10 μl ddH2O for TLC or 100 μl ddH2O containing 10% glacial acetic acid if in preparation for reverse-phase HPLC.

Reverse-phase High-performance Liquid Chromatography (RP-HPLC) for the Separation of Trypsin Digests or for the Separation of L7 from L12. In both cases, a C18 reverse-phase column from Waters Inc. was used on the Hewlett-Packard diode-array detector system. For the trypsin digest fragment separation: The trypsin fragments were added directly to the C18 column (200 μls) developed with a linear gradient of 20 mM tertiary butylammonium

acetate, pH 6.0, to 20 mM tertiary butylammonium acetate, pH 6.0, and 50% acetonitrile (v/v) over a one hour period at 0.2 ml/min. Detection was at 230 nm. Results are shown in Chapter 5.

For the separation of L7 from L12: 10% acetic acid was added to wild type L7/L12 or to cysteine mutants already reduced in 1% β-mercaptoethanol and protein was subsequently added to the C18 column (200 μls) equilibrated with 0.1% trifluoroacetic acid (TFA) in water and developed on a linear gradient of 5-40% of 0.1% TFA in acetonitrile for 10 min, 40-70% same buffer for 60 mins, and 70-100% same buffer for 10 mins. Flow rate was 0.5 ml/min and detection was at 230 nm. Results are shown in Chapter 5.

Amino Acid Sequencing of L7/L12 Trypsin Fragments. All amino acid sequencing was performed by Dr. Neil Riemer at the Molecular Biology Instrumentation and Training Facility, University of Hawaii at Manoa, on an Applied Biosystems Edman Degradation Amino Acid Sequencing Machine.

Purification of Ribosomes from E. coli. 70S and 50S ribosomes were purified by the well-established and lengthy procedures already described (Kenny et al, 1979) and stored at -70°C to preserve the RNA component or prevent L7/L12 methionine oxidation.

Preparation of 70S and 50S Ribosomes Lacking L7/L12. L7 and L12 were extracted from the ribosomal subunits using the methods already described (Hamel et al, 1972; Tokimatsu et al, 1981). Briefly, the extraction is performed 2x at 0°C with 2 mg/ml ribosomes in 10 mM Tris-HCl (pH 7.2), 150 mM ammonium chloride, 10 mM magnesium chloride, 3.5 mM β-ME, and 50% (v/v) ethanol. The final pellet was resuspended at 1mg/ml in TMNB (14 mM β-ME) and stored at -70°C in small aliquots.

Reconstitution of L7/L12 on to the 50S or 70 Ribosome Cores (lacking L7/L12). The reconstitution procedure is a slight modification of that first developed

by Hamel et al, in 1972 and involves simply adding desired excess of L7/L12 dimers over ribosomes at 37°C (although other temperatures work) and incubating no longer than 10 mins. Non-reconstituted L7/L12 can be removed by either 1) centrifuging 5 hr at 58000 rpm in a Beckman Ti65 rotor through a 9-ml cushion of 10 % (w/v) sucrose followed by resuspension of the ribosomal pellet or 2) separating via SE-HPLC, in which the ribosome-reconstituted L7/L12 comes out in the void volume.

Poly-phenylalanine Synthesis Activity Assays of L7/L12 Variants. This procedure was done at the University of California, Davis with materials purified in their laboratory as well as materials purchased from various sources. The usual TMND (except 20 mM Tris-HCl, pH 7.5 and only 1 mM DTT) buffer was used as well as 0.5 mM calcium chloride, 1 mM spermidine, and 5 mM sodium phosphate. First, 80 pmol L7/L12 is first reconstituted into the 70S ribosomes (lacking L7/L12) for 10 mins at 37°C in TMN. Each 100 μl reaction mixture contained in addition 1 mM ATP, 1 mM GTP, 6 mM phosphoenolpyruvate, 1 μg of pyruvate kinase, 10 μg polyuracil, 200 μg of total *E. coli* tRNA, 10 μl of S100 enzymes (containing various necessary factors as previously decribed, Kenny et al, 1979), 5000 pmol of [^{14}C]phenylalanine, and 10-20pmol of 70S ribosome cores (lacking L7/L12 and added last). Incubation is for 30 mins at 37°C. The amount of radioactive phenylalanine incorporated in protein synthesis is quantified by liquid scintillation as previously described (Jelenc and Kurland, 1979).

Anti-Fluorescein Antibodies. An IgG polyclonal antibody, Fab fragment, and a single chain Fab have been previously well characterized (Voss, 1984; Voss, 1990; Voss et al, 1993); they were provided to us as a generous gift from Dr. Ed Voss at the University of Illinois, Urbana and details and individual uses are described throughout the subsequent chapters.

FLUORESCENT PROBES

The fluorescent probes used in the present study were as follows: tetramethylrhodamine-5-(and-6)-iodoacetamide (TMRIA), 5-iodoacetamido-fluorescein (IAF), 5-(2((iodoacetyl)amino)ethyl)-amino)naphthalene-1-sulfate (IAEDANS), 5-dimethylaminonaphthalene-1-sulfonyl chloride (Dansyl-Cl) 1-pyrenemethyliodoacetate (PMIA), fluorescein isothiocyanate (FITC), and 7-diethylamino-3-(4'-maleimidylphenyl)-4-methylcoumarin (CPM). The structure of the above probes are illustrated in Figure 9 (except Dansyl-Cl, similar in structure to IAEDANS), and were all purchased from Molecular Probes, Inc, Eugene, Oregon. Extinction coefficients given in this chapter are approximations taken from values measured by Molecular Probes, Inc and in Chapters 4-6 actual measured extinction coefficients for chromophores attached to L7/L12 protein variants are presented. *The author shall mention here that, although each of the probes mentioned in Figure 9 lose some of their atoms subsequent to chemical reaction (e.g., IAEDANS loses its iodide and becomes AEDANS), the same abbreviations as given in Figure 9 will be used throughout this dissertation.*

DYE LABELLING PROCEDURES

Fluorescent Probe Labeling of Wild Type L7/L12. Wild type L7/L12 was labeled with either 1,5-IAEDANS in pH 9.4 carbonate buffer or fluorescein isothiocyanate (FITC) in pH 9.0 (modification of Lee et al, 1981). In the case of IAEDANS labeling, the protein buffer was exchanged into pH 9.4 carbonate buffer (containing 50 mM sodium carbonate, 100 mM potassium chloride) via one Biospin 6 column (a polyacrylamide based column with a 6 kD MW exclusion limit from Bio-Rad) chromatography purification step. Subsequently, 30-40 x excess of IAEDANS (in excess of monomeric L7/L12) was added and incubation was for 2-4 hours in the dark. Excess unlabeled probe is

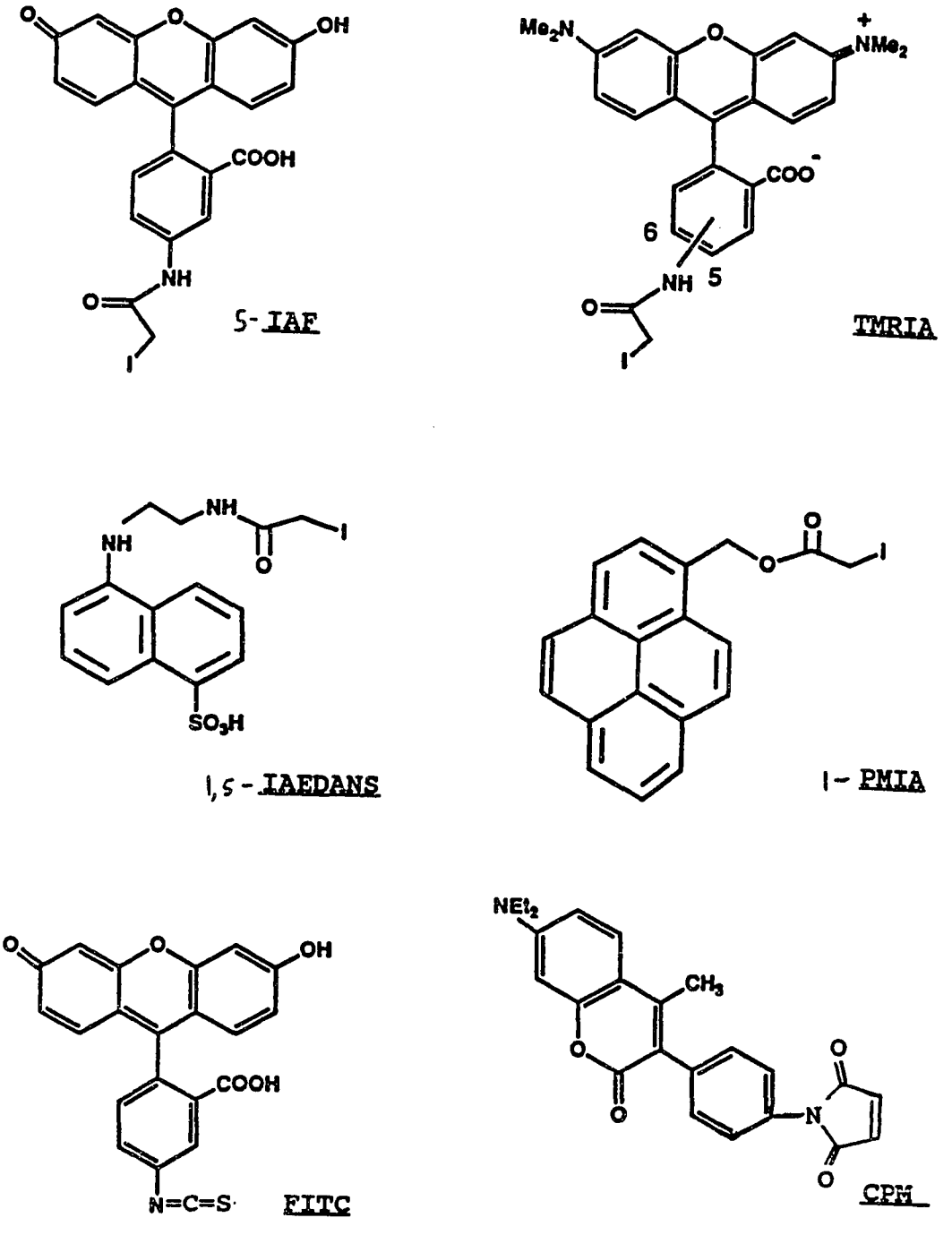

Figure 9: Chemical structures of various probes used in the presented study (see text)

removed by one of the following procedures: two Biospin purifications, one G25 PD10 sephadex column chromatography run, one SE-HPLC run (see Chapter 4) or overnight dialysis. Specificity is putatively 90-100% at the N-terminal lysine as judged by 2-D gel electrophoresis of tritiated protein followed by autoradiography (Lee et al, 1981A) although for our measurements it was never necessary to verify this specificity. Labeling efficiencies were always ~0.25-0.6 IAEDANS/subunit of L7/L12 as judged by IAEDANS and protein concentrations. IAEDANS concentrations were determined either via an extinction coefficient at 340 nm of 5700 $cm^{-1}M^{-1}$ (from Molecular Probes Catalogue) or, if concentration of IAEDANS was too low for accurate optical density determination it could be roughly quantified by comparing emission intensities (340 nm excitation) to that of free IAEDANS in an appropriate percentage of ethanol possessing equivalent fluorescent lifetime (see next section) and emission maximum (see Hudson and Weber, 1973).

Wild type L7/L12 was labeled with FITC by simply exchanging protein into pH 9.0 borate buffer (50 mM sodium borate, 100 mM potassium chloride) via Biospin-6 column, adding 10 x excess of FITC, incubating for 5-10 mins at room temp., and subsequent removal of free dye by any one of the above procedures listed for free IAEDANS removal. Specificity was putatitivey ≥80% (Lee et al, 1981) but our trypsin digestion and subsequent RP-HPLC suggested much lesser specificity (no more than 60%--see chapter 4). Furthermore, amino acid sequencing of the primary fluorescein-containing peptide gave an ambiguous and very surprising indication that the serine 15 was labeled (see Chapter 5). Labeling efficiencies were usually ~0.1-0.25 FITC/subunit of L7/L12 as judged by FITC optical density at 495 nm (extinction coefficient is ~82000 $cm^{-1}M^{-1}$).

Fluorescent Probe Labeling of the Various L7/L12 Cysteine Mutants. The four different iodoacetamide derived fluorophores (including IAEDANS) seen in Figure 9 were attached to all five different cysteine mutations as well as the Cys-89 hinge deletion mutant (each are illustrated in Figure 7). The CTF C-89 and NTF mutants have only been labeled with 5-IAF and FITC, respectively. Finally, the Cys-33 and Cys-89 mutants were also labeled with the one maleimide probe seen in Figure 9.

The procedure used for labeling the different L7/L12 cysteine mutants with IAEDANS or IAF was as follows (adapted from Allen, 1981): The IAF and the IAEDANS were each first dissolved in dimethylformamide (DMF); 1) 1-4 mgs/ml L7/L12 cysteine mutants disulfide bonds (if any) are reduced with ~1% β-mercaptoethanol for 30-60 minutes at 37°C; 2) excess β-mercaptoethanol is removed via spin through Biospin-6 column previously equilibrated with TMN buffer, pH 7.8-8.3 containing 3 mM fresh dithiothreitol (DTT)--this step is the most crucial one of the entire procedure, the DTT essentially keeps cysteines reduced as well the rapid Biospin-6 column buffer exchange which simultaneously, essentially removes all β-mercaptoethanol that would interfere with subsequent iodoacetamide labeling; 3) ~8-10 mM of the iodoacetamide derivative probe (essentially in excess of the 3 mM DTT) is then added (usu. ~4 μls) and 4) labeling proceeds for 40-75 mins at 37°C; 5) excess probe is removed by either *three* Biospin-6 purifications (most expensive, but most rapid), 3x2 liters dialysis each for ~3-5 hours (most time consuming), Sephadex, or SE-HPLC (see next chapter). Labeling efficiency is nearly always 100% (i.e., all cysteines labeled) as verified by optical density readings of the IAF at ~495 nm (extinction coefficient is ~82000 $cm^{-1}M^{-1}$) and 340 nm for IAEDANS (extinction coefficient is ~5700 $cm^{-1}M^{-1}$). Specificity was initially verified prior to labeling as described above

(see subsection above titled Determination of Cysteine Mutant Sulfhydryls) and after labeling via simple comparison to wild type control which contains no cysteines and is virtually free of IAF or IAEDANS subsequent to the above labeling procedure (IAEDANS does not label wild type L7/L12 at pH 8.0 as judged by total lack of any emission upon 340 nm excitation). All proteins remained active subsequent to labeling (see Chapter 4).

Labeling of the cysteine mutants with PMIA or TMRIA was slightly more difficult with the two interesting exceptions of the Cys-12 and Cys-33 N-terminal domain mutations. Labeling of Cys-12 and Cys-33 with PMIA or TMRIA followed nearly the same procedure as labeling with IAF or IAEDANS except a large amount of probe precipitation occurs with the former pair of probes at the labeling incubation step. The only difference in the procedures for Cys-12 and Cys-33 when labeling with PMIA or TMRIA is that the samples must be centrifuged subsequent to the labeling incubation; the resulting supernatants are put through the Biospin-6 column once (to remove excess dye), centrifuged (still usually small amount of precipitant), and either 1) dialyzed 2x2 liters each for ~3 hours or 2) put through the SE-HPLC (usual procedure). Washing of the SE-HPLC of the SE-HPLC with 6 M urea is required after each run of samples labeled with TMRIA or PMIA to remove probe which stuck to the column. Even though precipitation occurred in the labeling reaction, nearly 100% labeling efficiency was always obtained (although protein yield usually only 50%). Quantitation of TMRIA was performed essentially in 3 M Gu-HCL (see Chapters 5 and 6) where the 555 nm extinction coefficient is 76000 $cm^{-1}M^{-1}$. PMIA quantitation was at 338 nm where the extinction coefficient was 46000 $cm^{-1}M^{-1}$. Full protein activity remained for the above samples (see Chapter 5).

Labeling of the C-terminal domain cysteine mutants (C-63, C-89, and C-99) with PMIA or TMRIA is more tedious. The labeling reaction was done via usual procedures except 50% DMF was required to keep probe and therefore protein solubilized. Each completed labeling reaction was spun one time through a 6 M urea equilibrated Biospin-6 column (urea essentially prevented protein loss via probe precipitation). Finally, the proteins were put through SE-HPLC pre-equilibrated with TMN/6 M urea (urea once again essential to prevent serious protein loss) and the resulting protein fractions were then dialyzed 2x2 liters to remove urea. Nearly 100% complete labeling was obtained with this method as determined from extinction coefficients and protein assays and furthermore, full activity remained. Neither PMIA or TMRIA labeled even the slightest fraction of a percent the wild type L7/L12. Why labeling of the C-terminal with PMIA or TMRIA leads to co-precipitation of protein with probe, whereas, labeling of the N-terminal does not, is a very intriguing question.

Labeling of C-33 and C-89 with CPM (a maleimide) followed the same procedure as for the iodoacetamides except the pH was kept at 7.5. Labeling efficiencies approached 100% for C-33 and never better than 35% for C89 (even when labeling was performed in 50% DMF, although higher efficiency was not pursued further for C-89) as judged from a 390 nm extinction coefficient of 30000 $cm^{-1} M^{-1}$.

CHAPTER 3:
FLUORESCENCE METHODOLOGIES AND INSTRUMENTATION

INTRODUCTION

Fluorescence is the emission of photons from electronically excited singlet states. The basic definition for the understanding of fluorescence was introduced by Einstein (see 1917) and was stated as follows: "Any excited state of the system, characterized by an electronic energy E_1, higher than the ground state energy E_0, decays spontaneously (i.e. in the absence of any radiation) to the lower energy state E_0 by emitting a photon of angular frequency ω such that

$$h\omega = E_1 - E_0 \qquad (1)$$

where h is the Planck's constant."

It was well known at the time of Einstein, via the initial observations of Stokes in 1852, that stimulated emission (as opposed to the spontaneous emission process described in Equation (1) could occur via the *absorption of light* in the ultraviolet or violet electromagnetic region and its subsequent emission in the blue and red region, i.e., at longer wavelengths (now known as the Stokes shift). Scientists such as Einstein, Bose, and Planck subsequently laid down the initial equations describing spontaneous emission (see der Haar, 1967 for detailed discussion). A full explanation of the origin of fluorescence was later described via the development of quantum mechanics and included: the quantization of the electromagnetic field first developed by Dirac and Heisenberg in the twenties; the transition between electronic states being dependent on a Hamiltonian electron/photon interaction term; and the Fermi excited-to-ground state transition probability rate equation (for a

detailed description of the quantum theory of absorption and emission of light, see Louden, 1983).

It was later shown by Franck and Condon (1926) that vibronic bands exist within electronic transitions and that the emission always occurs from the lowest vibrational state of the lowest electronic excited state (S_0). They also found that vibrational relaxation as well as relaxation from higher electronic states (S_1) is *much faster* than the deexcitation of S_1 to S_0 (see Figure 10A). As seen in the Jablonski diagrams (Fig. 10A/B): 1) the spectrum of emitted light should be independent of the wavelength of excitation; 2) most or all of the fluorescence spectrum will be shifted to lower energies (i.e., longer wavelengths than the longest wavelength absorption band; alias the "Stokes shift"); and 3) the shape of the emission band will be approximately a mirror image of the longest-wavelength absorption band.

The time that elapses between absorption of light and subsequent emission is known as the excited state lifetime (also nominated the fluorescence lifetime, equal to the *average* time of the emission decay, e^{-1}). During the excited state lifetime a number of processes occur that allow the investigator to obtain information on the particular system. As mentioned in Figure 10, collision with neighboring molecules can lead to deexcitation and therefore quenching of the excited state lifetime (and essentially emission of photons). Hence, the excited state lifetime itself can give information on the particular fluorescent molecule environment. During the excited state lifetime the fluorophore can rotate or more specifically change excited dipole orientation relative to its position upon absorption of light; this reorientation is the basis for steady-state as well as time-resolved polarization measurements described in the next two subsections. Furthermore, excited state reactions such as resonance energy transfer to a neighboring chromo-

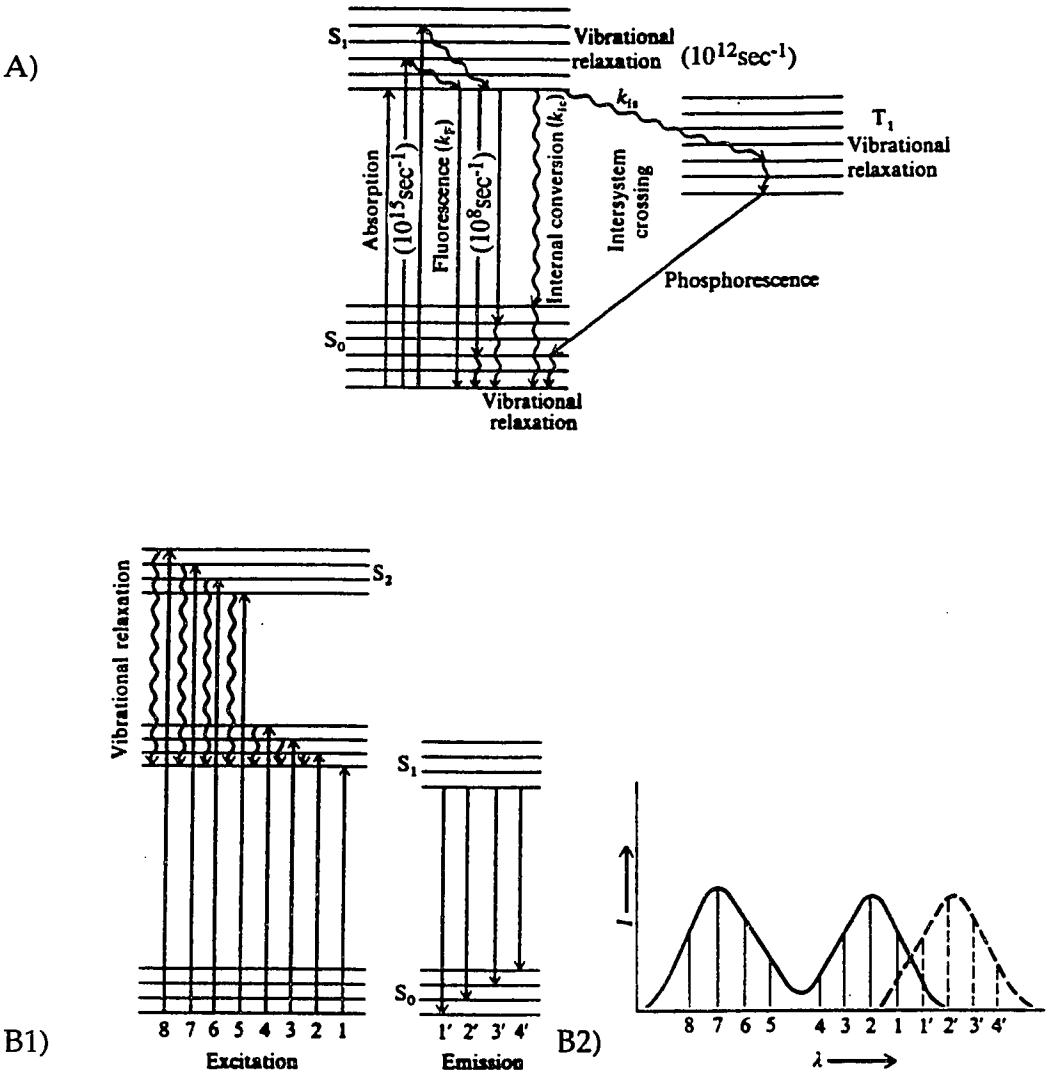

Figure 10 (modification of Cantor and Schimmel, 1980): A) a Jablonski diagram illustrating the phenomena and time scales for excitation and emission of fluorescence. It is also noteworthy that some molecules are capable of undergoing conversion from an excited singlet state to the nominal forbidden excited triplet state wherein phosphorescence occurs. Deexcitation to the ground state can also occur via collisions with other molecules, a process known as quenching; B) demonstration of relation between the electronic and vibrational energy states (B1) of fluorophores and their absorption/emission spectral properties (B2); see text for explanation.

phore can occur during the excited state lifetime and can lead to deexcitation as described in the last section of this chapter.

STEADY-STATE FLUORESCENCE

Steady-state polarization measurements were done with an SLM-8000 fluorometer (see Figure 11A) where the excitation source is either a xenon arc lamp or a Spectra-physics 2025 argon-ion laser (only for pressure studies discussed later).

Emission spectra, corrected for photomultiplier tube and emission monochromator wavelength biases, were obtained on an ISS K2 instrument (Urbana, IL) by using parallel polarized excitation light and adding parallel polarized emission to twice the perpendicular emission (effectively abolishing any polarization biases) and therefore obtaining the total emission. For emission spectra, the optical density of the samples was usually kept at ~0.1 or less to abolish any significant inner-filter effects (inner-filter effects refer to the fact that absorption of an appreciable amount of exciting light by the sample may reduce the observed fluorescence since the fluorometer optics usually focus on the center of the cuvette and the exciting beam is attenuated as it traverses the cuvette; see Jameson, 1984).

Polarized emission subsequent to excitation with light plane polarized parallel to the vertical laboratory axis can be defined by the equation (Perrin, 1926)

$$P = (I_{\parallel} - I_{\perp}) / (I_{\parallel} + I_{\perp}) \qquad (2)$$

where $I_{\parallel}$ is the light emitted parallel to the laboratory vertical axis and $I_{\perp}$ is the light emitted perpendicular to the laboratory vertical axis (see Figure 11B). Furthermore (Weber, 1966):

$$P = [(3/2)\cos^2\theta - (1/2)] / [(1/2) + (\cos^2\theta/2)] \qquad (3)$$

where θ is the angle made between the excitation and emission vector. Steady-state polarization is therefore a measure of the average angle $\cos^2\theta$ through which the fluorophore or probe rotates during its excited-state

(fluorescence) lifetime (see Equation 3; Fig. 11B). The limits for positive and negative polarizations (P_0) of any fluorophore (i.e., no rotation during the molecule's excited-state lifetime; also, the depolarization resulting simply from the molecule's intrinsic electronic transition dipole resulting from the absorption of specific electromagnetic waves) are calculated to be +1/2 and -1/3, respectively (see Weber, 1966 and next chapter for more details). Apparent polarizations greater than the limiting polarization can only be observed when at least some of the light is simply scattered ($\theta = 0°$ and $P = 1$) and then passes through the emission cut-on filter.

Quite often the term fluorescence anisotropy (r) is used in the literature rather than fluorescence polarization. The anisotropy of fluorescence is calculated by simply multiplying the perpendicular component in the denominator of Equation (2) by two. Polarization values can be readily converted to anisotropy as $r = 2P/(3-P)$ or $P = 3r/(2 + r)$. The primary reason for using anisotropy rather than polarization is that the former simplifies the derived mathematical expressions for complex cases in which multiple rotational modes exist (although both contain identical information). In the case of multiple rotations:

$$r = \sum_i f_i r_i \qquad (4)$$

where f_i and r_i are the fractional emission contribution and the emission anisotropy for the *i* th species, respectively. Similarly, the additivity of polarization has the form (Weber, 1952):

$$(1/P - 1/3)^{-1} = \sum f_i (1/P_i - 1/3)^{-1} \qquad (5)$$

thus, $1/P - 1/3$ is the harmonic mean of the individual polarizations, P_i, weighted according to their fractional contributions to the total fluorescence intensity.

According to the theory developed by Perrin (1926;1934;1936) the partial

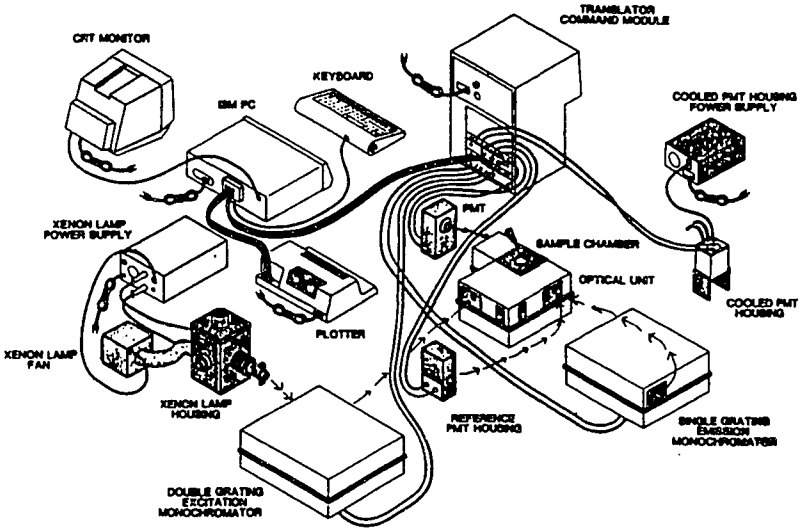

A)

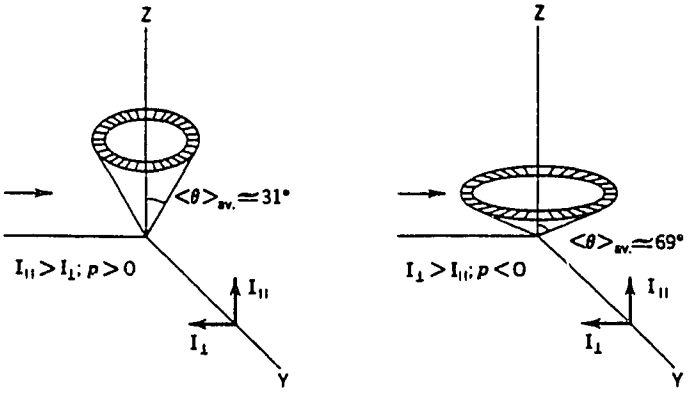

B1) B2)

Figure 11: A) SLM-8000 instrument (Urbana, IL) used for steady-state fluorescence measurements; emission/excitation spectra are taken through left PMT and polarization measurements through the right PMT; polarizers are calcite prisms; B) Schematic of the concept of steady-state polarization, demonstrating the origin of positive (B1) and negative (B2) polarizations (taken from Weber, 1966; see text and Eqn. 3 for details).

polarization of the emission associated with spherical molecules is dependent upon the relation of their rotational relaxation time to the excited state (fluorescence) lifetime:

$$1/P - 1/3 = (1/P_0 - 1/3)(1 + 3\tau/\rho) \quad (6)$$

where P is the observed polarization, P_0 is the intrinsic polarization (highest possible polarization at a *given wavelength*, i.e., a measure of the dipole reorientation during the excited-state), τ is the lifetime of the excited state, and ρ is the harmonic mean of the rotational *relaxation time* of the fluorophore (the time taken to rotate in a fixed direction through an angle equal to arccos $e^{-1} = 68°$). The rotational relaxation time is often confused with the rotational *correlation* time (ambiguously symbolized in literature as τ_c, σ, or ϕ) which is simply one-third the magnitude of the former. For a spherical molecule the rotational relaxation time is described by the Stokes-Einstein relation of diffusion:

$$\rho = 3\eta V/RT \quad (7)$$

where η is the viscosity of the medium (in centipoise,cP), V is the hydrated molecular volume monitored by the probe (vide infra), and T is the absolute temperature (K). The hydrated molecular volume, V, is equal to the molecular weight monitored by the probe times the sum of the specific volume (in units of ml/g; this term can be calculated from amino acid composition in proteins; see Cohn and Edsall, 1943) and the hydration state (Kuntz, 1971; ranging from 0.2-0.4 ml H_2O/g protein). ρ is therefore (in nanoseconds; ns), in the case of a rigid spherical rotator roughly equal to its molecular weight divided by ~700-950 dependent on the degree of hydration (see Chapter 4). Furthermore, ρ is inversely proportional to twice the *rotational* diffusion coefficient, D, for a simple isotropic, spherical rotator. Equations 6 and 7 were later expanded to account for ellipsoidal rotations

(Weber, 1952) and more recently for flexible or hinge motions (see Chapter 4, for extensive details), both of which exhibit conspicuous deviations from Equations (6) and (7).

Since a typical fluorophore has an average excited state lifetime of about 10 ns and a rotational relaxation time in buffer on the order of 0.2 ns, it is easy to understand that its emission should be almost completely depolarized. When the same 10 ns lifetime fluorophore is attached to a spherical 24 kD protein, we would expect a ρ of 30-36 ns at 20°C (from equation 6) and hence, a much higher polarization (closer to P_0). The greatest uncertainty of Equation (6) is the degree of hydration, which is discussed in detail in Chapter 4.

One must remember from the Chapter One subsection on protein dynamics that macromolecules possess a hierarchy of motions which can further lead to depolarization of emission and hence, P_0 is rarely reached in practice. Depolarization of a particular fluorophore attached to a macromolecule is therefore not only due to overall or "global" rotational motion of the targeted macromolecule but quite often additionally due to motions "local" to the reporting fluorophore. "Local" motions can be attributed to all motions *excluding* the "global" rotation expected of a rigid body to which it is attached (Jameson and Sawyer, 1993). These so-called "local" motions (see Table 1 in previous chapter) can therefore be attributed to internal domain motions as well as rapid motion around the point of attachment of the probe or the amino acid side chain. The use of non-covalent probes, which associate simultaneously at multiple contact points on a macromolecule (and therefore possess negligible rapid local motion), tend to weigh more the global or domain motions of a protein. Conversely, covalent probes (and intrinsic fluorophores such as tryptophan or tyrosine), attached by a single bond, can

rotate as fast as the amino acid side chain to which they are attached (recall Table 1; see also Gratton et al, 1986A). The use of non-covalent probes therefore allows the spectroscopist to directly monitor protein tertiary and quaternary structure and dynamics without the interference of rapid depolarization occurring at a single amino acid side chain. Elucidation of various rotational modalities in a macromolecule (with *either* covalent or non-covalent probes) is greatly enhanced by modern time-resolved fluorescence methods discussed in the next subsection.

The T-format polarization configuration is used for most of our polarization studies and the L-format polarization configuration is used for high-pressure studies. Essentially, the difference between T-format and L-format polarization is that in the former case, the parallel and perpendicular components of the emission are monitored by separate photomultiplier tubes, whereas, in the latter method only one photomultiplier tube is used and the parallel and perpendicular components are monitored sequentially by rotating the emission polarizers (see Figure 11). In both cases emission is taken at right angles from the excitation vector to help further separate exciting light from emitted light. Equation 2 is used in the partial calculation of the polarization values reported in this text. Furthermore, a g-factor (originally shorthand for grating factor) is calculated from the emission obtained via perpendicular excitation light to account for any biases in the PMT (s) response to parallel or perpendicular polarized light. Emitted light is separated from exciting light via the use of cut-on filters which allow transmission starting at a wavelength red-shifted from that of the excitation as exciting light is purely parallel polarized and would interfere with the true polarization (remember, perpendicular exciting light only used for g-factor calculation).

Finally, high-pressure steady-state polarization measurements were obtained via the use of a high-pressure bomb made of Vasconax 300 (Teledyne Vasco Company, Chicago, IL) with windows made of fused quartz (details are given in Paladini and Weber, 1981A). Correction factors, to account for the birefringency of the windows induced upon pressurization, were obtained by the use of fluorescein in 95% glycerol at 0°C (at the P_0 where no depolarization can occur unless birefringency occurs) and using the equation deduced by Paladini and Weber for an L-format optical configuration:

$$p_L' = P(1-3\alpha)/(1-P\alpha) \qquad (8)$$

where p_L' is the apparent polarization, P is the true polarization, and α is the birefringency correction factor (further details are given in Chapter 5).

TIME-RESOLVED FLUORESCENCE

Time-resolved fluorescence is a method used for the determination of various excited state decay times (lifetimes) as well as the elucidation and distinction of the various rotational relaxation time components (dynamic polarization) of a fluorescent molecule. The two most common methods for acquiring time-resolved fluorescence data are: 1) the pulse method in which the sample is illuminated by a repetitive pulse of exciting light and the fluorescence decay is monitored; and 2) the harmonic multi-frequency phase and modulation method (Spencer and Weber, 1969), which is used in these studies and described below (instrument shown in Figure 12).

Lifetime and dynamic polarization measurements were accomplished with an ISS multifrequency phase and modulation cross-correlation fluorometer (from ISS in Urbana, IL) based on the Gratton design (Spencer and Weber, 1969; Gratton and Limkeman, 1983) (see Figure 12). Excitation is obtained with a Spectra Physics 2045 argon ion laser (vide infra); specific wavelengths in the mid-UV (337nm-364nm) and the visible (457nm-528nm)

were selected with a quartz prism. An interference filter was placed in the path of the excitation when in the mid-UV to eliminate plasma glow and other slight contaminating wavelengths.

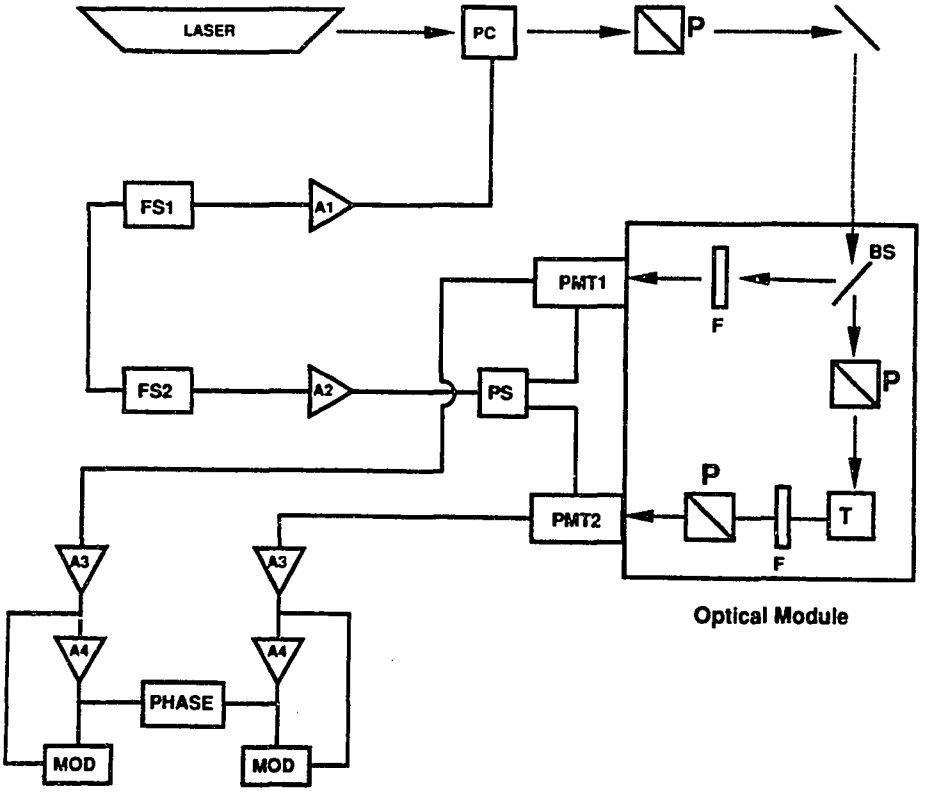

Figure 12: A cross-correlation multifrequency phase and modulation fluorometer based on the Gratton design (see text). Abbreviations are as follows: PC, Pockel's Cell; P, polarizer; BS, beam splitter; F, filters; T, sample turret; PMT, photomultiplier tube; PS, power splitter; A, amplifier; FS, frequency synthesizer; PHASE, phase.

In the multifrequency phase and modulation technique the intensity of the exciting light is modulated continuously and sinusoidally via the use of an electro-optical Pockel's cell. One frequency synthesizer provides the modulated signal to drive the Pockel's cell. A second frequency synthesizer, locked in phase with the first (i.e., same frequency), provides the signal that modulates the photomultiplier tube's response; this synthesizer provides an additional 40 Hz (the cross-correlation frequency) at the last dynode of the

PMTs. This cross-correlation procedure essentially transfers the phase and modulation information to the low frequency (40 Hz) mode (see Spencer and Weber, 1969; Jameson et al, 1984). The phase shift and relative demodulation of the sinusoidally emitted light (taken through the magic angle of 55° which effectively eliminates any polarization biases) are determined with respect to the excitation (monitored using scattered light) or known lifetime standard (Figure 13). Essentially, since frequency is the inverse of time and typical excited-state fluorescence lifetimes range from 1 to 100 ns, the sinusoidally modulated frequencies of excitation usually vary from 1 to 250 Megahertz (Figure 13). The investigator must choose a fluorescent probe that possesses an excited-state lifetime in the range of roughly 1/10 to 10X the time frame of the event being monitored (Valeur, 1991).

Phase and modulation lifetimes at each frequency are calculated using the equations shown (Duchinsky, 1933):

$$\tan [P] = \omega\tau^P \quad (9)$$

$$M = [1 + (\omega\tau^M)^2]^{-1/2} \quad (10)$$

where P is the phase shift, M the relative modulation {the time-dependent components divided by the time-independent components (i.e., AC/DC ratios), of the emission and excitation waveforms; $M = (AC/DC_{em})/(AC/DC_{ex})$} and ω the angular frequency ($\omega = 2\pi f$ where f is the linear modulation frequency set on the synthesizers). The phase shift and relative modulation are always measured relative to a standard fluorophore (or scatterer) of known lifetime. Two independent lifetimes, τ^P and τ^M, are thus obtained. An emitting system characterized by a single exponential decay will yield identical phase and modulation lifetime values irrespective of the modulation frequency. In the case of heterogeneous emitting systems (multiple, non-interacting fluorescent species). The phase lifetime values

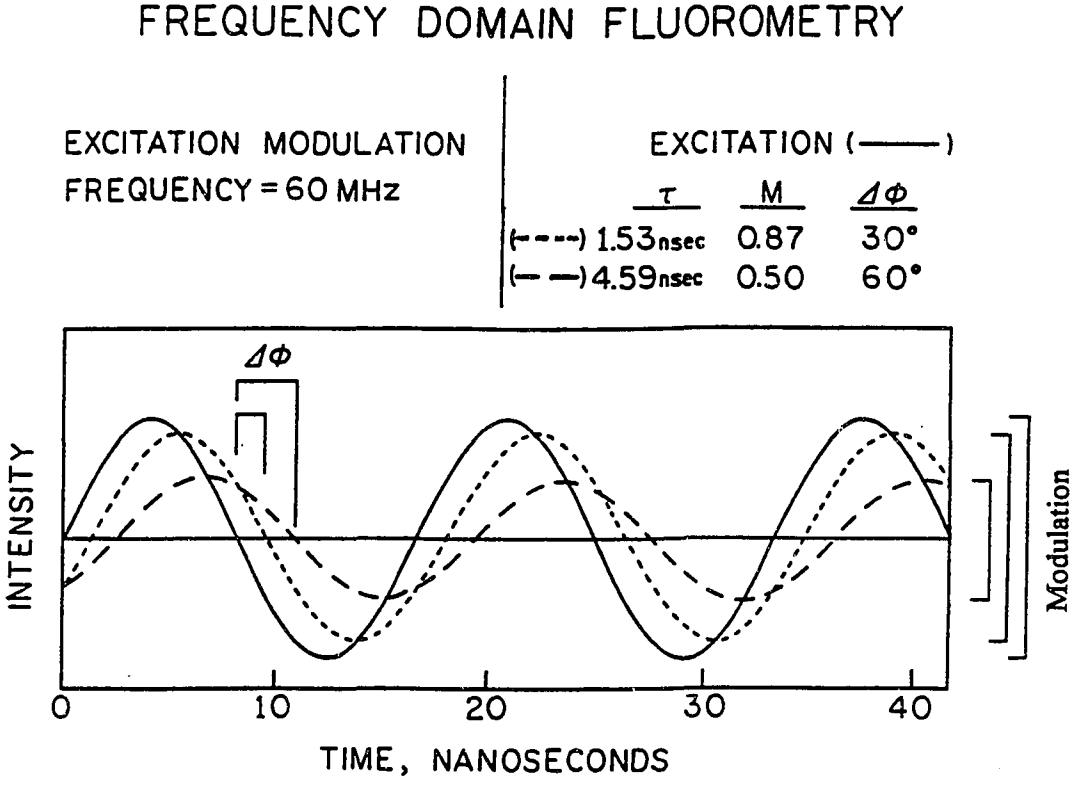

Figure 13: Schematic of the observed phase-lag and demodulation of the emission waveform relative to the excitation waveform. It is important to realize that these waves are the sinusoidal *intensities* of light (y-axis) versus time (x-axis), *not* electromagnetic waves. The shift in phase and demodulation of sinusoidally modulated emission of light relative to sinusoidally modulated exciting light for a hypothetical 4.59 nanosecond excited-state molecule and a hypothetical 1.53 nanosecond excited-state molecule. The DC component is the intensity of the trough of the waves and the AC component is the intensity of the peaks of the waves.

will be less than the modulation lifetime values. These lifetime values will be dependent upon the modulation frequency, specifically decreasing as the modulation frequency increases (Spencer and Weber, 1969). This dependence of the phase and modulation lifetimes on the modulation frequency forms the basis of the methodologies used to characterize the nature and extent of the system's heterogeneity. A simulation of data expected for two different single exponential decay fluorophores as well as one double exponential decay fluorophore is given in Figure 14.

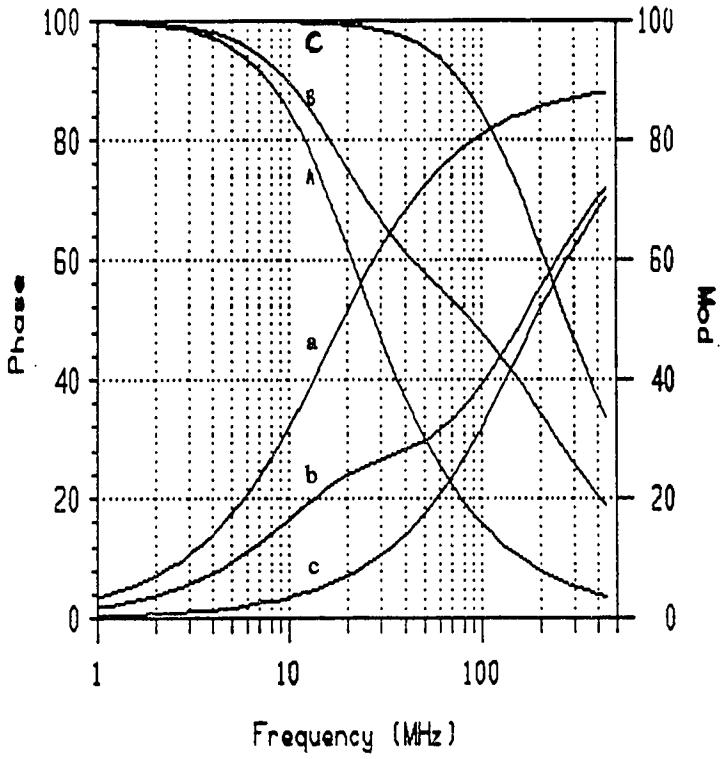

Figure 14: Simulation of phase delay (lower case letters) and % modulation (upper case letters) for a 10 nanosecond lifetime probe (a, A), a 1 nanosecond lifetime probe (b,B), and an equal fractional intensity (f, see text) mixture of a one nanosecond lifetime probe and a 10 nanosecond lifetime probe (c,C).

The measured phase and modulation values may be analyzed as a *sum of exponentials* (or a single exponential) by using a non-linear least squares procedure (Jameson and Gratton, 1983; Gratton et al, 1984A/B; Jameson et al,

1984) wherein the goodness of fit to a particular model (for example, single or multiple exponential lifetimes) is judged by the value of the reduced chi-square (χ^2) as defined by :

$$\chi^2 = \Sigma \{[P_c - P_m / \sigma^P] + [(M_c - M_m) / \sigma^M]\} / (2n-f-1) \quad (11)$$

where the sum is carried over the measured values at n modulation frequencies and f is the number of free parameters. The symbols P and M correspond to the phase shift and relative demodulation values, respectively, while the indices c and m indicate the calculated (*for a particular model*) and measured values, respectively. σ^P and σ^M typically correspond to the standard deviations of each phase (0.2°) and modulation (0.004) measurement, respectively. These standard error values are chosen as default values and are based on accumulated personal experience on the instrument performance. An example of good and bad fits between measured and calculated (described in next paragraph) phase and modulation data are shown in Figure 15.

The *calculated* values of phase and modulation used for modeling are obtained using the equations (Weber, 1981):

$$P = \tan^{-1}[S(\omega)/G(\omega)] \quad (12)$$

$$M^2 = S(\omega)^2 + G(\omega)^2 \quad (13)$$

where the functions $S(\omega)$ and $G(\omega)$ have different expressions depending on the fitting model utilized.

For the fit using a sum of exponentials, the functions $S(\omega)$ and $G(\omega)$ are given by:

$$S(\omega) = \Sigma f_i \omega\tau_i / (1+\omega^2\tau_i^2) \quad (14)$$

$$G(\omega) = \Sigma f_i / (1+\omega^2\tau_i^2) \quad (15)$$

$$\Sigma f_i = 1 \quad (16)$$

where the index i depends on the number of exponentials used for the fit; f_i is the contribution to the steady-state fluorescence intensity of the ith

component; τ_i is its lifetime and ω is the angular frequency of light modulation.

The discrete exponential analysis in the frequency domain method has been fine-tuned over the last decade and a more recent, and still evolving

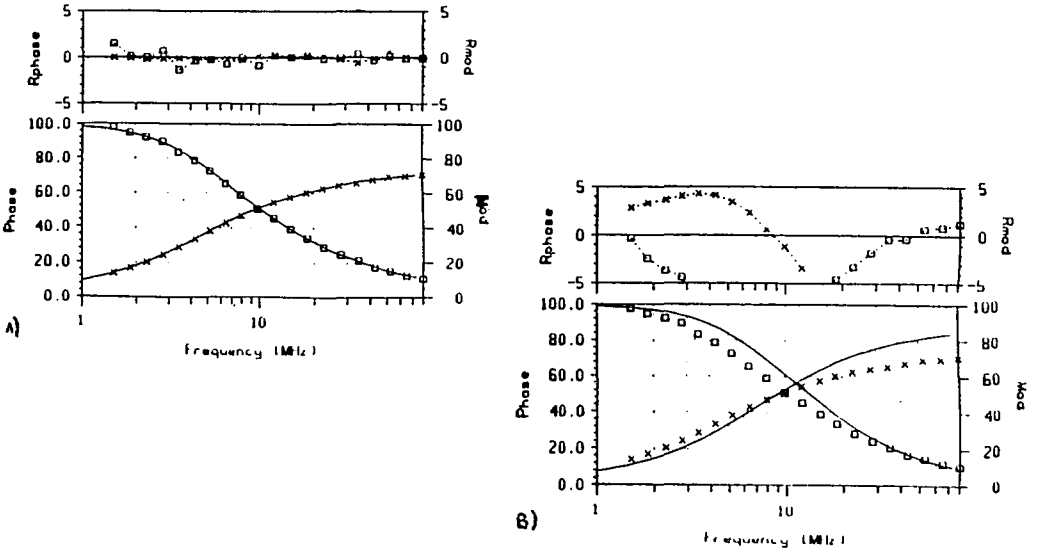

Figure 15: Good (A, $\chi^2 = 0.9$) and bad (B, $\chi^2 = 309$) fits for respectively, a three-component or one component excited-state decay. Hollow squares and x's respectively, represent modulation and phase. Taken from early data on a dansylated (Dansyl-Cl is similar in structure and properties as IAEDANS, shown in Fig. 9 earlier) wild type L7/L12 with three component lifetimes of 31.8 (f=0.82), 8.8 (f=0.16), or 1.6 (f=0.02) ns.

analytical method for handling time-resolved fluorescence data is the continuous distribution approach (for more details see Alcala et al, 1987). For the fit using a continuous distribution of lifetime values, $S(\omega)$ and $G(\omega)$ functions are given by:

$$S(\omega) = \int f(\tau)\omega\tau/(1 + \omega^2\tau_i^2)d\tau \quad (17)$$

$$G(\omega) = \int f(\tau)/(1 + \omega^2\tau_i^2)d\tau \quad (18)$$

$$\int f(\tau) = 1 \quad (19)$$

where $f(\tau)$ is an appropriation function. The choice of function (i.e., Lorentzian, Gaussian, etc.) will depend upon the particular system being examined, but in the case of most fluorescent biomolecules studies to date the Lorentzian function has proved useful (Alcala et al, 1985; 1987). In the case of a Lorentzian distribution, the function, $f(\tau)$, utilized is:

$$f(\tau) = A/[1 + 4(\tau - \tau_0)^2/W^2] \qquad (20)$$

where A is determined by the normalization condition, τ_0 is the center of the Lorentzian, and W is its full width at half maximum.

In addition to fluorescence lifetime determinations, the multi-frequency phase and modulation method permits characterization of the rotational modes of fluorophores (i.e., Lakowicz et al, 1985; Jameson and Hazlett, 1991; present study) and this method is known as differential phase fluorometry (also known as dynamic polarization). As seen in equation 6, the steady-state polarization allows us to calculate a *mean* harmonic rotational relaxation time. On the contrary, the time-resolved dynamic polarization method allows us to directly distinguish the*various* rotational relaxation times without variation of solvent viscosity.

In dynamic polarization measurements, the sample is illuminated by light polarized parallel to the vertical laboratory axis with intensity modulated at variable frequencies. Similar to lifetime measurements, low and high frequencies differentially weigh slow and fast rotational modes. The measured difference in phase delay, $\Delta\phi$, between the perpendicular and parallel components (phase delay of perpendicular minus that of parallel) of the emission can then be directly determined and for a *single, spherical rotator* the values of $\Delta\phi$ can be related to the rotational parameters by the expression (Weber, 1977):

$$\Delta\phi = \arctan \left[(18\omega r_0 R) / (k^2 + \omega^2)(1 + r_0 - 2r_0^2) + 6R(6R+2k+kr_0) \right] \quad (21)$$

where ω is the angular modulation frequency, r_0 the intrinsic anisotropy, k, the radiative rate constant ($1/\tau$) and R, the rotational diffusion coefficient (*R is usually replaced in most literature by the symbol D*). One also obtains the modulation ratio (Y) of the AC components of the perpendicular and parallel signals (perpendicular modulated amplitude divided by parallel) which, for the single spherical rotator case described above, is related by the expression (Weber, 1977):

$$Y^2 = \left[(1-r_0)k+6R \right]^2 + (1-r_0)^2\omega^2 \right] / \left[(1+2r_0)k+6R \right] + (1+2r_0)^2\omega^2 \quad (22)$$

Equations 21 and 22 are therefore time-resolved versions of the Perrin Equation (6). As is the case with the lifetime data, rotational data usually do not fit well to a simple single exponential spherical rotator as proteins for example, possess an array of motions (recall Table 1, Chapter 1). The results are therefore normally analyzed with multi-exponential rotational models. The goodness of fit between measured and calculated differential phase and modulation values is judged by a reduced χ^2 similar in form to Equation 11. Multi-exponential rotations are described by the following time-domain equation (similar to the steady-state Equation 4):

$$r(t) = r_0 \Sigma\, \alpha_i e^{-t/\tau ci} \quad (23)$$

where r(t) is the anisotropy at time t, r_0 is the limiting anisotropy, α_i is the pre-exponential factor of the i^{th} component (associated fractional amplitude of the particular rotating component), and τ_{ci} is the rotational correlation time of the i^{th} component (recall that τ_c equals $\rho/3$). A Fourier transformation converts Equation 23 into one suitable for analysis of frequency-domain data.

Further details on the analysis of the multifrequency phase and modulation data are given elsewhere as well as in the next chapter of the present text (Weber, 1977; Gratton et al, 1984A/B; Jameson and Hazlett, 1991). A simulation of dynamic polarization data expected for a 4 nanosecond lifetime fluorophore free or bound to a typical 25 kD protein is shown in Figure 16.

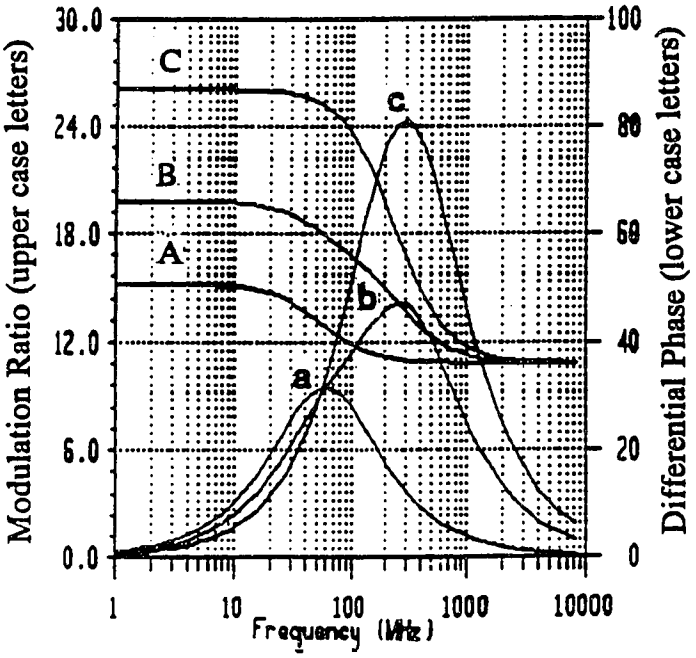

Figure 16: Dynamic polarization data for a 4.05 ns lifetime probe such as fluorescein. a) Fluorescein bound to 24 kD (30 nanosecond global ρ) protein with no local motion; b) fluorescein bound to 24 kD protein with 50% anisotropy decay attributed to ~1.2 ns local ρ motion; c) free fluorescein with 0.5 nanosecond ρ. *Note how the modulation ratios converge in all cases at very high frequencies; this point of convergence is essentially related to the r_0 by one minus the modulation ratio divided by one plus the modulation ratio; hence, the r_0 here is 0.370.*

Finally, Dr. Gratton (personal communication, 1993; Laboratory of Fluorescence Dynamics, University of Illinois, Urbana) recently developed a method that allows a distributional analysis of dynamic polarization data similar in form to that described above for lifetime data (Equations 17-19).

The software used for the analysis of lifetime and rotational data in the present study was obtained from ISS (Urbana, IL) and Globals Unlimited (Beechem et al, 1986, 1988, 1991,1992; from the Laboratory of Fluorescence Dynamics, Urbana, IL). The details of their individual uses are given in subsequent chapters.

NON-RADIATIVE FLUORESCENCE RESONANCE ENERGY TRANSFER (FRET)

The first observation of non-radiative fluorescence resonance energy transfer was made by Cario and Franck (1922) who studied a mixture of mercury and thallium atoms in the vapor phase, which, when irradiated with the light of a mercury resonance line, displayed emission characteristic of both atoms. Since thallium atoms do not absorb at the mercury excitation wavelength and trivial radiative reabsorption of mercury emission by thallium in the vapor phase was impossible, they concluded this transfer of energy from the *donor* atom mercury to the *acceptor* atom thallium must be non-radiative.

J. Perrin (1927) used classical physics and was followed by his son F. Perrin (1932) who used quantum-mechanics to explain the phenomenon but the modernly accepted explanation of resonance energy transfer was not fully derived until Förster (1946;1951). Förster explained this phenomenon as a transfer of resonance energy occurring from a donor molecule when an electron in its highest vibronic band of its first electronic excited state (see Figure 10) falls to the lowest vibronic band of its first electronic excited state (also known as thermal relaxation) simultaneously exciting the acceptor only if the energy difference occurring when dropping from the highest to lowest vibronic bands corresponds exactly to that necessary for excitation of the acceptor molecule.

The equations used for calculating distances between two fluorophores using the steady-state emission intensities method are as follows (Förster, 1967):

$$E = 1 - [F_{da} - F_d(1-f_a)f_d / F_d] \quad (24)$$

where E is the efficiency of energy transfer, F_d is the fluorescence intensity of the donor, F_{da} is the intensity of the donor in the presence of the acceptor, f_d is the fraction of donor molecules, and f_a is the fraction of acceptor molecules. E can then be used to calculate the distance between the two fluorophores (Förster, 1946; 1948):

$$E = R_0^6 / (R_0^6 + R^6) \quad (25)$$

where R_0 is the critical transfer distance between the two fluorophores (where 50% of excitation energy is transferred) and R is the measured distance between the two fluorophores. R_0 is calculated from the following fundamental parameters of resonance energy transfer (not to be confused with r_0, the limiting anisotropy):

$$R_0 = 9.78 \times 10^3 (n^{-4} Q \kappa^2 J)^{1/6} \text{Å} \quad (26)$$

where n is the refractive index (taken usually as 1.4), Q is the quantum yield of the donor, κ^2 is the orientation factor (of the donor/acceptor fluorophore) which takes on values between 0-4 (and is therefore the most ambiguous parameter of the equation; it arguably can be calculated from the steady-state polarizations of the donor and acceptor), and J is the overlap integral between donor emission and acceptor absorption given in $M^{-1}cm^3$ and is calculated as follows (Förster, 1946):

$$J = \Sigma F_d(\lambda)\varepsilon_a(\lambda)\lambda^4\Delta\lambda / \Sigma F_d(\lambda)\Delta\lambda \quad (27)$$

where $F_d(\lambda)$ is the fluorescence intensity of the donor expressed in an arbitrary unit, $\varepsilon_a(\lambda)$ is the extinction coefficient of the acceptor expressed in $M^{-1}cm^{-1}$. In our calculations, the summation was taken over 5 nm intervals ($\Delta\lambda$ = 5 nm)

and wavelengths were of course only those existing within the overlap region (between the donor emission and acceptor absorption). Emission spectra were essentially corrected for any polarization biases of the PMTs.

Extinction coefficients for fluorophores bound to L7/L12 were determined as follows: 1) The extinction coefficient of the fluorophore bound to its specific amino acid is compared to that of the fluorophore known to exist in a specific medium; 2) the extinction coefficient of the fluorophore bound to L7/L12 is then compared to that in which the protein is denatured in 6M guanidine-HCl. The extinction coefficient of the fluorophore bound to to the denatured protein should therefore be nearly identical to that of the fluorophore bound to the amino acid.

Quantum yields were determined for a given optical density of IAEDANS by comparing its total emission (correcting for polarization biases) to that of an identical concentration of quinine sulfate in 0.1 N sulfuric acid (where quantum yield for quinine sulfate is 0.60, Weber and Teale, 1970). Similarly, the quantum yield of the various fluorescein conjugates was determined in comparison to free fluorescein in 0.1 N sodium hydroxide (where quantum yield for free fluorescein is 0.92, Weber and Teale, 1957).

The κ^2 term is defined by the equation (Förster, 1946; see Dale et al, 1979; described in further detail in subsequent chapters):

$$\kappa^2 = (\cos\theta_T - 3\cos\theta_d \cos\theta_a)^2 \qquad (28)$$

where θ_T is the angle between the emission dipole of the donor and the absorption dipole of the acceptor, θ_d and θ_a are the angles between the vector joining the donor and acceptor and the emission and absorption dipoles, respectively. κ^2 is usually taken to be 2/3 assuming that the fluorophore dipoles sample all orientations during the interval of the excited state (i.e., isotropic) but putatively more accurate methods for determining this value

using the fluorophores polarization values at the exciting wavelength are available (Dale and Eisenger, 1974; Haas et al, 1978; see Chapter 5). The maximum value of 4.0 for κ^2 is obtained when the donor and acceptor dipoles are perfectly aligned. Dale et al (1979) later, however, published a paper demonstrating that only upper and lower limits of the κ^2 can be obtained due to the fast motions of the local probe regions as well as the dynamics of the macromolecules to which they were attached (for a more recent discussion see Wu and Brand, 1992 and references therein). Therefore, unless indicated otherwise, we have used 2/3 as the value for κ^2 (see Chapter 6 for more details).

Finally, since macromolecules are in fact dynamic we used the time-resolved method as our quantitative energy transfer determination method since this method allows determination of distance distributions (see Lakowicz et al, 1988; Cheung et al, 1991; James et al, 1992; Wu and Brand, 1992). The equations used for the determination of energy transfer via time-resolved methods are very similar to the steady-state method given in Equation (23) in that emission intensities are directly dependent on the excited-state lifetimes; hence, emission intensities are simply substituted by lifetimes (see Chapter 5 for more details). Furthermore, the time-resolved method is superior in that its quantitative data are not susceptible to photobleaching, slight shifts in the orientation of the cuvettes subsequent to mixing (!), trivial reabsorptions due to emission inner-filter effects, or finally, inherent ambiguities in the analysis of spectral changes (see Chapter 6).

Energy transfer also occurs between identical fluorophores with appropriate spectral overlap (Förster,1948; Weber, 1954), which results in a depolarized emission. This phenomenon results when an acceptor molecule's emission oscillator is oriented at an additional angle (to θ) relative

to that of the donor molecule's emission oscillator (Weber 1954; 1966). Dr. Weber has previously calculated distances between two identical fluorophores by their steady-state polarization; since this calculation is esoteric and still novel (even after 27 years) we present it in detail in Chapter 6.

Energy transfer distances can also be calculated from changes in rotational relaxation times using the steady-state polarization method (Weber and Anderson, 1969) or the time-resolved pulse method (Weber, 1989A; Burten-Bastiaens, 1992) and we approach this concept with the multifrequency phase and modulation time-resolved method in subsequent chapters.

CHAPTER 4:
PROBING THE CONFORMATIONAL AND ROTATIONAL HYDRODYNAMICS OF RIBOSOMAL PROTEIN L7/L12

INTRODUCTION

L7/L12 function is apparently dependent on its ability to flex and extend. Evidence from fluorescence studies, crosslinking, and immune electron microscopy indicates that one dimer is extended away from the ribosome body forming the stalk while the other flexes inward interacting with elongation factors and promoting poly-phenylalanine synthesis (Chapter 1, Figure 6B; see also, Girshovich et al, 1981). The Traut, Kirsebom, and Gudkov groups have all demonstrated that L7/L12 flexibility and function are dependent on the hinge region where mutations and deletions result in loss of poly-phenylalanine activity as well as erroneous proofreading. Bushuev and co-workers (1989) directly showed by proton NMR that the sharp resonance peaks of L7/L12 indicative of its flexibility disappeared when the hinge was mutated or deleted, clearly demonstrating the correlation between L7/L12 flexibility and function.

Evidence for the elongated structure of L7/L12 comes from analytical ultracentrifugation, translational diffusion, viscometry, and low-angle x-ray scattering studies (recall Chapter 1, pg. 7) which all described L7/L12 as a highly elongated *rigid rod* (see Table 2). However, the Österberg x-ray scattering group later, after apparently more sophisticated analysis, published data which suggested that L7/L12 possesses a distribution of conformations (in Möller and Maassen, 1986) although very little discussion of the data

analysis was given. The possibility of a stable, antiparallel, and unstaggered tetramer of L7/L12 also suggests a lack of mobility (recall Chapter 1, Figure 4C).

Obviously, some ambiguity exists in the literature on the conformational and rotational hydrodynamics of L7/L12 (see Table 2). A more technical discussion of the various symbols in Table 2 is presented later in the chapter (see pgs. 138-141). In this chapter elucidation of the following questions are sought: Is L7/L12 a highly elongated rigid rod or does it possess an array of conformational and rotational modalities? Is L7/L12 flexibility, if any, in fact dependent on the putative flexible hinge region? Do the C-terminal domains interact and rotate dimerically (as a single unit) as present models suggest or is it possible that they rotate independent of one another? Is L7/L12 flexibility, if any, best described by a hinge, swivel, or wobble, model? What are the angular limits of the putative rotational mobility? Answers to these questions should provide valuable insight on the details of the molecular mechanism of L7/L12 in protein biosynthesis.

The primary technique used in our laboratory for studying the hydrodynamics of macromolecules is fluorescence spectroscopy. Dr. Gregorio Weber and colleagues was the first to study hydrodynamic aspects of proteins using fluorescence spectroscopy in the early 1950's primarily on the rather ellipsoid-shaped and monomeric bovine serum albumin proteins (see Weber 1952 and 1953). Weber and colleagues (vide infra) subsequently derived the equations for correlating polarized emission to ellipsoidal rotations (vide infra) expanding the earlier work of Perrin (recall that the Perrin Equation (3) correlates polarized emission to strictly spherical rotators). More recently, steady-state and time-resolved fluorescence polarization methods have been

Table 2: A Summary of L7/L12 Hydrodynamics Results Prior to the Present Study*

Case & Method	f/f_0	v	δ	S	D	R_G	Axial Ratios	Comments
A (1974)	2.0	0.735	0.26	1.4	5.59	37.0	130x17.3	rod
B (1976)	–	0.729	0.28	–	–	41.0	180x32x12	rigid rod
C (1979)	1.8	0.753	–	1.6	–	–	190x30x10	rigid rod
D (1981)	1.6	0.755	–	–	–	27.0[a]	–	–
E (1986; 1987; 1993)	–	–	–	–	–	–	variable	flexible, dynamic
F (1989)	1.7	0.755 0.770	0.55	3.0	5.40	36.4	100x53	oblate, rigid tetramer
G (1993)	–	0.755	0.45	–	–	–	–	–

* In all cases except (F), measurements were done on putatively dimeric L7/L12. [a] Stokes radii. Description of symbols and units: f/f_0 is the frictional coefficient ratio of that measured for L7/L12 (f) to that expected for a sphere (f_0); v is the partial specific volume in ml/g; δ is the degree of hydration of L7/L12 in g/g; S is the sedimentation coefficient at 20°C x 10^{-13} /sec; D is the translational diffusion coefficient x10^{-7}cm^2/sec at 20°C; R_G is the Stokes radii of gyration in Å. Case A) All values except δ and R_G, which were calculated from low-angle x-ray scattering, were calculated from sedimentation velocity and diffusion methods (Wong and Paradies, 1974); Case B) all values except v, which was calculated from densitometry, were calculated from low-angle x-ray scattering data (Österberg et al, 1976); Case C) All values except v, which was calculated from amino acid composition, were calculated from sedimentation velocity data (Luer and Wong, 1979); Case D) Stokes radii were calculated from partition coefficients in gel chromatography; other values calculated from sedimentation velocity (Kar and Aune, 1981); Case E) Rotational flexibility as determined from low-angle x-ray scattering (Möller and Maassen, 1986), fluorescence and NMR (Liljas and Gudkov, 1987 and references therein), and zero-length crosslinking (Makarov et al, 1993 and references therein); Case F) S was calculated from sedimentation velocity; D was calculated from photon correlation spectroscopy; was calculated from either amino acid composition or densitometry; the tetramer state was deduced from gel chromatography and sedimentation equilibrium studies; the other values were calculated from low-angle x-ray scattering data (Georgalis et al, 1989). Case G) specific volume and degree of hydration calculated from L7/L12 amino acid composition by methods of Cohn and Edsall (1943) and Kuntz (1971), respectively (vide infra for more details).

successfully used or elucidating important hydrodynamic information on flexible (or hinged) dimeric proteins such as myosin (i.e., Wegener, 1982; Cheung et al, 1983 and references therein), actin (i.e., Tawada et al, 1978), troponin I and C (Wang and Cheung, 1986; Wang et al, 1993), and different immunoglobulins (i.e., Hanson et al, 1985 and references therein; Oi et al, 1984); each of these proteins possess flexibility via a structureless hinge region similar to that of L7/L12 (vide infra for more details). The equations used in the present study for distinguishing ellipsoidal and segmental (i.e., flexible) rotations from simple spherical rotations are presented in detail (vide infra).

All previously published data using fluorescence techniques to characterize L7/L12 have been on the wild type phenotype. The Leiden group (i.e., Möller, Maassen, Thielen, Zantema references mentioned earlier) used tedious chemical modification procedures to label wild type L7/L12 at putatively specific sites. They deduced information on the location of L7/L12 in the strong ribosome-binding site relative to L7/L12 in the weak binding site via fluorescence resonance energy transfer (FRET). In many cases, significant biological activity was lost in the process. Alternatively, the Lee and Cantor group (1981A/B) modified wild type L7/L12 at putative specific sites by simply altering the pH prior to labeling. Their data suggested specific labeling at the C-terminal lysine with IAEDANS at pH 9.4 and semi-specific labeling of an undetermined location with FITC at pH 9.0. Energy transfer experiments were subsequently performed on the ribosome to elucidate any possible interaction or proximity of L7/L12 with tRNA. Due to the simplicity of the labeling procedures Lee and Cantor used, initial experiments were performed in our laboratory with wild type L7/L12 labeled with FITC or IAEDANS.

In the present study, initial time-resolved fluorescence studies indicated that wild type L7/L12, labeled semi-specifically at an N-terminal

serine with FITC (~3.6 ns lifetime) suggested that L7/L12 possesses some segmental (i.e., domain) mobility. After labeling wild type L7/L12 at its' C-terminal lysine with the longer lifetime (~15 ns) probe IAEDANS or at an unknown position with an even longer lifetime probe (~27 ns) 2-dimethylaminonapthalene-5-sulfonyl chloride (Dansyl-Cl, similar in structure to IAEDANS), a rather long rotational relaxation time was observed indicative of a possible ellipsoidal rotation of L7/L12. Difficulties in the interpretation of the data arose due to the lack of available probe-specific sites on L7/L12.

As mentioned in Chapter 2, the Traut laboratory has created several cysteine mutants of L7/L12 via the use of site-directed mutagenesis. Furthermore, the Traut laboratory has created several deletion mutants allowing novel fluorescence investigations on specific fragments of L7/L12 as well as the hinge-deleted mutant mentioned in Chapter 2. In the present work, cysteine mutants were labeled with sulfhydryl-specific probes. Our initial findings, as in the case of wild type L7/L12, suggested segmental mobility within the protein, as the longer lifetime probes monitored a longer rotational relaxation time relative to that monitored by the shorter lifetime probes; the > 100 ns excited-state lifetime of 1-PMIA indicated the existence of highly aggregated form of L7/L12

We later discovered via SE-HPLC chromatography that the longer rotational relaxation times essentially corresponded to a higher aggregate of L7/L12; dimeric L7/L12 rotational relaxation times indicate segmental (domain) mobility, independent of the excited-state lifetimes of the various probes used. More sophisticated time-resolved fluorescence experiments and analysis on hinge-intact L7/L12 and the various deletion mutants (see Figure 7, Chapter 2) verify that the two C-terminal domains and dimeric N-terminal

domain rotate independently. The nature of this L7/L12 segmental global mobility is presented as well. Preliminary hydrodynamic data on ribosome-reconstituted L7/L12 suggest that this independent C-terminal domain mobility persists upon binding .

Data are presented chronologically in this chapter to gradually introduce the reader to the concepts, pitfalls, and potentials of the fluorescence methodologies used for characterizing rotational dynamics of macro-molecules.

INITIAL FLUORESCENCE CHARACTERIZATION WITH FITC: L7/L12 IS *NOT* A HIGHLY ELONGATED RIGID ROD. EVIDENCE FOR SEGMENTAL MOBILITY.

Initial Fluorescence Characterization of Wild Type L7/L12 Labeled with Fluorescein Isothiocyanate (FITC). Since fluorescein isothiocyanate is one of the most thoroughly characterized fluorescence probes known, initial studies of L7/L12 were carried out in our laboratory with this probe. Furthermore, high sensitivity (due to the high extinction coefficient and near unity quantum yield) and an approximate four ns excited-state lifetime made FITC an appropriate probe for studying a 24 kD protein such as L7/L12 (recall, a fluorophore can accurately monitor events of up to ~1/10 or 10x that of its excited-state lifetime). Assuming *dimeric* L7/L12 were *spherical*, possessed a consensus degree of hydration of 0.3 g H_20/g protein, and its partial specific volume of 0.75 ml/g, we could expect a global rotational relaxation time of roughly 31.5 ns at 20°C (from Equation (7) on pg. 54). If the actual global rotational relaxation time of L7/L12 were much greater than 40 ns (i.e., rigid ellipse or tetramer), our analysis procedures could probably resolve it but with less accuracy than if we used a probe with a more appropriate excited-state

lifetime than that of FITC (see Beechem et al, 1986; Hazlett et al, 1989; Gratton et al, 1992; Wang et al, 1993; *vide infra*).

In Table 3 we see the resultant labeling stoichiometry for FITC to wild type L7/L12 under various labeling conditions in the present study and in comparison to results of Lee and Cantor (see 1981A/B). Essentially, in the present study, identical results were obtained for L7-FITC and L12-FITC (data not shown).

Here we report a high dependence of labeling stoichiometry on the conditions used in the labeling reaction. Specificity is highly dependent on the ratio of probe to protein used in the labeling reaction, which is easily

Table 3: Results of labeling wild type L7/L12 with FITC*

Study	Labeling Buffer	Labeling Buffer pH	FITC/ L7/L12[1]	Average S.S.P[2]
Present Study	Borate	8.0	0.1	.235
	"	9.0	0.5[a]	.235
	"	9.0	1.0[b]	.231
	"	9.0	1.4[c]	.224
	"	9.0	5.2[d]	.208
	Carbonate	9.4	1.5	.219
Lee and Cantor (1981)	Borate	9.0	0.6-0.8	?
	Carbonate	9.4	1.3-1.8	?

*Labeling procedures were as described in Chapter 2 Materials and Methods of this dissertation with the exceptions of the alterations indicated. [1]Molar ratios of FITC per subunit of L7/L12--values given are averages of greater than three separate labeling reactions; results of labeling in the presence of molar excess FITC/(L7/L12) as follows: [a]10x; [b]30x; [c]60x; [d]150x; [2]S.S.P. is steady-state polarization at 488nm excitation; given values were calculated averages of greater than three separate labeling reactions and values were obtained at 20°C with Schott 085 emission cut-on filter begins passing significant light red-shifted to 520 nm eliminating any scattering of excitation light.

judged by the resulting polarization of pure FITC-L7/L12 conjugates. Furthermore, as the pH of the labeling buffer is raised, the numbers of reactive amino acids increase (as Lee and Cantor previously reported). Lee

and Cantor claimed that labeling of L7/L12 with 20-40x excess of FITC resulted in ~0.6-0.8 FITCs/L7 monomer and high specificity at an undetermined site; no steady-state polarizations of the resulting free FITC/L7 conjugates were given. Furthermore, most of the original L7/L12 poly-phenylalanine activity remained when L7/L12 was only lightly labeled perhaps suggesting insignificant conformational changes (see next two chapters for more detail).

As seen in Table 3, specificity reaches its maximum when the pH is kept at 9.0 or less, or if the pH is 9.0 and the concentration of FITC present in the labeling buffer is less than 15x greater than that of the L7/L12 monomer concentration. Since polarization is highly sensitive to the environment of the fluorophore (either via a change in lifetime or local dynamic aspects), one can expect very different polarizations from a particular fluorophore bound at different sites (as we shall see throughout the rest of this dissertation). This sensitivity to environment is one possible origin of the change observed in FITC polarization as the ratio of FITC/(L7/L12) is raised as new sites are labeled. It is also possible that the depolarization of FITC emission observed when the number of FITCs bound to L7/L12 increases, is due to fluorescence resonance energy transfer (FRET) (recall chapter 3, page 69). Since fluorescein has such a large extinction coefficient, quantum yield, and spectral overlap (i.e. small Stokes shift) it is very efficient at self-energy transfer (homotransfer) (vide infra). As we see in Figure 17, FRET is one cause for the depolarization of FITC emission when on average more than 0.5 FITCs are bound to L7/L12 and this energy transfer appears primarily via two FITCs bound to the same subunit (*intrasubunit* homotransfer; see next chapter for more details). Conversely, when on average only 0.1 FITCs are bound to L7/L12 (monomers), we observe insignificant energy transfer as expected. The fact that energy transfer still exists when L7/L12 is dissociated

with 8 M urea (see next chapter), indicates that the two fluorophores exhibiting FRET on each subunit are very near in primary structure (since 8 M urea would denature much of the secondary structure). Hence, binding of FITC to wild type L7/L12 appears rather cooperative.

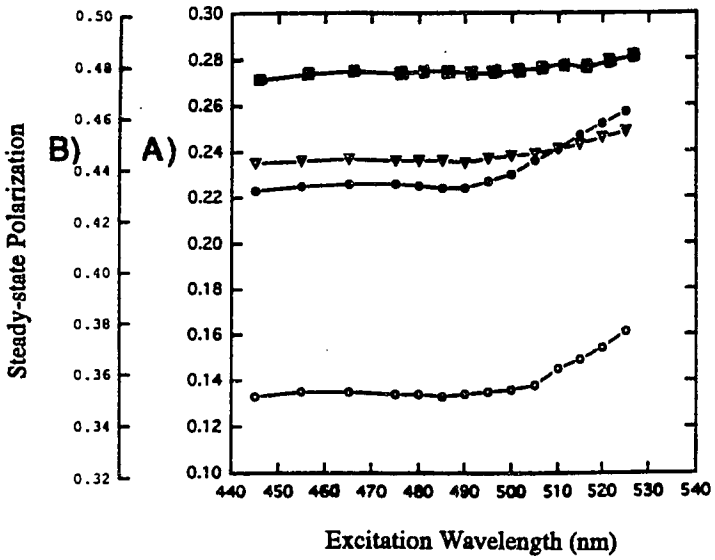

Figure 17: Effects of FRET on the depolarization of FITC emission when bound to wild type L7/L12 at 20°C (with 085 emission filters). In A), hollow triangles represent 0.1 FITC/(L7/L12); filled circles represent 1.2 FITC/(L7/L12); and hollow circles represent 1.2 FITC/(L7/L12) denatured in 4 M Gu-HCl. In B), filled squares represent the actual P_0's of fluorescein in 98% glycerol and 0°C whereby no rotation occurs during the excited-state. Essentially, FRET is increasingly lost at the red-edge of fluorescein's absorption spectra resulting in an increase in polarization (see Weber and Shinitzky, 1970 for more details of concept).

FRET between identical fluorophores located at different sites on a protein can result in significant alterations in the fluorescence lifetime (see Erijman and Weber, 1993) and rotational relaxation time observed (Weber and Anderson, 1969; Anderson and Weber, 1969). A comparison between 0.2 FITC-L7/L12 and 1.2 FITC-L7/L12 is made via time-resolved fluorescence and data is given in Figure 18. We observe fairly insignificant changes in the

fluorescence lifetime but three noticeable changes in the dynamic polarization analysis: 1) the global rotational relaxation time was 4-5 ns shorter in the sample exhibiting FRET and 2) the limiting anisotropy, r_0, was considerably less in the sample exhibiting FRET (0.338 instead of 0.375 as determined in 98% glycerol or 0.365 as in the 0.1 FITC-L7/L12 sample); 3) the fractional emission of the faster ρ (0.45) is proportionally greater than the slower ρ (0.55) in the case in which FRET is occurring; conversely, when FRET is <u>not</u> occurring, the respective fractional emissions are 0.35 and 0.65.

The reduced global rotational relaxation time can be explained via transfer of resonance energy from a donor probe that has an absorption dipole oriented normal to a long (polar) axis of rotation of L7/L12, to an acceptor probe with an absorption dipole oriented parallel to a more equatorial (short, rapidly rotating) axial rotation of L7/L12 (see Weber and Anderson, 1969; Figure 19). The shorter rotational relaxation time observed upon energy transfer may be conceptually explained via an additional "apparent" ρ created via the *rate* of energy transfer (Burten-Bastiaens, 1992). The *rate* of energy transfer, k_T, was first defined by Förster in the 1940's:

$$k_T = (1/\tau_D)(R_0/R)^6 \qquad (29)$$

where τ_D is the excited state lifetime of the donor fluorophore in the absence of any acceptor of resonance energy. In the case of energy transfer between identical fluorophores, assuming no change in lifetime at the red-edge of the absorption spectra (Knopp and Weber, 1969), we can calculate the R_0 from the overlap integral as described in Equation (26) in Chapter 3. The overlap integral was calculated from the absorption and emission spectra of FITC seen in Figure 20 (see Equation 27, page 65). The extinction coefficient of FITC bound to L7/L12 was 65000 $M^{-1}cm^{-1}$ at 488 nm and the quantum yield was

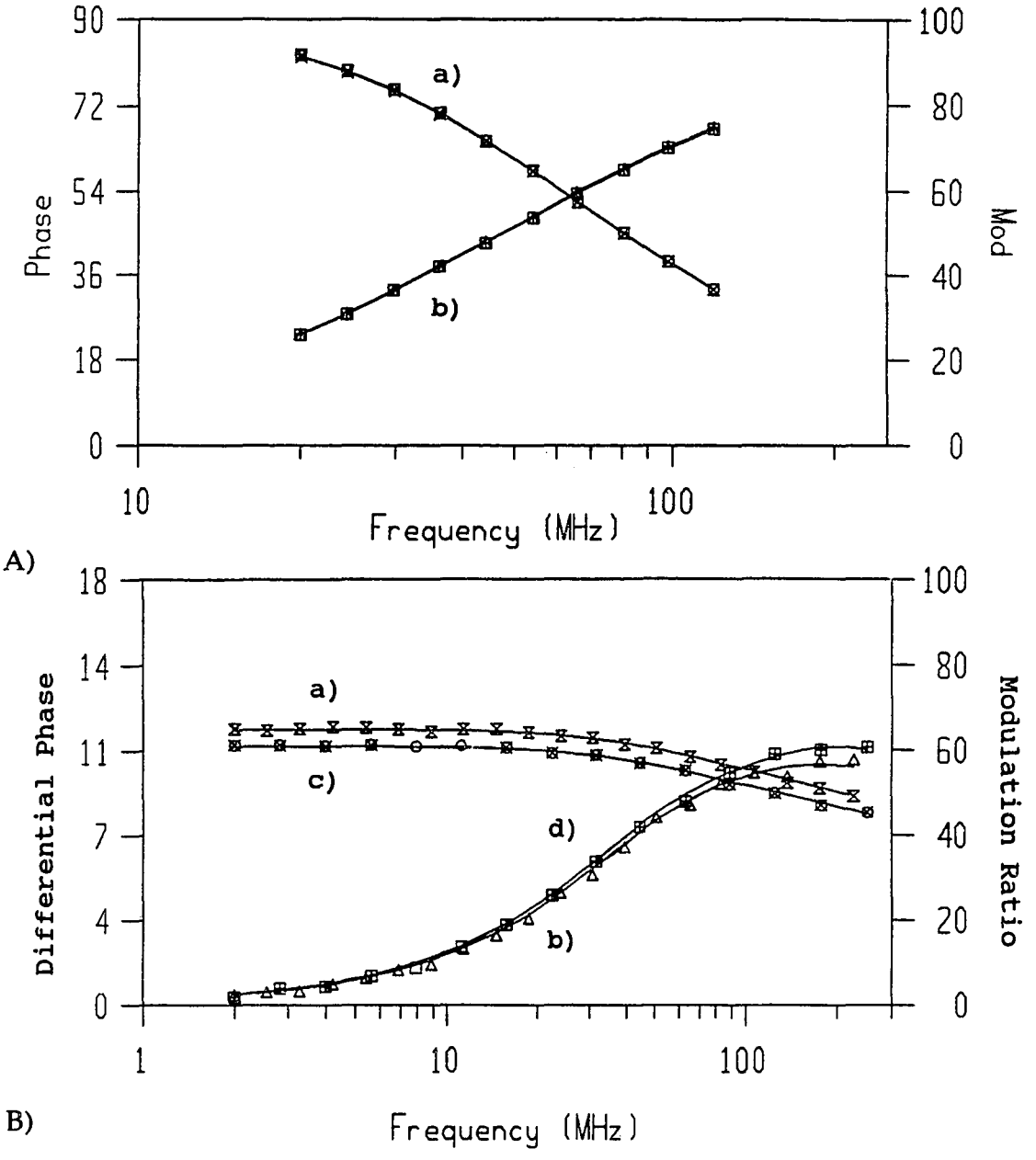

Figure 18: Time-resolved fluorescence data of wild type L7/L12 labeled with 0.1 or 1.2 FITCs per monomeric subunit of L7/L12 at 20°C with an 085 emission filter and 488 nm excitation. A) Lifetime data, where a) represents the demodulation curve and b) represents the phase delay; the lifetimes of each sample were within 50 picoseconds; B) Dynamic polarization data, where a) and b) are respectively, the modulation ratio and differential phase of the 0.1 FITC-L7/L12 sample; c) and d) are respectively, the modulation ratio and differential phase of the 1.2 FITC-L7/L12 sample. Data were from Global linkage analysis of three different preparations of each sample. See text for details of the results of the analyses.

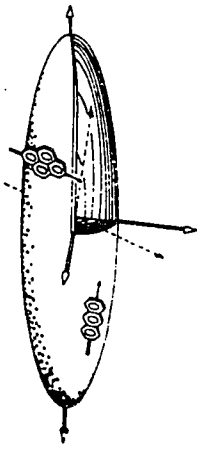

Figure 19: Orientation of FRET donor and acceptor fluorophores parallel to the polar (long) or equatorial (short) rotational axes, respectively, assuming a prolate ellipse for L7/L12 (from Beechem et al, 1986).

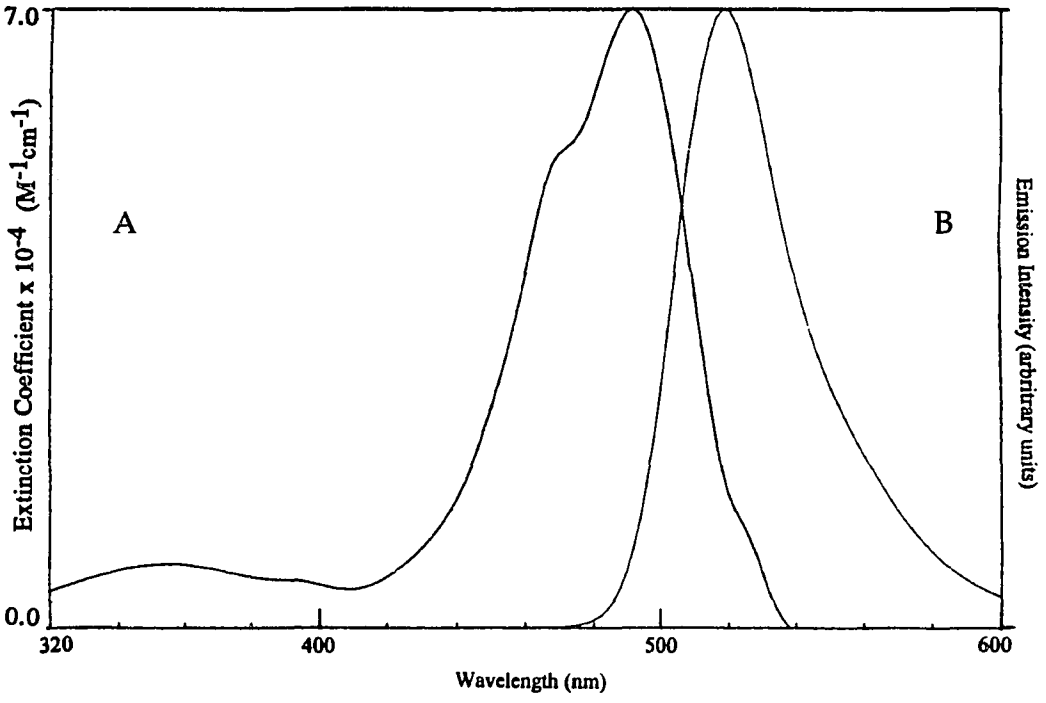

Figure 20: Overlap of 1.0 FITC/(L7/L12) absorption spectra (A) and corrected emission (B) spectra at 20°C. From this overlap, the overlap integral, J, is calculated. Emission was obtained via 488 nm excitation.

determined to be 0.72 (see page 65 for experimental methods). Integration over every five nanometers of the spectra (recall Chapter 3, pg. 66) led to an overlap integral of 3.1×10^{-14} $M^{-1}cm^3$. Substitution of the overlap integral, J, into Equation (27) and assuming a K^2 of 2/3, we find that the R_0 is approximately 40Å. Since the excited-state lifetime (τ_D) is 3.6 ns, we find from Equation (29) that an R of 40Å would result in a k_T of 0.29/ns. Since the rotational *correlation* time, ø, is $1/(2k_T)$ we would expect an *additional rotational relaxation time* (recall ρ equals 3ø) component *created by energy transfer* (let us nominate, ρ_T) of 5.1 ns (Burten-Bastiaens, 1992). If the two fluorophores were 50Å apart, k_T would become 0.097/ns and ρ_T is now 15.5 ns. Since the multifrequency phase and modulation technique is not able to resolve rotational relaxation times that are close together (i.e., when ρ's differ by less than two fold) in time, a ρ_T of 15.5 ns would only reduce the *actual* global rotational relaxation time and might explain the observed differences seen in Fig. 19. The reader should keep in mind that the distances above are average distances (the degree of error is discussed later in this text) of what might be a distribution of distances as described more quantitatively in Chapter 6. Alternatively, one might argue that the reduced global ρ in the samples exhibiting FRET is simply due to a new FITC binding site oriented with a different axis of L7/L12 rotation (as depicted in Figure 19). This latter explanation is supported by the results in Figure 17, as the FITCs undergoing FRET are probably close in primary structure (i.e., the probes undergoing FRET are much less than 40 or 50 Å apart).

What then would explain the missing limiting anisotropy observed in the sample exhibiting energy transfer? Let us assume that the fluorophores exhibiting energy transfer are within 10Å apart (i.e., R = 10Å). We can now easily calculate a k_T and ρ_T of 1187/ns and ~one *picosecond*, respectively. A

one picosecond ρ cannot be monitored with our available excitation modulation frequencies of ~250-300MHz (or our instrument's precision of 5-20 picoseconds) and would therefore result in a *missing anisotropy* (i.e., the total anisotropies do not add up to the limiting anisotropy) in the analysis. Phenomenologically, missing anisotropy can thus be defined as a depolarized emission of light from a fluorophore (i.e., one undergoing FRET) at a rate immeasurable with the time-resolved instrument. Missing anisotropy via energy transfer between identical molecules (i.e., tyrosines in the protein Troponin C) was also recently (although, very qualitatively) reported via the use of the pulse method of time-resolved fluorescence (Wang et al, 1993). It should also be mentioned here that excitation of the 1.2 FITC-L7/L12 sample at 528 nm results in reappearance of most of the missing anisotropy (data not shown; see Chapter 6 for more details), since 528 nm is near the red-edge of fluorescein's absorption spectra (recall Fig. 17) and, as Weber and Shinitzky demonstrated (1970), homotransfer fails at the red edge of the absorption band.

Clearly, the observed shortened global rotational relaxation time and missing anisotropy might be a result of rapid (less than a few hundred picoseconds) energy transfer from a donor fluorophore to an acceptor fluorophore oriented at slightly different angles with respect to the rotational axes. Since the *local* rotational relaxation time (~1.5 ns) is not significantly changed upon energy transfer (~1.2 ns), ρ_T is likely, in fact, less than one ns. Furthermore, the ~1.5 ns local ρ is quite typical and indicative of fluorophore rotations about the amino acid side chains to which they are attached (vide infra for more details). Finally, the *proportion* of the fractional emission intensity of the local ρ to the global ρ is greater when FRET occurs, indicating that some of the fractional emission intensity of the local ρ was due to the

missing anisotropy (see Chapter Six for more details). Hence, the data here clearly demonstrate the effects (and possible ambiguities) of FRET on the observed rotational diffusion of a macromolecule and a more refined, practical, and quantitative example of missing anisotropy (see also, Chapter Six).

Significance of the Rotational Relaxation Time of FITC Bound to Wild Type L7/L12: Evidence for Segmental Mobility. The initial goal of our investigation of L7/L12 hydrodynamics was to use fluorescence spectroscopy to determine its approximate shape and compare results to other methods. All previously published papers on *quantitative* L7/L12 hydrodynamics (recall Table 2) ultimately reported an axial ratio and model for its *structure*. Only one study reported the possibility of flexibility or conformational mobility (Österberg, unpublished x-ray scattering results). In contrast, NMR and crosslinking studies qualitatively verified some flexibility *must* exist in L7/L12. We shall attempt, in this subsection, to qualitatively describe the mobility of L7/L12 using modern fluorescence methodologies. A*quantitative* description of L7/L12 rotational hydrodynamics is the ultimate goal of this chapter.

In the previous subsection, the author demonstrated the potential artifacts and complications imposed when a sample is undergoing FRET. Clearly, elucidation of protein hydrodynamics via dynamic polarization measurements is simplified by using samples that possess no transfer of resonance energy between fluorophores. We shall see later in this chapter that knowledge of the precise location of the fluorophore is necessary to quantitatively characterize the dynamics of a protein. *Our initial characterization with wild type L7/L12 labeled at a previously (vide infra) unknown position were therefore simplified by using only samples not exhibiting FRET.*

In Figure 18, we see that the excited-state lifetime of 0.1 FITC-L7/L12 was 3.6 ns (without energy transfer) with a distribution half-width of 0.2 ns. This lifetime value was the average of 5 different samples globally linked to find the average best fit lifetime (see Globals Unlimited Technical Reference for more details of linkage scheme, LFD, Urbana, Ill). The 3.6 ns lifetime is slightly lower than other reports of FITC bound to protein, typically around 3.8 ns (see Erijman and Weber, 1993; Chen and Scott, 1985). This slight reduction of FITC excited-state lifetime may be the result of quenching by a neighboring amino acid side chain. The FITC lifetime remains at 3.6 ns even in the presence of 4.0 M Gu-HCl or 8 M urea indicating that, if quenching by a nearby residue occurs, it could be near the FITC labeling site in the primary structure (see Chapter 5 for discussion of FITC location).

If we know the excited-state lifetime of the FITC, its steady-state polarization, and its limiting polarization at the wavelength of excitation, we can calculate its *mean* harmonic rotational relaxation time using Equation (6) (Perrin Eqn., Chapter 3). The limiting polarization of FITC bound to L7/L12 at 488nm excitation (where absorption and emission dipoles are nearly colinear in the absence of rotation) is 0.475 (limiting anisotropy is 0.375) as determined in 98% glycerol at 0°C. Since the steady-state polarization at 488 nm excitation is 0.235 (Table 3) and the lifetime is 3.6 ns (Fig. 18) we can calculate a mean ρ of 9 ns. As described earlier, Equation 6 assumes a rigid, spherical shaped rotator and furthermore, covalently attached probes usually exhibit rapid depolarization (or rotation) around the bond or amino acid side chain to which they are attached. Rapid local motion would therefore decrease the mean ρ calculated from Equation 6.

As described in the previous subsection, we can separate this mean (9 ns) ρ into "global" and "local" rotational components via time-resolved

fluorescence measurements. The rapid (~1.5 ns) "local" rotation was attributed to the expected rotation of FITC around the amino acid side chain (designated ρ_C) and contributed to 35% of the decay of anisotropy during the 3.6 ns FITC lifetime. The global rotational relaxation time of 22 ns was unexpected for a putatively rigid prolate ellipsoid as previous ultracentrifugation and x-ray scattering studies had indicated for L7/L12 (vide infra). Furthermore, from Equation (7), assuming a spherical shape and a degree of hydration of 0.2-0.45 ml H_20/g L7/L12, we might expect a global rotational relaxation time for dimeric L7/L12 of 29-36 ns at 20°C. Since the mean harmonic ρ (ρ_h) of a rigid prolate or oblate ellipse is in theory and practice always greater than 95% that expected for a sphere (ρ_O; Weber, 1953; Tao, 1969; Tao et al, 1970), the observed global ρ of 0.53-0.66(ρ_O) can be attributed to *segmental* global mobility for L7/L12. We shall quantitatively clarify these distinctly different types of rotations in the next subsection.

Theory of Ellipsoidal Macromolecular Rotators in Relation to Anisotropy Decay. In this subsection, the equations used for discriminating oblate and prolate ellipsoid rotators from spherical rotators are given. In the case of a general ellipsoid, it was shown by Perrin (1934) and verified (by Weber, 1952; Belford et al, 1972; see also Small and Isenberg, 1977) that we can expect five possible rotational relaxation times. Under the simplified conditions of a symmetric prolate (i.e., elongated and cigar-shaped as shown in Fig. 19) or an oblate (i.e., flattened, plate-like) ellipsoid, where two of the three axes are equivalent, the equations for correlating anisotropy decay are simplified to three possible rotational relaxation times (see Small and Isenberg, 1977; Bucci and Steiner, 1988; or Brunet et al, 1993 and references therein for more details).

Recall that the decay time of anisotropy is a sum of exponentials:

$$r(t) = \sum \beta_j e^{-t/\phi j} \quad (30)$$

where r(t) is anisotropy at time (t), ϕ is the rotational correlation time of the jth component and for a symmetrical *ellipsoid*, j =1-3:

$$\beta_1 = 0.1\ (3\cos^2\theta_a - 1)\ (3\cos^2\theta_e - 1) \quad (31)$$

$$\beta_2 = 0.3\ \sin^2\theta_a \sin^2\theta_e \cos^2\theta_{ae} \quad (32)$$

$$\beta_3 = 1.2\ \sin\theta_a \cos\theta_a \sin\theta_e \cos\theta_e \cos\theta_{ae} \quad (33)$$

where the angles θ_a, θ_e, and θ_{ae} are the angles between the absorption oscillator and the symmetry axis, the angle between the emission oscillator and the symmetry axis, and the angle between the projections of the absorption and emission oscillators on to the equatorial plane, respectively (see Figure 21).

$$\phi_1 = (6D_{per})^{-1} \quad (34)$$

$$\phi_2 = (2D_{per} + 4D_{par})^{-1} \quad (35)$$

$$\phi_3 = (5D_{per} + D_{par})^{-1} \quad (36)$$

where:

$$D_{per} = 3/2\ D_s\mu\ \{(2\mu^2 - 1)S - \mu\} / (\mu^4 - 1) \quad (37)$$

$$D_{par} = 3/2\ D_s\mu\ \{\mu - S) / (\mu^2 - 1)\} \quad (38)$$

where D_s is the diffusion coefficient for a sphere of equivalent volume, V, which can be equated by the Debye-Stokes-Einstein relation to the rotational coefficient for a sphere (*recall Equation* 7). μ is the axial ratio, which is less than one for an oblate ellipsoid and greater than one for a prolate ellipsoid and hence:

$$S_{(oblate)} = [1/\sqrt{(1-\mu^2)}]\ \tan^{-1}[\sqrt{(1-\mu^2)}/\mu] \quad (39)$$

$$S_{(prolate)} = [1/\sqrt{(\mu^2-1)}]\ \ln[\mu + \sqrt{(\mu^2-1)}] \quad (40)$$

It is essential to realize that μ is less than one for an oblate simply because its axis of symmetry (short axis) is the polar or longitudinal axis, as

opposed to the prolate ellipsoid where the axis of symmetry (short axis) is the equatorial axis.

An ellipsoid of revolution may therefore be characterized by 3 rotational relaxation times but only two rotational diffusion constants. From Equations 30-40 one can calculate the predicted harmonic mean rotational relaxation time (recall, ρ_h is 3ø) expected for prolate and oblate ellipsoids of various axial ratios, μ (see Tao, 1969; Wahl, 1975) as:

$$1/\text{ø}_h = 1/3\,(\,1/\text{ø}_1 + 1/\text{ø}_2 + 1/\text{ø}_3\,) \qquad (41)$$

It is easy to see from equations 31-33 that excitation at various limiting polarizations (recall P_0) where the average angles between the absorption and emission oscillators change relative to a specific axis, a probe might monitor

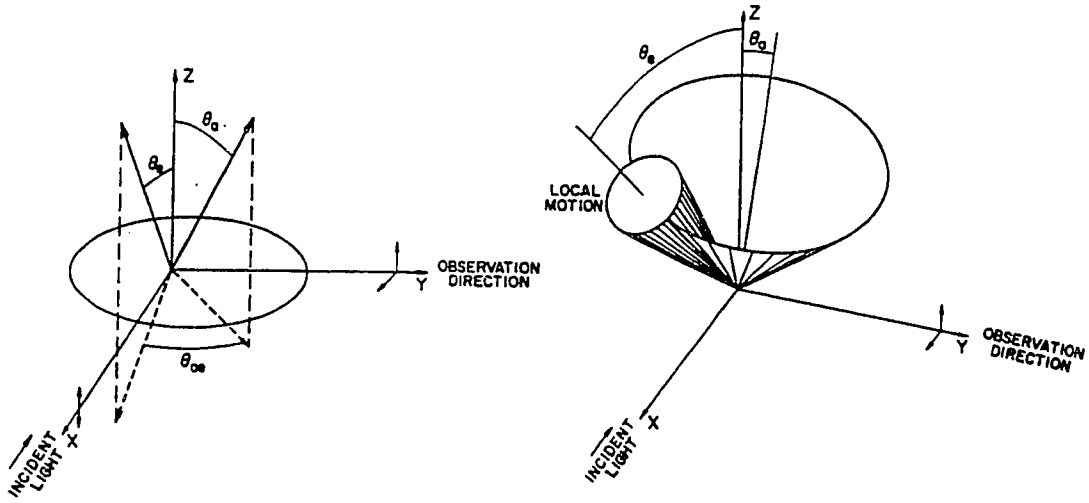

A) B)

Figure 21: A) Schematic of the angles θ_a, θ_e, and θ_{ae} described in Equations 31-33 and B) effects of local motion (taken from Brunet et al, 1993). Compare to Fig. 12.

quite different rotational relaxation times (Weber and Anderson, 1969; Beechem et al, 1986; vanderMeulen et al, 1990; Brunet et al, 1993). Gryczynski

et al (1990) have observed the three rotational correlation times for a prolate ellipse by this method of variable P_o excitation (also, vide infra).

From Equations 30-41 it is clear that prolate and oblate ellipsoid rotators are easily distinguished from spheres or proteins exhibiting segmental mobility using the method of time-resolved fluorescence by the following criteria (see Table 4): 1) the global rotational relaxation of a prolate or oblate ellipse is almost always greater than that expected for a sphere; 2) only the global rotational relaxation time (observed by anisotropy decay) of a prolate ellipse is dependent on the excitation wavelength; 3) the various oblate ellipsoidal ρ's increase linearly with axial ratio, whereas, prolate ρ's level off with increasing axial ratio (see Weber, 1952; 1953).

From Table 4, the global rotational relaxation time of L7/L12 labeled with 0.2 FITC can only be attributed to segmental global mobility for L7/L12. *The possibility of a highly elongated rigid rod (prolate ellipse; Table 2) appears completely abolished.* We see that even if L7/L12 was a prolate ellipsoid with an axial ratio of only 2:1, it would have to be *completely dehydrated* and the FITC would have to be perfectly aligned parallel with the short axis of rotation!!! Interestingly, the global ρ for FITC bound to L7/L12 fits well to a spherical rotor of 16 kD and hydration of 0.3 (vide infra); the state of aggregation of L7/L12 is investigated later in this chapter. Finally, the higher axial ratios presented in Table 4 demonstrate the expected ρ's according to the previous models of L7/L12 as a highly elongated rigid rod. Table 4 shall also serve as a reference for data presented later in the chapter.

Effects of Solvent Viscosity on the Rotational Relaxation Time of L7/L12. At this time, the data strongly suggested segmental global mobility for L7/L12, but the nature of the phenomenon was still undetermined. From the Stokes-Einstein-Debye Equation (6), Ch. 3, different rotators (i.e., ellipses, spheres,

Table 4: The Rotational Relaxation Times Expected for a 24 kD Oblate Ellipse, Prolate Ellipse, or Spherical Rotator as a Function of Axial Ratio and Degree of Hydration (modified from Tao, 1969; Steiner and Norris, 1987).*

Axial Ratio[1]	Degree of Hydration	ρ_1	ρ_2	ρ_3	ρ_h
1.0 (sph)	0.3	32	32	32	32
2.0 (pro)	0.3	48	42	31	39
2.0 (pro)	0.0	33	29	21	27
2.0 (obl)	0.3	36	37	42	38
4.0 (pro)	0.3	109	67	31	64
4.0 (obl)	0.3	59	61	67	49
10.0 (pro)	0.3	428	104	32	71
10.0 (obl)	0.3	138	140	148	142
20.0 (pro)	0.3	1338	119	32	74
20.0 (obl)	0.3	273	275	283	277
L7/L12-F	??	??	??	??	22

* at 20°C and assuming the experimentally verified (recall Table 2) specific volume for L7/L12 of 0.745 ml/g.

[1] abbreviations: pro is prolate ellipse; obl is oblate ellipse; sph is spherical rotor; F is FITC.

segmental, etc.) will exhibit different slopes when the reciprocal of their rotational relaxation time (or polarization) is plotted versus temperature/ viscosity (T/η). If L7/L12 is undergoing segmental global mobility, then we might expect to see deviations (such as non-linearities as discussed below) in the Perrin plot when compared to strictly rigid spherical rotors (vide infra).

In Figure 22, we see a Perrin plot for wild type (presumably dimeric) L7/L12 labeled with a molar ratio of 0.2 FITCs (values are averages of two sets of data). Essentially, when the viscosity of the solvent is increased upon addition of sucrose (or T/η decreases), in accordance to the theory of Perrin (1926; 1929), the *inverse* of the rotational relaxation time ($1/\rho$) and steady-

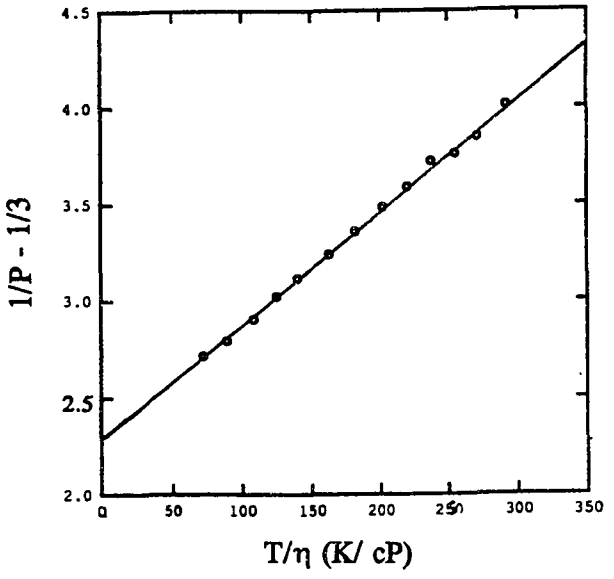

Figure 22: Perrin plot of wild type L7/L12 labeled with 0.2 FITCs at 20°C and 488 nm excitation. Emission greater than 515 nms was collected via a Schott 085 cut-on filter. The standard deviations are negligble.

state polarization ($1/P - 1/3$) of the spherical rotating fluorophore should decrease *linearly*. Deviations in the linearity, in fact, occur at viscosities greater than 10 centipoise where the local rotation of the fluorophore is attenuated. Hence, only viscosities greater than 10 centipoise should attenuate

free rotations (ρ_C) of fluorophores about their covalent bond attachments (i.e., to amino acid side chains; see Weber, 1952 and 1953 for detailed discussion). Hence, the slope obtained in Perrin plots in the viscosity ranges of 1-10 centipoise should ideally be linear and lead to a y-intercept of $1/P_0$-1/3. The P_0 obtained in this manner should reflect the P_0 in the absence of rapid local motion (vide infra). The global rotational relaxation time (ρ_G) can then be calculated by simply plugging this extrapolated value of P_0, the initial polarization (P) at 1 cP, and the determined lifetime, τ, (lifetimes are usually not significantly altered by the sucrose) into Equation (6). Clearly, a fluorophore bound to an ellipsoid that has a higher initial (global) ρ and lower 1/P-1/3 than that of a sphere, should have a significantly lower slope leading to an essentially identical y-intercept. Similarly, if segmental global mobility exists in L7/L12 we might expect changes in the rotational freedom of the hinge or joint at these rather low viscosities (1-10 cP), resulting in anomalous curvatures (Weber, 1952;1953; Waxman et al, 1993); in fact, no significant anomalies were observed with FITC (vide infra for desired effect). Usually, in the absence of rapid local motion (i.e., a non-covalent probe), one can simulate the predicted slope for a sphere or ellipse of desired molecular weight (i.e., Arellano et al, 1988). Unfortunately, in the steady-state method for Perrin plots, the contribution of the local motion to the overall polarization at various viscosities cannot be easily quantified. For wild type L7/L12 labeled with 0.2 FITCs we can calculate from the y-intercept and Equation (6) a ρ_G of ~17 ns, or, somewhat less than that obtained with the time-resolved method (Figure 18). Weber (see 1953; also Wahl and Weber, 1967) has discussed in detail the effects of rapid local motion on the extrapolated y-intercept, which usually leads to a slightly smaller ρ_G than in the absence of rapid local motion. The existence of rapid local motion can

therefore complicate analysis of Perrin plots obtained by the steady-state polarization method. We do, however, see a very slight deviation in the curve at very low viscosities (higher T/η) that might indicate some heterogeneous rotational behavior of FITC-L7/L12 (vide infra).

The *time-resolved* fluorescence method, which separates global from local motion by magnitude and amplitude at each given viscosity is a more informative method for studying viscosity effects on protein hydrodynamics. The time-resolved method essentially allows the investigator to account for lifetime changes that may occur (FITC bound to L7/L12 decreases in fluorescence lifetime from 3.8 to 3.6 ns when temperature increases from 4°C to 44°C). Furthermore, the method of changing T in the T/η term allows information on slower ρ's relative yo the method presented in Figure 22. In Figure 23 we see a plot of the*inverse* of the global rotational relaxation times of FITC bound to L7/L12 versus T/η in which T is altered. According to the Stokes-Einstein theory (origin of Perrin theory), diffusion *rates* (recall $\rho = 1/2D$) of rigid spherical bodies should exhibit a linear relation with the temperature/viscosity ratio. We see some deviation of L7/L12 when compared to that expected and simulated for a 16 kD spherical protein (recall that our 22 ns global ρ fits well to a spherical 16 kD protein) at $T/\eta >$ than 400 K°/cP. This non-linearity of L7/L12-FITC global rotation verses T/η can be attributed to one of the following: experimental error, thermal activations of a segmental mobility, mobility of an ellipsoidal *domain,* or a heterogeneous state of aggregation in the sample. The first explanation seems unlikely since the experiment was repeated twice and similar results were obtained on mutant forms of L7/L12 described later in this chapter; thus, the standard deviation of the measurements cannot readily account for the non-linearity. Thermal activations have been previously discussed in detail (Weber, 1952;

Weber, 1953; 1966; Knopp and Weber, 1969; Rawitch et al, 1969; Benecky et al, 1990) and are usually attributed only to rapid local motions of the fluorophore about an amino acid side chain. It seems possible that thermal activation might result in increased domain mobility of a protein such as L7/L12 since

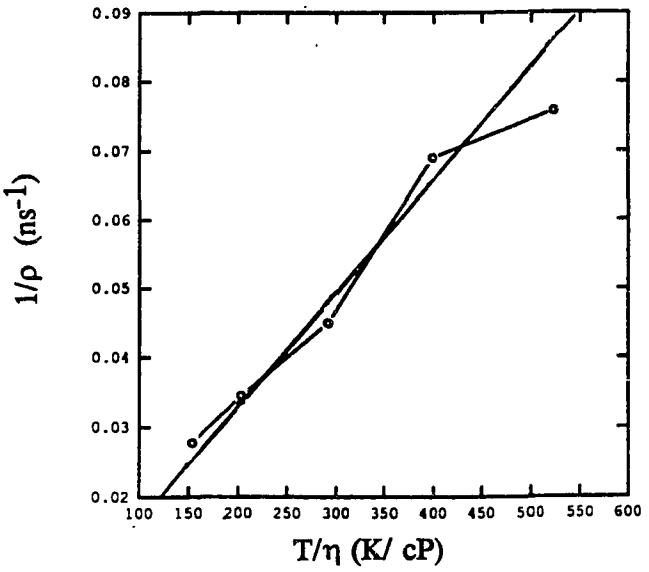

Figure 23: Stokes-Einstein plot of wild type L7/L12 labeled with 0.2 FITCs. Solid line represents simulation for a sphere (see text for details).

the origin of segmental mobility is in fact partially attributed to the C_α-C_β side chain bonds in amino acids located within structureless random coil conformations (Careri et al, 1975; Chou and Fasman, 1974). We cannot therefore, exclude the possibility of thermal activations as the cause of the deviation beginning at T/η = ~280 or 380 $K°cP^{-1}$ in Figure 23. Furthermore, if one of the domains of L7/L12 (recall CTF and NTF), or even L7/L12 as a whole, is ellipsoid in structure then we would expect a deviation (a reduced slope) in the Stokes-Einstein plot relative to the curve plotted for a sphere of identical molecular weight. As described earlier the slope of a plot of rotational relaxation versus T/η for an ellipsoid should be quite different than that of a sphere. The explanation is simple: The curves should eventually merge around 10 cP or T/η = ~30 °K/cP (recall the y-intercept in

Perrin plots) and an ellipsoidal rotator will almost always have a higher initial ρ (at 1 cP) than that of a sphere with an equivalent volume (as seen in Table 4). Finally, the possibility of dissociation with temperature at the protein concentrations measured (~2 μM) was excluded (see next chapter). The existence of multiple aggregation states had not yet been investigated in our lab and this fourth possibility (of heterogeneous states of aggregation) could not be excluded (vide infra). The data point at 44°C (T/η = ~380) might actually reflect a very slight aggregation of L7/L12 that putatively occurs at such temperatures (Casiano, 1992).

The viscosity data are consistent with some rather unusual rotational behavior of the L7/L12-FITC samples. At very high values of T/η (Fig. 23) L7/L12 shows signs of aggregation. When T/η is lowered to values of ~200, another form of L7/L12 rotation monitored by FITC is revealed, possibly indicating a new mode of segmental mobility of the domain to which the FITC is attached. Since the location of the probe was still ambiguous (see next chapter), we could only conclude that the Stokes-Einstein plot (at low viscosities relative to the Perrin plot) of L7/L12-FITC indicated unusual, non-spherical rotation of an apparent domain of L7/L12. See Figure 38 later in this chapter for typical experimental data obtained for a spherical rotor.

COVALENT ATTACHMENT OF 1,5-IAEDANS AND DANSYL-CL: EVIDENCE FOR SEGMENTAL MOBILITY WITHIN AN ELLIPSOIDAL L7/L12.

Numerous studies on immunoglobulins and muscle proteins using time-resolved fluorescence anisotropy have determined that flexibility exists in these proteins. For example, in one study of immunoglobulin G,*two* global rotational relaxation times were measured; the shorter one was attributed to flexibility of an internal domain and the longer one, to the

overall tumbling of the protein (Yguarabide et al, 1970). In two later studies of pure monoclonal IgG (a molecular weight of 150 kD), each of the two global rotational relaxation times were attributed to internal domain flexibility (segmental) with the longer one attributed to *restricted* segmental mobility (Hanson et al, 1981; Oi et al, 1984); in both studies a 25 ns lifetime probe Dansyl-Cl was used and the two ρ's were ~45 ns and ~300 ns. Since the 150 kD IgG is primarily ellipsoidal with an axial ratio of ~10:1 (from sedimentation), they concluded that neither ρ represented global tumbling. *Only in one case,* has the author found a publication describing elongated global ρ's (global tumbling) for a putatively flexible immunoglobulin (see conclusions in this chapter for more details): Liu et al (1981) have used pyrene to report two different global mobilities for IgA, which, like IgG, possesses a molecular weight of ~150 kD. One ρ was >3000 ns (global tumbling) and the other was the usual ~45 ns (segmental flexing). Interestingly, the *average* lifetime of their pyrene-conjugate was a mere 10 ns, and the author finds it difficult to believe that a >3000 ns rotational relaxational time could significantly depolarize a fluorophore with a mere 10 ns fluorescence lifetime (the investigators attributed 30-50% of the anisotropy decay to this "global tumbling"!!!). Similar dependencies of the excited-state lifetime of the probe used, on the rotational relaxation times monitored were reported for the flexible muscle proteins (Harvey and Cheung, 1977; Mendelson and Cheung, 1978; Burghardt and Thompson, 1985; see conclusions of this chapter for more details). Dependence of the rotational relaxation time monitored, on the fluorescence lifetime used, has also been demonstrated by the determination of ρ's in the presence of various concentrations of the quencher acrylamide (Lakowicz et al, 1987). It seemed inevitable that we next try labeling L7/L12

with longer lifetime fluorophores that might enable us to see a slower rotational mode of L7/L12 such as global tumbling.

Initial Fluorescence Characterization. Since the fluorescence lifetime of FITC bound to L7/L12 was only 3.6 ns, it was desirable to use probes with longer lifetimes. Lee and Cantor (1981) reported highly specific labeling of wild type L7/L12 at its C-terminal lysine although very little details on its subsequent fluorescence characterization were given (i.e., only estimated lifetimes, no ρ's, and no polarizations of free L7-IAEDANS). Furthermore, Lee and Cantor showed that full poly-phenylalanine synthesis activity persists subsequent to low labeling levels of IAEDANS, suggesting minimal, if any, conformational changes in the protein upon labeling. The location of the Dansyl-Cl binding sites were unknown and, as with FITC or IAEDANS, not required for *initial* hydrodynamics characterization.

Since neither IAEDANS nor Dansyl-Cl bound to L7/L12 exhibit significant spectral overlap (Figure 24), and both possess rather small extinction coefficients and quantum yields, we would not expect any significant self energy transfer (R_0's <<10Å). Verification of the absence of energy transfer for wild type L7/L12 labeled with IAEDANS is shown in Figure 25 and essentially similar results were obtained for Dansyl-Cl (data not shown). Upon labeling at pH 9.4, we obtained ~0.1-0.3 IAEDANS/(L7/L12) subunit, a result similar to that reported by Lee and Cantor. No attempts were made to achieve higher labeling ratios. Using a pH 8.0 carbonate buffer, we obtained ~0.2 Dansyls/ (L7/L12) subunit.

Time-resolved Fluorescence Results. In Tables 5A and 5B we see a summary of fluorescence lifetime and dynamic polarization data, respectively, obtained for L7/L12 putatively labeled at its C-terminal lysine with IAEDANS or at an unknown site with Dansyl-Cl.

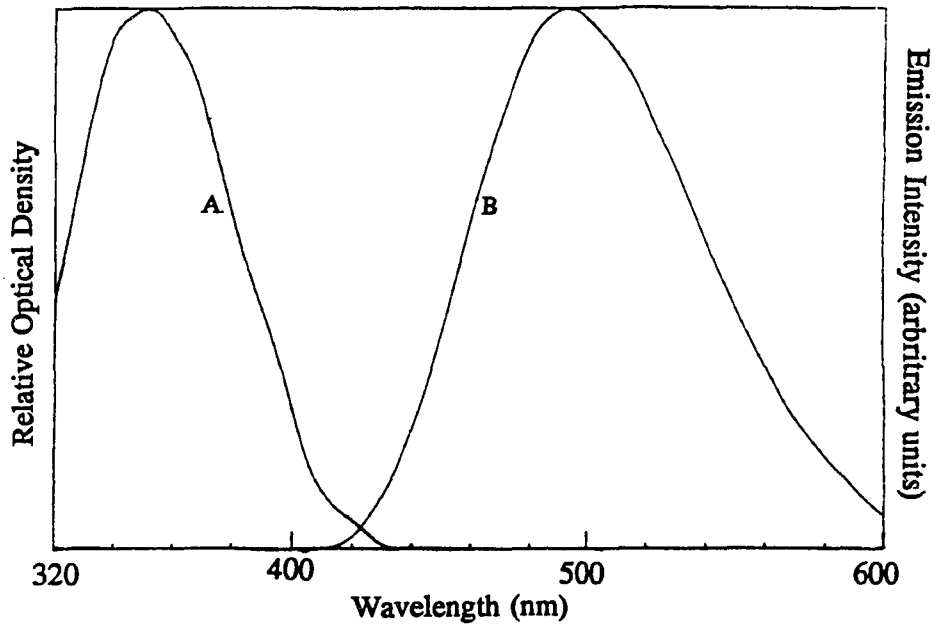

Figure 24: Absorption (A) and corrected emission (B) spectral overlap of 0.2 IAEDANS bound to L7/L12 at 20°C. Emission spectrum was achieved via 351 nm excitation.

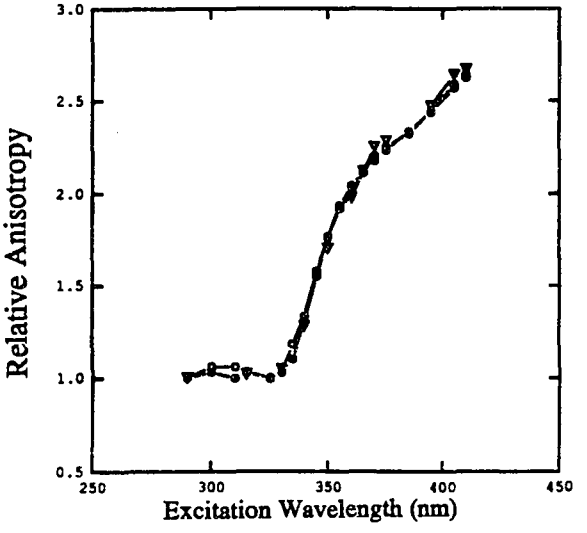

Figure 25: Normalized (to 290 nm) excitation anisotropy spectra demonstrating lack of energy transfer between IAEDANS' bound to L7/L12. Filled circles represent L7/L12 bound IAEDANS, hollow circles represent IAEDANS in 98% glycerol, filled triangles represent L7/L12 bound IAEDANS and denatured in 4 M Gu-HCl. Emission collected with KV399 filters.

The average excited-state lifetime of ~15 ns for IAEDANS is close to what Lee and Cantor predicted and the two-component decay is not unsual for IAEDANS. The ~15 ns excited-state lifetime and rather blue-shifted absorption and emission spectra, indicate that the IAEDANS is in a somewhat non-polar environment (Hudson and Weber, 1973) as opposed to the x-ray structure of L7/L12 (Leijonmarck and Liljas, 1987), which indicates that the C-terminal lysine is one of the more solvent accessible amino acids. Further proof for IAEDANS' location in a restricted or hydrophobic environment comes from the fact that the "local" mobility component is longer in comparison to those observed for FITC-L7/L12 (~3 ns as compared to ~1.5 ns). Investigation of this disagreement goes beyond the scope of this dissertation.

Essentially, the 15 ns lifetime of IAEDANS expanded our "time-window" for monitoring events in L7/L12 from the ~40 ns maximum range (as with FITC) to the ~150 ns maximum range. As previously shown in Table 4, we might therefore, with IAEDANS, be able to monitor an ellipsoidal (up to 10:1 axial ratio) *global tumbling* of L7/L12 as previous sedimentation and low-angle x-ray scattering data suggested should exist. As seen in Table 5B, the IAEDANS did in fact, monitor a global ρ of over 40 ns. The data suggested that the longer fluorescence lifetime probe revealed a rotational mode of L7/L12 not detected by FITC (vide infra, for more discussion). The longer lifetime probe Dansyl-Cl might monitor even slower events.

Interestingly, the ~27 ns average lifetime of dansyl bound to L7/L12 fit best to a tri-exponential decay. The dansyl lifetime data analysis allowed us to make two theories about the dansyl binding site environment: 1) the relatively long average lifetime of 27 ns indicates that the dansyl is somewhat shielded from the solvent (like IAEDANS; see Wahl and Weber, 1967); 2) the

dansyl samples several different environments during its excited-state. In the the dynamic polarization analysis we assumed that the three-component decay could all be attributed to one dansyl (i.e., non-associative decay).

Global linkage analysis of the dynamic polarization data for three separate samples of L7/L12-dansyl resulted in a rather typical local rotational

---

Table 5A: Fluorescence Lifetime Data for Wild Type L7/L12 Labeled with IAEDANS (A) or Dansyl-Cl (B).[1]

	τ_1	f_1	τ_2	f_2	τ_3	f_3	χ^2	τ
A*	15.9	0.928	1.04	0.072	-----	-----	1.9	14.83
B#	31.0	0.820	8.30	0.140	1.40	0.040	1.3	26.64

[1]All data were acquired at 20°C and 351 nm excitation, with Schott KV399 cut-on filters. The symbol's τ_i, f_i, and χ^2 are essentially the lifetimes, fractional intensity contributions and error as described in Eqns. 11-16 in Ch. 3 (also, see text below); τ is the average lifetime simply = S $\tau_i f_i$. All τ's are given in ns

*Two sets of data were globally linked using Globals Unlimited analysis software to find the average best fit.

#Three sets of data were globally linked.

Figure 5B: Dynamic Polarization Data for Wild Type L7/L12 Labeled with IAEDANS (A) or Dansyl-Cl (B).[1]

	ρ_1	β_1	ρ_2	β_2	r_0^*	χ^2	S.S.P#
A	40.1	0.384	2.78	0.616	.272	4.3	0.068
B	55.0	0.401	1.88	0.599	.318	3.1	0.094

[1] All data were acquired at 20°C, 351 nm excitation, and through KV399 filters and are results of global linkage as in Fig. 5A. The symbols ρ and β are the rotational relaxation time (given in ns) and pre-exponential of the ith component like in Eqn. 30, r_0 is the limiting anisotropy, χ^2 is the error (like in Eqn. 11, Ch. 3), and S.S.P. is the steady-state polarization.

* True r_0's at 351 nm for IAEDANS and dansyl were measured in 98% glycerol at 0°C and are .282 and .338, respectively; hence, the time-resolved method can nearly pick up the r_0's in buffer and 20°C--the lesser values probably reflect very rapid motion detected only beyond the frequency range used in the measurements (0-150MHz).

Steady-state polarizations were acquired primarily on the SLM fluorometer (recall Ch. 3; SLM and ISS instruments have good agreement) and are averages of at least four separate preparations. The polarizations were added to this table and subsequent time-resolved fluorescence tables for two primary reasons: 1) θ can be calculated from S.S.P or vice versa (recall eqn.3, pg. 52); 2) the steady-state polarization can be calculated from the time-resolved rotational parameters and average lifetime via combination of eqns. 4 or 5 and 6. The S.S.P. calculated by this method (from the time-resolved data)is usually in excellent agreement (within 5 or 10%) with the measured S.S.P.'s unless a particular rotational parameter is difficult to measure with the particular probe or instrument (or if their is missing anisotropy).

relaxation time of ~1.8 ns and a global rotational relaxation time of ~55 ns. Once again we observed a dependence of the observed rotational relaxation time on the length of the excited-state lifetime, indicating possible global tumbling. If this global tumbling relaxation time of ~55 ns represented that of a prolate ellipsoid with an axial ratio of greater than 4:1 (from Table 4), then we would expect to see a noticeable difference in a Stokes-Einstein plot when the slope of the data is compared to a hypothetical equivalent sphere. In Figure 26, we in fact see a very non-linear and reduced slope for L7/L12-dansyl compared to a hypothetical spherical rotator (with 55 ns rotational relaxation time at 20°C like L7/L12-dansyl). The data supported the existence of an either ellipsoidal L7/L12, thermal activation of hinge-induced segmental mobility, or possible existence of a higher aggregate form of L7/L12 (see Figure 38, CTF C-89 for typical experimental results for a spherical rotor).

What motions, then, does IAEDANS monitor? At this point we had data from three different fluorophores monitoring different global rotational relaxation times. Furthermore, all three data sets fit quite well to the reported rotational models. The 3.6 ns lifetime fluorescein derivative monitored a 22 ns segmental mobility of L7/L12 and the 27 ns lifetime dansyl derivative monitored a 55 ns mobility (something much larger than that expected for a spherical 24 kD L7/L12). Interestingly, the 15 ns IAEDANS lifetime monitored a rotational relaxation time of 42 ns, intermediate to the other two values. Unfortunately, the IAEDANS data fit very poorly to a three-exponential anisotropy decay. It was tempting to attribute the 42 ns ρ to another rotational axis of a *prolate* L7/L12, i.e., it was possible that the absorption and emission dipoles of IAEDANS were oriented at different angles from that of the dansyl. From Table 4, the data implied that L7/L12 was a prolate ellipsoid (recall,

prolates are distinguishable from oblates by λ_{ex} dependence which originates from conspicuous differences in ρ dependent on the orientation of the fluorophores' transition dipole) with an average axial ratio in the 15-25 ns time

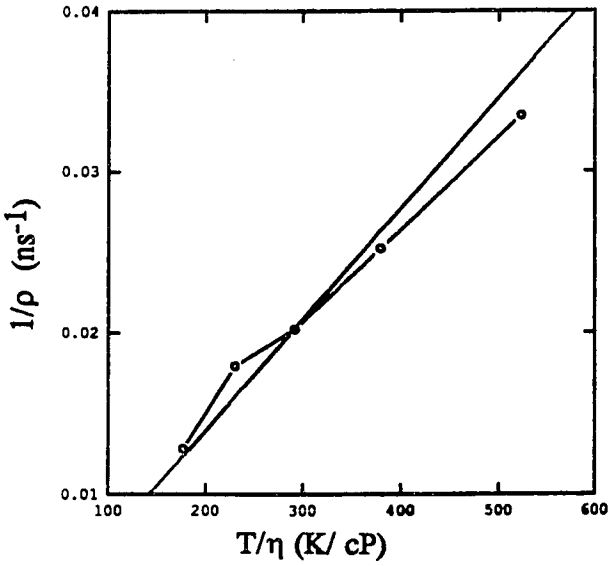

Figure 26: Stokes-Einstein plot of wild type L7/L12 labeled with Dansyl-Cl at an unknown position (hollow symbols) and a simulated slope of a 50 kD sphere (solid line).

scale of *roughly* 4:1 (vide infra). Furthermore, the data indicated that L7/L12 possesses a predominant ~22 ns segmental mobility.

Many questions still remained before any concrete conclusions could be made. How do we know L7/L12 is only a dimer? This question can be answered in the affirmative since all data published to date, with only one exception (i.e., under high salt conditions Georgalis et al, 1989 claimed that L7/L12 is purely tetrameric), had demonstrated that L7/L12 is dimeric. One study (Österberg et al, 1976) suggested that a *small percentage* of L7/L12 might form a tetramer. Our dynamic polarization data indicated that nearly 50% of the anisotropy decay was due to a rotational relaxation time much greater than that expected for a spherical dimer of L7/L12. Hence, we temporarily

excluded this possibility (vide infra) in favor of the possibility of an ellipsoidal L7/L12.

Why don't the longer lifetime probes monitor fast segmental mobility? One must consider the time scale of the fluorescence decay. If the segmental rotational time is relatively fast (22 ns) and the global tumbling relaxation time is long (~60 ns), then the 3.6 ns decay of fluorescein should predominately monitor the 22 ns ρ (plus, of course, any rapid local mobility). The underlying concept is simple, i.e., very little emission from the FITC occurs after ~30 ns (remember, a given excited-state lifetime is the *average* decay, 1/e, of the fluorescence). In the case of a 27 ns lifetime such as dansyl, sufficient light is available to monitor events occuring beyond 100 ns. If the "real" global tumbling is, say, 80 ns and the dansyl is *oriented* such that it monitors a slower segmental mobility (say 40 ns), then our analysis procedures may not be able to discriminate between the two and the data will therefore fit to something in between (recall discussion on page 13 of this chapter). Similar analogies could be made for the IAEDANS case. Fortunately, the Globals Unlimited analysis software is sufficiently sophisticated so that this type of situation can be considered. In Figure 27, we see a χ^2 surface analysis of the global rotational relaxation time of wild type L7/L12 labeled with either Dansyl-Cl or FITC. Here we see the opposite is true: the FITC is monitoring primarily the segmental motion, but also seems to be monitoring a slightly slower motion. The dansyl on the other hand, strictly monitors a 55 ns rotational*relaxation* time. The skewing of the χ^2 confidence curves of FITC towards the more "global tumbling" relaxation time is not difficult to imagine, but why the dansyl derivative cannot sense any of the same 22 ns ρ is open to speculation. One intriguing possibility is that the dansyl is oriented such that it monitors a rather hindered hinge mobility (like the

immunoglobulins) and that the true global tumbling of L7/L12 (i.e., the 20:1 axial ratio theory) can only be observed with a longer lifetime probe such as pyrene. This theory is tested in the next section.

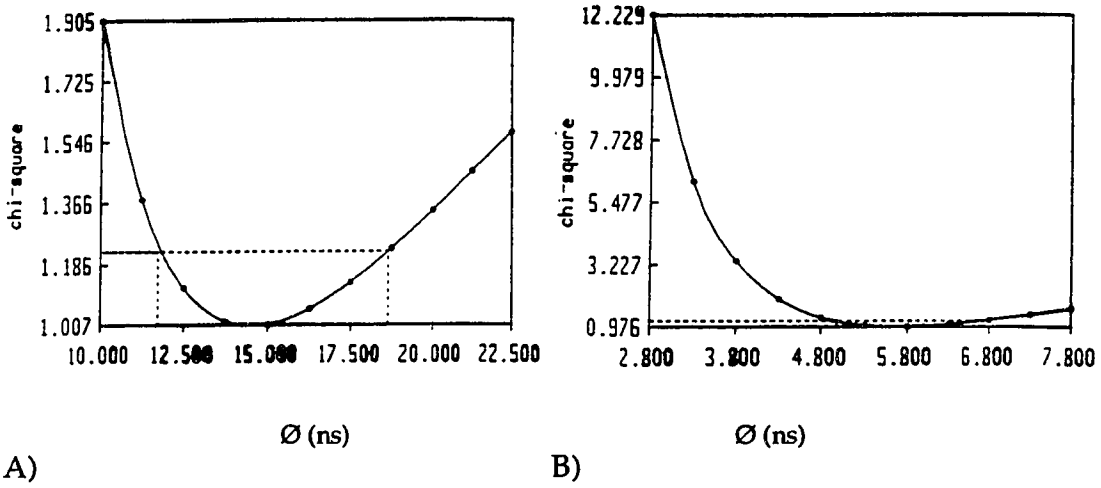

Figure 27: Typical χ^2 surface analysis of the global rotational *correlation* time of wild type L7/L12 labeled with either Dansyl-Cl (A) or FITC (B). Y-axes represent the global Ø's (in ns). The dashed lines represent a single standard deviation wherein 67% confidence exists. χ^2 surfaces are calculated similar to equation (11), pg. 63 for different values of Ø (recall Ø = 1/3 ρ; see also text above). Results here are from a typical, single set of data.

INITIAL FLUORESCENCE CHARACTERIZATION OF THREE SITE-SPECIFIC CYSTEINE MUTANTS OF L7/L12: EVIDENCE FOR INDEPENDENT C-TERMINAL DOMAIN MOBILITY WITHIN A HIGHLY ELONGATED DIMER OR A HIGHER AGGREGATE.

The various cysteine mutants created in the laboratory of Dr. Robert Traut at UC Davis were illustrated in Figure 7 (Chapter 2). In this section, data are presented for the C-33, C-63, and C-89 cysteine mutants. The author chose to present data for the other mutants later in this chapter since they were expressed and characterized only recently.

Initial Time-resolved Fluorescence Data. Three different sulfhydryl-specific probes, each with considerably different fluorescence lifetimes, were individually attached to each of the three different mutants. Initial fluorescence lifetime and dynamic polarization data for the various fluorophore-L7/L12 conjugates are presented in Tables 6 and 7, respectively.

The three mutants were first labeled and characterized with 5-iodoacetamidofluorescein (5-IAF). Labeling stoichiometries of 0.8-1.0 IAF/(L7/L12) subunit were typically obtained. Furthermore, there was absolutely no trace of fluorescein bound to wild type L7/L12 and therefore the 5-IAF labeling was highly specific for the cysteine mutant. Essentially, nearly identical results were obtained each time with each labeling preparation. The 5-IAF derivative has a lifetime of ~4.1 ns and hence, gives us nearly the same time-scale of information as the ~3.6 ns FITC. Furthermore, a 4.1 ns lifetime is quite typical for 5-IAF (see chapter 6 for more details on the 5-IAF lifetimes).

The global rotational relaxation times reported at the two C-terminal cysteines (C-63 and C-89) were not significantly different from the one N-terminal cysteine (C-33) mutant. All three ρ's here are similar to those reported earlier for FITC bound to wild type L7/L12. Since we knew by now that L7/L12 exhibited substantial flexibility, probably via its flexible hinge which separates its C-terminal domains from its N-terminal domains, it seemed quite logical that we might observe differences when each domain was separately labeled. According to speculations based on the x-ray structure, the C-terminal domains, each possessing a molecular weight of ~7100 daltons, might form a complex. The N-terminal domains on the other hand, putatively responsible for dimerization, each have a molecular weight of ~3750 daltons. Dimers of the C-terminal domains and N-terminal domains, respectively, would thus have molecular weights of 14.2 kD and

Table 6: Initial Fluorescence Lifetime Data for Three Different L7/L12 Cysteine Mutants.*

	τ_1	f_1	τ_2	f_2	τ_3	f_3	χ^2	τ
33-F[1]	4.09	1.00	-----	-----	-----	-----	1.2	4.09
63-F	4.05	1.00	-----	-----	-----	-----	1.7	4.05
89-F	4.15	1.00	-----	-----	-----	-----	0.8	4.15
33-I[2]	12.97	0.96	.001	0.04	-----	-----	1.9	12.5
63-I	11.94	0.96	.001	0.04	-----	-----	2.2	11.5
89-I	12.43	0.97	.001	0.03	-----	-----	2.7	12.0
33-P[3]	151.9	0.85	4.65	0.15	-----	-----	5.6	129.8
63-P	127.2	0.58	14.46	0.13	3.52	0.29	1.8	76.7
89-P	137.0	0.60	41.02	0.27	4.37	0.15	4.8	93.9

* All X-axis symbols are essentially as indicated in Table 5A and lifetimes are again in ns. Average lifetimes were rounded off to the nearest tenth.

[1] "F" symbolizes 5-iodoacetamidofluorescein; data are the best fit global linkage of three different sets of data at 20°C, 488nm excitation, and emission through 085 cut-on filters.

[2] "I" symbolizes 1,5-IAEDANS; data are the best fit global linkage of two sets of data at 20°C, 351 nm excitation, and with KV399 emission cut-on filters.

[3] "P" symbolizes 1-pyrenemethyl iodacetamide; data are the best fit global linkage of two sets of data for C33 and C63; C89 data are the result of one experiment. Data were collected at 20°C, 351nm excitation, and with Schott 057 cut-on filters. *All samples were flushed with 99.99% Argon for 1 mins. prior to measurements; higher lifetime's could be obtained with more tedious treatment's, which were unnecessary at this time in the interpretation of L7/L12 hydrodynamic information (see last section of this chapter).* Lifetimes given are peaks from a Lorentzian distribution (recall Ch.3).

Table 7: Initial Dynamic Polarization Data for Three Different L7/L12 Cysteine Mutants.*

	ρ_1	α_1	ρ_2	α_2	r_0**	χ^2	S.S.P.#
C33-F	24	0.27	2.1	0.73	0.288	1.8	0.148
C63-F	23	0.24	1.1	0.77	0.341	2.7	0.112
C89-F	28	0.49	2.1	0.51	0.372	2.1	0.200
C33-I	326	0.21	3.0	0.79	0.272	0.9	0.118
C63-I	39	0.14	2.7	0.86	0.278	3.2	0.081
C89-I	42	0.24	3.6	0.76	0.285	1.3	0.090
C33-P	721	0.18	2.5	0.72	0.120	0.8	0.043
C63-P	605	0.13	2.6	0.87	0.126[F]	3.2	0.041
C89-P	1146	0.22	3.1	0.78	0.126[F]	3.5	0.048

* All y-axis symbols and conditions are as described in Table 6; All symbols in the x-axis are as described in Table 5B.

Polarizations for fluorescein samples were averages of five separate labeling reactions; IAEDANS polarizations were averages of three separate labeling reactions; pyrene polarizations were averages of two separate labeling reactions.

** True r_0's were measured at the reported excitation wavelengths (noted in Table 6 caption) in 98% glycerol and 0°C; for fluorescein 0.375; IAEDANS 0.282; Pyrene 0.126 (a lightly labeled pyrene butyrate-WT L7/L12 conjugate).

[F] In some cases (some pyrene data) values needed to be fixed since the analysis resulted in obviously higher than allowed numbers (see text for details).

7.5 kD (excluding the fact that the C-terminal domains are more hydrated). Hence, we would expect to see obvious differences between these two protein preparations. Assuming that the probes were not preferentially aligned with a particular axis, it seemed quite logical that the C-terminal domains (MW = 7100 daltons) were each rotating independently, whereas, the N-terminal domains rotated as a dimeric unit (MW = 7500 daltons). Still, many questions needed to be answered. Could it be that the probes were interfering with the C-terminal domain interaction? If this were the case then the C-terminal domain interaction would have to be at most, very weak, since the N-terminal domain complex was apparently not effected by the probes. Furthermore, Dr. Oleinikov had verified that labeling C-89 or C-63 with bulky crosslinking agents, which we could expect to effect the interaction more than the fluoresceins, has absolutely no effect on biological activity (personal communication) and hence, a C-terminal complex must have at most, little biological significance.

One other interesting phenomenon was observed in the fluorescein data: 5-IAF attached to the C-33 and C-63 mutants displayed missing anisotropy (recall first section of this chapter). The r_0 for free fluorescein at 488 nm excitation as determined in 98% glycerol is 0.375, which is what we observe from the time-resolved fluorescence data analysis for C-89 labeled with 5-IAF. When 5-IAF is attached to C-33 and C-63, we observed limiting anisotropies of 0.288 and 0.340, respectively. The data suggested some small extent of intersubunit energy transfer between fluoresceins located at the C-63 position and large amounts of intersubunit energy transfer at the C-33 position (see Chapter Six). Hence, the data further supported the idea that the C-terminal domains, in solution, were rather far apart and the N-terminal domains were rather close. We will find out later, more quantitatively, that

energy transfer does not occur between IAFs at C-63 (See Chapter Six). Further hydrodynamics characterization of cysteine mutants labeled with IAF are shown in the next three sections.

The three mutants were then labeled separately with IAEDANS (usually 1 IAE/(L7/L12) subunit). IAEDANS does not measurably bind to wild type L7/L12 under the specified labeling conditions (recall, labeling buffer pH 8.0). The ~12 ns lifetimes obtained for IAEDANS bound to the three mutants indicated that, in all cases, it is rather exposed to the solvent (see Hudson and Weber, 1973). When IAEDANS is simply attached to N-acetylcysteine (N-cys-IAEDANS is used as our standard in lifetime measurements in the mid-UV excitation), its fluorescent lifetime is 10.4 ns in buffer; conversely, when IAEDANS is buried (like when attached to phosphofructokinase-2, Jameson, 1993, personal communcation), its lifetime can be greater than 20 ns. Hence, it is not surprising that the IAEDANS is rather exposed to the solvent as the cysteines were strategically placed within structureless loops on L7/L12. Furthermore, as was the case with 5-IAF, the C-63 position is especially exposed to the solvent (τ = ~11.5 ns), whereas, the 33 and 89 positions are less solvent exposed (τ = ~12.5 ns). Further support for this theory comes from the rapid local motion always observed at C-63 regardless of what probe is used (vide infra for more details).

A striking finding appeared when the C33-IAEDANS dynamic polarization data was analyzed. The global rotational relaxation time monitored was greater than 320 ns. Analysis of the C63-IAEDANS and C89-IAEDANS dynamic polarization data resulted in an ~40 ns global ρ. *Interestingly, the IAEDANS-labeled C63 and C89 mutants (both are C-terminal domain mutants) appeared nearly identical to IAEDANS attached to the C-terminal lysine of wild type* (with respect to global ρ; recall last section).

It seemed possible that the IAEDANS bound to C-33 was aligned parallel to the long (polar) axis of a prolate L7/L12, whereas the three IAEDANS located in the C-terminal domain preferentially aligned parallel to a more short (equatorial) axis of rotation. Furthermore, IAEDANS bound to the C-terminal domains might be monitoring a rather restricted (slower) 40 ns segmental mobility that goes undetected by the fluorescein. Finally, one might begin to wonder from these results whether or not the fluorescein probe, with its rather short fluorescence lifetime was actually even monitoring a segmental mobility (recall Fig. 27, how the fluorescein data appeared rather skewed towards the longer rotational relaxation times). The IAEDANS data (Table 4) therefore suggested a more rigid 10:1 axial rotation for L7/L12!! The possibility of an aggregated L7/L12 had not yet been investigated and offered yet another possible explanation for the data. This latter possibility was somewhat supported by the fact that the local motions were considerably higher than that expected for a fluorophore *freely* rotating around an amino acid side chain; the data therefore suggested that the fluorophores might be in a rather restricted environment perhaps expected if aggregation had occurred. Hence the data might be consistent with some flexibility of the C-terminal domains within an aggregated form of L7/L12.

Labeling of the three cysteine mutants with pyrene presented us with yet another ambiguity. First, several difficulties were encountered in the labeling procedure (recall Materials and Methods) such as slight precipitation when the dye was added. The stick pyrene was readily soluble in organic solvents but the 8-10 mM pyrene necessary for labeling, was apparently insoluble in buffer resulting in aggregation of the probe. Surprisingly, the C-33 still labeled quite efficiently {~0.6-0.8 PMIA/ (L7/L12) subunit}. In contrast, the C-63 and C-89 C-terminal mutants exhibited rather low labeling

efficiencies {each ~0.2-0.4 PMIA/ (L7/L12) subunit} as one might expect under conditions that precipitate the probe. However, the 1-pyrenemethyliodo-acetamide derivative essentially did not label wild type L7/L12. Second, enormous global rotational relaxation times were observed subsequent to labeling. In all cases, a global rotational relaxation time greater than 600 ns was observed and in one case, that of C-89, the ~100 ns fluorescence lifetime of pyrene (vide infra) monitored a global ρ of greater than 1100 ns.

Why were we no longer observing obvious segmental mobility ability with the pyrene and IAEDANS labeled proteins? The χ^2 surface analysis plot in Figure 28 demonstrates an even greater chi-confidence for the ~4.1 ns lifetime probe IAF than with the ~3.6 ns lifetime probe FITC (Fig. 27), in monitoring the apparent segmental mobility. Conversely, the ~12 ns lifetime IAEDANS and ~100 ns lifetime pyrene probes each monitored significantly slower motions with nearly equal chi-confidence as the IAF (see Figure 28).

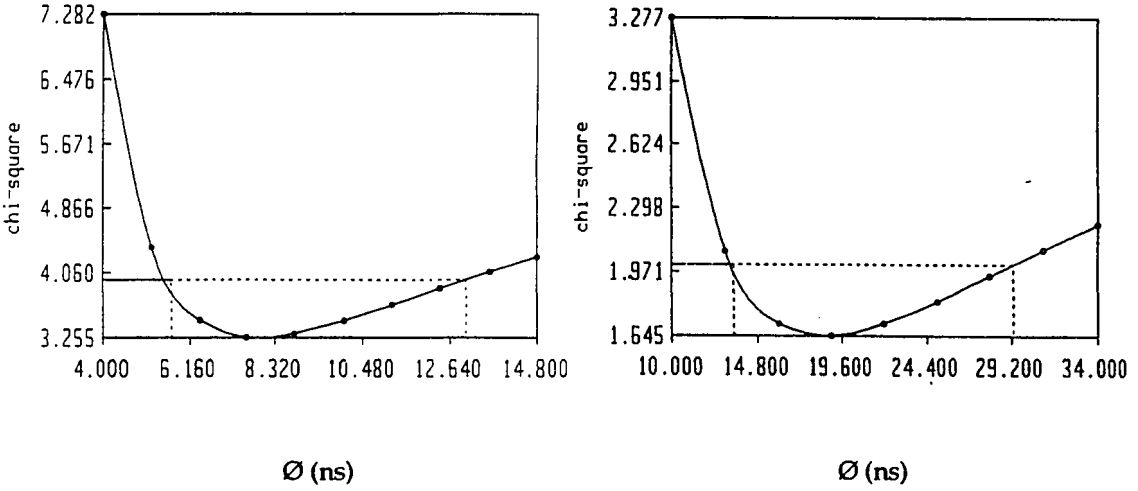

Figure 28: Chi-confidence plots for the global Ø's of A) C63-IAF; B) C63-IAEDANS (compare to Figure 27, pg. 112 for more details).

Analytical Model for Dimeric L7/L12. The 1100 ns global mobility monitored by pyrene rendered the author highly suspicious that an aggregated form of L7/L12 was present. A 20:1 axial ratio prolate (from pyrene data and Table 4) simultaneously possessing high flexibility (as monitored by the IAF) seemed incompatible. Wong and Paradies (1974) claimed with low-angle x-ray scattering to have observed a small axis with a diameter maximum of 17.3Å. They did not, however, at that time attribute the 17Å diameter to any particular structure within L7/L12. Wong and Luer later (Luer and Wong, 1979) created a model from additional sedimentation and viscosity data in which they claimed that one C-terminal domain had one axis that was 10Å!! Their data agreed well with Österberg et al (1976) who claimed that with small angle x-ray scattering they were able to detect an axis with a diameter of 12Å (recall Table 2). In 1987, Liljas and Leijonmarck published x-ray scattering data which concluded that the C-terminal domains have axial dimensions of 35x35x25Å, nullifying the previous model of Luer and Wong (1979, C-terminal short axis of 10Å). Most would agree by now that the 10Å value probably reflects the diameter of single α-helices within L7/L12.

Both the Österberg et al (1976) and the Luer and Wong studies (1979) indicated a 30-32Å axial diameter exists within dimeric L7/L12. If L7/L12 is purely dimeric and the smallest quaternary structure diameter in existence is that of a coiled-coil (which is ~30Å - O'Shea et al, 1991), then the present author attributes the 30 Å axial diameter to a coiled-coil structure perhaps existing in the N-terminal domain as suggested by Tsurugi and Matsui (1991).

The Österberg et al (1976) group and the Wong and Paradies duo both agree that L7/L12 could reach maximum lengths of ~180-190Å. The model presented by the author in Figure 29 predicts maximum axial extension of ~130-170 Å. The assumptions are as follows: 1) The ~six N-terminal residues

are arguably disordered (Möller and Maassen, 1986 and references therein)--the distance between amino acids in random coils is ~3.6Å (21Å max.; 9Å min. if the six amino acids partake in α-helix formation); 2) a stable coiled-coil region possessing 28-35 amino acids has *maximum* dimensions of ~30x45Å (O'Shea et al, 1991; *next chapter for more details*) and minimum dimensions of 25Åx40Å; 3) if residues 33 (max.) or 37 (min.) through 50 (min.) or 52 (max.) are part of a random-coil (see Bushuev et al, 1989)--the maximum and minimum length of the structureless hinge would respectively be 47 or 68Å; and finally, 4) the C-terminal domains possess ~three-dimensional axes of 35x35x25Å (Leijonmarck and Liljas, 1987). The minimum and maximum calculated dimensions for the model depicted in Figure 29 are therefore 131-165Å (longest extended axis) x 25-50Å (depending on relative angular alignment of the two C-terminal domains) x 25-30Å (coiled-coil). Rapid

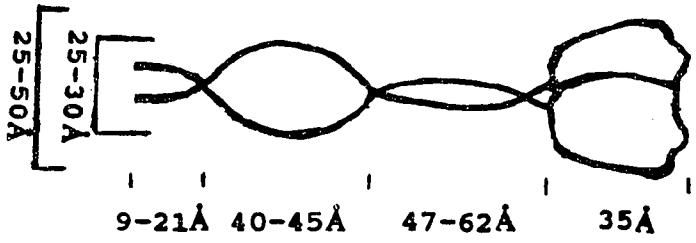

Figure 29: Model demonstrating unlikeliness of a 24 kD L7/L12 dimer possessing global tumbling at the 1,000 ns time scale (20:1 axial ratio that pyrene suggests) and simultaneously exhibiting flexing or rotation of its C- and N-terminal domains at the ~25 ns time scale (as the fluoresceins suggest). Any flexing of these domains would result in an axial ratio of less than 6.6:1. A conserved gly-pro sequence in the hinge is depicted as inducing a flexible sharp turn (suggested from data of Bushuev et al, 1989; also, see Richardson and Richardson, 1990) and is important for function (Bushuev et al, 1989).

segmental movement of the putative random-coil six N-terminal amino acids, should go undetected by a fluorophore located at the C-33, C-63, C-89, or lysine 120 positions. We are therefore left with a maximum possible axial ratio detected by any fluorophore in the above amino acid positions of 165Å x 25Å (6.6:1), assuming a rigid and extended conformation for L7/L12. An axial ratio of 6.6:1 for a 24 kD rigid dimer would result in maximum detectable rotational relaxation times (from Table 4, or Equations 30-41 of ~200 ns (depending on relative orientation or interaction of the two C-terminal domains, the maximum rotational relaxation time could be much less than 200 ns) for a prolate and less than 100 ns for an oblate. Clearly, a higher aggregate of L7/L12 or some other contaminant exists and at this time we became aware from the Traut group that another form of L7/L12 did in fact exist in our samples (see next section for details). The model in Figure 29 shall be discussed more quantitatively in terms of dimeric L7/L12 flexibility and axial ratio distribution later in this chapter.

SIZE-EXCLUSION HIGH-PERFORMANCE LIQUID CHROMATOGRAPHY (SE-HPLC) STUDIES. EXISTENCE OF AN UNUSUALLY LARGE OLIGOMERIC FORM OF L7/L12 IN ADDITION TO THE DIMERIC FORM.

Initial Calibration of The Column: In Table 8, a list of published hydrodynamic information for the proteins used as standards in the calibration of our SE-HPLC column, is presented. Several interesting conclusions are made from Table 8. Obviously, the translational diffusion rate increases as the molecular weight of the protein decreases. Conversely and predictably, the sedimentation rate increases with the molecular weight of the protein. Deviations from this general trend usually reflect significant differences in shape or to a lesser extent, the degree of hydration of the protein (see Cantor and Schimmel, 1980). Shape changes are clearly accompanied by conspicuous

our SE-HPLC column, is presented. Several interesting conclusions are made from Table 8. Obviously, the translational diffusion rate increases as the molecular weight of the protein decreases. Conversely and predictably, the sedimentation rate increases with the molecular weight of the protein. Deviations from this general trend usually reflect significant differences in shape or to a lesser extent, the degree of hydration of the protein (see Cantor and Schimmel, 1980). Shape changes are clearly accompanied by conspicuous changes in the frictional coefficient ratios (f/f_0). Note how the lower molecular weight protein chymotrypsin (21.6 kD) actually has a smaller translational diffusion coefficient than the rather spherical carbonic anhydrase (31 kD). The frictional coefficient ratio is quite often called the Perrin shape factor and is used to directly calculate changes in axial ratio (see Cantor and Schimmel, 1980). The frictional coefficient ratio or axial ratio

Table 8: Comparison of Published Hydrodynamic Characteristics for the Various Proteins used as Standards in the Calibration of the SE-HPLC Column (compare to Table 2, L7/L12 data; also, see text).*

Protein	MW (kD)	$S_{20}x10^{-3}$	$D_{20}x10^{-7}$	V_{20}	f/f_0
LDH	109.0	6.93	5.95	0.741	1.127
BSA	68.0	4.58	6.42	0.740	1.250
HP	44.0	3.48	7.05	0.699	1.357
CA_B	31.0	3.23	10.66	0.739	0.989
CHYM	21.6	2.40	10.21	0.736	1.130
CYT_C	13.4	1.71	11.40	0.728	1.191

*All hydrodynamic data were obtained from CRC Handbook of Biochemistry, 1992; Chem. Rubber Co., Cleveland, OH); Abbreviations: LDH = pig heart lactate dehydrogenase (from Sigma); BSA = bovine serum albumin (from Pierce); HP = horseradish peroxidase (from United States Biochemicals); CA_B = human RBC carbonic anhydrase (from Sigma); CHYM = bovine pancreas Chymotrypsin α (from Sigma); CYT_C = bovine heart cytochrome C (from Sigma); all other symbols were described in Table 2.

can be calculated from numerous types of hydrodynamic methods including *rotational* diffusion from fluorescence spectroscopy (recall Eqns. 30-41 in this chapter) and *translational* diffusion from radiative scattering methods (including photon correlation, low-angle x-ray scattering and viscometry; Tables 2 and 4), and sedimentation (a form of *translational* diffusion; Table 2; Table 4). *All* of these techniques can be used to at least indirectly calculate gyration or Stokes' radii. SE-HPLC is another common method for directly determining Stokes' radii and macromolecular volume and weight (and to a lesser extent, shape; recall Ch 2, Materials and Methods; vide infra for more details).

Hence all of the above hydrodynamic methods can be mathematically interrelated with proper consideration of differences in rotation and translation dynamics. In Figure 30, we see a semi-logarithmic plot of the proteins used as molecular weight standards (listed in Table 8) versus elution volume (in ml/min.). All data presented in this section are from our Toso-Haas G2000SW column described in the Materials and Methods, Chapter 2. Of the six proteins listed in Table 8, horseradish peroxidase has the highest known axial ratio of ~3:1 computed from fluorescence data (see Brunet et al, 1993), with BSA around 2.5:1 (from frictional coefficient), and the others are less than ~1.8:1 (Kuntz and Kauzmann, 1974). The 31 kD carbonic anhydrase is nearly a perfect sphere (from frictional coefficient). The elution volume of 50S ribosomes was added as an indicator of the void volume of the column (10.5 mls) and beta-mercaptoethanol was added as an indicator of the total included volume of the column (~24 mls).

Very little deviation could be detected in Figure 30, as all proteins elute in order of log molecular weight as expected for fairly symmetric molecules (see Ackers, 1975 for more details of the method). Our silica-based molecular sieve columns putatively possesses a linearity in the protein molecular

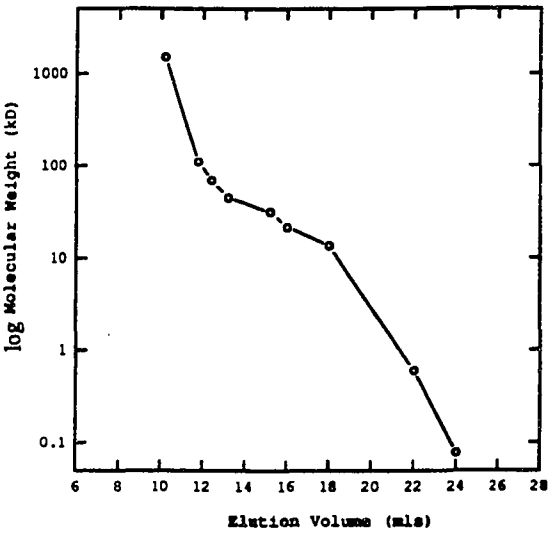

Figure 30: Semi-logarithmic plot for log molecular weight (y-axis) of SE-HPLC standards versus elution volume (in mls; x-axis). Flow rate was 1 ml/min. (details of conditions were described in the Materials and Methods, Chapter 2). Proteins elute by descending molecular weight as described in Table 8 except the first point represents 50S ribosomes (MW = 1500 kD), and the last two points represent 5-IAF (i.e., 5-iodoacetamidofluorescein; MW = 0.57 kD) and BME (i.e., β-mercaptoethanol; MW = 0.078 kD). Values given were averages of at least two separate runs at constant pressure (~370 p.s.i.).

weight range of ~10 kD to ~150 kD (Phenomenex and Toso-Haas data). The horseradish peroxidase and BSA proteins presented us with the most potential error or deviation (as seen in Figure 30) as their rather elongatedness cannot be easily accounted for with the SE-HPLC method (vide infra for more details). The largest deviations in the linearity at the above molecular weight range (plotted in Fig. 30) is between horseradish peroxidase (largest frictional coefficient ratio) and carbonic anhydrase (smallest frictional coefficient ratio) as they have the largest difference in shape.

SE-HPLC of Various Unmodified and Modified Forms of L7/L12. In Figure 31 we see a typical chromatogram for wild type L7/L12 and methionine oxidized wild type L7/L12. It should be noted that all data presented in this subsection

are for forms of L7/L12 overexpressed using the molecular biology techniques described in Chapter 2. It is possible that the overexpression system used in the present studies can lead to an aggregated and/or unfolded state of L7/L12 nominated "Peak1" from SE-HPLC purification. In Fig. 31 we see that Peak1 is approximately the same concentration as "Peak2". The Peak2 has been well characterized in the Traut laboratory as a purely dimeric form of L7/L12 (Zecherle et al, 1992A/B; Oleinikov et al, 1993A/B; Makarov et al, 1993; Traut

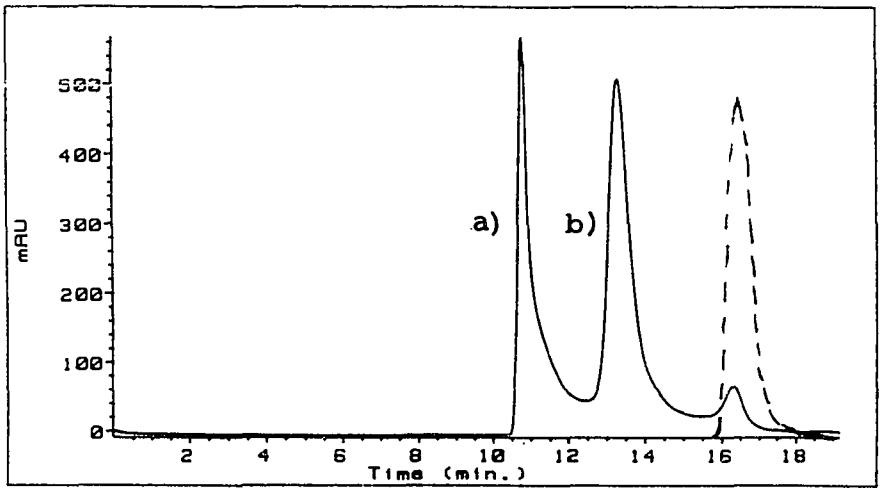

Figure 31: Typical SE-HPLC chromatogram for recombinant wild type L7/L12, where a) represents peak one and b) represents peak two. Y-axis is optical density at 220 nm and X-axis is the elution volume. Also included (dashed line) is the typical elution profile of monomeric (methionine oxidized) L7/L12.

et al, 1993). When one compares the elution volume of Peak1 (10.8 mls) to that of the standards shown in Figure 30, we find that it elutes closer to the void volume than that of the 109 kD protein LDH. The Peak1 elution volume was quite different to that of L7/L12 reported by Georgalis et al (1989), who claimed that a rather oblate (axial ratio of ~2:1) 49 kD tetrameric form of L7/L12 eluted slightly slower than an ellipsoidal (axial ratio of ~3:1) 149 kD protein rabbit muscle aldolase and significantly sooner than the ellipsoidal

(axial ratio ~2.5:1) 66 kD protein BSA. The present author finds it difficult to imagine how 49 kD tetramer of L7/L12 with an axial ratio of only 2:1 could elute near to a 149 kD ellipse with axial ratio of 3:1. *Furthermore, it seems unlikely that this putative tetramer of L7/L12 to elute much sooner than the 66 kD ellipsoidal BSA.* Conversely, our results indicate the possibility of Peak1 being much larger than a "tetrameric" protein putatively observed by Georgalis et al (Figs. 30 and 31 above). Finally, it is noteworthy that peak one can be reconstituted into the ribosome and is equally active as the peak two dimers of L7/L12 in poly-phenylalanine synthesis activity (Oleinikov, personal communication).

The dimeric (Peak2) 24 kD form of L7/L12 elutes maximally at around 14 milliliters. Conversely, the rather spherical protein (axial ratio of ~1.8:1) with molecular weight of 21.6 kD, chymotrypsin, elutes maximally at around 16 milliliters. Furthermore, the perfectly spherical 31 kD protein carbonic anhydrase elutes maximally at 15.2 milliliters. Horseradish peroxidase, with an axial ratio of ~3:1 and molecular weight of 44 kD, elutes maximally at around 13.2 milliliters. If we assumed that all proteins in Figure 30 as well as L7/L12 were spherical, then dimeric L7/L12 would appear to be about 40 kD. Obviously, the shape of dimeric L7/L12 somehow promotes unusually rapid flow through the column; the results were consistent with an asymmetric dimeric L7/L12 although not its putative high frictional coefficient of ~1.7 (recall Table 2). A more quantitative approach to the data is given later in this chapter.

Since the 12.2 kD methionine oxidized form of L7/L12 elutes at around 16.3 milliliters (*nominated Peak3 in subsequent text*) and the rather spherical 13.4 kD protein cytochrome C elutes at 18 milliliters, we can postulate that oxidized L7/L12 has an asymmetry similar to the dimeric form (elutes where

an expected 20 kD protein should). A trace (~5-8%) of monomeric L7/L12 usually eluted in untreated samples of L7/L12 (no methionine oxidation), which indicated that either some protein was dissociated prior to injection (i.e., already near dimer/monomer Kd), dissociated in the column, or was oxidized at ambient conditions. We will discover in the next chapter that the L7/L12 methionines can become oxidized in the absence of reducing agent at temperatures greater than -20°C, if stored for relatively long periods of time (see next chapter). Furthermore, we shall find that dimeric L7/L12 is not ~5-8% dissociated until 0.1 μM (next chapter); all fluorescence measurements in this chapter are at concentrations greater than 0.1μM and as mentioned earlier, all chromatograms presented in this chapter were the result of loading greater than 5 μM L7/L12 onto the SE-HPLC column (assume ~10x subsequent dilution on the column).

In Figure 32A, we see a chromatogram typical for all the various cysteine mutants of L7/L12 labeled with tetramethylrhodamine-5-iodoacetamide (TMRIA), 5-IAF, or IAEDANS. Interestingly, the concentration of Peak1 is noticeably reduced when a L7/L12 cysteine mutant is labeled with one of these three probes. Furthermore, labeling of wild type L7/L12 with FITC results in similar reduction of Peak1 concentration. How these fluorophores (maybe even the labeling procedure) induce this phenomenon is further discussed in the next chapter. In Figure 32B, a chromatogram of L7/L12 C33-IAF microconcentrated to nearly the protein concentration prior to the first chromatogram shown in Fig. 32A, demonstrates that dimeric (Peak2) L7/L12 cannot be converted into Peak1. The small bump seen at 10.8 milliliters is simply the ~8% Peak1 that was contaminating peak two in Fig. 32A (so we can easily conclude that samples need to be put through the SE-HPLC twice to remove all the "aggregated" Peak1 L7/L12). It seems quite

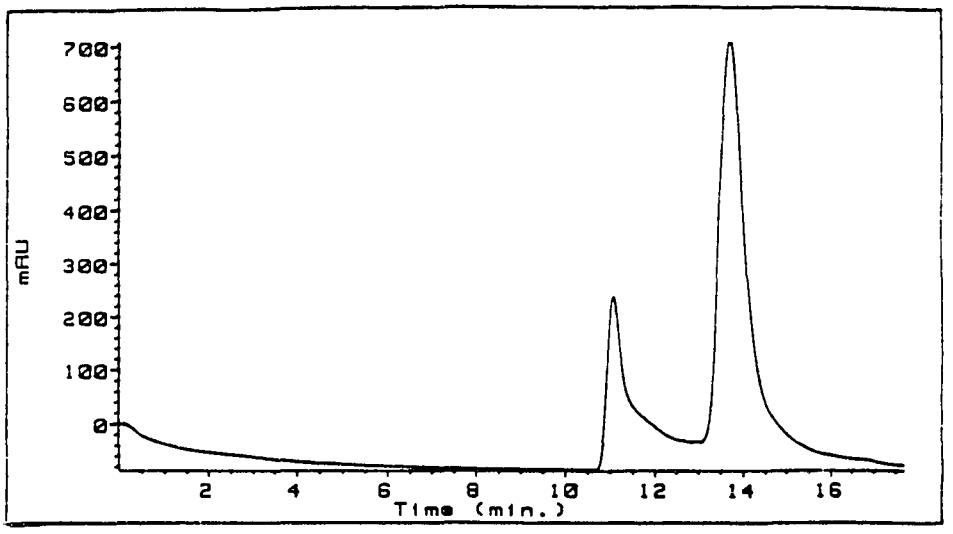

A)

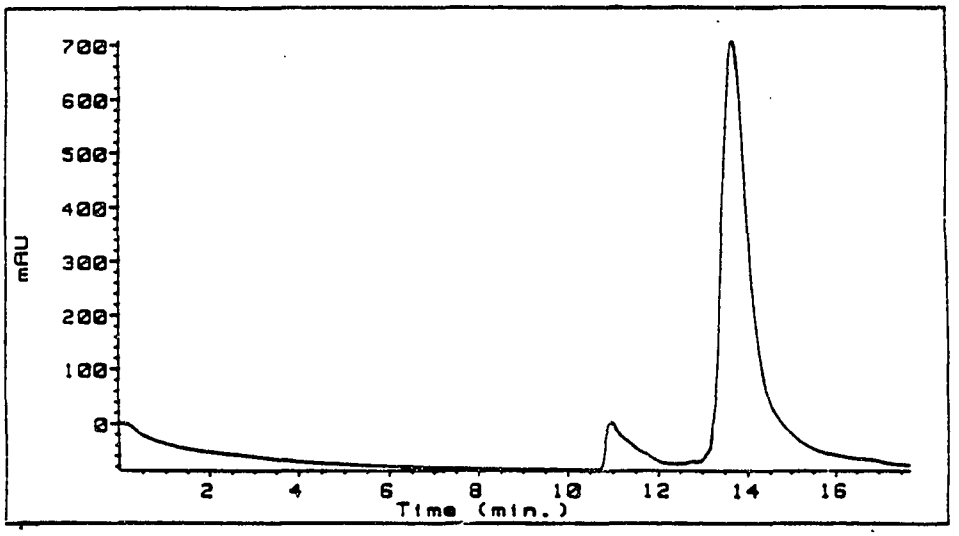

B)

Figure 32: A typical chromatogram for the various L7/L12 cysteine mutants labeled with TMRIA (only C-33), 5-IAF, or IAEDANS (see text for details), or wild type with FITC. A) first chromatography run; B) second chromatography run (of Peak2 L7/L12 reconcentrated from first run eluate).

likely, therefore, that peak one is not in any equilibrium with dimeric (Peak2) L7/L12 (see next chapter for more details). The data therefore agrees with the theory (Oleinikov, Traut, and Makarov, personal communication) that peak one is an unnatural form of L7/L12 that is the by-product of overexpression. The Traut laboratory is presently investigating whether insufficient heat shock protein (GroE) results in the aggregation of overexpressed proteins (personal communication). Finally, Makarov (unpublished, 1992) has putatively determined that Peak1 does not exist in samples of L7/L12 simply prepared by Hamel extraction from wild type ribosomes (described in Chapter 2; not genetically manipulated). This concept is discussed in further detail in the next chapter.

In Figure 33, we see that when C-63 or C-89 are labeled with PMIA, the equilibrium is shifted to a higher state of aggregation. The C89-PMIA sample forms primarily an oligomer that elutes around 12.7 milliliters or, very similar to the 68 kD ellipsoid, BSA (vide infra for more details). The C-63 sample peaks become much broader and peaks one and two become more similar. Conversely, labeling of C-33 with PMIA has little effect on its state of aggregation as its chromatogram looks quite similar to those of other fluorophores bound to the various L7/L12 cysteine mutants (previously shown in Fig. 32). It seems, therefore, that labeling of the C-terminal cysteines with pyrene results in aggregation. Similarly, as mentioned in the materials and methods (Chapter 2), labeling of the C-terminal cysteine mutants with TMRIA leads to an aggregation that can only be prevented by constant presence of high denaturant concentrations. We have not yet tried labeling the C-terminal cysteine mutants with PMIA in the presence of high urea. Each of the SE-HPLC purified proteins are characterized via time-resolved fluorescence in the next section.

Finally, chromatograms for the N-terminal fragment, the C-terminal fragments and the hinge deletion mutant (each illustrated in Fig. 7, Ch. 2) are presented in Figure 34. *The most striking finding was that the hinge deletion mutant eluted at close to the void volume!!* Although Oleinikov et al (1993A) have published crosslinking data stating that the hinge deletion mutant is purely dimeric, both our SE-HPLC data and theirs have demonstrated this unusual elution pattern. The present author finds it

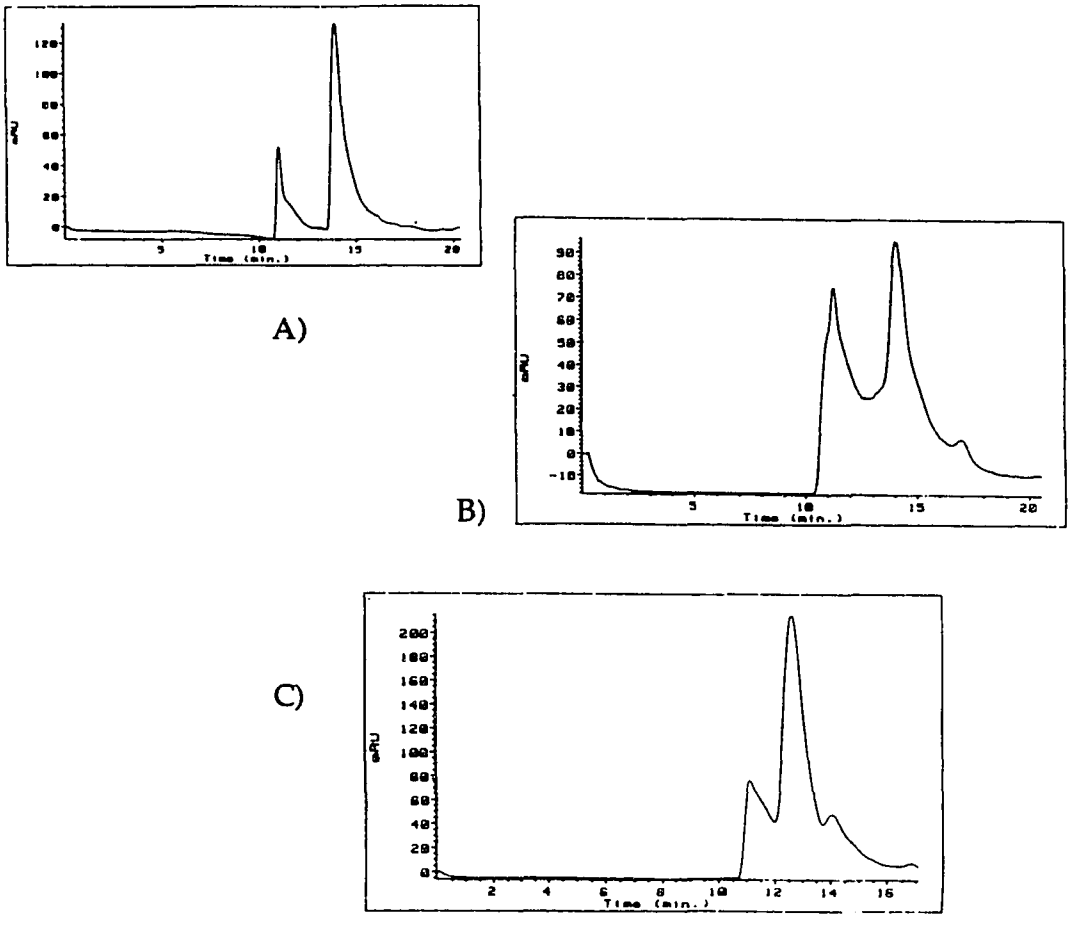

Figure 33: Chromatograms for C-33 (A), C-63 (B), and C-89 (C) each labeled with PMIA (see text for details).

difficult to believe that simple hinge deletion could produce such profound conformational changes that it could make a 21 kD protein elute equivalent

to a >200 kD protein. Our time-resolved fluorescence data presented in the next section bare on this issue. The NTF and CTF proteins either labeled or unlabeled, elute at ~16.5 milliliters and ~18.5 milliliters, respectively. The NTF is dimeric and possesses the amino acids existing in the hinge region as well as the putative coiled-coil region together adding up to a MW of ~11.5 kD. It is therefore not surprising that it elutes with a similar retention time as the methionine oxidized L7/L12 monomer (MW = 12.2 kD). Furthermore,

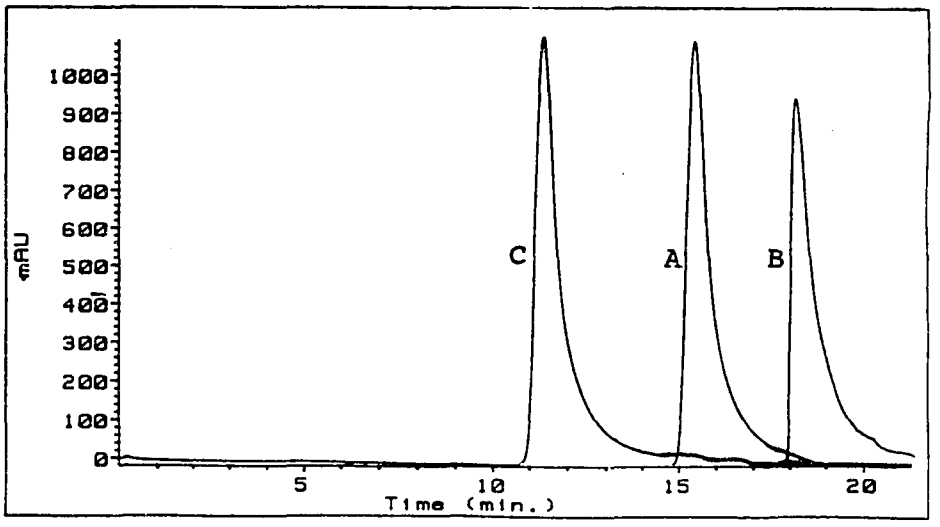

Figure 34: Typical chromatograms for NTF (A), CTF (B), and the hinge deletion mutant (C) (see text for details).

the NTF, like the methionine oxidized L7/L12, appears quite asymmetric in shape, as it elutes equivalent to a sphere with MW of ~20 kD. One should not be surprised by this elution pattern since the NTF and hinge region of L7/L12 are the regions that putatively bestow L7/L12 with elongatedness. Finally, the CTF, being primarily spherical with a MW of 7.1 kD, eluted quite near to that expected for a ~9 kD spherical protein (compare its ~19 milliliter elution to Figure 30). Neither the NTF nor the CTF exhibited any signs of aggregation like the hinge-intact (Peak1) or hinge-deleted mutants of L7/L12.

TIME-RESOLVED FLUORESCENCE CHARACTERIZATION OF SE-HPLC PURIFIED FORMS OF L7/L12. CHARACTERIZATION OF L7/L12 SEGMENTAL MOBILITY.

Time-resolved Fluorescence Characterization of SE-HPLC Purified Forms of L7/L12 C-33, C-63, and C-89 Labeled with 5-IAF. Subsequent to SE-HPLC, the purified forms of L7/L12 could be more quantitatively characterized via time-resolved fluorescence techniques (see Tables 9 and 10). For total purification of the dimeric (Peak2) L7/L12, or methionine oxidized (monomeric) L7/L12, it was necessary to microconcentrate the eluates from the first round of SE-HPLC, and then separate a second time on SE-HPLC.

In Tables 9 and 10, we see that the 5-IAF time-resolved fluorescence data was primarily unaffected by the removal of peak1. The data unequivocally determined that fluorescein, with its four ns fluorescence lifetime, was unable to significantly monitor events much beyond 30 ns. The skewing of χ^2 confidence plots in Figures 27 and 28, towards higher rotational relaxation times does, in fact, reflect decreased accuracy in the dynamic polarization data

Table 9: Comparison of Time-resolved Fluorescence Lifetime Data for SE-HPLC Purified forms of L7/L12 C-33, C-63, and C-89 each Labeled with 5-IAF. *

	Cysteine	τ_1	f_1	τ_2	f_2	χ^2
Peak1	33	4.122	0.995	.001	.005	1.65
"	63	4.092	0.994	.001	.006	1.22
"	89	4.144	0.992	.008	.008	0.82
Peak2	33	4.140	0.998	.001	.002	1.18
"	63	4.080	1.000	-------	-------	0.62
"	89	4.158	1.000	-------	-------	0.72
Peak3	33	4.090	1.000	-------	-------	0.88
	63	4.061	1.000	-------	-------	0.76
	89	4.133	1.000	-------	-------	1.01

*Conditions and symbols as described in Table 6 and in text below.

Table 10: Comparison of Time-resolved Fluorescence Dynamic Polarization Data for SE-HPLC Purified forms of L7/L12 C-33, C-63, and C-89 each Labeled with 5-IAF.*

	Cys	ρ_1	α_1	ρ_2	α_2	r_0	χ^2	S.S.P.
Peak1	33	43.6	0.388	2.21	0.612	0.318	1.00	.156
"	63	30.0	0.419	1.76	0.581	0.340	0.90	.138
"	89	45.2	0.490	2.03	0.510	0.372	1.21	.208
Peak2	33	20.2	0.359	1.82	0.641	0.303	1.15	.145
"	63	15.1	0.288	0.95	0.712	0.356	0.60	.105
"	89	21.0	0.524	1.45	0.476	0.364	0.90	.191
Peak3	33	13.8	0.274	1.82	0.726	0.310	0.70	.097
"	63	14.9	0.300	1.02	0.700	0.345	1.40	.101
"	89	17.9	0.519	1.41	0.481	0.366	1.01	.178

*Conditions and symbols as described in Table 6 and in text below. Steady-state polarizations are averages of at least 4 different preps.

at lower frequencies, i.e., frequencies which weight the emission corresponding to longer lifetimes.

In Figure 35 we see a typical χ^2 confidence plot for 5-IAF covalently attached to peak two (dimeric) L7/L12 C-89. We no longer observe the skewing of χ^2 confidence towards longer rotational relaxation times as observed with samples "contaminated" with the peak one aggregates. Similar results were obtained with the other mutants (data not shown). Furthermore, we see fairly high χ^2 confidence (data not shown) for the global ρ of the Peak1 samples labeled with IAF *suggesting* that Peak1 L7/L12, like Peak2, possesses significant segmental mobility.

Interestingly, removal of peak one had very little effect on the recovered global rotational relaxation time for 5-IAF bound to dimeric L7/L12. The primary reason is simple: very little Peak1 (<10%) existed in the samples labeled with IAF or FITC (recall chromatogram, Fig. 32). The Peak1 aggregate, therefore, promoted the slight skewing of the global rotational

relaxation times to erroneously higher values (recall Table 7). The global rotational relaxation times given in Table 10 should therefore truthfully reflect the segmental global mobility of L7/L12 of ~15-25 ns. The slight variation in global ρ's of IAF samples may reflect one or both of the following: 1) the orientation of the fluorophores with particular axes of rotation; 2) in the case of C-63, skewing of the χ^2 confidence towards more rapid apparent global motions, might be due to the predominance of the rapid local mobility (data not shown). Recall from various discussions earlier in the text, how significant local motion and amplitude can attenuate the accuracy of the determined global rotational relaxation times.

Data for C-12 and C-99 labeled with 5-IAF was not included as they look nearly identical to C-33 and C-63, respectively; we can therefore conclude that the two pairs of cysteine mutants are located in very similar environments. We shall find in Chapter 6 that the C-33 and C-12 mutants labeled with 5-IAF

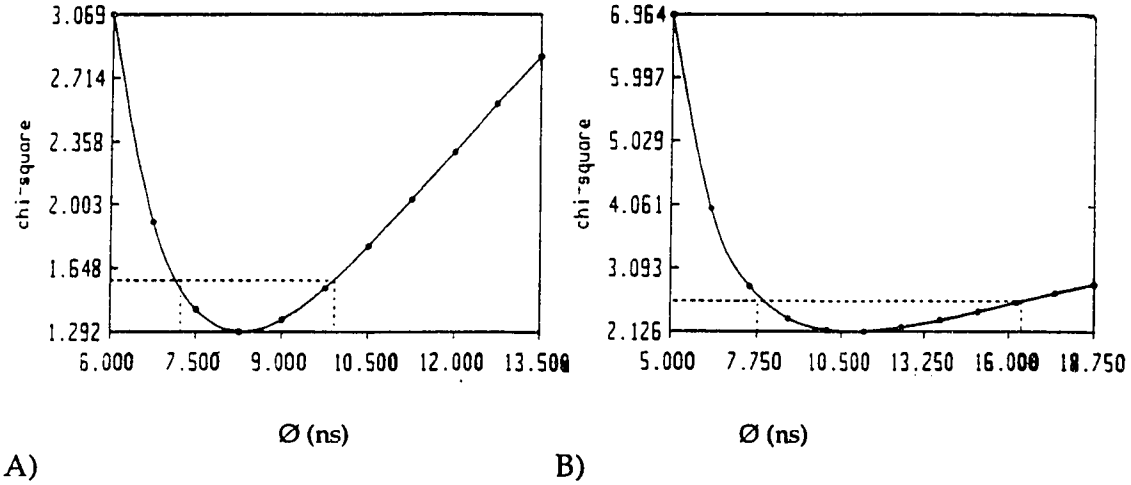

Figure 35: Chi-square confidence plots for the global Ø's of A) pure Peak2 (dimeric) and B) peak one contaminated samples of L7/L12 C-89 each labeled with 5-IAF. Compare to Figs. 27 and 28 and see text for further details.

possess large "local motion" anisotropy amplitudes primarily due to rapid energy transfer between the two fluorophores. When this energy transfer is

abolished via subunit exchange, the 5-IAF fluorescence properties of these two mutants are nearly identical to 5-IAF labeled on C-89. Furthermore, the global rotational relaxation times are increased by three to five ns upon loss of energy transfer, from the values reported in Table 10. What then is the cause of the unusually rapid local motion at the C-63 and C-99 sites? The answer to this question is presently open to speculation.

The data for methionine oxidized L7/L12 cysteine mutants labeled with 5-IAF was also presented in Table 10 and is discussed in more detail in the next chapter. We see that practically no changes are observed in the C63-IAF fluorescence (time-resolved or steady-state polarization) upon methionine oxidation. This phenomenon is explained as follows: the C-terminal domains (within which the C-63 exists) are rotating independently in both the dimeric and monomeric forms of L7/L12. Upon dissociation, this segmental "global" mobility is practically unchanged (recall from SE-HPLC data that shape is hardly changed upon dissociation). Furthermore, no changes in the local motion should occur as the C-terminal domains are unlikely to be involved in the dimerization process. Then why do we see changes, albeit slight, in the polarization of C89-IAF upon dissociation? The changes observed with C89-IAF upon dissociation are quite minuscule (compare to C33-IAF); nevertheless, as mentioned in the previous paragraph, C63-IAF depolarization is dominated by local motion and likely monitors with much less accuracy (less fractional anisotropy amplitude) the global motion than 5-IAF labeled at C-89. Furthermore, it's possible that the segmental mobility monitored by 5-IAF at C-63 is quite different than at C-89 (recall significance of fluorophore orientation with respect to rotational axes).

In the case of C33-IAF, three conspicuous changes occur upon dissociation:

1) The global rotational relaxation time becomes considerably less. If the N-terminal fragments (NTF's) are responsible for dimerization, then we could expect segmental mobility of a monomeric NTF (~50% reduction in molecular weight of rotating unit) instead of a dimeric NTF upon dissociation subsequently resulting in a reduced ρ;

2) A more rapid and higher amplitude local motion is observed. Similar increases in local motion occur in tryptophan-containing proteins upon dissociation as tryptophan is usually somewhat buried in the interface (i.e., see Xu and Weber, 1982). We might therefore conclude that the 5-IAF is somewhat restricted in mobility when located at the C-33 position of dimeric L7/L12 (i.e., intersubunit interaction of 5-IAF);

3) An unusual amount of missing anisotropy is still present, even when no intersubunit energy transfer should exist. It seems quite likely that a new, rather undetectable third form of rapid depolarization is unleashed upon dissociation, which might partially explain the large increase in local anisotropy amplitude.

The dimer/monomer equilibrium of L7/L12 is described in detail in the following chapter. *Here, methionine oxidized L7/L12 was presented as further evidence for independent segmental mobility of the two C-terminal domains and a dimeric N-terminal domain within dimeric L7/L12.*

Additional direct proof for independent C-terminal domain mobility was accomplished by an intersubunit cysteine oxidation at the 89 positions and subsequently labeling with FITC; both methods were described in detail in Chapter Two. Oxidation of the cysteines *prior* to labeling with FITC was necessary since FITC was found to react with the cysteines (data not shown). The global rotational relaxation time reported by FITC increases from 24 ns to 32 ns, as the FITC (located at least partially in a C-terminal domain; vide infra)

now monitors segmental mobility of two C-terminal domains oxidized to one another (data not shown). Furthermore, the steady-state polarization increases from .232 to .246 when the C-terminal domains are oxidized to each other. Although we are certain that some of the FITC binds to the N-terminal domain of L7/L12, the result indicated that much of the FITC binds to the C-terminal fragment (see next chapter for more details). Verification of lack of interdimeric oxidation was accomplished by SE-HPLC (data not shown). An even greater effect might be expected when oxidized C-89 is labeled with IAEDANS at its C-terminal lysine (see next subsection). The possibility of conformational changes in C-89 compared to wild type L7/L12 is investigated in the next chapter.

Time-resolved Fluorescence Characterization of SE-HPLC Purified, IAEDANS Labeled Forms of C-33, C-63, and C-89. The 5-IAF data presented clear evidence for a 15-22 ns segmental mobility of purified dimeric L7/L12. It seemed likely that the IAEDANS probe, with its longer fluorescence lifetime, might be more drastically affected by the presence of the Peak1 aggregate. In Tables 11 and 12, we see the time-resolved fluorescence data for various SE-HPLC separated forms of L7/L12 C-33, C-63, and C-89 labeled with IAEDANS. No measurements have yet been acquired with the C-12 or C-99 mutants labeled with IAEDANS. Methionine oxidation was performed with the C-89 and C-63 mutants labeled with IAEDANS and subsequent time-resolved fluorescence data looked very similar to the 5-IAF data (therefore, not included in Tables 11 or 12; see next chapter for details).

The data in Tables 11 and 12 verify that the Peak1 aggregate, which was approximately 30% of the total concentration of L7/L12 reported in Table 7, led to our erroneous suspicions that IAEDANS was monitoring a more elongated rotational mode of dimeric L7/L12. The dynamic polarization

values reported in Table 12 also verify that L7/L12 possesses a segmental rotational relaxation time of ~15-27 ns, just like the 5-IAF data. The ~12 or 13 ns lifetime of IAEDANS monitors nearly the exact same rotational modalities on L7/L12 as the ~4.1 ns lifetimes of 5-IAF. Similarly, both IAEDANS and 5-IAF data demonstrate a slightly higher global ρ for probes labeled in the NTF than probes labeled within the CTF. The data can be explained in that the NTF has a more prolate shape (recall Fig. 29) than that of the CTF.

The slightly higher global ρ values obtained with IAEDANS probably reflects either slight monitoring of a global tumbling, or else incomplete

Table 11: Comparison of Time-resolved Fluorescence Lifetime Data for SE-HPLC Purified forms of L7/L12 C-33, C-63, and C-89 each Labeled with 5-IAEDANS. *

	Cysteine	τ_1	f_1	τ_2	f_2	χ^2
Peak1	33	13.502	0.986	.001	.014	2.41
"	63	11.988	0.994	.001	.006	1.22
"	89	11.608	1.000	-------	-------	0.66
Peak2	33	12.874	0.997	.001	.003	1.00
"	63	12.270	1.000	-------	-------	0.66
"	89	12.010	0.998	.001	.002	1.55

Conditions and symbols as described in Table 6 and in text below.

Table 12: Comparison of Time-resolved Fluorescence Dynamic Polarization Data for SE-HPLC Purified forms of L7/L12 C-33, C-63, and C-89 each Labeled with 5-IAEDANS.*

	Cys	ρ_1	α_1	ρ_2	α_2	r_0	χ^2	S.S.P.
Peak1	33	354.9	0.439	5.57	0.561	0.269	1.14	.167
"	63	110.9	0.223	4.55	0.777	0.265	0.45	.098
"	89	96.0	0.267	4.31	0.733	0.267	1.64	.100
Peak2	33	27.5	0.270	3.02	0.730	0.267	3.12	.075
"	63	16.1	0.295	1.96	0.705	0.268	3.20	.059
"	89	24.2	0.257	2.72	0.743	0.272	1.71	.072

*Conditions and symbols as described in Table 6 and in text below. Steady-state polarizations are averages of at least 4 different preps.

removal of Peak1. Conversely, as opposed to 5-IAF, the IAEDANS monitors with sharp χ^2 confidence (data not shown), a global rotational relaxation time for Peak1 L7/L12 of ~100-350 ns depending on the location of the fluorophore.

It is quite interesting that IAEDANS fluorescence is especially affected when located in the C-33 position in Peak1 L7/L12; the fact that its lifetime is signif-icantly enhanced, indicates that it is in a different environment than when bound to Peak2. The data might indicate that aggregation within Peak1 occurs via the NTF's or conversely, the NTF's are completely unfolded (and swollen with water). In all cases, IAEDANS local mobility is apparently restricted in peak one L7/L12 and its fluorescence lifetime is more indicative of more hydrophobic environment. Hence, the time-resolved fluorescence data support the idea of an aggregated form for Peak1 L7/L12. According to the IAEDANS data, Table 4, and the SE-HPLC data, Peak1 L7/L12 fits well as a >100 kD prolate octamer with an axial ratio of >4:1. The author shall leave the more quantitative characterization of Peak1 to future investigators (although, see next chapter for more details).

At this point it seemed unequivocal to us that dimeric L7/L12 possesses segmental global mobility, presumably via its flexible hinge, in which the individual C-terminal domains and dimeric N-terminal domain are able to rotate, wobble, or flex. Preliminary results were also recently obtained with disulfide (oxidized) bridged (like with FITC on page 129) dimeric C-89 L7/L12 labeled with IAEDANS at its C-terminal lysine (recall experiments in section starting page 98). The lifetime of IAEDANS increases ~1.0 ns (from ~15 ns to ~16 ns) upon intrasubunit disulfide bondage. Furthermore the IAEDANS steady-state polarization increases from .059 (compare to Table 5B, pg. 99 where Peak1 not removed) to .082 corresponding to an increase in global rotational relaxation time from ~28 ns to ~52 ns (data not shown). The data

once again demonstrated that the two C-terminal domains rotate independently of one another and furthermore, a fairly similar mode of rotation can exist when the two domains are oxidized to one another (i.e., "free" rotation of the disulfide oxidized domains). This piece of data is still incomplete as we have not yet determined the extent of disulfide formation. Finally, SE-HPLC results indicated that no intersubunit disulfide formation had occurred between two dimers of L7/L12 (i.e., no sign of higher aggregates; data not shown). Very similar results are reported later in this chapter with the non-covalent probe Bis-ANS.

Interestingly, even with an ~13 ns fluorescence lifetime such as IAEDANS, which is able to monitor rotational events up to 130 ns, we were still unable to monitor any significant global tumbling (as opposed to segmental domain mobility) of the entire dimeric L7/L12. The data therefore suggested (from Table 4) that at the 4-13 ns time-scale, perhaps L7/L12 tumbled globally as an ellipsoid with axial ratio much greater than 4:1 (a >8:1 axial ratio oblate ellipsoid should be easily monitored by IAEDANS, whereas, with proper absorption or emission dipole alignment, a >>6:1 prolate might go unnoticed). Furthermore, the fact that IAEDANS can accurately monitor a global relaxation time of greater than 350 ns (recall Peak1Table 12) implies that it should be able to detect an ellipsoidal L7/L12 with an axial ratio of greater than 10:1 (from Table 4). *Clearly, an ellipsoid of L7/L12 with axial ratio greater than 7:1 is unfeasible. (Figure 29). The considerable local mobility of the covalently attached probes should give an excellent estimation of the mean harmonic rotational relaxation time of any feasible shape of dimeric L7/L12 with axial ratio up to 10:1* (recall, ρ_{h_v} Table 4 and Equation 41). If the axial ratio of L7/L12 is much greater than 10:1 the IAEDANS' fluorescence lifetime might be insufficient to *significantly detect it*, which might explain

the very slight increase in global ρ relative to the 5-IAF data (see pyrene data below). Since an axial ratio for dimeric L7/L12 greater than 7:1 is unfeasible, it seems likely that the slight increase in global ρ's detected by IAEDANS (16-27 ns, in comparison to 5-IAF, which detected segmental ρ's of 15-23 ns) might rather reflect a more bended, *average* conformation of L7/L12 undergoing *global tumbling* (vide infra).

Time-resolved Fluorescence Characterization of SE-HPLC Purified, 1-Pyrenemethyl Iodoacetamide (1-PMIA) Labeled Forms of C-33, C-63, and C-89. In Search of L7/L12 Global Tumbling. As mentioned previously, an ~120 ns probe such as a typical pyrene probe should be able to monitor events up to ~1200 ns. From Table 4, even an L7/L12 with maximum axial ratio of 20:1 should be easily monitored with 1-PMIA. In Tables 13 and 14, time-resolved fluorescence data for L7/L12 C-33, C-63, and C-89 labeled with 1-PMIA are presented. Neither C-12 nor C-99 have been labeled with 1-PMIA. Furthermore, no methionine oxidations have been performed on L7/L12 labeled with 1-PMIA (as opposed to the 5-IAF and IAEDANS labeled samples).

As described earlier (Table 6 notes), we have not rigorously attempted to remove all of the ambient oxygen from our pyrene-containing samples. The lifetime values for pyrene labeled samples presented in this dissertation cannot, independently, be used for any quantitative determination of the local environment of their binding sites. The values given are only semi-quantitative in that they are all the result of samples that have been flushed with 99.999% argon for one minute. Hence, the pyrene lifetimes are essentially only used for quantitative determination of the various rotational relaxation times. In all cases, we obtain average fluorescence lifetimes between between 90 and 140 ns, which is fairly typical for pyrene probes rather exposed to the solvent (Knopp and Weber, 1969; Reinhart and Lardy, 1980)

Table 13: Comparison of Time-resolved Fluorescence Lifetime Data for SE-HPLC Purified forms of L7/L12 C-33, C-63, and C-89 each Labeled with 1-PMIA. *

	Cys	τ_1	f_1	τ_2	f_2	τ_3	f_3	χ^2	τ
Peak1	33	235	0.398	99.8	.283	6.9	.319	0.22	124
"	63	178	0.522	47.3	.204	5.5	.274	1.22	104
"	89[1]	137	0.597	40.4	.256	4.3	.147	2.10	93
Peak2	[a] 33	167	0.816	-----	-----	6.7	.184	2.18	138
	[b] 33	154	0.742	-----	-----	5.4	.258	2.40	116
"	[a] 63	149	0.558	28.5	.156	3.9	.286	1.85	89

*Conditions and symbols as described in Table 6 and in text below. Unless otherwise indicated, each value given was result of two separate preparations.

[1]As shown in Fig. 33, insignificant amounts of true peak one C89-Pyr could be isolated; similarly, no true Peak2 can be isolated as labeling with pyr at C-89 results in the intermediate peak described here. This sample was purified and measured only once.

[a]After one SE-HPLC separation of Peak1 from Peak2, ~20% of Peak1 still exists in Peak2 eluates.

[b]After second SE-HPLC purification of peak two, less than one or two % Peak1 exists in Peak2 eluates. This sample was purified and measured only once.

Table 14: Comparison of Time-resolved Fluorescence Dynamic Polarization Data for SE-HPLC Purified forms of L7/L12 C-33, C-63, and C-89 each Labeled with 1-PMIA*

	Cys	ρ_1	α_1	ρ_2	α_2	r_0	χ^2	S.S.P.
Peak1	33	1041	0.498	3.3	0.502	0.126[F]	2.66	.068
"	63	624	0.732	21.0	0.268	0.111	1.60	.064
"	89[1]	423	0.218	1.6	0.782	0.126[F]	5.22	.049
Peak2	[a] 33	888	0.229	24.3	0.771	0.132	0.99	.030
"	[b] 33	42	0.512	2.8	0.488	0.126[F]	5.66	.016
"	[a] 63	567	0.310	21.5	0.690	0.134	0.95	.025

*Conditions and symbols as described in Tables 7/13, and in text below unless otherwise indicated. Polarizations are averages of three separate samples except "Peak1 C89-pyr" and Peak2 C33-pyr (b), which were both only purified and measured once.

[F]In some cases, for reasons not fully known, the r_0's needed to be fixed because of impossibly high values obtained from analysis of the data.

and is expected in our case if the mutations were within random coil loop structures in L7/L12.

The data in Table 14 indicate that the Peak1 aggregate possesses a global rotational relaxation time of >1000 ns. Since 1040 ns (Table 14) is close to the maximum possible for a 124 ns average lifetime of 1-PMIA bound to C33, the actual global rotational relaxation time of Peak1 might be significantly greater. The SE-HPLC data suggest that Peak1 is quite possibly greater than 500 kD (or else an extremely unusual conformation of L7/L12). The Peak1 pyrene and IAEDANS data strongly support the idea of a high molecular weight form of L7/L12: 1) If Peak1 was an unfolded form of L7/L12 (i.e., random coil) it would elute at low volumes as is the case, but it would appear as mostly pure local motion by time-resolved fluorescence (see Gratton et al, 1992); 2) we will find in the next chapter that Peak1 secondary and tertiary (as judged from resistance to Gu-HCl denaturation) are still quite intact; 3) in all cases, the lifetimes of the fluorophores are *greater in Peak1* than Peak2 or Peak3; the lifetime of *pyrene or IAEDANS will always decrease in more polar,* solvent exposed environments as described earlier. The data therefore suggest once again that Peak1 is some sort of large aggregate form of L7/L12 (see Conclusions section of this chapter for quantitative discussion). Finally, it is interesting to note that in one Peak1 sample (from SE-HPLC) and both singly purified (from SE-HPLC) Peak2 samples, the usual ~22-24 ns segmental global rotational relaxation times are observed in addition to ρ's of greater than 600 ns (see Tables 13 and 14). In Figure 36 a χ^2 confidence plot is presented, indicating that the 22-24 ns segmental ρ is predominantly monitored even when using a 120 ns lifetime probe. The data also suggests that C-terminal domains are freely moving even in Peak1 samples. Although, we did not see any segmental 24 ns ρ's with IAEDANS-labeled Peak1 samples (Table 12), the

conspicuous increase in local ρ is most likely attributed to an average between the usual ~1.5 ns local ρ and the usual ~24 ns segmental ρ (data not shown).

The Peak2 data presented in Table 14 demonstrate the necessity for complete removal of Peak1 L7/L12 in determining meaningful information from pyrene fluorescence. Similar, but not so drastic effects were seen with

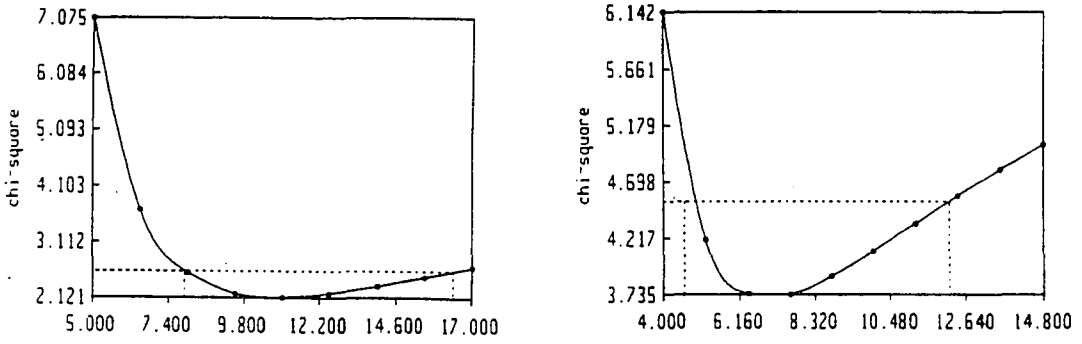

Figure 36: Chi-square confidence plots for the segmental Ø's of A) Peak1 C-63 pyr or B) singly purified Peak2 C-33-pyr. See text for further details.

IAEDANS labeled samples (data not shown). Essentially, after two cycles of SE-HPLC, nearly complete removal of Peak1 L7/L12 C33-pyrene was evident. The global rotational relaxation time given in Table 14 for doubly HPLC-purified Peak2 L7/L12 C33-pyrene is only 42 ns. The 42 ns global ρ for dimeric L7/L12 C33-pyrene is somewhat higher than that obtained with C33-IAEDANS (~27 ns) or C33-IAF (~22 ns). The average fluorescence lifetimes of 1-PMIA, IAEDANS, and 5-IAF each independently bound to dimeric C-33 are ~120, 13, and 4 ns, respectively and so the data might be explained in one of the following ways: 1) with increasing fluorescence lifetime of the probe, a

simultaneous increase occurs in the sensitivity to incomplete removal of a large Peak1 aggregate; 2) with increasing fluorescence lifetime of the probe, a simultaneous increase in sensitivity to a particular rotational modality of L7/L12 occurs. After two rounds of SE-HPLC, not greater than *one or two* percent Peak1 could be contaminating the Peak2 samples (data not shown). If we assume that Peak1 L7/L12 has a global rotational relaxation time of at least 1000 ns with relative fractional anisotropy amplitude of 50%, than from Equations (4) and (6), the global rotational relaxation time of pyrene bound to dimeric (Peak2) C33 could not increase by more than a couple ns. The data therefore strongly suggested that a longer lifetime probe seemed to weigh more strongly a rotational mode of L7/L12 slightly slower than that characterized earlier as hinge-induced flexing or wobbling of the C- or N-terminal domains. We can attribute this slightly slower rotational mode of L7/L12 to either global tumbling of its average overall conformation or to increased sensitivity to a slower segmental mobility (see Conclusions of this chapter for more detail). The fact that we saw a 24 ns ρ in some Peak1 or singly-purified Peak2 samples indicates that this 42 ns mobility was somewhat obscured earlier by the much slower global tumbling of Peak1.

Time-resolved Fluorescence Characterization of the L7/L12 Cys-89 Hinge-deletion (Δ35-52) Mutant Hydrodynamics. Evidence for a Rigid Prolate with an Axial Ratio of ~4:1. As a control for L7/L12 hinge mobility, a mutant with 17 amino acids deleted from its putative hinge region (Δ35-52) and a cysteine substitution at position 89, was labeled separately with various fluorescent probes. Since we know from SE-HPLC results that labeling of C-89 with pyrene leads to aggregation (page 122), we have not included this sample in any subsequent studies. In Tables 15 and 16, the time-resolved fluorescence data for L7/L12 Δ35-52 C-89 successfully labeled with 1,5-IAEDANS or 5-IAF is

presented. L7/L12 Δ35-52 C-89 has also been characterized with the non-covalent probe Bis-ANS and its subsequent fluorescence data is presented two subsections from now. Data for hinge-intact L7/L12 C-89 labeled with 5-IAF or IAEDANS were presented earlier (see Tables 6 and 7; 9-12). Several interesting conclusions can be made from Tables 15 and 16. First, however, several points must be considered. Recall the SE-HPLC chromatograms of L7/L12 Δ35-52 C-89 labeled with 5-IAF or IAEDANS look identical (Fig. 34; page 123). The chromatograms on page 123 indicated that L7/L12 Δ35-52 C-89 is either a higher aggregate form of L7/L12 or else, possesses enormous conformational differences from hinge-intact forms of L7/L12. On page 123, we doubted that a conformational change, such as increased rigidity upon hinge-deletion, could account for such an enormous decrease in elution volume (~void volume!). Since SE-HPLC is primarily sensitive to relative Stokes radii (R_s, recall SE-HPLC section above), the Stokes radii of the 109 kD lactate dehydrogenase

Table 15: Fluorescence lifetime data for IAEDANS or 5-IAF bound to L7/L12 Δ35-52 C-89*

Probe Used:	τ_1	f_1	τ_2	f_2	χ^2
5-IAF	3.6	0.99	0.001	0.01	0.99
IAEDANS	13.4	1.00	---------	---------	0.82

*Temperature as usual 20°C; cut-on filters as described earlier for 5-IAF or IAEDANS; excitation for 5-IAF was 488nm and for IAEDANS, 351 nm (see Chapter 3 or text below for more details). Symbols and units as previously described (i.e., Table 6). Data are the result of averaging two separate preps.

Table 16: Dynamic polarization data for IAEDANS or 5-IAF bound to L7/L12 Δ35-52 C-89*

Probe Used:	ρ_1	α_1	ρ_2	α_2	r_0	χ^2	S.S.P.
5-IAF	18.1	0.363	1.32	0.637	0.276	1.60	0.111
IAED	70.1	0.278	4.10	0.722	0.251	0.92	0.102

*Temperature as usual 20°C; cut-on filters as described earlier for 5-IAF or IAEDANS; excitation for 5-IAF was 488nm and for IAEDANS, 351 nm (see Chapter 3 or text below for more details). Symbols as previously described (i.e., Table 7). Data are the result of two separate preps except polarizations, which are average of three preps.

(elutes at ~12 minutes) is calculated from its putative translational frictional coefficient (Cantor and Schimmel, 1980), f/f_0, which equals 1.127 (from Table 8). Since f_0 for a hydrated spherical 109 kD protein is given by:

$$f_0 = 6\pi\eta(3V_h/4\pi)^{1/3} \quad (42)$$

where η is the viscosity of the medium (one centipoise = 0.01 g $cm^{-1}sec^{-1}$), and V_h is the hydrated molecular volume of the spherical protein in $Å^3$ calculated from:

$$V_h = (M/N_0)(V_2 + \delta_1 V_1) \quad (43)$$

where M is the molecular weight, N_0 is Avogadro's number, V_2 is the partial specific volume of the protein (0.741 ml/g for lactate dehydrogenase, V_1 is the partial specific volume of water (inverse of its density), and δ_1 is the degree of hydration (~0.3 g water/g lactate dehydrogenase). We can therefore calculate a V_h of 1.9 x 10^5 $Å^3$ for lactate dehydrogenase. Hence, f_0 equals ~7 x 10^{-8} g sec^{-1} and f = ~7.8 x 10^{-8} g sec^{-1} (since $f/f_0 = 1.127$ from Table 8) and R_s for a hydrated ellipse is given by:

$$f = 6\pi\eta r_h F \quad (44)$$

where F (Perrin shape factor) = f/f_0, η is the viscosity of the medium in units of 1 cP, and r_h is the *mean* Stokes radius of a hydrated ellipsoid. Hence, we can expect a Stokes radius of ~36.7 Å for lactate dehydrogenase. Furthermore, the Stokes radius of L7/L12 Δ35-52 C-89 must be significantly greater than ~36.7 Å (close to 45Å from Figure 30); its frictional coefficient ratio, F, *assuming a dimeric molecular weight of 21 kD*, can be calculated from the Stokes radii initially ignoring shape factors:

$$f = 6\pi\eta r_h \quad (45)$$

where r_h is the hydrated Stokes radius, equal to ~45Å for L7/L12 Δ35-52 C-89 as described above. Hence f equals 8.4 x 10^{-8} g sec^{-1}. Since f_0 equals 3.8 x 10^{-8} g/sec for a 21 kD hinge-deleted L7/L12 (calculated from equations 42 and 43

assuming δ = 0.3 g water/g protein, and v = 0.75 ml/g), the frictional coefficent ratio, f/f_0 (= F = J. Perrin shape factor), would equal 2.2. If the L7/L12 Δ35-52 C-89 is only 21 kD, then it would (from J. Perrin's shape factor equations shown in Cantor and Schimmel, 1980, page 561) theoretically possess an axial ratio of >25:1, which is impossible for a hinge-deleted form of L7/L12 (*from Figure 29 the maximum axial ratio possible for a hinge-deleted dimeric L7/L12 would be 4:1*). Hence, we might conclude that L7/L12 Δ35-52 C-89 exists as a somewhat higher aggregate form than a dimer. According to Oleinikov et al (1993A), crosslinking of L7/L12 Δ35-52 C-89 with dimethylsuberimidate results in a subsequent SDS-PAGE band corresponding to molecular weight of ~24 kD. Hence, their data strongly suggested that higher aggregates than a dimer of this protein were unlikely.

The SE-HPLC and crosslinking data obviously conflict. Like the case of Peak1 hinge-intact L7/L12 (pages 131-135), one might argue that L7/L12 Δ35-52 C-89 elutes earlier because of a somewhat unfolded secondary (2°) or tertiary (3°) structure. We shall see in the next chapter that L7/L12 Δ35-52 C-89 does in fact, appear to have a somewhat unfolded 2° and 3°. In Chapter 6, we discover that L7/L12 Δ35-52 C-89 in fact has significant (even rather strong) quaternary (4°) structure in agreement with Oleinikov et al (1993A).

With the above considerations in mind, let us now interpret the fluorescence data presented in Tables 15 and 16. First, a significant decrease in the fluorescence lifetime of C89-IAF occurs when the hinge is deleted (from 4.2 ns to 3.6 ns). The data were highly suggestive of excited-state reactions such as energy transfer and/or collisional quenching with neighboring amino acids upon deletion of the flexible hinge region. We find in Chapter 6 that significant amounts of both energy transfer and collisional quenching occur among 5-IAFs labeled at the C-89 position in the hinge deleted samples. The

fact that energy transfer can only occur between IAFs labeled at C-89 if the flexible hinge is removed, indicated that flexibility is essential for significant distance separation of the C-terminal domains (see Chapter 6 for more details). We shall also find out in Chapter 6 that the collisional quenching of 5-IAF is with amino acids on the neighboring subunit.

Interestingly, the IAEDANS bound to L7/L12 Δ35-52 C-89 has an *increased* fluorescence lifetime relative to when the hinge is present. Two possible explanations for the result are given: either 1) IAEDANS is buried between two subunits when bound to a "normal" dimeric L7/L12 Δ35-52 C-89, or 2) IAEDANS is buried between two or more subunits when bound to an "abnormal" aggregated form of L7/L12 Δ35-52 C-89. The dynamic polarization data in Table 16 might allow us to distinguish (vide infra).

Three obvious distinctions can be made between hinge-intact dimeric L7/L12 C89-IAF (Table 10) and L7/L12 Δ35-52 C89-IAF (Table 16): 1) the limiting anisotropy is reduced from 0.37 to 0.27, respectively; 2) the fractional anisotropy contribution of the former is ~48% and in the latter, 64%; 3) the global ρ monitored is reduced from ~22 ns to ~18 ns, respectively. All three distinctions can be partially explained by rapid energy transfer. In case one, much of the missing anisotropy with the L7/L12 Δ35-52 C89-IAF samples is caused by rapid energy transfer between the IAFs (explained on pgs. 85-88; also, see Chapter 6) and some of it is caused by increased local motion due to attenuated (with respect to resistance to Gu-HCl denaturation) secondary/tertiary structure (Chapter 5) when the hinge is deleted. Rapid energy transfer and increased local motion due to attenuated secondary or tertiary structure explains the large change in fractional contribution of the anisotropy associated with the local motion (i.e., case two). Why do we see a decrease in the global rotational relaxation time when the hinge is deleted?

We know from earlier discussions (recall Table 4) that no rotational axis in an ellipsoid can be monitored by any fluorescence probe, as a ρ of less than 95% of that expected for a sphere of equivalent volume. The expected global ρ of a spherical 21 kD (such as dimeric L7/L12 Δ35-52 C-89) protein with specific volume of 0.75 and hydration of 0.3, is ~27 ns at 20°C. In Chapter 6, we find that this case is a drastic example of how energy transfer can effect the reported global rotational relaxation time (recall ρ_T, pgs. 84-88) as the ρ_T between IAFs located at C-89 on L7/L12 Δ35-52 is ~8 ns (see Chapter 6). This phenomenon is obviated when one looks at the rather broad χ^2 confidence plot of L7/L12 Δ35-52 C89-IAF in Figure 37. The true global rotational relaxation time of L7/L12 Δ35-52 C89-IAF, in the absence of energy transfer is ~28 ns at 20°C. The data therefore suggest that 5-IAF bound to L7/L12 Δ35-52

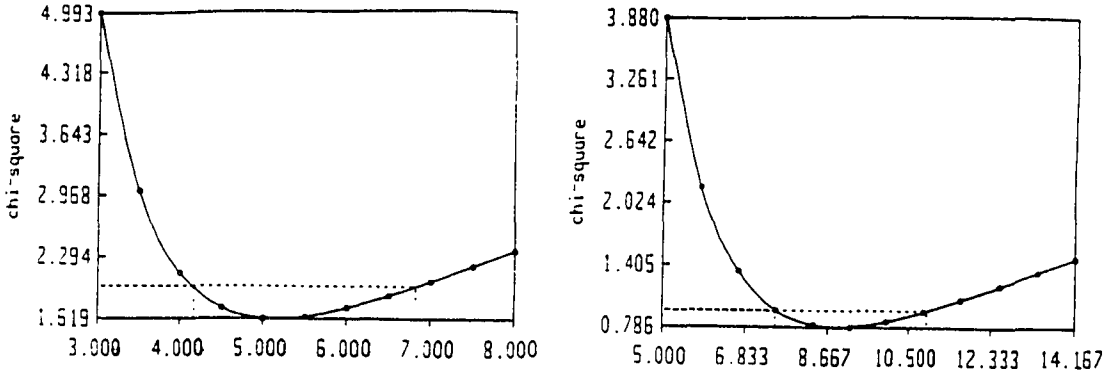

Ø Ø

A) B)

Figure 37: Chi-square confidence plot of apparent rotational relaxation time of A) fully 5-IAF labeled L7/L12 Δ35-52 C89 or B) L7/L12 Δ35-52 C89-IAF exchanged with 10X unlabeled and reduced L7/L12 Δ35-52 C89.

C-89 monitors either a rather spherical rotating protein, or that the 5-IAF is somewhat preferentially aligned with a rather short axis of rotation of a more

ellipsoidal protein. Although, the enormous local motion of 5-IAF bound to the hinge deletion mutant makes it rather difficult to imagine how the fluorophores' transition dipoles could still be aligned so normal to a single axis of rotation. One might wonder at this point if a small amount of segmental flexibility still persists with the hinge deletion mutant.

When IAEDANS is covalently attached to C-89 on L7/L12 Δ35-52, its fluorescence lifetime is considerably longer than that of 5-IAF (13 ns as opposed to 3.7 ns) and we might therefore expect to monitor a different rotational mode of the protein. Furthermore, it is not difficult to imagine that the IAEDANS should have a somewhat different direction of its electronic transition dipole than 5-IAF, and hence could be monitoring a different rotational axis. In Table 16, we see that IAEDANS does in fact report a significantly greater rotational relaxation time of ~70 ns (compare to hinge-intact L7/L12 C89-IAEDANS data in Table 12). Furthermore, very little changes were apparent in the associated fractional anisotropy amplitudes or limiting anisotropy, as opposed to the 5-IAF just described above. The local rotational relaxation time when compared to hinge-intact is somewhat greater, possibly indicating some restricted mobility. The restricted mobility is probably due to the same reasons indicated above for the increased fluorescence lifetime (i.e., intersubunit interaction). It is obvious that IAEDANS and 5-IAF sense quite different environments when bound to L7/L12 Δ35-52 C-89; both are probably the result of some sort of intersubunit interaction (more in Chapter 6).

Since energy transfer is negligible, what can we conclude from the 70 ns global rotational relaxation time monitored by IAEDANS bound to L7/L12 Δ35-52 C-89? From equations 30-41, the 70 ns global ρ for a 21 kD dimeric L7/L12 Δ35-52 C89-IAEDANS and the ~28 ns global ρ detected by 5-IAF, fit

excellently to a rigid prolate protein with axial ratio of 4:1. Furthermore, IAEDANS bound to hinge deleted L7/L12 C89 exhibited a significantly sharper χ^2 confidence for its global ρ than IAEDANS bound to to hinge-intact L7/L12 C-89 (data not shown); the data provided further evidence for the IAEDANS in the C-terminal domains sampling a more extensive range of freedom when the hinge was intact in L7/L12.

Hence, the fluorescence data presented in this subsection, the analytical model described in Figure 29 (and pages 111-113), and the crosslinking data of Oleinikov et al (1993A), are all consistent with a rigid prolate L7/L12 Δ35-52 with an axial ratio of ~4:1. The only ambiguity presented in this subsection (seen also in Figure 34) is the SE-HPLC data. We shall confront this ambiguity later.

Time-resolved Fluorescence Characterization of the Hydrodynamics of L7/L12 NTF and CTF Fragments. The Extent of Hinge-promoted Angular Mobility in L7/L12. Recombinant N-terminal fragments of L7/L12 (NTF's), comprising amino acid residues 1-53, and C-terminal fragments (CTF's), comprising residues 52-120, were recently created in the laboratory of Dr. Robert Traut (recall Figure 7 in Chapter Two). The Traut laboratory is currently characterizing cysteine mutant forms of NTF, but in this chapter we present data on "cysteine-less" NTF labeled with FITC using the same FITC labeling procedure described in detail earlier. Furthermore, the Traut laboratory is currently characterizing a CTF with no cysteine substitutions. We present material in this chapter for CTF C-89 already characterized somewhat in the Traut laboratory (unpublished) and in the present study (next chapter).

The CTF was labeled with 5-IAF via the same protocol already described in Chapter Two for iodoacetamide labeling and the labeling

efficiency is as usual, nearly 100%. Labeling of NTF with FITC at pH 9.0 results in an efficiency of ~0.15 FITC/(L7/L12) subunit, indicating very indirectly that ~30% of the typical ~0.5 FITC/(L7/L12) subunit obtained with wild type L7/L12 are bound to the NTF (recall Table 3 above; Figure 17; see Chapters 5 and 6 for more details). Hence, intersubunit energy transfer should be minuscule (since 15% of the subunits possess FITC, ~15% of the dimers *that possess a FITC (see next chapter for details of the Bernoulli distribution equations)*, will possess two FITCs that may undergo intersubunit homo-FRET (see also Chapters 5 and 6).

In Tables 17 and 18, we see the time-resolved fluorescence data for L7/L12 NTF-FITC and L7/L12 CTF C89-IAF. Initial comparisons of the data should be made with hinge intact wild type L7/L12-FITC (Figure 18) and C89-IAF (Tables 9 and 10). Further comparisons of the data are given in the next subsection. We have not yet labeled either fragment with IAEDANS (although the fluorescence data should be nearly the same as that with a fluorescein derivative). Furthermore, we shall see in Chapter Five that the NTF-FITC protein is primarily dimeric at 5 μM concentrations, and then begins to dissociate upon further dilution. Hence, all the fluorescence data reported in Tables 17 and 18 are the result of measurements at dimer concentrations of ~5 μM. The dimeric state of NTF-FITC is further supported by the SE-HPLC data presented in Figure 34 as was the monomeric state of CTF C89-IAF. The dimeric and monomeric states of NTF and CTF, respectively, are further supported by crosslinking and SDS-PAGE results of Oleinikov (personal communication).

The fluorescence lifetime of FITC bound to NTF is slightly greater than that of lightly FITC-labeled wild type L7/L12 (Figure 18), although no simple conclusions can be made from the lifetime alone. The very slight

intersubunit energy transfer seen earlier in Figure 17 for wild type L7/L12-FITC probably solely attributed to the FITC labeled in its NTF region (as we discover in the next two chapters that intersubunit energy transfer is evident within NTF-FITC). This small amount of energy transfer does not significantly alter the data presented in Table 18, with the possible exception of a slight increase in missing anisotropy attributed to the very rapid rate of

Table 17: Fluorescence Lifetime Data for L7/L12 NTF-FITC and L7/L12 CTF C89-IAF.*

Sample	τ_1	f_1	τ_2	f_2	χ^2
CTF-IAF	4.174	0.998	0.001	0.002	0.6
NTF-FITC	3.769	0.984	0.001	0.016	1.3

*Symbols and units in the x-axis are as described in Table 15. Symbols in the y-axis are as described in the text of the present subsection. Conditions are as previously described (i.e., 20°C; 085 filters, and 488nm excitation) for IAF (Table 15) or FITC (Fig. 18). NTF samples were measured at protein concentrations of ~5 μM to ensure a fully intact protein dimer state exists.

Table 18: Dynamic Polarization Data for L7/L12 NTF-FITC and L7/L12 CTF C89-IAF.*

Sample	ρ_1	α_1	ρ_2	α_2	r_0	χ^2	S.S.P.
CTF-IAF	13.26	0.539	0.975	0.461	0.365	1.4	0.152
NTF-FITC	24.90	0.376	1.482	0.624	0.338	0.9	0.172

*Symbols and units in the x-axis are as described in Table 16. Symbols in the y-axis are as described in the text of the present subsection. Conditions are as previously described (i.e., 20°C; 085 filters, and 488nm excitation) for IAF (Table 16) or FITC (Fig. 18). NTF samples were measured at protein concentrations of ~5 μM to ensure a fully intact protein dimer state exists (see text).

energy transfer expected between probes located on each subunit in the N-terminal coiled-coil domain (see Chapter 6 for extensive detail). Furthermore, a slight increase in the fractional anisotropy amplitude of the local motion component of NTF-FITC is noticed in comparison to wild type-FITC (shown previously, in Figure 18); this slight increase is probably due to slight intrasubunit energy transfer as well as a slightly different environment

of the NTF-bound FITC than the CTF-bound FITC (s) occurring in wild type L7/L12 (in fact, we shall find in Chapter 6, that this missing anisotropy is primarily due to a *very* rapid motion similar to that occurring with C63-IAF). The very exciting discovery made with FITC-labeled NTF was that the global rotational relaxation time monitored was nearly the same as wild type L7/L12!! Before we elaborate on the significance of this result let us evaluate the time-resolved data presented for CTF C89-IAF in Tables 17 and 18. Absolutely no differences are observed in the fluorescence lifetime of 5-IAF when bound to CTF C-89 in comparison to 5-IAF bound to fully-intact L7/L12 C-89. Furthermore, we see only a slight difference in the fractional anisotropies in that the fractional anisotropy associated with the global ρ increases about 5-10%. Once again, no missing anisotropy or energy transfer are observed as expected (since CTF is a monomer). The data further supported the idea of insignificant intersubunit CTF interaction within native dimeric L7/L12 and furthermore, the data indicated that very little communication occurs between the CTF and NTF in native dimeric L7/L12. The very interesting finding here is that the global rotational relaxation time monitored by 5-IAF for CTF C-89 is ~13.3 ns. From Equation 7, Chapter Three, we can predict a global rotational relaxation time for a spherical 7 kD CTF of 10.2 ns considering a calculated (method of Kuntz, 1971) hydration of 0.45 and partial specific volume (Cohn and Edsall, 1943) of 0.755 at 20°C. Hence, the experimentally observed value of ~13 ns is in fairly good agreement with a rather spherical (globular) CTF. Since 5-IAF bound to CTF still has considerable local motion, it seems likely that the 13.3 ns value given in Table 18 is a rather average global ρ. From Table 4 and equations 30-41, CTF appears somewhere between a perfect sphere and an ellipsoid with axial ratio of no greater than 2:1. Hence, our time-resolved fluorescence data are in excellent

agreement with the x-ray crystal structure of a single C-terminal domain (Figure 5). Furthermore, the data is in excellent agreement with the theoretical work of Wegener (1981), who predicted that the rotation of a sphere about a fully flexible hinge tethered to a nearly equal molecular weight domain, should possess a rotational relaxation time of ~1.2-1.5 times greater than that of a freely rotating single C-terminal domain. The segmental rotational relaxation times obtained with 5-IAF or IAEDANS attached to C-terminal cysteines on fully intact L7/L12 (21 ns) fall within the range of 1.15-1.66x greater than that reported in this subsection for free CTF C89-IAF (13 ns).

What then does the global rotational relaxation time reported for NTF in Table 18 tell us about NTF structure or dynamics? From Eqn. 7, Chapter 3, we can predict a global rotational relaxation time of 14.4 ns for a hypothetical spherical dimeric NTF, with molecular of 10,250 daltons, hydration of 0.35 (calculated from amino acid sequence by method of Kuntz, 1971), partial specific volume of 0.752 (Cohn and Edsall, 1943), and at 20°C. Under similar conditions we can calculate a global ρ of 10.6 ns for NTF *minus the hinge* . If residues 1-6 and 37-53 are random coil, then the only structure that could give L7/L12 an elongated appearance due to its rigidity would be the putative coiled-coil region. Hence, from Table 4 and Equations 30-41, our data (25 ns global ρ) suggests that the NTF is somewhat ellipsoidal with an axial ratio of ~3 or 4:1 (see Conclusions of this chapter for more detail). It seems unlikely that a coiled-coil of only 28 amino acids, such as that predicted for L7/L12 (recall Fig. 29), would have an axial ratio much greater than 2:1. The data is obviously somewhat complicated by the existence of the hinge region in these NTF fragments. One explanation for the rather long global ρ monitored by FITC bound to NTF is that the FITC is aligned quite parallel to the longest axis of rotation in a prolate NTF with axial ratio of 2:1. The data are still quite

consistent with data presented earlier for C-33 (also within the NTF) labeled with various probes, in which the segmental global mobility is nearly the same as that reported here for NTF-FITC (see next subsection and Conclusions section for more discussion). Data for NTF labeled with the non-covalent probe (no local motion) Bis-ANS is presented in the next subsection, which agrees well with the data presented in this subsection. The data presented in this subsection provides us with excellent evidence for a nearly perfectly flexible hinge within L7/L12 that allows nearly, if not full, free angular mobility of the dimeric N-terminal domains and the monomeric C-terminal domains.

Comparative Hydrodynamics of Various Hinge-intact, Hinge-Deleted, CTF, and NTF Forms of L7/L12. In this section we shall analyze more closely the segmental rotational mode of CTF and NTF within hinge-intact and hinge-deleted L7/L12. The data are directly compared to free CTF and NTF in order to obtain more structural and dynamical information about these various domains of L7/L12. Finally, Bis-ANS data are presented verifying the rigidity or higher aggregate form of the hinge deleted mutant, the segmental mobility of hinge-intact L7/L12, and the rather prolate ellipsoidal structure of the NTF.

In Figure 38, we see a Stokes-Einstein plot for hinge-intact L7/L12 C89-IAF and C12-IAF, hinge-deleted L7/L12 C89-IAF (exchanged with unlabeled to prevent FRET), CTF C89-IAF, and NTF-FITC. To prevent ambiguities, all data presented in Figure 38 are for samples not undergoing FRET (since one might argue that viscosity or temperatures changes might simply result in conformational changes leading attenuated or augmented FRET and hence, ρ_T). Since dimeric C12-IAF is less stable than wild type L7/L12 (next Chapter) and exhibits enormous FRET (Chapter 6), it was necessary to exchange subunits with 10 x excess of unlabeled wild type L7/L12 (see Chapter 6 for

details). Similarly, NTF-FITC was exchanged with 10 x excess unlabeled NTF. The time-resolved fluorescence data for C12-IAF/10 x wild type is nearly identical to C33-IAF/10 x wild type, with the exception that we see a slightly greater (~three ns) global rotational relaxation time with IAF located at the C-

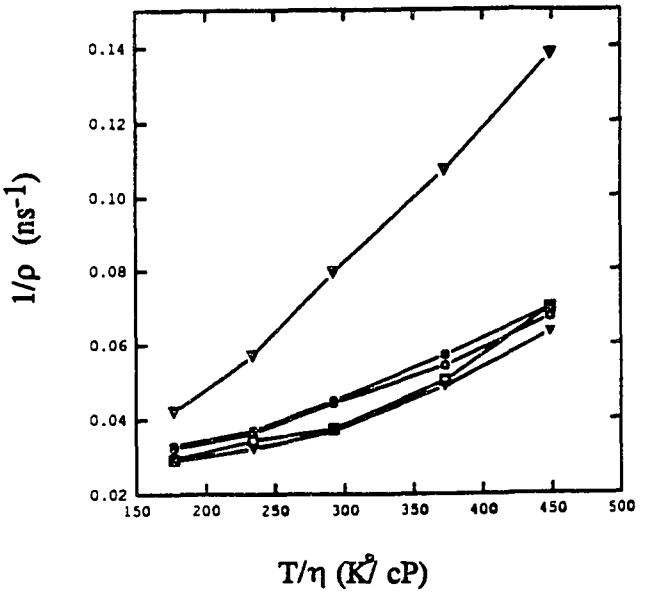

Figure 38: Stokes-Einstein plot of hinge-intact L7/L12 C89-IAF (filled triangles) and C12-IAF/10x unlabeled, exchanged wild type (hollow squares), hinge-deleted L7/L12 C89-IAF (filled sircled), CTF C89-IAF (hollow triangles), and NTF-FITC (hollow circles).

12 position than at the C-33 position (27 instead of 24 ns), probably due to the fact that the C-12 is much more distant to the highly flexible hinge than C-33. Hence, C12-IAF should be a fairly equivalent comparison to C89-IAF, which is very distant in the C-terminal domain from the flexible hinge.

Since all SE-HPLC purified mutants studies in this section, regardless of what probe was used, exhibit predominant global ρ's of approximately 15-27 ns, all data presented in Figure 38 are for 5-IAF labeled samples. The reasoning is simple, 5-IAF is the simplest and most sensitive of the fluorescent probes and its lifetime is sufficient to detect L7/L12 segmental

mobility as well as the global mobilities of the various deletion mutants. Several conclusions can be made from the Stokes-Einstein plot in Figure 38: 1) The CTF C89 samples exhibit nearly perfect spherical global rotation, as the ratio of $1/\rho$ at four and 20°C is as predicted for a sphere (~1.6); 2) the $1/\rho$ versus T/η slopes for the hinge-deletion and NTF mutants are, like CTF, quite linear as expected. Conversely, their slopes are much smaller than that of CTF, indicative of their rather ellipsoidal shape (recall pages 88-94); 3) The slopes for C-12 and C-89, both possessing their flexible hinge, are parabolic in shape relative to the T/η axis. The data are fully consistent with a thermal activation, or change in hinge mobility with T/η.

Perrin plots, via addition of sucrose, were additionally performed to see if similar deviations in the slopes occur at higher viscosities (in absence of FRET once again) and are shown in Figure 39. Two things were concluded from the Perrin plots of 5-IAF bound to the given cysteine mutants: 1) As opposed to the Stokes-Einstein plot, the slopes for all five mutants are all quite linear, the reason most likely being the absence of thermal activation (Perrin Plots done isothermally); 2) the slope for the rather spherical CTF C-89 was conspicuously less than the other mutants, probably as a result of the spherical shape of CTF (like the Stokes-Einstein plot, Figure 38). Furthermore, the y-intercept for CTF is noticeably higher than the other four mutants. The data might simply be the result of the fact that CTF C89-IAF possesses the least intrinsic local motion of the five (although, not much less than C-89). Interestingly, the slopes of the other four mutants are all quite similar in that they reach the ~same y-intercept. C-89 and C-33/(10x wild type) have obviously lower initial (at $T/\eta = 292$) $1/P - 1/3$ values simply because they have higher molecular weight and less anisotropy associated with local motion. Finally, we no longer see the small hump around $T/\eta = 292$ as we

did with unpurified (no SE-HPLC) wild type L7/L12-FITC (recall Fig 22), probably indicating the fact that Peak1 is removed from the samples reported here in Figure 39.

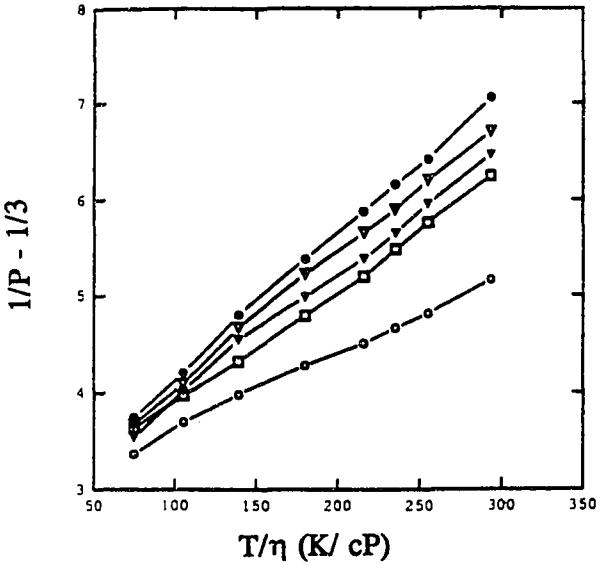

Figure 39: Perrin plots for NTF (filled triangles) labeled with FITC or Δ7 C-89 (+10x exchanged, unlabeled, and reduced Δ7 C-89; hollow triangles), CTF C-89 (hollow squares), C-89 (hollow circles), and C-33 (+10x exchanged, unlabeled wild type L7/L12; filled circles) each labeled with 5-IAF.

In conclusion, both sets of viscosity data suggest a rather spherical shape for CTF and unusual rotational behavior for the other four mutants. The data were still consistent with flexible mobility of C-89 (monitors the CTF) and C-33 or C-12 (both monitoring the NTF) and rigid ellipsoidal rotational behavior for NTF or Δ7 C-89. If NTF and Δ7 C-89 were *prolate* ellipsoids as suspected, then the rotational relaxation times monitored by fluorophores bound to them should be dependent on the wavelength of excitation (recall Eqns. 31-33). The reasoning is simple: since the limiting

anisotropy of the fluorophore is dependent on the wavelength of excitation, the relative orientation of the absorption and emission dipoles of the fluorophore is wavelength dependent. Hence, since the orientation of the absorption and emission dipoles differs with the wavelength of excitation, so should its alignment with respect to a particular rotational axis of a protein. Thus, the observed rotational relaxation of CTF C89-IAF should not exhibit a significant dependence on the wavelength of excitation if it is spherically symmetric (no difference in rotation around any axis). As mentioned earlier, an asymmetric prolate ellipse should exhibit conspicuous differences in rotation around its various axes. We cannot, however, predict whether or not 5-IAF at the C-terminal C-89 or N-terminal C-33 position will exhibit a rotational relaxation time dependent upon the wavelength of excitation, since we do not yet know the angular rotation mobility (recall previous subsection; also, see Conclusions of this chapter) of this segmental rotation. If the angular rotation mobility is perfectly free then we might expect the data perfectly consistent with a rotation reflecting the shape of the *individual* CTF's or NTF.

Preliminary time-resolved fluorescence data for the five mutants each labeled with 5-IAF upon excitation at 351 nm (*where the limiting polarization is -0.03*) has been obtained (data not shown). Since the only set of time-resolved data taken for the five mutants at 351 nm excitation was rather inaccurate, the author chose not to present the data in this dissertation (works in progress). Nonetheless, a few preliminary conclusions could be made from the data: 1) as expected, practically no fluorescence lifetime dependence on the wavelength of excitation was observed (in comparison to the data from 488 nm excitation data in Tables 9, 15, and 17). Only the 5-IAF bound to Δ7 C-89 exhibits any change in fluorescence lifetime (from 3.60 to 3.74 ns); this slight

change in fluorescence lifetime probably simply reflects a change in the κ^2 parameter for energy transfer--recall Eqn. 28, p. 66 (since this measurement was done in the presence of FRET; 2) very little differences in the rotational relaxation times (plus or minus a ~two ns) of the hinge intact C-89 mutant or CTF C-89 were observed indicating a fairly spherical rotational pattern for both; furthermore, the data once again supported free hinge-promoted mobility of the independent C-terminal domains; 3) interestingly, the C-33 or C-12 mutants labeled with 5-IAF (both exchanged with unlabeled wild type L7/L12 to prevent FRET-induced ambiguities) did in fact appear somewhat ellipsoid in rotation as a reduction of the "global" ρ monitored (in comparison to the 488 nm data) of three or four ns occurred; 4) unfortunately, the data for the Δ7 C-89 mutant labeled with 5-IAF was highly inaccurate (χ^2 no better than 15) and hence, inconclusive; 5) a fairly accurate (χ^2 ~4) decrease in the global ρ of 5-IAF bound to NTF from 25 ns at 488 nm excitation (presented in Table 18), to 18.4 ns at 351 nm excitation was observed; it was tempting to attribute this last finding to a difference in axial alignment of the 5-IAF, indicative of a prolate ellipsoidal NTF (in support of the C-33 or C-12 data described above). In conclusion, it should be interesting in the near future to obtain more precise data for these five mutants upon 351 nm excitation subsequent to a more fine tuning of the time-resolved fluorometer.

Finally, as a last control, data was obtained on L7/L12 labeled with the *non-covalent* binding fluorophore, Bis-ANS (see Molecular Probes catalogue for structure). All data presented in this dissertation prior to this point have been obtained from covalently bound fluorophores that exhibit a large amount of rapid local motion. Bis-ANS, a covalent dimer of two ANS' , putatively has a very strong affinity to nucleotide binding sites of nucleotide binding proteins (see Yoo et al, 1990). Without going into great details (see

Rosen and Weber, 1969 for more subtle details), it is necessary that the reader becomes aware that both Bis-ANS and ANS have an extremely low quantum yield in buffer, which is enhanced (total emission can be enhanced several hundred-fold with Bis-ANS; vide infra) upon binding to non-polar macromolecules. Initial studies by Gudkov et al (1980) as well as the present author, demonstrated that *ANS* binds to dimeric and monomeric forms of L7/L12 with a fluorescence enhancement of about 5x. Since the fluorescence is enhanced only 5x, we could still expect ~20% of the anisotropy decay a result of rapid motion of the free probe. A colleague (Mr. Alex Rietveld, personal communication, 1993) visiting our laboratory made the interesting discovery that*Bis-ANS* fluorescence is enhanced at least a hundred-fold (data not shown) upon binding to wild type L7/L12. This result enabled Mr. Rietveld to initially characterize L7/L12 hydrodynamics via time-resolved fluorescence with a probe possessing no significant local motion (any free probe emission --less than a fraction of a percent, would go practically unnoticed). Interestingly, Mr. Rietveld discovered that the Bis-ANS, with its ~10 ns lifetime, monitored a global rotational relaxation time of ~100 ns for L7/L12. Unfortunately, it was shortly after Alex left that we discovered the effects of Peak1 contamination.

In Tables 19 and 20, data are presented for Peak2 C-89, Δ35-52 C-89, and NTF each labeled with Bis-ANS. Similar enhancement of Bis-ANS emission was observed (in comparison to results of Mr. Rietveld) upon binding to pure Peak2 L7/L12. The data suggested that Bis-ANS binds fairly equally to Peak1 or Peak2 L7/L12 (although, this theory has not yet been directly examined). Interestingly, Bis-ANS binds slightly more efficiently to the NTF than the CTF's as theorized by Mr. Rietveld (data not shown); conversely, a preliminary study by the present author indicated that *ANS* does not bind to

the CTF but binds rather tightly to the NTF (data not shown). Hence, the data presented in Tables 19 and 20 for Peak2 wild type L7/L12 should reflect an average of the segmental motions of both the CTF's and NTF (since both have fairly equaly affinity for Bis-ANS at these ~micromolar concentrations). Finally, it is interesting to note that the emission of Bis-ANS is enhanced by ~400 x upon binding to the hinge-deletion mutant (data not shown, although this higher affinity is reflected in the relatively augmented fluorescence lifetime seen in Table 19).

In Table 19 we see that the fluorescence lifetime of Bis-ANS bound to wild type L7/L12 exhibits a rather typical two-component decay. The average fluorescence lifetime of Bis-ANS bound to wild type L7/L12 is ~7 ns as opposed to Bis-ANS free in buffer, which is <1.0 ns. The exciting finding is shown in Table 20, where we see that the global (or segmental) ρ for wild type L7/L12 is ~28 ns. Hence, the data verified that the rapid local motion of the covalent probes described throughout this chapter had very little, if any, significant effect on the observed global (or segmental) rotational relaxation times. The time-resolved data for NTF (~27 ns global ρ) once again verified the rigidity of this domain in L7/L12 and gave further support for the theory that the segmental domain mobility of L7/L12 is quite unrestricted (see conclusions). No time-resolved data has yet been obtained with Bis-ANS bound to the CTF's, although the steady-state polarization of this probe/ protein conjugate (.212) indicated (from the Perrin equation) a global ρ of once again ~18 ns.

The rather startling result presented in Table 20 was that Bis-ANS monitors a global ρ of ~160 ns when bound to the hinge-deletion mutant. The data once again verified the rigidity and elongation of of the hinge-deletion mutant. From Table 4 and data in Tables 16 and 18 (when 5-IAFs are <u>not</u>

undergoing FRET, pg. 80), the monitoring a prolate with axial ratio of ~5 or 6:1 appears possible (assuming that the Bis-ANS is aligned parallel to the long axis of rotation, the 5-IAF along the short axis, and the IAEDANS with the average axial rotation). Alternatively, we cannot yet rule out the possibility

Table 19: Fluorescence Lifetime Data for Bis-ANS Bound to Wild Type L7/L12, L7/L12 Δ35-52 C-89, or NTF.*

Sample	τ_1	f_1	τ_2	f_2	χ^2
Wild Type	8.105	0.876	2.578	0.124	0.98
Δ35-52 C-89	10.754	0.755	4.412	0.245	3.21
NTF	7.761	0.773	2.392	0.227	1.07

*Excitation was with 364 nm light at 20°C and emission was collected with a Schott KV399 cut-on filter. Symbols as described in Table 7 and data as described in the text.

Table 20: Dynamic Polarization Data for Bis-ANS Bound to Wild Type L7/L12, L7/L12 Δ35-52 C-89, or NTF.*

Sample	ρ_1	α_1	ρ_2	α_2	r_0	χ^2	S.S.P.
Wild Type	28.4	0.905	1.43	0.095	0.152	0.4	0.223
Δ35-52 C-89	166.0	0.959	1.32	0.041	0.165	4.2	0.333
NTF	26.9	0.922	1.44	0.078	0.157	7.1	0.227

*Conditions as described in Table 19. Symbols as described in Table 7 and data as described in the text.

of this hinge-deletion mutant existing as an aggregate larger than a dimer; this possibility is rather attractive when one looks once again at Fig. 29, which depicts a maximum possible axial ratio of ~4:1 for the hinge deleted mutant (or if one considers again the SE-HPLC data). Finally, we cannot rule out (at least with our particular SE-HPLC columns where Δ7 elutes very near to the void volume) the possibility of Bis-ANS inducing a higher state of aggregation for the hinge-deletion mutant; since Bis-ANS possesses such a large Stokes' shift (data not shown), little if any FRET could have obscured the results.

CONCLUSIONS TO CHAPTER FOUR

In the first section of Chapter Four (excluding the introduction), fluorescence data from FITC bound to wild type L7/L12 demonstrated the potential artifacts that occur in the presence of homo-FRET. More specifically, the author presented a simple mathematical explanation for the "missing anisotropy" phenomenon that appears in the analyses of time-resolved fluorescence data. Both the multifrequency phase and modulation (present study) or pulse methods (Burten-Bastiaens, 1992; Wang et al, 1993) for time-resolved fluorescence indicate in the presence of FRET between identical fluorophores, a limiting anisotropy less than that expected in the absence of FRET. Phenomenologically, the attenuated limiting anisotropy occurring in the presence of FRET is a result of transfer of energy between fluorophores more rapid than that measurable (or resolvable) with the time-resolved instruments (in the present case FRET occurring faster than ~100 picoseconds).

Dynamic polarization data for wild type L7/L12 labeled with FITC clearly demonstrated evidence for a segmental, or independent domain mobility for L7/L12. This experimental data was in excellent agreement with present theories on the relation of fluorescence anisotropy to macromolecular volume and rotation (Weber, 1952; Tao, 1969; Belford et al, 1972). The modern theory predicts that the overall rotation relaxation time (or global tumbling) of any hydrated molecular volume or shape shall always be greater than 95% that calculated by Equation 7 for a hydrated spherical rotator (the Stokes-Einstein relation; pg. 53, Ch. 3). Hence, since the FITC monitors a rotational relaxation time for wild type L7/L12 of only 69% that predicted for an equivalent sphere, it was likely that the FITC was monitoring a domain motion of L7/L12. Since the excited-state lifetime of FITC (~3.6 ns) should be

sufficient to monitor ρ's of ~125% that expected for a spherical rotating L7/L12 (recall from Table 10 that 5-IAF could monitor Peak1 rotations of nearly 50 ns), the author attributed this highly reproducible ρ to domain (or segmental) motions of L7/L12. Thermal viscosity data (Stokes-Einstein plot) gave support for thermal activation of the putative segmental mobility. Both the Stokes-Einstein (temperature alteration) and Perrin plots (sucrose viscosity data) indicated the possibility of a slightly aggregated form of L7/L12.

In the second results section of this Chapter, time-resolved fluorescence data for IAEDANS or Dansyl-Cl probes bound to L7/L12 revealed another rotational mode of L7/L12. The average fluorescence lifetimes of IAEDANS and Dansyl-Cl were respectively, 4.2 and 7.4 times longer than that of FITC. Since the rotational relaxation times monitored by FITC, IAEDANS, and Dansyl-Cl were respectively, 22, 42, and 55 ns, it became obvious that a multitude of rotational modes existed within our L7/L12 samples. It was tempting to attribute these increases in apparent global ρ's to a proximity (within 2 or 3X in magnitude) of the global tumbling relaxation time (ρ_G) to the segmental rotational relaxation time (ρ_S). The data were in agreement with a segmental mobility within a rather ellipsoidal L7/L12. The χ^2 surface analyses of the various apparent global ρ's gave support to this theory, but additionally indicated the possibility of a higher aggregate form of L7/L12.

In the third section of this chapter, three different cysteine substituted mutants of L7/L12 were labeled with several different sulfhydryl-specific probes. More specifically 5-IAF, IAEDANS, and 1-PMIA were each separately attached to the three mutants. Two of the three cysteine mutations were in the C-terminal domains (C-63, C-89), whereas, the other (C-33) in the N-terminal domain. Since the probe labeling was highly specific, we essentially knew the location of the probes. The 5-IAF data, each possessing fluorescence

lifetime of ~4.1 ns, revealed once again the segmental ~15-25 ns rotation mode of L7/L12. Furthermore, the C-33 and C-89 5-IAF data appeared nearly identical to the wild type-FITC data indicating that this apparent segmental motion of L7/L12 monitored by fluorescein-derived probes was equally present in both major structural domains of L7/L12. IAEDANS, with its longer fluorescence lifetime, monitored a very slow (~300 ns) global rotational relaxation time when located in the C-33 (N-terminal) position. Conversely, when IAEDANS was bound to either of the C-terminal cysteine mutants it monitored the same ~40 ns global ρ as IAEDANS bound to the wild type C-terminal lysine. The data were fully consistent with a higher aggregate form of L7/L12, in which its N-terminal domains were aggregated and hence, monitoring a global tumbling of an aggregated form of L7/L12; furthermore, in this aggregate the C-terminal domains might still able to rotate and hence, their segmental ρ's would be skewed more towards a slower global tumbling time (than dimeric L7/L12). Contrastingly, the IAEDANS data might be consistent with preferential long axis alignment when bound at the C-33 position, but aligned with a rather average axis of rotation when bound to the C-terminal domains (from Table 4, consistency with an axial ratio of 8-10:1); this possibility seems unlikely since the extent of local motion in all cases indicates that the probes sample each rotational axis during the probes' excited-state. Finally, labeling with the pyrene derivative 1-PMIA resulted in average 1-PMIA fluorescence lifetime of 90-135 ns. This fluorescence lifetime range allowed revelation of global ρ's in the range of ~600-1200 ns and indicated a prolate of ~15-20:1 for dimeric L7/L12. The author subsequently produced an analytical "consensus" model for the quaternary structure of dimeric L7/L12 that indicates the simple impossibility of elongation greater than ~6.8:1. Hence, the data in this section fully

supported the possible existence of an aggregated form of L7/L12 in which some segmental mobility still remains, especially in the C-terminal domains.

The SE-HPLC data presented in the fourth section of this chapter unequivocally demonstrate the existence of two major forms of L7/L12. It is important to realize that we have dealt with recombinant L7/L12 throughout this chapter and the Traut laboratory has suspected that overexpression of L7/L12 may lead to this higher aggregate form (Peak1) of L7/L12. Further proof for this idea comes from past studies with L7/L12, which argued that native L7/L12 is nearly 100% dimeric at ~1-20 μM concentrations (vida supra). Furthermore, Makarov (personal communication) has indicated that when L7/L12 is simply extracted from native ribosomes using the Hamel procedure (recall Materials and Methods), only the dimeric form (Peak 2) is observed with SE-HPLC. Alternatively, Oleinikov (personal communication) has proposed the possibility of this Peak1 L7/L12 existing as a rather unfolded form. Our SE-HPLC results cannot exclude this theory, nor can the time-resolved data presented in the previous section. In the next chapter, we shall see that Peak1 L7/L12 2° and 3° structure does in fact appear intact and hence, the author tends to believe that Peak1 is a large aggregate form (supported in the last section of this chapter as well). Furthermore, a hinge-deletion mutant of L7/L12 eluted at the same spot as Peak1 hinge-intact L7/L12. Oleinikov (1993A) has indicated via chemical crosslinking that this hinge-deletion mutant is fully dimeric. The data here are hence, apparently consistent with a very rigid and elongated hinge deletion mutant, or conversely, consistent with a rather unfolded (but still dimeric) hinge deletion mutant (consistent with data presented in the next chapter). Furthermore, SE-HPLC verified unusual conformations for dimeric L7/L12, monomeric L7/L12, and the NTF (apparently dimeric). Conversely, the CTF appeared quite spherical. Finally,

the SE-HPLC method verified that, labeling of the C-terminal mutants with 1-PMIA or TMRIA, resulted in significant protein aggregation as well as probe precipitation; this problem could be bypassed by labeling (only checked with TMRIA) in the presence of 6 M urea.

In the last results section of this chapter, SE-HPLC purified forms of L7/L12 were fully characterized using contemporary steady-state and time-resolved fluorescence methods. In that section, many conclusions could be derived: 1) doubly-purified Peak2 L7/L12 C-33 or C-89 labeled with 5-IAF, IAEDANS, or 1-PMIA, respectively exhibited apparent global rotational relaxation times of ~20, 25, or 42 ns. The data were fully consistent with a *segmental (domain) mobility* of ~20-25 ns and an *average global tumbling* of greater than 40 or 50 ns. In fact, it is not difficult to imagine that the true average global tumbling time for dimeric L7/L12 is similar to that of the hinge-deletion mutant (~70 nanoseconds); more specifically, the 42 ns ρ observed with pyrene might simply be the average of the ~25 nanosecond segmental ρ and a 60 or 70 nanosecond global tumbling. χ^2 surface analyses were excellent for each of these sets of data.

The global rotational relaxation times for 5-IAF bound to CTF or FITC bound to NTF were very similar to that of 5-IAF bound to C-89 or C-33 in fully-intact L7/L12. The independent domains rotate ~1.1-1.6 x faster than when tethered via the flexible hinge of fully-intact L7/L12, in agreement with the theoretical work of Wegener (1982) for unrestricted hinge mobility. Segmental mobility of the C-terminal and N-terminal domains appears dependent on the putative hinge region as a conspicuous increase in the global rotational relaxation time is monitored by the various probes bound tothe hinge-deletion mutant relative to the hinge-intact protein. Preliminary results demonstrate that substitution of this flexible hinge region with poly-

proline result in a 3 ns increase in the global rotational relaxation (data not shown); thus, the poly-proline hinge appears very slightly more rigid then the native alanine rich protein (see Chapter 6 for more details on the poly-proline hinge mutant).

What, then, do we mean by a 20-25 ns segmental mobility (or ρ) and a 50 or 70 ns average global tumbling? In Figure 40A, the author illustrates how a protein with the quaternary structure depicted earlier (author's consensus model, Fig. 29), can possess an average global tumbling rotation similar in magnitude to that of the hinge-deletion mutant (Figure 40B). Since the segmental rotation within hinge-intact L7/L12 dominates the anisotropy decay of the shorter lifetime probes, very little global tumbling is monitored. Only the pyrene derivative, with an excited-state lifetime significantly greater than the segmental ρ, is able to significantly monitor the 50 to 70 nanosecond global tumbling ρ. In the case of the hinge-deletion mutant, where presumably no segmental rotation exists, the shorter lifetime (i.e., 12 nanoseconds) probe IAEDANS is able to easily monitor the true global tumbling of ~70 nanoseconds (consistent with a rather prolate average shape for L7/L12; see Table 4).

The models presented in Figures 40A and 40B are in excellent agreement with all steady-state and time-resolved fluorescence data and SE-HPLC data presented in this chapter. The two figures are also in agreement with previous publications on L7/L12 that indicated considerable flexibility via the hinge (vide supra). The data in this chapter are the first that directly and rather quantitatively indicate that the two C-terminal domains of dimeric L7/L12 rotate independently. Although the previous zero-length crosslinking data (Oleinikov et al, 1993B; Traut et al, 1993) indicated the possibility of rather free C-terminal mobility, it did not directly prove that the

mobility is as unrestricted and independent as that depicted in Figure 40. The time-resolved fluorescence data presented in this chapter indicate that the angular mobility of the C-terminal domains or N-terminal domain induced by the flexible hinge region is apparently unrestricted. Furthermore, this independent C-terminal domain mobility was even apparent within the Peak1 "aggregated" form of L7/L12. The data presented in this chapter

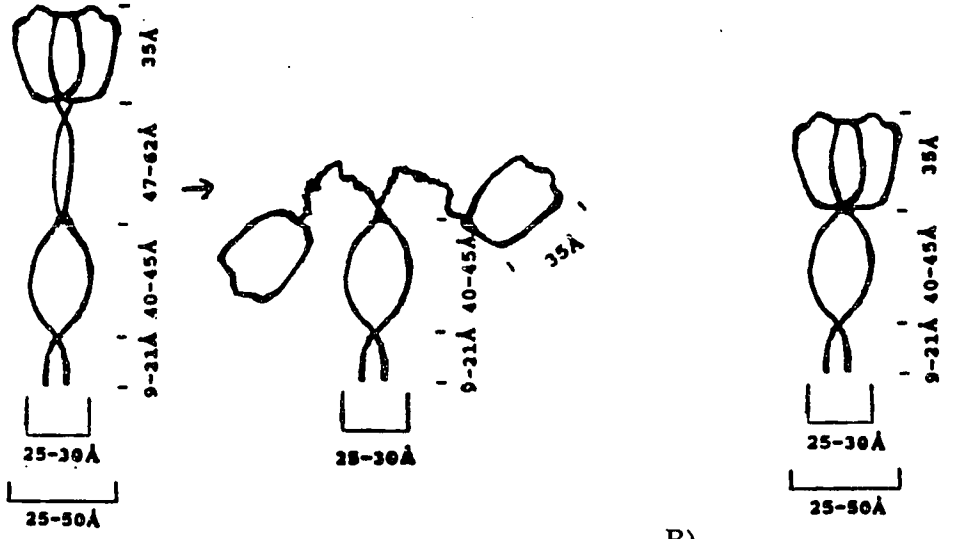

A) B)

Figure 40: Schematic depicting A) the feasibility of a global tumbling rotational relaxation time of ~50-70 ns and a domain flexing of ~20-25 ns for hinge-intact L7/L12 or B), the rigidity (~70 ns global ρ) of hinge-deleted L7/L12. In A) a rather average global conformation of L7/L12 is depicted.

strongly suggest that future interpretations of L7/L12 function in protein synthesis should consider the possibility of independent C-terminal domain motions. Hence, the data here suggest that four independent (monomeric), rather than two complexed (or dimeric) C-terminal domains rotate or flex on the ribosome. The significance is questionable since L7/L12 is still fully functional in poly-phenylalanine synthesis promotion when its two C-terminal domains are complexed (disulfide oxidized--Oleinikov et al, 1993B); of course, this result would not exclude the possibility that independent C-terminal domain mobility is involved in, for example, proofreading. The

data presented in this chapter fully support the theory that L7/L12 should be able to flex via its hinge towards rather distant or seemingly restricted regions on the ribosome (as depicted earlier in Figure 6, Chapter One; see also Chapter Seven for more details). Preliminary data suggest that this independent C-terminal domain mobility persists when L7/L12 is reconstituted into the ribosome (see Hamman et al, 1993); more specifically, when pyrene is attached to the C-terminal domain (but not the N-terminal domain which is putatively rigidly bound to L10), it still monitors an apparent C-terminal domain flexing.

CHAPTER FIVE:
ELUCIDATION AND CHARACTERIZATION OF THE L7/L12 DIMER TO MONOMER DISSOCIATION CONSTANT. COMPARATIVE CHARACTERIZATION OF L7/L12 STRUCTURE, DYNAMICS, AND STABILITY

INTRODUCTION

The author has already presented a brief general summary of the present state of the art of protein dynamics elucidation in relation to fluorescence spectroscopy in Chapter One (pages 22-25). In the last chapter the reader was presented with a model (Figure 40) depicting native L7/L12 as a highly flexible dimeric protein capable of appearing highly elongated. The section in Chapter Four on SE-HPLC data for various recombinant forms of L7/L12 suggested that native L7/L12 is dimeric at protein concentration ranges of ~0.2-50 micromolar. The SE-HPLC data verified that three forms of recombinant L7/L12 exist: 1) an apparently aggregated or unfolded and unnatural Peak1 phenotype; 2) the putative dimeric and "extremely stable", well-characterized (or natural) form of L7/L12; and 3) a monomeric form of L7/L12, putatively formed from ambient O_2 oxidation of methionines 14, 17, and 26. The relative amounts of each form depends strongly on the history of each sample (vide infra). Furthermore, the time-resolved fluorescence data presented for wild type L7/L12 and various amino acid substitution or deletion mutants of L7/L12 present us with a semi-quantitative picture of dimeric L7/L12 dynamics: all sets of data presented in the previous chapter strongly agree that the two C-terminal domains in all forms of L7/L12,

including SE-HPLC peaks one (maybe only partially), two, and three, experience nearly unrestricted rotational movement relative to the N-terminal domain via the structureless hinge region.

Most of the previous studies on L7/L12 stability have concluded that L7/L12 is nearly a pure and "extremely stable" dimeric protein (Möller et al, 1972; Wong and Paradies, 1974; Gudkov and Behlke, 1978; Luer and Wong, 1979; Luer and Wong, 1980; Lee et al, 1981 A/B; Zantema et al, 1982 A/B; Thielen et al,1984). However, the possible existence of tetrameric (Österberg et al, 1976; Kar and Aune, 1981; Georgalis et al, 1989) or monomeric (Kar and Aune, 1981) forms of L7/L12 "naturally" occurring at ~0.4-40 μM concentrations of native L7/L12 has been proposed.

Only in one case in the literature has the author seen experimental data used to quantify the "stability" of L7/L12 quaternary structure (Kar and Aune, 1981). More specifically, Kar and Aune proposed that the L7/L12 is naturally in an equilibrium mixture of tetramers, dimers, and monomers with association constant (K_a) of merely $3.5 \times 10^4\ M^{-1}$! Their association constant (discussed extensively later) indicated that L7/L12 is about 90% monomeric at one micromolar concentrations and hence, the dimeric form of L7/L12 is quite unstable!! The reader should be aware that the pressures induced by an analytical centrifuge exceed 100 atmospheres (Josephs and Harrington, 1967), pressures which can be sufficient to partially dissociate many oligomeric macromolecules (please see Weber, 1992 or Ruan and Weber, 1993 and references therein); furthermore, since oligomeric proteins undergo cycles of reassociation and dissociation (described on pages 22-25 in Chapter One of this dissertation; also, see Chapter 6), it is feasible that the equilibrium of dimers such as L7/L12 can be artificially "pulled" towards the monomeric form in the analytical centrifuge (Weber, 1993, personal

communication). Kar and Aune proposed via ultracentrifugation experiments, an equilibrium between tetrameric, dimeric, and monomeric forms of L7/L12; their data was criticized by Zantema et al (1982B) as being contaminated with an unnatural, methionine oxidized, monomeric form of L7/L12 resulting from purification and storage in the absence of sufficient reducing agent. Furthermore, the present author is concerned about the extremely harsh conditions (*i.e., 50% acetic acid, 8 M urea*) that Kar and Aune used in their preparations of L7/L12--as L7/L12 aggregates in acid pH (Luer and Wong, 1980), which might explain their putative tetramer. As mentioned in the previous chapter (SE-HPLC section), Makarov (1992, personal communication) has putatively demonstrated via SE-HPLC that L7/L12 is purely dimeric when purified using the Hamel extraction procedure (described in the Materials and Methods, Chapter Two of this dissertation). The present author demonstrated in Figure 32B of the previous chapter that the Peak1 (aggregate?) form of L7/L12 is not in equilibrium with peak two L7/L12, as Peak2 could not be converted to Peak1 via reconcentration. Finally, the ~5% monomeric L7/L12 only rarely appears in the SE-HPLC experiments and is attributed to minor amounts of methionine oxidation (via ambient O_2) that occurs when samples were kept at 0-8°C for extensive periods of time (weeks to months). Hence, the results reported earlier in the present study agree with the majority of previous L7/L12 studies, that L7/L12 is dimeric in its natural form or biological concentration (~ micromolar). *Thus, some ambiguity exists in the literature on the "stability" of dimeric L7/L12 and the author shall clarify the issue with experimental data later in this chapter.*

Several papers, utilizing circular dichroism (Boublik et al, 1973; Boublik et al, 1979; Luer and Wong, 1980 and references therein) methodologies, have studied the effects of denaturants, pH, temperature, salt,

and alcohol on L7/L12 secondary (2°) and tertiary (3°) structure. All three studies agreed that L7/L12 2° and 3° structures are quite heterogeneous with regards to stability and the present author shall describe more details about these results later in this chapter.

Most of the material presented in this chapter pertains to the fluorescence characterization of the relations of L7/L12 structure, dynamics, and stability. Fluorescence spectroscopy, as described in Chapter One, is an excellent method for elucidating dissociation constants and other macromolecular thermodynamics parameters: 1) fluorescence spectroscopy is a biophysical method that is highly sensitive to changes in the *rotations* of macromolecules. Obviously, from equation 7 in Chapter Three, as the molecular weight of an oligomeric is decreased upon dissociation, so is the global rotational relaxation time (or steady-state polarization) monitored spectroscopically by an extrinsic or intrinsic fluorophore (see pages 22-25, Chapter One for some references); 2) if the fluorophore being studied possesses a lifetime insufficient for monitoring significant changes in global rotational relaxation times upon dissociation, it may be sensitive to changes in its local mobility upon dissociation (i.e., if it is located at a subunit interface, its local mobility may change upon dissociation; there are tryptophan residues for example, which demonstrate this phenomenon--see Gratton et al, 1992 or Ruan and Weber, 1993 and references therein); 3) fluorescence spectroscopy allows the investigator to monitor concentration-dependent changes in macromolecular conformation in the concentration ranges of ~sub-nanomolar to greater than 10 micromolar, depending on the particular spectroscopic characteristics of the fluorophore used; only dangerous radioisotopes provide comparable sensitivity and very little can be elucidated about the protein conformation by simple labeling with

radioisotopes; 4) no potentially ambiguous extrinsic physical or chemical procedures are necessary for investigation; although, of course, if one is using extrinsic fluorophores, they must determine if the probe has any effect on the natural conformational equilibrium of the macromolecule (see Chapter One).

One of the primary goals of biochemists at this time is to determine the relation between the amino acid sequence and the final protein conformation, dynamics, stability, or function (see King, 1989 for an excellent review). The combination of site-directed mutagenesis and protein conformation characterization presented in this chapter should provide an excellent experimental and theoretical contribution to this problem. Thus, the primary goals of this chapter include the following: 1) elucidate the dimer to monomer dissociation constant of various wild type and mutated forms of L7/L12 using primarily equilibrium fluorescence methodologies; 2) characterize the relation of specific structural domains of L7/L12 to the 2°, 3°, and 4° stability of L7/L12; and 3) characterize and quantitate the physical forces involved in the "stability" of L7/L12.

In the first section, the author demonstrates an unusual and complex artifact that can occur when one is using fluorescence spectroscopy to elucidate the subunit equilibrium of a highly flexible macromolecule. Essentially, if the fluorophore observed was located in the C-terminal domain of L7/L12, very little (nearly zero) changes in fluorescence polarization occurred upon dissociation into monomers. This result was in excellent agreement with time-resolved data presented in the previous chapter for methionine oxidized L7/L12 monomers--if the probe was labeled at cysteines located in the C-terminal domains insignificant changes were monitored in the segmental rotation (in that domain) upon monomerization. This concept is unequivocally demonstrated in the the next two sections of this chapter;

furthermore, data is presented verifying the essential and negligible contribution respectively, of the N-terminal domain or C-terminal domains of L7/L12 in the dimerization process. In the subsequent section, a general thermodynamic treatment of the dimerization forces are described via high-pressure, temperature, denaturants, and kinetics; additionally, this section will include further characterization of the stability of L7/L12 2° and 3° structure and their relation to the 4° structure.

APPARENT LACK OF CONCENTRATION DEPENDENCE IN THE DISSOCIATION OF WILD TYPE DIMERIC L7/L12 LABELED WITH FLUORESCEIN ISOTHIOCYANATE

As mentioned in the first results section of the previous chapter, fluorescein, with its ~four ns fluorescence lifetime, seems ideal for following the rotational dynamics of an ~24 kD protein such as dimeric L7/L12. Hence, our initial studies in this chapter were accomplished with fluorescein isothiocyanate labeled at an unknown position within wild type L7/L12.

As shown on pages 75-85 in the previous chapter, the number of FITCs bound per subunit of L7/L12 is highly variable depending on the pH of the labeling buffer or the specific excess of probe to protein during the labeling procedure. When L7/L12 is only labeled to an average extent 0.1-0.5 FITC/subunit, minuscule fluorescence resonance energy transfer (FRET) is evident (recall Table 3 and Figure 17). Conversely, the extent of FRET rapidly increases as the average # of FITCs/subunit increases beyond 0.5. When ~1.2 FITCs are bound on average, per subunit of L7/L12, the FRET appears primarily as that between FITCs located on the same subunit. Hence, it seemed unlikely that any significant intersubunit FRET between FITCs could interfere with elucidation of the L7/L12 dimer to monomer dissociation constant; more specifically, if FRET was occurring between identical

fluorophores located on different subunits, and the local mobility of the probe does not increase upon dissociation, then we might expect an *increase* in steady-state polarization upon dissociation (recall, FRET between identical fluorophores results in depolarization of emission). Since we verified in Figure 17 (and in more detail in the next chapter) that *inter* subunit FRET is rather negligible, even when 1.2 FITCs are bound per subunit of L7/L12, very little *re* polarization is expected upon dissociation (that might "compete" with the *de* polarization expected upon a decrease in molecular weight by one-half). Hence, our initial attempts to elucidate the dissociation constant of L7/L12 were with samples labeled with ~1-1.2 FITCs/subunit; the rationale was simple: a larger amount of FITC bound to L7/L12 should allow greater sensitivity at dimeric protein concentrations of sub-nanomolar. Why sub-nanomolar? Since previous investigators had all described L7/L12 as "highly stable" and the dissociation constant (K_D) measured by many dimeric proteins were in the 0.1-100 nanomolar range (i.e., see Erijman and Weber, 1991 for a review), it seemed likely that it would be necessary to dilute L7/L12 samples to concentrations of less than nanomolar to observe significant concentration-dependent dissociation.

Excellent descriptions of the concept of oligomeric protein dissociation upon dilution have already been given (see Xu and Weber, 1982; or see Weber, 1992 for more details). The phenomenon can be described via changes that occur in the chemical potential (from the law of mass action--see Weber, 1992) of monomers that increase with the amount of time spent in the dissociated state. The span of a dissociation process is commonly defined as the concentration range encompassing 10% to 90% dissociation. Ideally, the log span of a dimeric compound will be 2.86 log units with the midpoint (50% dissociated) being equivalent to the dissociation constant (K_D). In fact, the log

span of the dissociation observed for several protein dimers is quite often less than two log units (~100 fold concentration range). For more details see the classic paper by Xu and Weber (1982) or later, in the present chapter.

Effects of Diluting Wild Type L7/L12 Labeled with FITC from 5 μM to 1 nM.

In Figure 41, a plot of steady-state polarization versus protein concentration is presented for wild type L7/L12 labeled, on average, with either 0.2 or 1.2 FITCs. Absolutely insignificant changes in polarization were observed in the dimeric L7/L12 protein concentration range of 10 μM to 0.1 nM for either sample!! The immediate conclusion was that the K_D of dimeric L7/L12 was significantly less than 1.0 nM. The conclusion of Kar and Aune (1981) based on their analytical ultracentrifuge data, suggested that L7/L12 was primarily monomeric at protein concentrations on the order of 1.0 μM was shown to be inconsistent with our SE-HPLC data which (Figures 31 and 32A) demonstrated that our samples consisted primarily of dimeric L7/L12 in the concentration range of 10 μM to 100 nM. The data presented in Figure 41 are for samples that were not purified by SE-HPLC and hence, some Peak1 (~20-25% from Figure 32A) L7/L12 was present. Nonetheless, a more recent experiment with pure Peak2 (dimeric) L7/L12 verified that the Peak1 contaminant had non-existent effects on the data (data not shown; vide infra). Thus, the highly reproducible (experiment repeated four times) data presented in Figure 41 verified that no changes in L7/L12 structure are monitored by the FITC in the given concentration range. Finally, the longer lifetime probes, pyrene butyrate or IAEDANS, with their limited sensitivity (respectively, ~0.05 or ~0.08 μM in this case, data not shown), monitored similar rotational behavior of wild type L7/L12 as FITC upon dilution (data not shown).

What sort of changes in the steady-state polarization of FITC can one expect upon dissociation of dimeric L7/L12? Recall from Figure 18 in the previous chapter that, in the absence of FRET, FITC monitors a global ρ of ~22

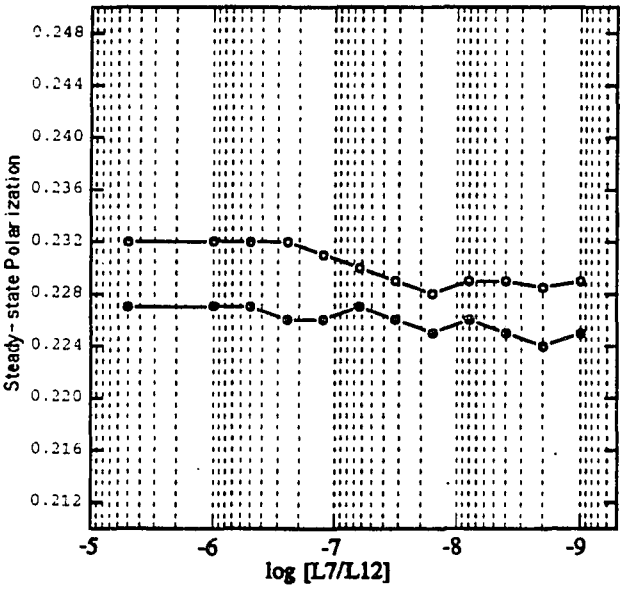

Figure 41: Absence of effects of dilution of dimeric L7/L12 from 5 μM to 1 nM as monitored by the steady-state polarization of 0.2 FITCs (hollow circles) or 1.2 FITCs (filled circles) bound per subunit. Excitation was achieved from 488 nm light at 20°C and 085 cut-on filters were used to collect emission red of 515 nm. Polarizations were essentially corrected for background when the FITC concentration becomes less than 10 nM. Changing the temperature (from 4°C to 37°C) or allowing the various diluted aliquots of L7/L12 to "incubate" for a couple of days had no effect on the apparent stability of dimeric L7/L12 in the protein concentration range depicted here (see next section).

ns and a local ρ of ~1.5 ns with respective fractional amplitudes of 0.65 and 0.35. If we consider the lifetime to be 3.6 ns and the P_0 to be 0.47, then we can calculate (from Equation 6, Chapter 3) steady-state polarizations for the two individual rotational components of 0.335 and 0.067. If we take the fractional amplitudes into consideration and substitute into Equation 5 (Chapter 3) the calculated steady-state polarization is 0.243, or, very close to that measured of 0.232. If we assume that the global ρ monitored by FITC reflects that of a dimeric rotating domain of L7/L12, then dissociation will result in a 50% reduction in molecular weight and hence, a 50% reduction in the global ρ

(from Equation 7, Chapter 3). If the fractional amplitudes of the rotational relaxation times are not changed upon dissociation, then the 50% reduction in global ρ would result in reduction of steady-state polarization from 0.243 to 0.193 (substitutions of equations 5 and 6). Hence, the slight decrease in polarization observed in Figure 41 (from 0.232 to 0.229) is insignificant.

At this time, two feasible explanations for the data presented in Figure 41 could be given: 1) the K_D of dimeric L7/L12 is much less than one nanomolar; or 2) the FITC was bound to an amino acid, or amino acids, located primarily in the C-terminal domains, which as described in the previous chapter, rotate freely and independently of one another. Thus, we would not expect any decrease in the steady-state polarization of a fluorophore attached to the C-terminal domains upon dissociation of L7/L12 (recall Peak3 fluorescence data in Table 10). Since the initial work in our laboratory was with wild type L7/L12 labeled with FITC, the first explanation was investigated in detail and the data is presented in this section (see next section for quantitative characterization of the second explanation).

Effects of Denaturants and High Pressure. In the previous chapter, data was presented in which the viscosity of the medium was altered via additions of sucrose. Glycerol is another small molecule that can be used to alter the viscosity of the medium without sensibly affecting the overall structure of the protein (see Reinhart and Lardy, 1980; Ruan and Weber, 1993). Sucrose and glycerol have been long known as stabilizers of biomolecules (see Timasheff, 1993 for review). Conversely, urea and guanidine-HCl (Gu-HCl), possessing similar structure, have the well known effect of denaturing or dissociating proteins (see also, Timasheff, 1993 and references therein for mechanistic details). Numerous studies, using fluorescence spectroscopy, have indicated that the dissociation constants of proteins less than that measurable by simple

dilution, can be elucidated by denaturants such as Gu-HCl or urea (see Timm and Neet, 1992, for an excellent example). The procedure is arguably straightforward (vide infra): by the law of mass action, increasing the protein concentration will increase the proportion of native dimeric protein at every denaturant concentration, and the midpoint of the sigmoidal curves will increase as the protein concentration increases. One can then calculate the Gibb's free energy (ΔG) of unfolding, (*assuming that it directly reflects dissociation*) at each denaturant concentration in the linear region of the curves and extrapolate the ΔG free energy of unfolding/dissociation at zero denaturant, which in the case of a dimer, should reflect the K_D (as of course, $\Delta G_D = -RT \ln K_D$). In Figure 42, the denaturation curves for 10 μM and 10 nM L7/L12 labeled with 0.2 FITCs are presented. Once again we see no concentration dependence in the denaturation/dissociation of dimeric L7/L12 as the two denaturation curves perfectly overlay one another!! Similar results were obtained with urea except that the midpoint was ~3.7 M urea (data not shown) rather than the ~1.8 M Gu-HCl depicted in Figure 42. In the case of β-nerve growth factor (Timm and Neet, 1992), which possesses a K_D of ~10^{-12} M, simply changing the protein concentration 15x (from 9.3 μM to 0.6 μM) resulted in shifting of the midpoint of the denaturation curve from 2.7 M to 2.2 M Gu-HCl. The data presented in Figure 42 could be explained as follows: either 1) L7/L12 is dissociating in a concentration independent manner (see Silva et al, 1989); 2) the FITC is attached primarily to the C-terminal domains of L7/L12; or 3) the protein is not actually dissociating, but rather, is simply denaturing. It is interesting that no significant changes in the polarization of FITC occur when the Gu-HCl concentration is raised from 3.6 M to 8 M. It seemed highly unlikely to the author that any protein dimer could resist dissociation in 8M Gu-HCl and hence, this third possibility was

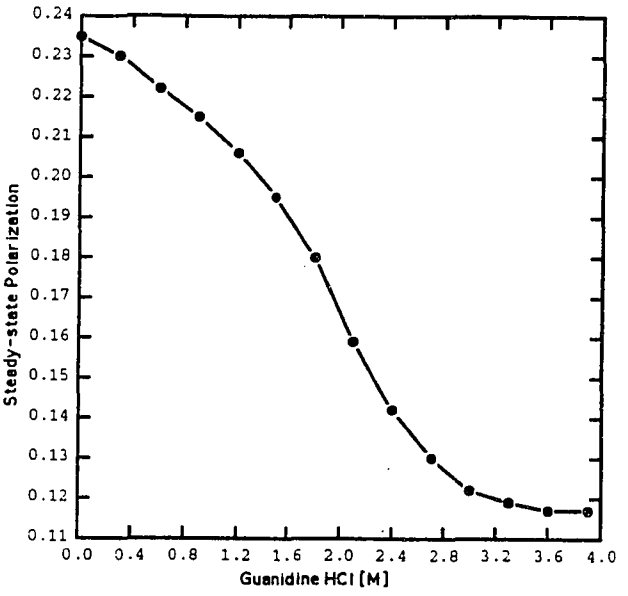

Figure 42: Guanidine-HCl induced denaturation/dissociation of 10 μM (hollow circles--not seen since the filled circles perfectly overlay) or 10 nM (filled circles) L7/L12 labeled with 0.2 FITCs at 20°C. Other conditions were as described in the caption of Figure 41.

temporarily excluded (see next section for experimental evidence). On the other hand, it is not unfeasible that excessive denaturation of L7/L12 2° and/or 3° structure in the region more local to the FITC obscures the concentration dependent dissociation (vide infra). In Figure 43, a plot of the global and local rotational relaxation times (and respective fractional amplitudes) of 0.2 FITCs bound to L7/L12 is given. This set of dynamic polarization data demonstrated nearly a 50% reduction of the global rotational relaxation time upon denaturation as expected for monomerization of the N-terminal domain. The local rotational relaxation time was not affected, *although its fractional anisotropy amplitude increased from 35% at zero denaturant concentration to 77% at 3.6 M Gu-HCl.* The data suggested that by far the predominant depolarizing force in the case of Gu-HCl additions was a three-fold increase in the fractional anisotropy ampli-

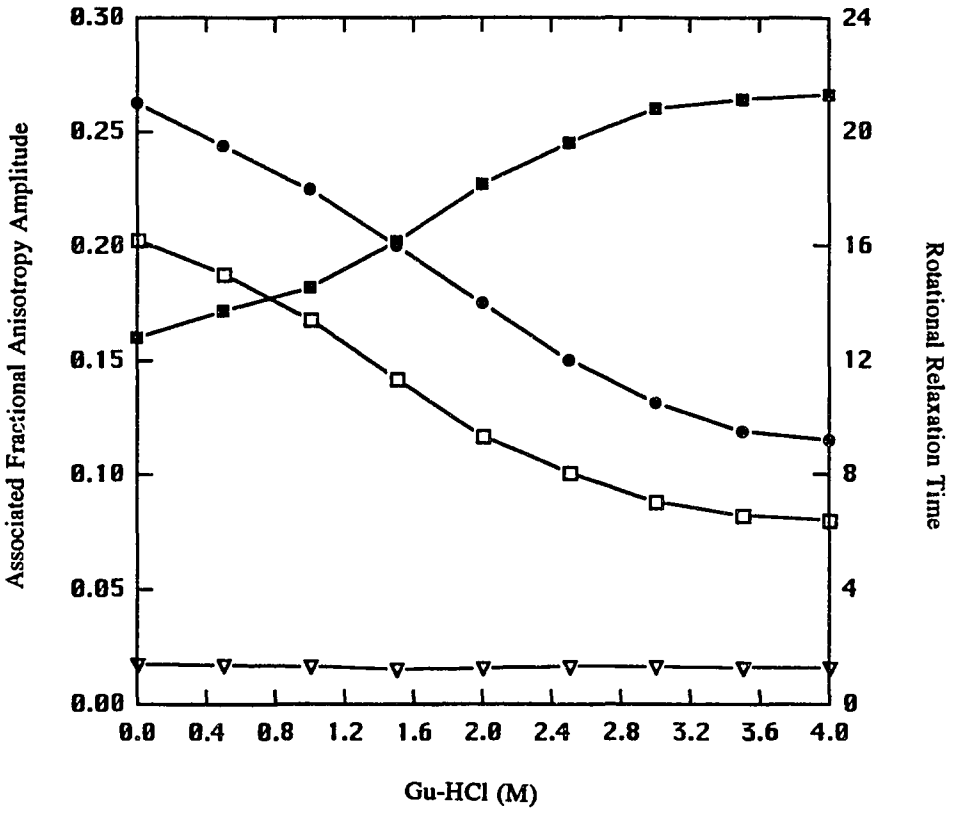

Figure 43: The dynamic polarization data for 0.2 FITCs bound per L7/L12 subunit at various denaturant concentrations. Filled circles and hollow squares respectively, represent the global rotational relaxation time and associated fractional anisotropy amplitude of FITC; hollow triangles and filled squares respectively, represent the local rotational relaxation time and associated fractional anisotropy amplitude of FITC. Dimeric L7/L12 concentration was 1.0 μM and other conditions were as described in Figure 42. Similar results were obtained with urea indicating similarity of action to that of Gu-HCl (data not shown). All denaturations were readily reversible upon removal of the denaturant (data not shown).

tude of the local motion, which might explain the obscuring of concentration dependent dissociation in Figure 42. Conversely, it is in fact, quite possible that the decrease in the global rotational relaxation time upon denaturant addition was simply due to unfolding of the C-terminal domains (E. Gratton, 1992, personal communication). Nonetheless, one can easily conclude that the depolarization upon denaturant addition resulted not from the dimer dissociation, but rather, from some sort of unfolding of L7/L12.

Protein oligomers can also be dissociated or denatured by high hydrostatic pressures (for an excellent review, see Weber, 1992, Chapter 15). Pressures in the range of 1-2000 atmospheres almost exclusively result in *dissociation* of oligomers, whereas, pressures greater than 2000 atmospheres can begin to result in *denaturation* of isolated subunits. Two primary forces are involved in the dissociation of oligomers in the range of 1-2000 atmospheres: 1) the putative filling of voids or dead spaces existent between the subunits. When the pressure is increased, the volume of the protein becomes smaller as these dead spaces are filled or replaced with the solvent; or similarly, 2) the phenomenon of electrostriction. In this case, charged amino acid side chains are preferentially hydrated upon pressure induction and are thus, less likely to reform salt bridges necessary for subunit interaction. Interestingly, these two explanations are not necessarily so different than that used for explaining the mechanism of denaturant action (vide infra). Nonetheless, excellent evidence exists for the lack of significant denaturation of proteins at pressures of 1-2000 atmospheres, as the steady-state polarization of fluorophores (either extrinsic or intrinsic) attached to monomeric proteins remains predominantly unchanged (see Li et al, 1976; Visser et al, 1977; Chrysomallis et al, 1981).

Hence, if L7/L12 were *dissociating* in a concentration independent manner as theorized above (previous figure) then treatment with high pressures should reveal more direct proof than denaturants. The reasoning is simple, since in the former case, depolarization should be more strictly due to dissociation rather than <u>both</u> denaturation <u>and</u> dissociation. The effects of high pressures were tested on L7/L12 using the instrument and methods described on pages 54 and 55 of this dissertation. As in the case with denaturants such as Gu-HCl or urea, the mid-point of the dissociation (or

denaturation) curves should shift to lesser denaturant concentrations or pressures (see Ruan and Weber, 1993 and references therein) as the protein concentration is reduced. In Figure 44, we once again observe no concentration dependence in the dissociation of L7/L12, as the sigmoidal curves of 10 μM or 100 nM L7/L12 labeled with FITC are nearly identical up to 2500 atmospheres!! As was the case with denaturants, very little (if any) changes occurred with additional alteration of the temperature (data not shown). The most startling fact depicted in Figure 44 is that the steady-state polarization of FITC decreased from ~.23 (at 1 atm) to ~.13 (at 2500 atm). As

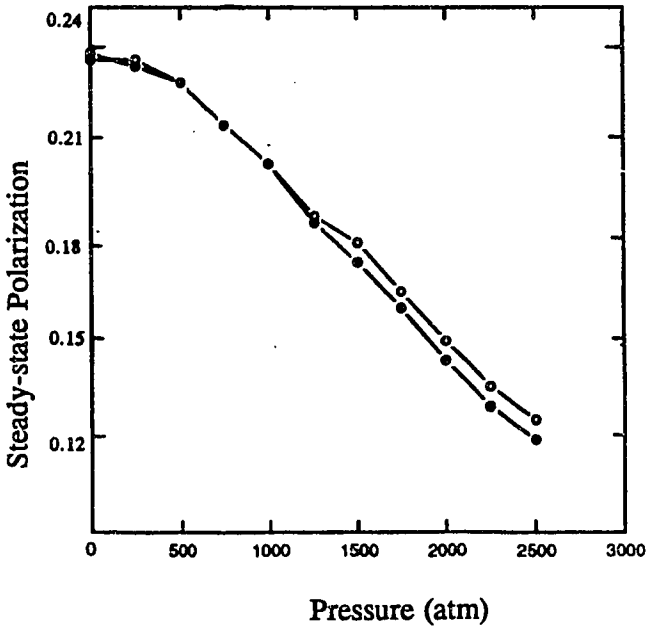

Figure 44: Effects of high-pressure on the stability of either 10 μM (hollow symbols) or 100 nM (filled symbols) L7/L12 labeled with 0.2 FITCs (see text below). All effects were readily (almost instantly) reversible upon decompression (data not shown).

the author calculated earlier (page 188), if only dissociation of dimeric L7/L12 occurs, the steady-state polarization of FITC should only decrease from ~.243 to ~.193. Hence, the data suggested that denaturation was occurring in addition to dissociation. When one looks at the previous high-pressure data

for a monomer such as a lysozyme (see Chrysomallis et al, 1981), clearly an ~20% reduction in rotational relaxation time occurs when the pressure is raised to 2500 atmospheres. Hence, the reduction of polarization seen in Figure 44 could be due to an unusual amount of "local" denaturation highly indicative of voids or pockets existing near the FITC binding location on L7/L12. The exact change in volume that occurs in the above pressure range can be calculated as follows (from Weber, 1992):

$$\langle dp \rangle = 2.302\, RT \log (729) \;/\; \Delta V \qquad (46)$$

where <dp> is the characteristic pressure span (i.e., the difference between pressures at which 10 and 90% dissociation are achieved), R and T are the gas constant and absolute temperature (293 K), respectively; and ΔV is the change in volume that occurs upon association of subunits. ΔV is assumed to be independent of the applied pressure as proteins are rather incompressible (see Gavish et al, 1983). Since anisotropy is directly additive (recall Equation 4, Chapter 3), it was used rather than polarization in Figure 44. Furthermore, since the degree of dissociation, α, is calculated from anisotropy or polarization and the change in quantum yield (see Xu and Weber, 1982), the quantum yield of the FITC was experimentally determined (recall page 66) to be nearly unchanged at the above pressures; hence, the anisotropy values given in Figure 44 should accurately reflect the degree of dissociation. Thus, since L7/L12-FITC is apparently denatured or dissociated 10-90% in the pressure range of 500-2200 atmospheres, ΔV is calculated to be 93 mls/mole at 20°C. Furthermore, if one assumes that the curves seen in Figure 44 represent dissociation occurring simultaneous to denaturation, a K_D can be calculated as follows (see Weber, 1992):

$$K_P = (4\alpha^2 C) \;/\; (1-\alpha) \qquad (47)$$

where K_P is the dissociation constant at pressure p and C is the protein concentration as dimer. K_P is related in turn to the dissociation constant at atmospheric pressure (K_D or K_{atm}) and ΔV by the relation:

$$K_P = K_{atm} \exp (p\Delta V / RT) \qquad (48)$$

Thus, K_P at 1350 atmospheres (see Figure 44 curve midpoint = p) and 1μM dimer concentration (as in Figure 44) is 2 μM and hence, K_{atm} is 10^{-8} M ($\Delta G^{"}_{diss}$ = 10.9 kcal/mole). One must exercise caution in that several assumptions were made in determining this "dimer to monomer" K_D of 10^{-8} M: 1) it was assumed that the pressure span of 500 to 2200 atmospheres actually represented dissociation. It is not unreasonable that some of the decrease in anisotropy was due to dissociation since pressures in this range putatively dissociate rather than denature proteins. Nonetheless, as described above, some denaturation must be occurring within L7/L12 at these pressures and hence, we cannot unequivocally argue that the calculated K_D is fully accurate; 2) furthermore, the author simply assumed that 2200 atmospheres represented 90% dissociation, even though the sigmoidal curves had not yet leveled off (representing the end of the dissociation). Since the curves seemed quite close to a leveling point, it seems most likely that the 2200 atmospheres is, in fact, quite close to the 90% point; 3) finally, the fact that we see no significant shift in the dissociation curves*implies* that we are not actually observing dissociation; conversely, concentration-independent dissociation has been reported in at least one study of a multimeric (12 subunits!) protein (i.e., Silva et al, 1989).

In conclusion, the following questions still remained: 1) does the dimer of L7/L12 actually dissociate in an apparently concentration independent manner, a phenomenon never before reported for any dimeric protein? This question could be explained in that the denaturation of the region local to the

FITC was so extensive that it obscured the depolarization that results from dissociation. Furthermore, the author found it difficult to imagine that a rather small dimeric protein such as L7/L12 could behave so similar to a large protein aggregate (as the 12 subunit protein studied by Silva et al, 1989); or 2), was it possible that the FITC was primarily located in the C-terminal domain? At this time it seemed rather crucial to determine where the FITC was located.

In Figure 45, two chromatograms of trypsin digests of L7/L12 labeled with either 1.2 (Fig. 45A) or 0.2 (Fig. 45B) FITCs are depicted (see Materials and Methods for procedures). The x's located at the top of the peaks represent fragments that contained FITC as judged simply by excitation with a UV hand lamp (recall from Fig. 20 in the previous chapter that fluorescein absorbs light quite efficiently in the mid-UV). Since L7/L12 possesses 13 lysines and 1 arginine, we should expect approximately 15 fragments. The trypsin digests of L7/L12 look quite similar to that previously reported (Zantema et al, 1982A) with the exception that we did not bother creating and removing the so-called tryptic cores; hence, we have a few more peaks. The interesting finding here was that so many different peaks possessed FITC: about 30% or 20-25% of the peaks respectively, for the 1.2 FITC/(L7/L12) or 0.2 FITC/(L7/L12) trypsin digests. One might argue that some of the peaks may be the result of an incomplete digest, but this seems highly unlikely since we do observe quite close to the expected ~16 peaks. *Hence, the data indicated that FITC labeling is not so highly specific as that previously described by Lee et al (1981A/B).* Nonetheless, the highest peak seen in Figure 45B (0.2 FITC/subunit of L7/L12), which was also the peak containing the highest amount of FITC (~20-30%), was given to Dr. Neil Riemer who subsequently did amino acid sequencing of the fragment (data not shown). Dr. Riemer determined that

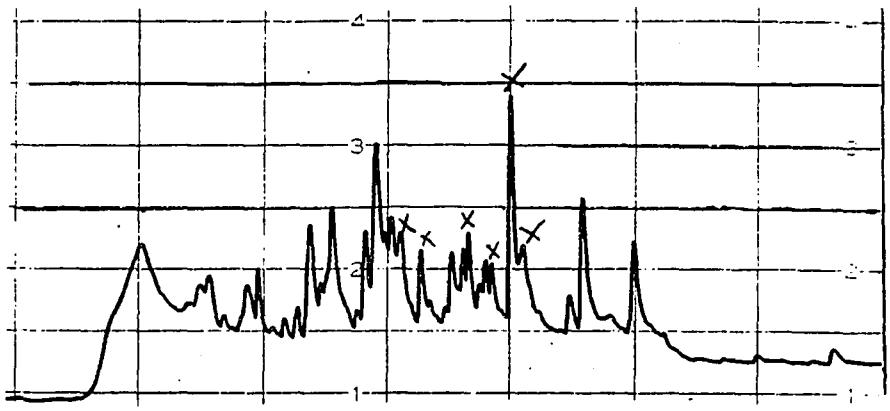

Elution Time (the initial peak at far left is at 30 minutes)

A)

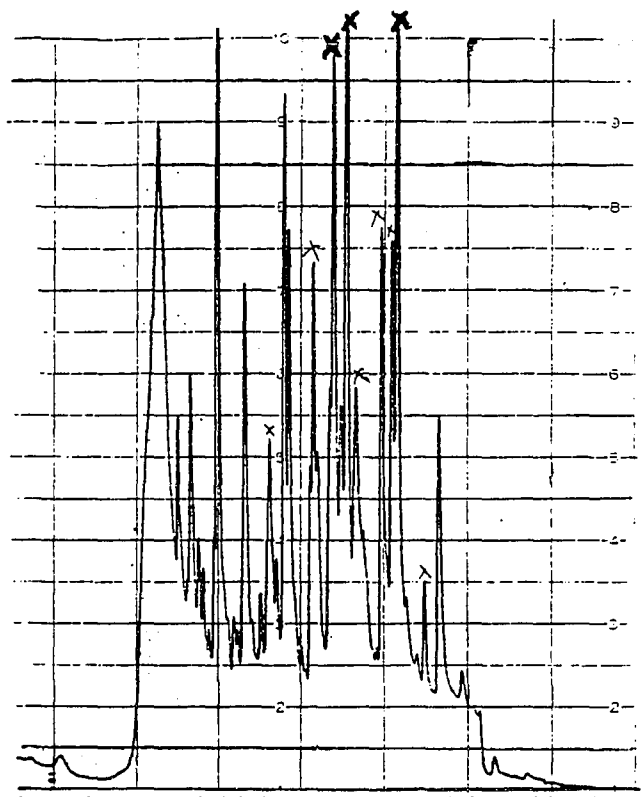

B) Elution Time (the initial peak at far left is at 30 minutes)

Figure 45: In A) the RP-HPLC chromatogram of a trypsin digest of L7/L12 labeled with 1.2 FITCs per subunit is depicted; x's represent peaks containing FITC; in B) the RP-HPLC chromatogram of a trypsin digest of L7/L12 labeled with 0.2 FITCs per subunit is depicted; x's represent peaks containing FITC. In both cases, the detector was set at 220 nm. See text for further details.

this fragment consisted of amino acids 15 through 22 of L7/L12, indicating that a cleavage had occurred at the carboxy terminal side of methionine 14! Hence, it appeared that some chymotrypsin contaminated our trypsin purchased from Sigma. Furthermore, Dr. Riemer determined that *serine* 15 had been covalently modified by FITC (data not shown). The present author has not seen anywhere in literature where an isothiocyanate can bind to a serine. In conclusion, it seemed likely that the FITCs were rather scattered throughout L7/L12, even when specificity initially appeared rather high (Lee et al, 1981; pages 75-78 of this dissertation). It is not difficult for the author to imagine the steady-state polarizations for 0.2 FITC bound per subunit of L7/L12 (given in Table 3, page 75) were the result of labeling at several similar environments within L7/L12. Conversely, when the labeling conditions are such that FITC can bind quite different environments within L7/L12, the S.S.P. becomes less (or maybe simply, FRET leads to the depolarization at higher labeling stoichiometries). Finally, the author cannot readily explain why Lee et al (1981) claimed such high specificity for FITC to L7/L12.

How, then, do the trypsin digests relate to the rather anomalous dissociation/denaturation behavior of L7/L12-FITC? In Figure 46, the amino acid sequence of L7/L12 is given. Eleven of the thirteen lysines and the only arginine are located in the C-terminal domain. Hence, it seems quite feasible that the majority of the FITCs should be in the C-terminal domain. Although, since FITC can *apparently* bind serine, it is not necessarily warranted that we attribute the lysines and arginines to the only FITC binding sites. If we assume from the amino acid sequence of L7/L12 that the majority of the FITCs were located in the C-terminal domains, then it seems quite likely that our apparent concentration-independent dissociation of L7/L12 was simply the result of the high mobility of the C-terminal domains. Hence,

only minuscule changes in rotation behavior (or FITC polarization) of the FITC should occur upon dissociation of L7/L12 into monomers. Furthermore,

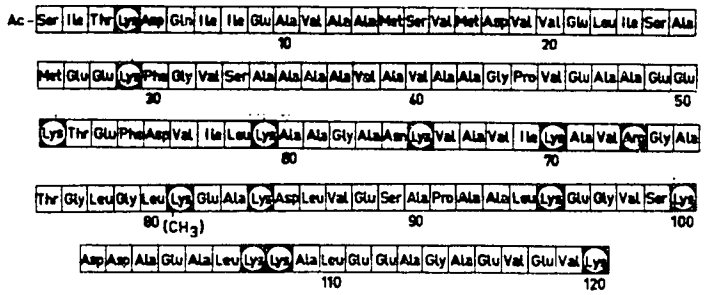

Figure 46: The amino acid sequence of L7/L12 (from Terhorst et al, 1973).

if only, say 10-20% of the FITCs were located in the N-terminal domain, then we would only expect minimal, if any, changes in the average overall polarization upon dissociation; this might explain the very small (.003) decrease in S.S.P observed with dilution of L7/L12.

ELUCIDATION OF THE DIMER TO MONOMER DISSOCIATION CONSTANT OF L7/L12 IS DEPENDENT ON THE LOCATION OF THE FLUOROPHORE. A STUDY OF VARIOUS OLIGONUCLEOTIDE SITE-DIRECTED SUBSTITUTION AND DELETION MUTANTS

In the previous section, elucidation of the dimer to monomer dissociation constant of L7/L12 via covalently attached FITC, appeared obscured by one or both of the following: 1) the majority of the FITCs may have been located in the C-terminal domains; or 2) the dissociation constant was so low (and/or complex, i.e. concentration independent dissociation) that none of the present fluorescence methods were able to detect it. Distinction between these two scenarios is the goal of this section.

Effects of Dilution of Three Hinge-Intact Cysteine Substitution Mutants. The C-33, C-63, and C-89 mutants of L7/L12 were obtained from the laboratory of Dr. R. Traut at about the time that we believed dissociation of dimeric L7/L12 might be concentration independent. Hence, we were able to directly

determine if in fact, the FITC was simply located primarily in the C-terminal domains and therefore unable to detect dissociation.

5-IAF, with its high extinction coefficient and quantum yield, is one of the best fluorescent probes for elucidating dissociation constants ranging from ~1.0 μM to sub-nanomolar. In Figure 47, we see the effects of dilution of *Peak2* (dimeric L7/L12) C-33, C-63, or C-89, each labeled with 5-IAF. Interestingly, initial dilutions of the three mutants were done before undertaking the SE-HPLC and hence, Peak1 aggregates contaminated the samples; nonetheless, the existence of ~15-20% Peak1 (recall Fig. 32A, pg. 120) had nearly no effect on the dilution curves depicted in Figure 47 (data not shown), which comes as no surprise as the polarization of 5-IAF is hardly affected by the Peak1 "aggregate" (compare polarizations in Table 7, pg. 106 and Table 10, page 125). Interestingly, the C89-IAF sample was affected the most by contamination with Peak1 as the polarization changes were slightly larger (0.200 to 0.179 or 0.197 to 0.172 one time when small amounts of free fluorescein was present); although we have not yet directly checked dilution effects on peak one C-89, we have checked the dilution effects with Peak1 C-33 (data not shown), which verify that Peak1 <u>is</u> some sort of higher aggregate that*begins* dissociating around 20 or 30 nM and the 50% dissociation point/ dissociation constant/K_D is estimated to be a little less than 1 nM (see also, next section of this chapter).

The immediate conclusion one can make from Figure 47 is that we were <u>not</u> observing concentration-independent dissociation in the first section but rather, the other possibility, that the FITCs are predominantly located in the C-terminal domains. The reasoning is as follows: 5-IAF attached to L7/L12 C-63 (in the C-terminal domain, recall Figure 7, page 28), like FITC attached to wild type L7/L12, shows practically no changes in

polarization when diluted from a few micromolar to one nanomolar. Furthermore, very little changes in the polarization of 5-IAF attached to

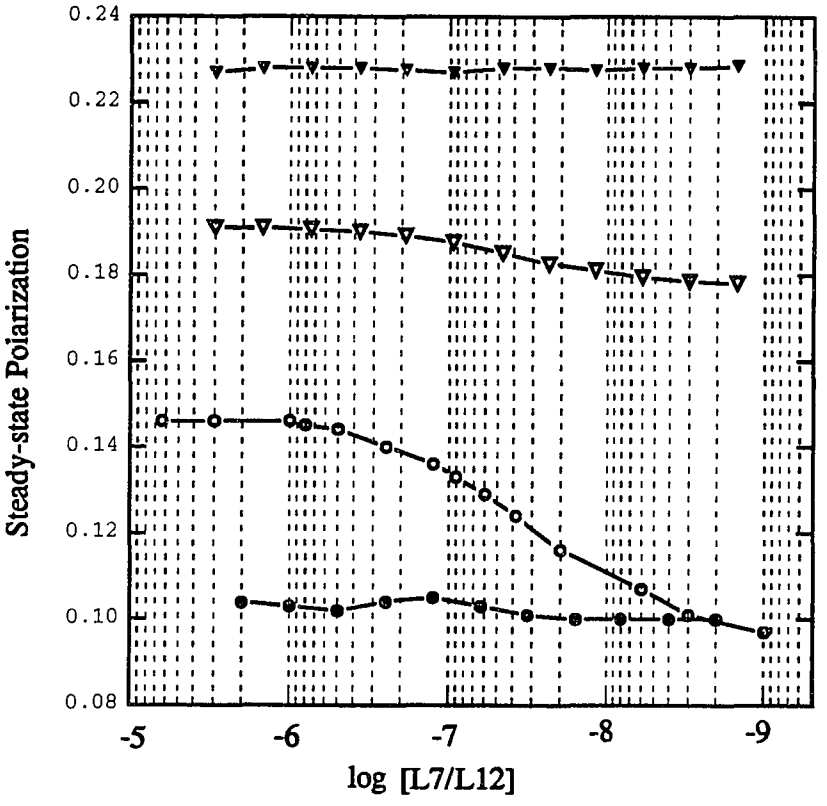

Figure 47: Effects of dilution of C-33 (hollow circles), C-63 (filled circles), or C-89 (hollow triangles), each labeled with 5-IAF. Conditions are as described in Figure 41 except temperature (and maybe time) were a factor (see next section, which includes the reversibility issue). As a control, lysozyme-FITC (filled triangles) is shown as well.

L7/L12 C-89 occur in the same concentration range (S.S.P. goes from 0.191 to 0.178). The key observation in Figure 47 is that L7/L12 C33-IAF (located in the N-terminal domains) undergoes a highly reproducible steep transition (10-90% dissociation span of ~2.2 log [dimeric L7/L12] units) beginning at ~0.3 μM (~10% dissociated). Furthermore, the midpoint of the transitions for both L7/L12 C-89 and C-33 labeled with 5-IAF is always around 38 ±2 nM. Essentially, the monomeric control, lysozyme-FITC, exhibits nearly identical

polarizations at all concentrations verifying the accuracy of our instruments and methodologies.

Many questions still needed to be answered before we could unequivocally claim that the K_D of *native or wild type* L7/L12 was 38 nM: 1) How do we know that the mutations don't result in attenuation of the subunit association? In theory, the simple fact that mutations in the C-terminal domain (C-89) result in exactly the same dissociation constant as when an amino acid is mutated in the N-terminal domain (C-33) already implied that the effects of the mutations on the dissociation were insignificant. The reasoning is as follows: in the previous chapter the author unequivocally verified that the C-terminal domains are distant from one another and hence, probably not involved in dimerization. Thus, mutations in the C-terminal domains should have little, if any, bearing on the dimer to monomer dissociation constant. Furthermore, the fact that *wild type* L7/L12 labeled with FITC primarily in its C-terminal domain appears to exhibit independent C-terminal domain rotation (first section of the last chapter and first section of this chapter) similar (if not identical) to L7/L12 C-89. If we assume that the mutation in the C-terminal domain has no effect on the K_D (in comparison to wild type L7/L12), then it must follow that mutation of serine to cysteine at position 33 in the N-terminal domain has no effect on the K_D as well since the K_D of both C-33 and C-89 labeled with 5-IAF are identical. A qualitative observation was made with SE-HPLC data in the previous chapter that wild type L7/L12 begins to dissociate slightly at around 0.3 μM. More significantly, an experimental comparison between wild type and mutant forms of L7/L12 are presented in the next section of this chapter (see also Figure 48); 2) then how do we know that the fluorophores are not affecting the equilibrium? Direct evidence is presented in the next chapter

demonstrating that the fluorophores have no effect on the equilibrium via the fact that all mutated forms of dimeric L7/L12 rapidly undergo subunit exchange with unlabeled wild type L7/L12. *Furthermore, as shown in Figure 48, the K_D of L7/L12 C33-IAF exchanged with a 10x excess of unlabeled wild type L7/L12 has essentially an identical K_D to L7/L12 C33-IAF (of 38 nM).* The data in Figure 48 are given as anisotropy since anisotropy is directly additive and hence, should give a more direct comparison to the degree of dissociation (and the relative quantum yields, given in the next chapter, are within 10-15% the same for 5-IAF bound to dimeric or monomeric C-33; 5-IAF bound to dimeric L7/L12 C33 has nearly the same quantum yield as when exchanged with unlabeled wild type). *Not surprisingly, the K_D is identical (38 nM) when anisotropy or polarization are used.* The one difference that could be noticed when comparing the anisotropy data of 5-IAF attached to C33 (and exhibiting enormous FRET) in Figure 49 to its polarization data in Figure 48 is that the dissociation span (10-90% dissociated) is decreased to 2.1 log [L7/L12] units (from 2.2) in the former; hence, in this case, steady-state anisotropy and polarization essentially possess the same information content (essentially via the fact the quantum yield of fluorescein is only changed 5-10% upon dissociation). Since the anisotropy term is directly linear, the author deems the true log dissociation span for fully 5-IAF labeled C-33 (exhibiting FRET) as 2.1 units. Furthermore, this log span is apparently increased to 2.4 units when C33-IAF is exchanged with 10x excess unlabeled wild type L7/L12. The author believes that this change in log dissociation span is purely a result of loss of the interfering FRET upon subunit exchange, but one might argue that the fluorophores interfered with the subunit equilibrium very slightly (when dimer fully labeled). The rise in steady-state polarization upon subunit exchange is simply the result of loss of energy transfer (see next chapter).

Hence, it seems unequivocal that the dimer to monomer K_D of unlabeled wild type L7/L12 is very near to 38 nM. What, then, is the significance of the log dissociation span? Dr. Weber and colleagues (recall page 26-27 on conformational drift in Chapter One of this dissertation) have shown in great deal that the theoretical log span of a simple dissociation of 2.86 units is in fact, an exception to the rule for dimeric proteins (for tetramers ~1.6). This

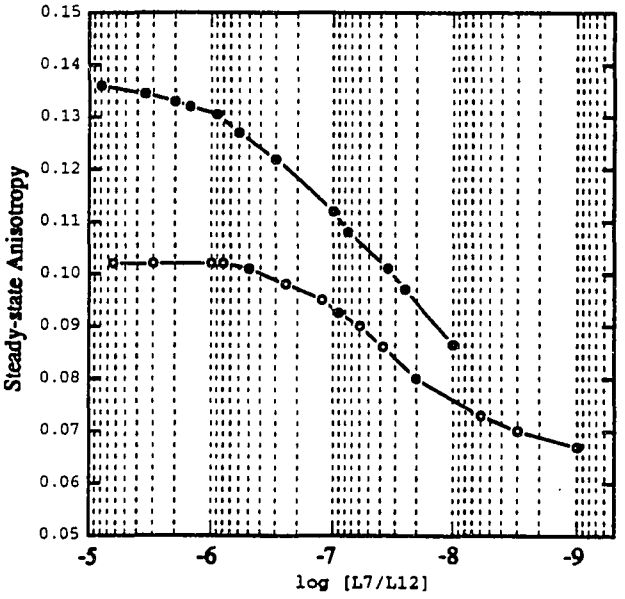

Figure 48: A plot of 5-IAF anisotropy, when bound to L7/L12 C33-IAF (hollow circles) or L7/L12 C33-IAF exchanged with 10x excess of unlabeled wild type L7/L12 (filled circles), versus concentration of L7/L12. Conditions as described in Figure 47.

shortened log span for L7/L12 dissociation is putatively caused by the conformational drift phenomenon defined on page 26 of this dissertation and previously well described experimentally by Weber and colleagues (and described in further detail for L7/L12 in the next section of this chapter). For the record, the author shall mention here that the dimer to monomer K_D of L7/L12 C33-IAF is independent of the Mg^{2+} concentration in the range of 0-20 mM, and salt concentration in the range of 0-300 mM (when the salt is greater than one molar, L7/L12 begins to aggregate--data not shown; see next section).

The author shall clarify more quantitatively the exact changes in polarization observed with 5-IAF when labeled to L7/L12 C-33 upon dissociation in the next section of this chapter (also, see pages 128-130). Here it should be mentioned once again (recall pages 128-130) that the small changes in polarization observed for 5-IAF bound to L7/L12 C-89 upon dissociation (from 0.191 to 0.178), as opposed to when bound to Peak2 C-63 (from .105 to .101), probably reflect minuscule monitoring of the overall global tumbling (i.e., the 5-IAFs, depending on their precise environment in the C-terminal domain, can monitor slightly the N-terminal domain). It is not unreasonable that 5-IAF bound to the C-terminal domain can monitor slightly the molecular volume of the N-terminal domain. Why does 5-IAF bound to the C-89 position monitor more effectively the N-terminal domain movement than when bound to the C-63 position?? The answer is obvious when one considers the time-resolved data displayed earlier for methionine oxidized samples (Table 10, pg. 125). When one considers that the fractional anisotropy amplitude of the local ρ (1.45 ns) of 5-IAF bound to C-89 is ~0.47 and when bound to C-63 is ~0.71 (local ρ is ~1 ns), it is clear that the global motion is somewhat obscured by the enormous local motion in the case of C-63. More specifically, let us assume that 5-IAF bound to C-63 or C-89 possesses the same fluorescence properties listed in Tables 10 and 11 of the previous chapter and that dissociation results in a decrease in global ρ by one-half (all other fluorescence properties staying the same). We can then calculate from Equations 5, 6, and 7 of the previous chapter (and assuming that the C-terminal domains do not rotate independnetly) that the steady-state polarization (S.S.P.) of 5-IAF bound to C-89 will drop from 0.191 to .146 and that the S.S.P. of 5-IAF bound to C-63 will decrease from 0.105 to 0.081; hence, the drop in polarization in the former should be nearly double that of the

latter and experimentally, the drop is only slightly larger (~3x) than that. This slight discrepancy (~33%) may simply reflect the relative axial orientations of the probes, which could explain why FITC, randomly bound primarily in the C-terminal domains of wild type L7/L12 monitors only ~5-15% the N-terminal domains. Hence, the data here suggest that 5-IAF may monitor slightly (~5-15% of the global ρ) the global tumbling of L7/L12, which may have increased its apparent global ρ by a few ns. Thus, the true segmental relaxation time of the C-terminal domain may be that reported for monomeric L7/L12 (~18 ns; see Table 10, pg. 125).

Effects of Dilution on Various other Substitution and Deletion Mutant Forms of L7/L12. After elucidating the dissociation constant of hinge-intact L7/L12, it seemed likely that elucidation of the dissociation constant might be considerably easier for a hinge-deleted mutant. The reasoning was simple: if the 21 kD hinge deletion mutant lacks independent C- or N-terminal domain mobility (i.e., more rigid, it should not matter where the fluorescent probe is bound as long as its fluorescent lifetime is sufficient to monitor changes in the global rotation. Since the hinge deletion mutant is ~21 kD, the ~four ns fluorescence lifetime of 5-IAF should easily monitor the global (tumbling) rotational relaxation time. As we saw in the previous chapter (Tables 15 and 16, pg. 138), the global rotational relaxation time of 5-IAF bound to L7/L12 Δ35-52 C-89 was ~18 ns; it was mentioned that if we eliminate FRET via subunit exchange, the global ρ increases to ~28 ns (axial ratio ~2-4:1; page 142) and we shall find in the next chapter that the S.S.P. rises from .109 to .148 upon complete subunit exchange.

In Figure 49, a plot of L7/L12 Δ35-52 C89-IAF protein concentration versus the S.S.P. of 5-IAF is presented. Interestingly, the polarization of 5-IAF rises slightly upon dilution from 4 μM protein dimer concentration and then

begins to drop slightly around 50 nM. The results were fairly inconclusive but appeared similar to the results of C63-IAF. One could only conclude one of two things: 1) either the protein was not dissociating; or 2), the 5-IAF could not accurately monitor the dissociation due to a unique binding environment. It is rather difficult to imagine how the 5-IAF could not monitor the dissociation of a rigid 21 kD protein and hence, the author initially concluded here that the hinge-deletion mutant was in fact not yet dissociating (i.e., a considerably more stable dimer than the hinge-intact forms of L7/L12). Although, the possibility of some unusual sort of mobility within the hinge deletion mutant could not be excluded. Further attempts in elucidating the K_D of the hinge deletion mutant with other probes such as TMRIA or IAEDANS, gave equally inconclusive results. The TMRIA data appeared very similar to the 5-IAF data and hence, is not shown here. Interestingly, the IAEDANS data appeared to demonstrate some sort of transition between ~30 μM (S.S.P. = .092) and ~35 nM (S.S.P. = .073) with a midpoint of about 0.8 μM; we have not repeated this experiment and question its significance since no change in SE-HPLC elution volume occurs in this dilution range (data not shown). Evidence is revealed before the end of this dissertation that the hinge-deletion mutant of L7/L12 appears oligomerically heterogeneous (vide infra). Preliminary results using the Gu-HCl method described above, were equally inconclusive (data not shown). We shall find in the next chapter that the K_D can be estimated by the rate of subunit exchange.

Only recently, four more mutants of L7/L12 were created in the Traut laboratory and sent to us: C-99, C-12, NTF, and CTF C89, and the hydrodynamics of each labeled with various fluorescein derivatives were initially described in the previous chapter. In Figure 49, the dissociation via dilution

curves of each are shown. As expected, the steady-state polarization of 5-IAF bound to CTF remains essentially unchanged from 10 μM to 1 nM concentrations once again verifying that the CTF's do not form a complex as originally suggested by Liljas in 1982 (although, once again, one might argue

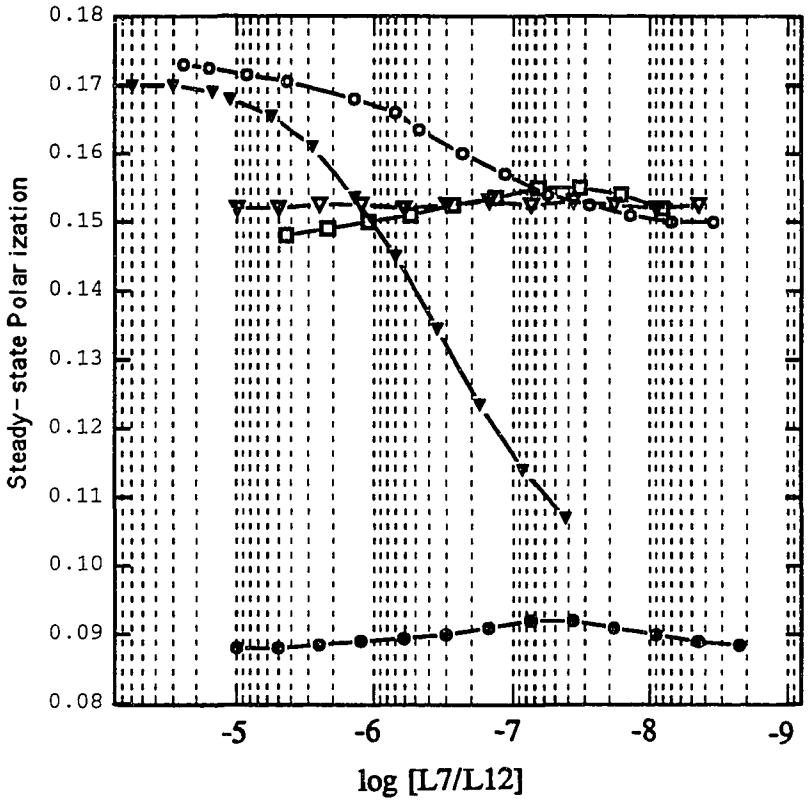

Figure 49: Effects of dilution on L7/L12 Δ35-52-IAF/10x unlabeled Δ35-52 (hollow squares), CTF C89-IAF (hollow triangles), C99-IAF (solid circles), NTF-FITC (hollow circles), and C12-IAF/8x unlabeled C-12 (filled triangles). Conditions as described in Figure 47.

that the fluorescein moiety or 5-IAF binding somehow dissociates the complex; if so, then the complex must be extremely weak and perhaps only able to form in the crystalline state). On the same note, the 5-IAF monitors nearly identical motional properties at the various protein concentrations when bound to C-99 as when compared to when bound to C-63 (recall Figure 47), verifying once again the independent C-terminal domain mobility. L7/L12 C99-IAF is described in slightly more detail in the next section and in

considerably more detail in the next chapter. As mentioned in the previous chapter, the extent of intersubunit FRET should be minimal if at all, and so it was unnecessary to exchange in unlabeled L7/L12.

Interestingly, the K_D of NTF-FITC was slightly higher (~0.3 μM) than that of C33-IAF (~0.04 μM). Hence, deletion of the C-terminal domain apparently destabilizes the NTF interaction by 8x. Interestingly, the log span of the dissociation remains at ~2.2. The drop in polarization from 0.172 to 0.150, is in good agreement with the time-resolved data (partially shown earlier for the dimer in Table 18, pg. 146; for monomer, global ρ of FITC is reduced to ~55% that of the dimer and α's ~unchanged--data not shown) and theory, which would predict a drop in S.S.P. of 0.172 to 0.152 upon simple dissociation!! The fact that we see such a minuscule drop in S.S.P. (0.022) of FITCs upon dissociation makes it not so difficult to imagine why we're unable to see a drop in S.S.P. of more than 0.003 upon dissociation of the intact wild type L7/L12 (with FITCs primarily located in the C-terminal domains).

Finally, the K_D of L7/L12 C12-IAF was determined to be "shifted" to ~0.32 μM (Figure 49)!! An 8 x excess of unlabeled and reduced C-12 was exchanged in to allow measurements at higher protein concentrations (no interference of inner-filter effects) and to eliminate contaminating energy transfer (although, fully-labeled dissociation constant is same, data not shown). Interestingly, the log dissociation span remains at ~2.3. The data can be explained in one of three ways: 1) either the mutation of alanine 12 to cysteine results in 10x destabilization of the putative coiled-coil (i.e., dimer of L7/L12); 2) labeling of cysteine 12 with 5-IAF results in a 10x destabilization of the dimer; 3) both effects are manifested. The present author believes that first option is most likely: 1) since alanine prefers to participate in α-helix

formation (see Richardson and Richardson, 1989) which is necessary for coiled-coil formation and cysteine is more commonly found in loops or disordered regions in proteins (see Richardson and Richardson, 1989); 2) the rather normal log dissociation span indicates that FITC does not destabilize significantly the average conformation of the pure dimer state of L7/L12 C12 (see Xu and Weber, 1982). In the next section, additional quantitative description of L7/L12 "stability" is given. Furthermore, the polarization of 5-IAF bound to C-12 drops similar in magnitude to when bound to C-33, subsequent to dissociation. *Thus, it seems likely that similar conformational changes occur local to the C-12 or C-33 residues upon dimer dissociation, whereas, the local environment of the FITC (s) bound to NTF does not seem to be significantly altered upon dissociation.*

CHARACTERIZATION OF L7/L12 STABILITY. CONSIDERATION OF THERMODYNAMICS AND KINETICS

Effects of Dilution, Temperature, and Guanidine-HCl on the Kinetics and Thermodynamics of L7/L12 Denaturation. Earlier, in Figure 41, the caption indicated that their was no apparent dissociation (as the FITC is not located at a site suitable for observation of dissociation) of diluted wild type L7/L12-FITC, regardless of the time or temperature of incubation. Furthermore, the Gu-HCl and high-pressure experiments exhibited little, if any, time or temperature dependence (i.e., effects were rapid). Conversely, it was mentioned that the *dissociation* of L7/L12 described in Figures 47-49 exhibited some temperature (maybe time) dependence (see next subsection). Hence, the data previously described in this chapter indicated that *denaturation* (2° or 3° structure via Gu-HCl, urea) or *unfolding* (of presumably 3° structure via high-pressure) of L7/L12 in the region local to the FITC lacks significant time (range of <10 seconds to several days) and

temperature dependence (from ~4°C to ~44°C; see Table 21). We obviously could not, however, exclude that denaturation of all structures or domains of L7/L12 were independent of the time or temperature of reaction; rather, only in the *given ranges*. The data in Table 21 indicate that the denaturation or unfolding of wild type L7/L12 in the region (s) of the FITC (s) is quite rapid and the subsequent 2° or 3° conformation of L7/L12 in the region of the probes are stable for up to several months depending on the temperature of storage.

Table 21: The Effects of Dilution, High Pressure and Temperature on the Kinetics of Changes in the Steady-state Polarization of FITC Bound to Wild Type L7/L12 Subsequent to Addition of Denaturants*.

Treatment of wild type L7/L12-0.2 FITC	Time scale of completion of the initial changes in S.S.P.	Time scale of *no further* changes in S.S.P.
dilution from 10 μM to1nM	<10 seconds	> 24hours (at 44°C) or three months (at 4°C)
addition of any aliquot of 0.2 - 6 M Gu-HCl	<10 seconds	same as dilution
addition of any induction increment of pressures between 1 and 3000 atm	<30 seconds	same as dilution except only observed up to three hours at various pressure inductions and/or T's.

*S.S.P. is steady-state polarization. See text for further details. Denaturants include Gu-HCl or urea.

The Gu-HCl denaturation (or 5-IAF fluorescence depolarization) curves for dimeric (1μM) and monomeric forms of C33, C63, C89, and NTF (5μM), each labeled with 5-IAF, are shown in Figure 50. Furthermore, the denaturation curves of the hinge-deletion mutant (10 μM; exchanged w/10x unlabeled; no FRET; Figure 50A) or CTF C-89 (Figure 50B) are given. Similar to wild type L7/L12 labeled with FITC, the denaturation of each was very

rapid (<10 seconds) and initial results determined that the denaturations on the short time scale (seconds) were independent of the temperature in the range of 4 to 44°C (see next subsection for more details). Conversely, in the case of a concentration-dependent dissociation process, we shall find that time and temperature in the ranges depicted in Table 21 can affect its kinetics and thermodynamics (see next sunbsection).

Several interesting conclusions can be made from the Gu-HCl denaturation transtions seen in Figure 50 for the various mutants:

1) The polarizations of 5-IAF bound to dimeric (1 μM) L7/L12 C-33 upon addition of the denaturant Gu-HCl unequivocally simulate those depicted in Figure 47 for the *dilution* of L7/L12. Hence, the data in the two figures demonstrates that the *denaturation of the region local to C-33 is closely (if not perfectly) coupled to the dissociation of L7/L12.* In fact, we shall see in the next subsection that dilution of L7/L12 C33-IAF prior to addition of denaturant results in shifting of the denaturation curves to lesser Gu-HCl concentrations (i.e., the effect desired but not observed earlier in Figure 42). Of further interest, addition of denaturants to the monomeric form of L7/L12 C33-IAF resulted in insignificant changes in the polarization of 5-IAF; more specifically, the protein region local to the C-33 already demonstrated considerable mobility in the monomeric form reached simply by dilution in the absence of chemical denaturants. *Furthermore, the time-resolved fluorescence data for L7/L12 C33-IAF denatured in 3.6 M Gu-HCl or diluted to 1 nM are nearly indistinguishable* (see Figure 51). Hence the data are consistent with NTF existing as a coiled-coil, which loses secondary structure subsequent to dissociation.

2) In contrast to the L7/L12 C33-IAF data, the NTF-FITC data did not display such apparent coupling between local unfolding and dissociation.

A)

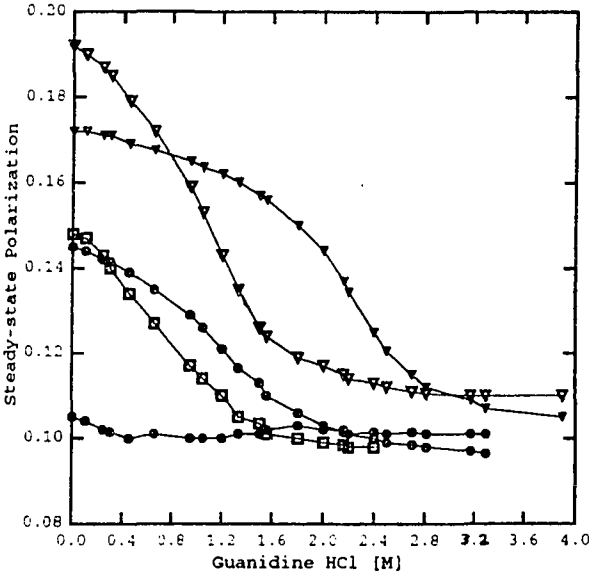

B)

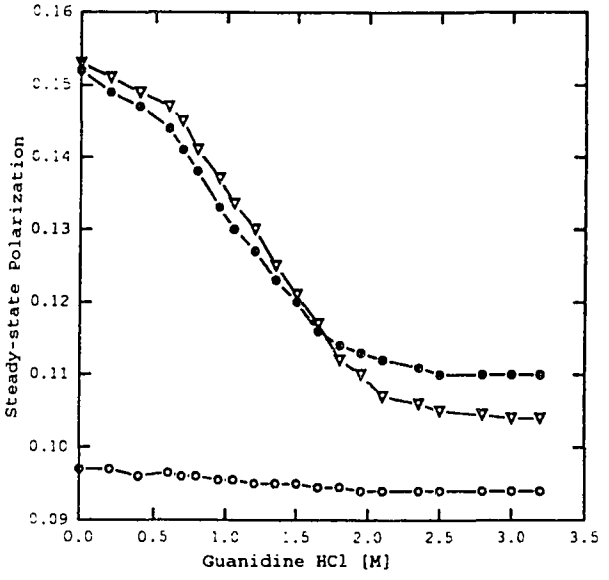

Figure 50: A) The Gu-HCl denaturation curves for dimeric (2.0 μM) L7/L12 C33 (hollow circles), C63 (filled circles), C89 (hollow triangles), and NTF (filled triangles); furthermore, the hinge deletion mutant labeled with 5-IAF and exchanged with 10x excess unlabeled (to prevent FRET) is shown as well (hollow squares); B) the Gu-HCl denaturation curves for monomeric (dissociated via dilution) forms of L7/L12 C33 (hollow circles), CTF (filled circles), and NTF (hollow triangles) are shown as well. Each of the above proteins were labeled with 5-IAF except NTF, which was 15% (molar/molar) labeled with FITC. Recall the midpoint of the Gu-HCl denaturation of dimeric or monomeric wild type L7/L12 labeled with FITC was ~2 M Gu-HCl (Figure 42). All measurements were taken at 20°C with 488 nm excitation of fluorescein derivatives (085 cut-on emission filters). *In all cases, the polarization changes were immediately reversible upon spin-column removal of Gu-HCl.*

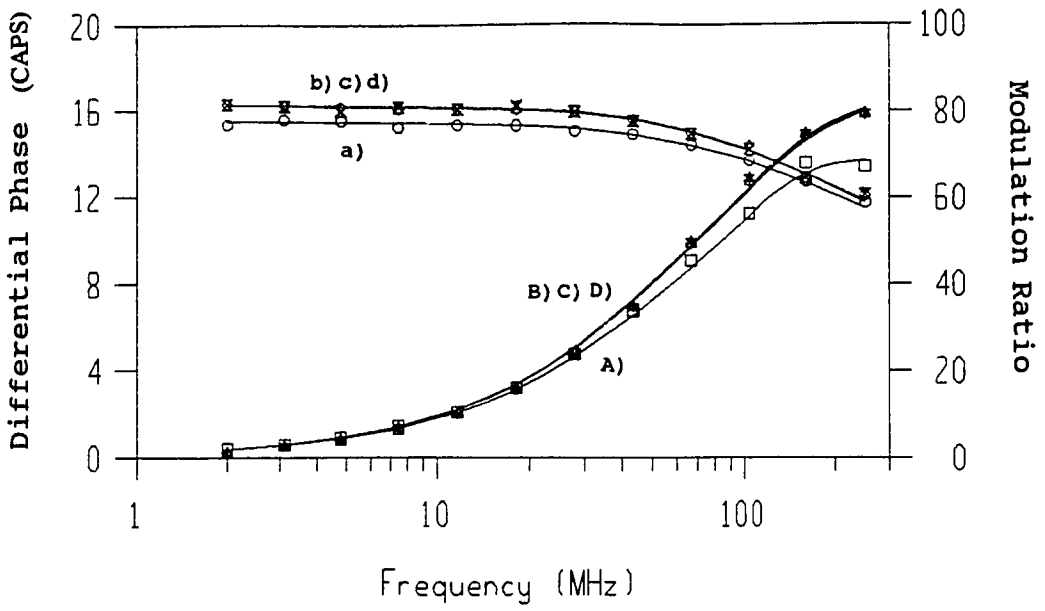

Figure 51: Dynamic polarization data of 5-IAF bound to dimeric L7/L12 C-33 (a,A), 3.6 M Gu-HCl denatured/dissociated L7/L12 C-33 (b,B), 1 nM (dissociated by dilution) L7/L12 C-33 (c,C), or methionine oxidized L7/L12 C-33 (d,D). All data were acquired at 20°C upon 488 nM excitation (085 emission cut-on filters). The rotational parameters acquired from the analysis of these data sets were partially presented in the previous chapter (Tables 9 and 10).

This result seems somewhat peculiar at first glance since both the IAF and FITC are bound to amino acid residues located in the N-terminal domain. The Gu-HCl denaturation of dimeric NTF results in a decrease in polarization from 0.172 to .105 (transition midpoint at 2.1 M), whereas, the dissociation via dilution of NTF-FITC results in a decrease from 0.172 to only 0.150 (recall Figure 49). Hence, the data here unequivocally determine that the secondary

structure of the region local to the FITC in the N-terminal domain, is not completely disrupted upon simple dissociation via dilution as was the case with C-33 (also, of course, in the N-terminal domain); this theory is further evidenced when one compares the Gu-HCl denaturation of dimeric *and* monomeric forms of L7/L12 C33-IAF or NTF-FITC. Similarly, no transition is observed when Gu-HCl is added to monomeric L7/L12 C33-IAF, whereas, a transition beginning at 1.3 M (rather than 2.1 M) Gu-HCl occurs with NTF-FITC. The simple fact that the midpoint of the transition for NTF-FITC is decreased from 2.1 M Gu-HCl for the dimer to 1.3 M Gu-HCl for the monomer, provides strong evidence that much (~60%) of the secondary and/or tertiary structure still remains in the region local to the FITC (s) subsequent to simple dissociation via dilution (vide infra for more details). In conclusion, it appears likely that the region local to C-33 undergoes a considerably more complete conformational change upon dissociation than that of the FITC binding site (s). The present author speculates that the C-12 and C-33 are located within the coiled-coil, whereas, the FITC is located within different structure in the NTF. In fact, using the extrapolation procedure described earlier (pages 175-177), one can determine that an additional 3 or 4 kcal/mole are needed to completely denature the region (s) local to the FITC (s) subsequent to dissociation via dilution (data not shown). Furthermore, it is also apparent that this procedure of correlating the free energy of Gu-HCl denaturation to that of dimer dissociation is less accurate in the case of NTF-FITC, i.e., when significant conformational change upon dissociation is not evident (data not shown). This theory becomes undeniable when one realizes that the midpoint and slope of the Gu-HCl-induced unfolding transition is shifted to higher concentrations of Gu-HCl in the case

of NTF-FITC, even though the NTF-FITC dimer is less stable (K_D is 0.15 μM instead of 0.038 μM as in the case od dimeric L7/L12 C33-IAF);

3) The denaturation curves of dimeric (1μM) or monomeric (2 nM) L7/L12 C-63 are nearly identical, further indicative of the inability of 5-IAF to monitor dissociation of L7/L12 when bound to C-63 (recall Figure 47). Furthermore, the data here further demonstrate that the region local to C-63 is *highly disordered* regardless of whether L7/L12 is a dimer or monomer;

4) The Gu-HCl denaturation of CTF C89-IAF resulted in a midpoint of 1.1 M Gu-HCl. Furthermore, the midpoint of the Gu-HCl denaturation of dimeric (1μM) or monomeric (2 nM) fully intact L7/L12 C89-IAF is ~1.1 M. The data indicated that the secondary/tertiary structure of the region local to the C-89 remains unchanged upon genetic deletion (i.e., or phenotypic deletion) of the hinge and NTF. Hence, the data here are in excellent agreement with the unchanged fractional anisotropy amplitudes of the ρ's of 5-IAF bound to CTF C-89 (Table 18) or L7/L12 C-89 (Table 10);

5) The denaturation of the hinge-deletion C-89 mutant (1 μM "dimer") is 50% complete by 0.75 M; hence, the data here indicates the deletion of the hinge (but not the NTF, as was the case with CTF C-89) results in conformational changes such that the region local to C-89 becomes apparently destabilized. Recall, in the previous chapter (144-147) that the time-resolved fluorescence data indicated a considerable increase in local mobility of the C-89 region upon hinge deletion. Hence, one intriguing explanation for the steady-state (Figure 50) and time-resolved (previous chapter) fluorescence comparison of 5-IAF bound to the hinge-deleted and hinge-intact L7/L12 C-89, is that the secondary and/or tertiary structure of the former protein is attenuated relative to the latter. Interestingly, we were unable to determine the K_D of the hinge-deletion mutant in the previous section, possibly

indicating greater stability (lower K_D). The author shall speculate now that the secondary/tertiary structure of the region local to the C-89 (maybe a large portion of the C-terminal domain) is destabilized upon hinge-deletion, but that the quaternary structure, predominantly determined by interactions between the two N-terminal domains, is augmented; this theory is not unreasonable when one considers also the SE-HPLC data (previous chapter) and finally, the author shall present more direct experimental evidence in the next chapter.

What, then, is the significance of the *midpoints* of the Gu-HCl denaturation transitions monitored by the fluorescent probes ? The various midpoints of the transitions of the various fluorophore-labeled forms of L7/L12 can be classified into four categories:

1) Those with transition midpoints of 1-1.3 M Gu-HCl. This category includes monomeric NTF-FITC, monomeric or dimeric C89-IAF, CTF C89-IAF, and *dimeric* C33-IAF (not greater than 2μM dimers; vide infra). Furthermore, *dimeric* C12-IAF (data not shown) or *Peak1* C33-IAF/C63-IAEDANS/C89-IAF possess denaturation midpoints of ~1.1M Gu-HCl. Data has been obtained for Peak1 C33-IAF and C89-IAF, which indicates that the secondary and tertiary structure of these forms of L7/L12 are fully intact (data for 5-IAF not shown; for IAEDANS, see Figure 52 below) or unaltered in comparison to Peak2 forms. It is interesting to note here that dissociation via dilution of NTF-FITC results in conversion to a local structural region of this category;

2) The hinge-deletion C-89 mutant has a unique transition of ~0.7 M Gu-HCl independent of the fluorophore used. In addition to 5-IAF, we have checked the transition with IAEDANS and TMRIA, which give nearly identical results (data not shown) as 5-IAF. In fact, as shown in Figure 52,

extending the fluorescence lifetime to 12 or 13 ns has no effect on the transition monitored for any of the proteins checked (except C-63, vide infra);

3) Those forms of L7/L12 which, as monitored by 5-IAF, do not undergo any conformational transition upon addition of Gu-HCl. These forms include dimeric or monomeric C-63 or C-99 and*monomeric* C33 (have not yet checked C12). Interestingly, a slight transition is observed in C-63 when labeled with 1,5-IAEDANS. It seems likely that the increased fluorescence lifetime simply extends the time-frame (and/or heterogeneity) of the rotational relaxation times monitored. The explanation for this lack of denaturation transition (from 0-8 M Gu-HCl) is simple: if their is no secondary structure to begin with, then their is no secondary structure to disrupt. Hence, *both* the steady-state (here) and time-resolved (previous chapter--recall the enormous local motion in the case of these particular probe/protein conjugates) fluorescence data unequivocally verify that the amino acid to which the probes are attached (in this category), reside within a random coil (or structureless) region;

4) Those forms of L7/L12 that undergo denaturation transitions of ≥1.8 M Gu-HCl. This category includes wild type L7/L12 labeled with FITC (Figure 41) or IAEDANS (data not shown), *high concentrations* (10μM) of dimeric C33-IAF exchanged with unlabeled wild type L7/L12 (see Figure 53), and dimeric NTF.

What can we conclude from the four transition midpoint categories? When the fluorophore is bound to a dimeric region or domain, it monitors a denaturation transition of increased Gu-HCl concentrations relative to that of the monomer. More specifically, assuming that the NTF of L7/L12 is a coiled coil, it appears that a coiled-coil (two α-helices) is considerably more resistant to Gu-HCl denaturation than a single α helix. An excellent example is the

NTF data, which upon dissociation via dilution, the transition is shifted from category four (≥2.1 M Gu-HCl) to category one (~1.3 M Gu-HCl). This observation is even more drastic when one looks closely at the C-33 data, where dissociation apparently results in complete loss of 2° structure! Furthermore, the results presented in this section are in good agreement with

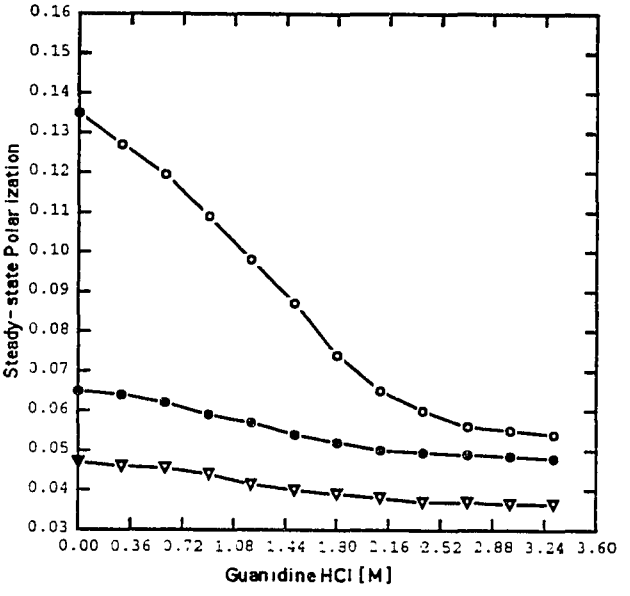

Figure 52: The Gu-HCl transitions of Peak2 (dimeric) C-33 (hollow circles) or C-63 (filled circles), and Peak1 C33 (hollow squares) each labeled with IAEDANS. Data were acquired upon 351 nm excitation and emission was collected via KV399 filters. Temperature was kept at 20°C and the times of the reactions subsequent to Gu-HCl addition were less than 10 seconds.

the early CD experiments on L7/L12 (mentioned in introduction of this chapter), that L7/L12 possesses a heterogenous structure with regards to stability. It is interesting to note that the midpoint of the transition of native L7/L12 in urea is ~3.6 M as judged by urea gradient PAGE (Oleinikov et al, 1993A). Similarly, the midpoint of the denaturation transition of wild type L7/L12 labeled with FITC in urea is also 3.6 M when judged from steady-state polarization data (data not shown). The PAGE method used by Oleinikov obviously reflects the *overall average* (2°, 3°, and 4° structure) conformational transition of L7/L12. Hence, it seems likely that the ~1.8 M Gu-HCl

transition midpoint for wild type L7/L12 labeled with FITC shown earlier in this chapter reflects the rather average transition midpoint of L7/L12 (also in good agreement with previous CD results, which indicate the overall midpoint of L7/L12 denaturation is ~1.5 M Gu-HCl; Luer and Wong, 1980). Conversely, when fluorophores are bound to *specific sites* within a protein, they monitor the unfolding transition of primarily the local 2° structure. One

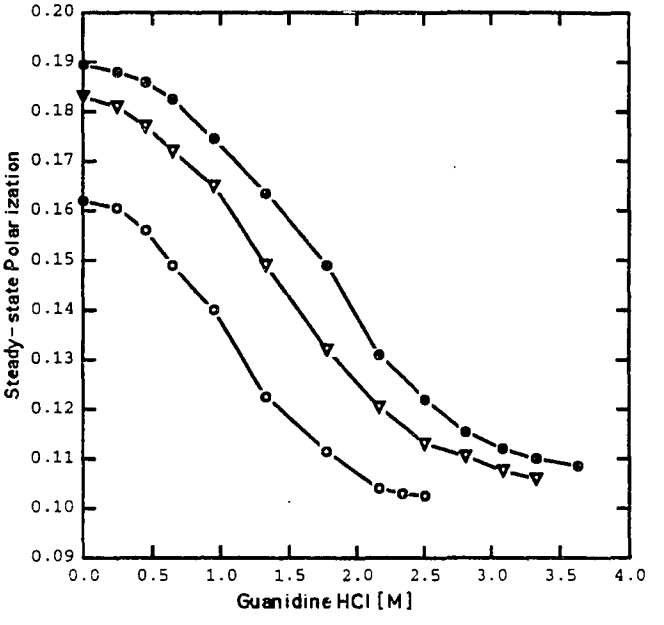

Figure 53: Dependence of the midpoint of the guanidine HCl-induced denaturation/ dissociation on the protein concentration of L7/L12 C33-IAF/10x wild type. Filled circles represent 8 μM L7/L12, hollow triangles represent 4.0 μM L7/L12, and hollow circles represent 0.5 μM L7/L12 all at 20°C. 5-IAF was excited at 488 nm and emission collected with 085 cut-on filters. A concentration dependent shift in the curves unequivocally verifies a dissociation process is occurring (compare to Figure 42 where dissociation is not monitored). If the K_D of a protein is too low to be detected, then these shifts can be used to calculate it (see Timm and Neet, 1992). *Note how the midpoint of the denaturation becomes nearly identical to that of dimeric C33-IAF (Figure 50) when the dimeric protein concentration essentially becomes ~0.5 μM.*

might argue that the fluorophores simultaneously monitor 3° and 4° conformational changes depending on its specific attachment site. The data here (category 3) indicate that if the fluorophore is bound to a local random

coil region, it cannot monitor any significant changes in the local tertiary or quaternary structure of L7/L12 regardless of its location (C-33 monomer, C-63, C-99). Conversely, if the probes are located in a rather structurally intact region within a domain rotating independent (i.e., segmental rotation) of the entire protein (i.e., global tumbling), it is not unreasonable that some tertiary structure (+ minor amounts of 4° structure) unfolding can be monitored. In the very unique case of L7/L12 (any form), changes in quaternary structure upon addition of denaturants, can only be significantly monitored by placing the probe within a structurally (2°) organized region of the domain (3°) responsible for dimerization (4°). The sole obscurant of this phenomenon is the structureless hinge region, which separates the two tertiary domains and allows their rather independent rotation. Further discussion of the data is given in the conclusions of this chapter.

Effects of Dilution, High Pressure, and Temperature on the Kinetics and Thermodynamics of L7/L12 Dissociation. In contrast to the denaturation of L7/L12 (shown in Figure 51), the *dissociation* of L7/L12 C-33 as monitored via fluorescence depolarization of 5-IAF appears somewhat more dependent on temperature in the range of 4°C to 37°C (see Figure 54). Interestingly, if a dimer of L7/L12 C-33 in TMND pH 7.4 buffer and fully labeled with 5-IAF is rapidly (few seconds) diluted to 4 nM at 20°C, the S.S.P. drops from ~0.146 to ~0.105, and then over several hours progressively and nearly linearly drops to 0.097 (data not shown). If the sample is left at 20°C for another 24 or 72 hours, respectively, the S.S.P. drops to 0.082 and 0.069 (data not shown; depolarization was not due to probe fall-off a s verified by dialysis)! At first glance, the author believed that this drop in S.S.P. over time may be attributed to some kinetic parameter of dissociation (e.g., bi-exponential rate constant), but after SE-HPLC of a 1μM sample left at 20°C for 48 hours, it

became quite evident that the drop in S.S.P. may have simply reflected degradation of some sort (rather small fragments, mostly greater in elution volume than the monomers, appeared in the chromatogram; data not shown). Similarly, degradation of L7/L12 becomes a problem after several hours at 37°C. The author has not rigorously attempted to track down the source of this degradation. Furthermore, since dissociation of L7/L12 via

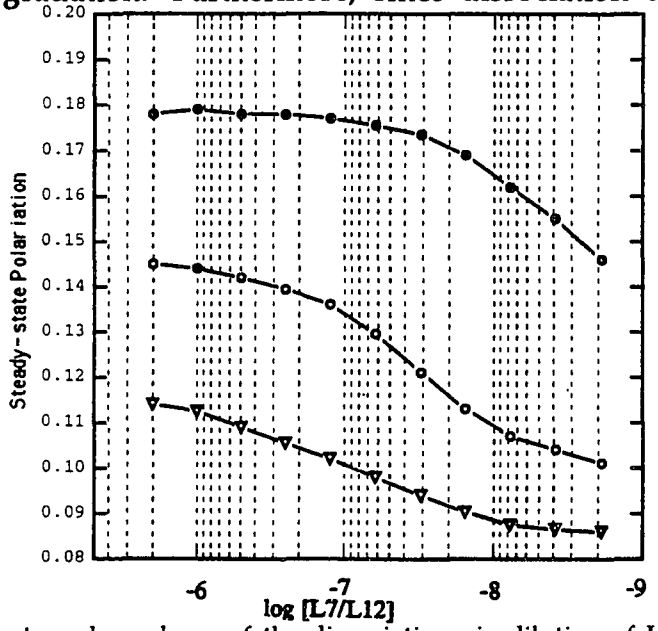

Figure 54: Temperature dependence of the dissociation via dilution of L7/L12 C33 fully labeled with 5-IAF, as monitored via fluorescence depolarization of 5-IAF. Dilutions and measurements were at 4°C (hollow circles), 20°C (filled circles), or 37°C (hollow triangles). Excitation was at 488 nm and emission was collected via 085 cut-on filters. Measurements were taken three minutes subsequent to dilutions. Data are the result of one experiment.

dilutions at either 4°C, 20°C, or 37°C is in fact always ≥90% complete in faster than 30-60 seconds, it did not appear necessary to identify the source of the degradation. Similarly, it seemed evident that this last 10% of depolarization that occurs over an ~two hour time-period represented a rather biexponential dissociation rate process (see Lin et al, 1993 for a nice description of bi- or multi-exponential dissociation rate constants in conjunction with experimental data representing the interaction between myosin subfragment-1 and actin; also, see next chapter for more details with L7/L12).

The primary conclusion made from Figure 54, is that raising the temperature to 37°C results in a new dimer to monomer dissociation constant for L7/L12 of ~100 nM. Conversely, lowering the temperature to 4°C results in a new K_D of an estimated 7 nM, although the data was obscured by the fact that we could not dilute all the way to completion of dissociation. Hence, in contrast to previous results with many other proteins (i.e., see Silva et al, 1986; Ruan and Weber, 1986; Ruan and Weber, 1993), dimeric L7/L12 is more stable at 4°C than 20°C or 37°C. The result is not, however, unreasonable since most papers published on the stability of coiled-coils have determined that raising the temperature destabilizes this rather unique structure (see Lau et al, 1984; Holtzer et al, 1984; Mo et al, 1991; Zhou et al, 1992; Thompson et al, 1993; Zhu et al, 1993; Zhou et al, 1993; Greenfield et al, 1993). Hence, the data here are qualitatively in agreement with the theory that L7/L12 dimerizes via a coiled-coil structure in its N-terminal domain. Interestingly and rather ambiguously, the author has noted repeatedly, that storage of L7/L12 C33-IAF at 4°C (in the refrigerator) for longer periods of time (overnight or longer) results in a decrease in the K_D; the significance of this result is questionable because it is quite possible that methionine oxidation is occurring in the refrigerator (hence, as mentioned in Chapter Two, storage at -70°C is considerably more safe).

Finally, the author shall simply note here that the dissociation appears readily reversible upon addition of several μM wild type L7/L12, although it appears that the reversibility is somewhat attenuated when L7/L12 is diluted to ~the K_D. Hence, it cannot be excluded here that dissociation via dilution is a rather two-state transition process. This issue has not yet been pursued, but indicates that some conformational drift occurs upon dilution to less than the

K_D, in contrast to the Gu-HCl studies in which reassociation was immediately reversible upon removal of the Gu-HCl (see below for more discussion).

Thermodynamically, what does the result in Figure 54 tell us about L7/L12? The change in enthalpy of association can be calculated as follows (from Ruan and Weber, 1993):

$$\Delta H = \Delta G_1 - dG(T/\delta T) \qquad (49)$$

where ΔG_1 is the free energy of association at the lower temperature, T, ΔG_1 + dG is the free energy of association at the higher temperature, and δT is the temperature differential. Since the free energy of association at 4°C and 37°C was respectively, -11.1 kcal/mol and -9.5 kcal/mol, the enthalpy of association of dimeric L7/L12 is -23.5 kcal/mol and $T\Delta S$ at 20°C (where ΔG = -10.1 kcal/mol) is -14.4 kcal/mol. Hence, the association of L7/L12 (like coiled-coils, in general) appears largely enthalpy driven according to equation 49 and the data in Figure 54 possibly indicative of a denaturation-type process.

Finally, in an attempt to gain more information on the nature of the dimerization of L7/L12, in Figure 55, a pressure-induced dissociation of L7/L12 C33-IAF at various protein concentrations is depicted. The author calculated the ΔV for "association" of wild type L7/L12 monomers via the span of the pressure dissociation. It seemed unlikely that the depolarization induced upon compression was really due to dissociation since their was no protein concentration-dependent shift in the midpoint of the curves to lesser pressures. In Figure 55, the desired effect is seen when 5-IAF is bound to L7/L12 C-33. This concentration-dependent shift can also be used to calculate the ΔV and ΔG of L7/L12 association as (see Weber, 1992):

$$dp\,(C_1,C_2) = (2.302\,RT/\Delta V)\log(C_1/C_2) \qquad (50)$$

where dp is the difference in the midpoint of the pressure dissociation of L7/L12 at two different protein concentrations (C_1,C_2). The author shall

nominate the ΔV calculated from this method as ΔV_C. Hence, ΔV and ΔG can be calculated by two separate methods from the pressure data.

The first conclusion that one can make from the data in Figure 55 is that the pressure dissociation results in essentially identical polarization change as the dissociation induced via dilution or Gu-HCl. Secondly, using

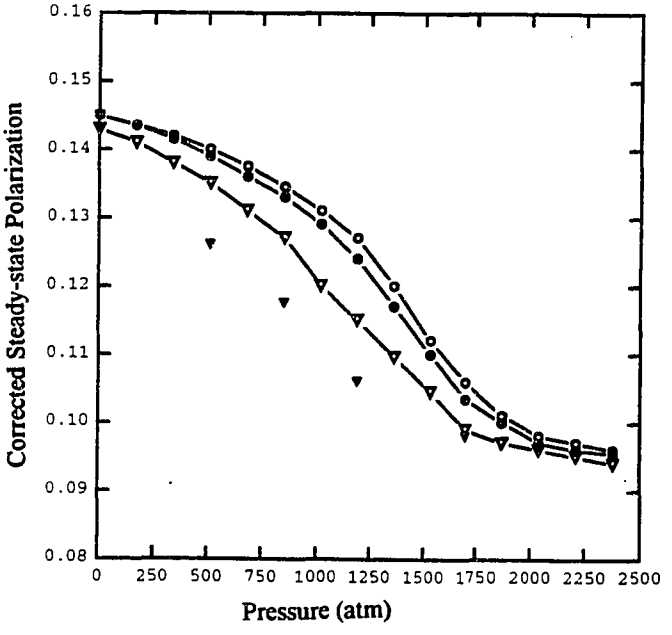

Figure 55: Pressure-induced dissociation of L7/L12 C33-IAF. Protein concentrations (calculated as dimers) were 5 μM (hollow circles), 2.5 μM (filled circles), and 0.5 μM (hollow triangles) and all data were acquired at 20°C with the instrument described in the Materials in Methods chapter of this dissertation. Excitation was at 488 nm and emission collected through 085 cut-on filters. Also shown is the decompression curve for 5 μM L7/L12 C33-IAF (filled triangles).

Equation (46) and the pressure-induced dissociation span for 5 μM dimer in Figure 55, one can calculate a ΔV (from Equation 46, let us nominate ΔV_P) of ~115 mls/mole and a K_D of (from equation 48) about 10 nM. Hence, the K_D calculated from the pressure-dissociation span is not so deviant from that actually measured via dilution. If we use equations 50 and 48 along with the

data in Figure 55, we can calculate a ΔV_C of ~135 mls, which is not so dissimilar to that calculated from the span (ΔV_P). A large discrepancy between the two calculated ΔV values occurs usually only in the case of tetramers or large protein aggregates, which is presumably the result of a very heterogeneous dissociation equilibria (see Erijman and Weber, 1991 and references therein). Hence, the pressure data for L7/L12 C33-IAF do not necessarily agree with idea that the quaternary structure of L7/L12 is thermodynamically unique among proteins, as opposed to what the temperature/dilution data (Figure 54) indicate. Since the data in Figures 54 and 55 were only acquired one time, it is necessary to repeat them again before one can make more quantitative conclusions. Finally, a slight hysteresis in the reassociation upon decompression of L7/L12 was observed subsequent to when L7/L12 is dissociated beyond ~50-60% (also shown in Figure 55). The data are in agreement with the reversibility of the dilution data mentioned above, that conspicuous conformational drift occurs when dissociation is greater than 60-90% (possibly consistent with a bi-exponential dissociation rate constant). The discrepancy between the reversibility of dissociation subsequent to dilution or pressure in comparison to Gu-HCl (in which the dissociation rate constant is apparently, on the time-scale of a few seconds necessary for a typical fluorescence polarization measurement, single exponential. This phenomenon should be investigated in more detail in the near future possibly with a stopped-flow apparatus. Furthermore, the conformational drift observed with the pressure (Figure 55) or dilution (data not shown) for L7/L12 are quite small in comparison to some other proteins (i.e., see Ruan and Weber, 1986 or 1989; Silva et al, 1986). Hence, the data presented here for L7/L12 indicate that the conformational changes that may

occur if a second dissociation rate constant is present, represent small differences in free energy.

CONCLUSIONS TO CHAPTER FIVE

The data presented in this chapter shed light on the problem of L7/L12 stability. The dissociation constant of dimeric L7/L12 is unequivocally elucidated in this chapter, clarifying the ambiguity that previously existed in the literature. The dimer to monomer equilibrium dissociation constant of L7/L12 is ~38 nM (ΔG_D~10.1 kcal/mol). A 38 nM dissociation constant should be classified among dimeric proteins as "normal" stability rather than "highly stable". The results here and in the previous chapter indicate that the published sedimentation results of Kar and Aune were obscured by several potential experimental artifacts (in their purification procedures). The preliminary temperature data presented in this chapter suggest that the dimerization is promoted primarily by a large enthalpy contribution. Hence, our results are inconsistent once again with Kar and Aune, who claimed that temperature is absolutely insignificant with respect to subunit association ($\Delta H = 0$). It is doubtful that the 38 nM K_D (Figs. 47-52) for dimeric L7/L12 C-33 or C-89 is more than a few percent different from that of wild type L7/L12, as the a 10x wild type (L7/L12)/(L7/L12) C33-F hybrid possesses an identical K_D. Finally, it is doubtful that our protein assay (Coomassie) is more than 5-10% erroneous as the desalted and dehydrated form of wild type L7/L12 was used as a quantitative standard (recall page 34, Chapter Two).

The results presented in this chapter strongly suggest that future fluorescence spectroscopy investigators should consider the possibility of heterogeneous rotational modalities when attempting to elucidate the dissociation constant of their macromolecule of interest. The results in this chapter verify once again the segmental mobility of L7/L12 and hence,

provide us with an unusual situation in which the fluorescence probe used must be located in the "dimerizing domain" in order to observe significant changes in polarization upon dissociation.

The pressure data presented in this chapter suggest that the volume of the space between the two subunits of L7/L12 is ~0.6% that of the entire L7/L12 (recall ΔV for the association of L7/L12 is ~100-140 ml mol^{-1}/ Avogadro's # = 166-232$Å^3$ and the volume of L7/L12 is ~$3.1x10^4$ $Å^3$ according to Wong and Paradies, 1974). Furthermore, the rate of dissociation of L7/L12 subunits (discussed more in the next chapter) appears to be primarily very rapid (less than a few seconds) as was the case with dilution of L7/L12, but similarly, both methods indicated the possibility of an energetically unique conformational state (conformationally drifted) of L7/L12 that begins at concentrations where 60-90% monomers form. Hence, initial observations indicate that the dissociation rate may be bi-exponential, i.e., dissociation occurs rapidly (seconds) to ~60-90% monomers, followed by a slow (hours) transition to a complete monomeric state (see next chapter for more details).

Furthermore, the results here indicate that heterogeneous 2° or 3° structures exist within L7/L12 as each probe/protein conjugate monitored a different stability with regards to Gu-HCl denaturation. It is tempting to attribute the category of probe/conjugates that do not undergo transitions upon Gu-HCl addition, to structureless regions within L7/L12 (local to the probe) such as flexible loops. In fact, this theory is in excellent agreement with the crystal structure (recall Chapter One), in which C-63 or C-99 are located within loops.

In cases where the probe monitors a steep depolarization transition upon addition of Gu-HCl, the transition appeared to be instant-aneous and single exponential at the time-scale of a few seconds (in contrast to dilution or

high-pressure studies). When probes are attached to the C-89 residue (which is also in a flexible loop region according to the x-ray structure) do, in fact, monitor a steep transition upon Gu-HCl additions. Hence the data here suggest one of four things: 1) the crystallization process results a conformational change such that the C-89 location appears within a loop; 2) when a probe is bound to this particular "loop" that C-89 resides within, it monitors better the local tertiary structure (i.e., the entire C-terminal domain); 3) the substitution of cysteine for serine results in a large conformational change; 4) all of the probes that have been attached to the C-89 interfere with the local "loop" region, i.e., they stabilize it. Elucidation of which possibility (maybe more than one) is true is left to future investigators.

The FITC (s) bound to wild type L7/L12 (mostly in the C-terminal domain) monitor less local motion (recall results in previous chapter) than 5-IAF bound to C-89 and a considerably more stable structure (midpoint at 1.8 M Gu-HCl rather than 1.1 M) with regards to guanidine HCl denaturation. Hence, the author shall speculate that the lesser the local motion monitored, the greater the sensitivity to the motions of structures geometrically more distant from the probe binding site. More specifically, when we consider the incredible local motion (~75-80% fractional anisotropy amiplitude; previous chapter) of 5-IAF bound to dimeric L7/L12 C-63 in conjunction with the C-89 and wild type data, it is apparent that unfolding of the entire C-terminal domain (3° structure) is more easily monitored with decreased motion local to the probes.

It is interesting that when a probe is bound to the C-33 position in dimeric L7/L12 (~1 or 2 μM dimers; although, as the protein concentration is raised above ~2 μM the chemical potential of the dimers becomes such that the midpoint of the transition is not reached until ~1.8 M Gu-HCl), it

possesses a very similar Gu-HCl transition as the C-89. This structure is completely abolished when L7/L12 becomes a monomer via *simple dilution*, further indicating the existence of a coiled-coil in dimeric L7/L12. Conversely, no such changes are observed with NTF-FITC upon dissociation. Hence, the NTF-FITC data indicate that the FITC (s) are located in structurally dissimilar region within the N-terminal domain as the C-33 (or C-12) region. A comparison of the Gu-HCl denaturation transition slopes and midpoints of NTF-FITC and C33-IAF in comparison to the simple dilution curves strongly suggests that the method of Gu-HCl denaturation in the determination of dissociation K_D's should be used with great caution.

Further evidence was presented in this chapter that the NTF is responsible for dimerization of L7/L12. More specifically, a concentration-dependent dissociation is observed upon dilution of NTF and contrastingly, no such transition was observed for the CTF C-89. The possibility of large structural changes occurring in the CTF C-89 upon deletion of the NTF and hinge are abolished as the CTF C-89 possesses identical local 2° and 3° stability as the the fully intact C-89 mutant. Interestingly, the association free energy (ΔG = 8.9 kcal/mol) of the N-terminal tails appears somewhat attenuated subsequent to deletion of the C-terminal domains, indicative of a loss in some sort of cooperative free energy.

In contrast to the CTF C-89 mutant, the hinge deletion C-89 mutant appears to have lost significant 2° or 3° structure upon deletion (as judged from Gu-HCl or time-resolved fluorescence data). Conversely, the 4° structure of the hinge-deletion appears at least as stable as the hinge-intact C-89 mutant. The data cannot at this time be readily explained (see next chapter).

Finally, the Peak1 (aggregated) mutants possess nearly identical stability with regards to Gu-HCl denaturation resistance as the peak two (dimers)

mutants. Hence, in conjunction with the time-resolved fluorescence and SE-HPLC data presented in the previous chapter, the author shall deem it unequivocal that the Peak1 mutants are in an aggregated state. The problem of L7/L12 stability and the kinetics of the dissociation/ reassociation process are further characterized in the next chapter.

CHAPTER SIX:
L7/L12 SUBUNITS EXCHANGE IN SOLUTION VIA RAPID CYCLES OF DISSOCIATION AND REASSOCIATION

INTRODUCTION

In the last decade, several papers were published on the subunit exchange of dimeric or oligomeric proteins (Hermann et al, 1982 and references therein; King and Weber, 1986A/B; Saad et al, 1986; reviewed by Jaenicke and Rudolph, 1989; Erijman and Weber, 1991A/B; Lin et al, 1993; Wendt et al, 1993). The concept of subunit exchange has been known since the early 1950s (Weber, 1993, personal communication): 1) Kaplan and Markert separately found that cyclic freezing and thawing of a mixture of lion and frog lactate dehydrogenase resulted in 10-15% hybridization as judged from electrophoretic techniques; 2) at about the same time, another group (reference temporarily unknown) found that hemoglobin S could exchange subunits with normal hemoglobin, also judged from electrophoresis. It was not until the 1970s that Ackers and co-workers found that the rate of subunit exchange was nearly equivalent to the rate of dissociation of tetramers and dimers of hemoglobin. A more quantitative and detailed description of subunit exchange has been revealed more recently via fluorescence polarization and energy transfer methods (starting with King and Weber, 1986A/B). Erijman and Weber (1991 A/B) found that the temperature dependence of the rate of subunit exchange between two forms of lactate dehydrogenase is accompanied with an increased *rate of dissociation* at the lower temperature as judged from high-pressure and dilution studies (like

those described in the previous chapter of this dissertation). In the last year, Erijman and Weber (1993) experimentally (using high-pressure or temperature shifts) determined that the rate of subunit exchange is *exclusively* dependent on the rate of dissociation as judged from fluorescence polarization and/or energy transfer techniques; more specifically, the rate of subunit exchange is concentration independent. Why should one believe that a concentration independent subunit exchange indicates that subunit exchange is exclusively dependent on the rate of dissociation? Let us lay forth the simple and well known relation that describes the dissociation constant of a complex (recall AD cycles; i.e., see Xu and Weber, 1982):

$$k_- / k_+ = K_D \tag{51}$$

where K_D of course, is the dissociation constant, k_- is the rate of dissociation, and k_+ is the rate of association. The rates of dissociation and association can be defined as follows (without rigorous mathematical treatment; for more details, see Johnson et al, 1974):

$$k_+ = 4\pi R(D)(N') \tag{52}$$

where R and D are respectively, the average radius of gyration and the diffusion coefficient of the individual constituents (in the case of L7/L12, the monomers), whereas, N' is Avogadro's number divided by 1000 (to allow conversion from milliliters to liters); furthermore (also known as the Arrhenius rate equation):

$$k_- = Ae^{-E/RT} \tag{53}$$

where A is a pre-exponential number of 10^{12} sec^{-1}, E is the energy of the dissociation (e.g., the total energy of the bonds), and RT is simply the product of the absolute temperature, T, and the gas constant, R. Hence, the concentration parameter is not apparent in the well established theory of dissociation rates; furthermore, the rate of dissociation is usually determined

experimentally. Phenomenologically, it is not difficult to see that the rate of subunit exchange is independent of the protein concentration as the changes necessary for the rate of dissociation, such as charge or conformation fluctuations (recall Table 1 and pgs. 23-25 from Chapter One of this dissertation), occur much faster than the rate of association (primarily diffusion controlled, but dependent on concentration); *thus,* dissociation is the rate limiting step in the case of subuit exchange. These equations will be discussed again later in this chapter.

In the case of L7/L12, with a K_D of 38 nM and a maximum (diffusion controlled; diffusion coefficent for monomeric L7/L12 is ~ 10^{-6} cm^2 sec^{-1}; average R is ~20Å) rate of association of $1.5x10^9$ M sec^{-1}, we can *in theory* predict a rate of dissociation of ~57 sec^{-1}. The efficiency of complex formation in protein dimers or oligomers may in practice be much less than that predicted from equations 50 and 51, since these equations were derived for simple chemical compounds. Hence, the rate of association of L7/L12 may be significantly less than the 57 sec^{-1}. If we assume that the rate of dissociation is equal to the rate of subunit exchange, we can in theory predict a halftime for subunit exchange of 18 milliseconds. Recall, that the data presented in the previous chapter (Figure 54) indicated that the dissociation rate of L7/L12 is primarily (if not completely) less than a few seconds. The results presented later in this chapter shall rather indirectly reveal (via subunit exchange) that rate of dissociation of L7/L12 is in fact within one order of magnitude that calculated above (from Equations 50-51; vide infra)

Obviously, it is of great significance to know whether or not the subunits of L7/L12 can exchange subunits in solution and especially whether or not it can exchange subunits on the ribosome. The earlier fluorescence results of Lee et al (1981), Zantema et al, (1982), and Thielen et al (1984), all

claimed that the subunits of L7/L12 were unable to undergo subunit exchange because the dimer of L7/L12 was "highly stable". More quantitatively, Thielen et al (1984) found that the subunits of L7/L12 bound to the putative "strong" binding site of the ribosome, do not undergo significant subunit exchange with subunits bound to the "weak" binding site (at the time scale studied). Very little details were given and thus, until this time, no group has truly verified whether or not the subunits of L7/L12 undergo dynamic exchange free, or on the ribosome.

Thus, the goals of the work presented in this chapter included: 1) to determine whether or not the subunits of L7/L12 can exchange; 2) if the subunits exchange, then what is the rate; 3) if the subunits of L7/L12 exchange, then we might use the phenomenon to directly measure specific intersubunit distances via FRET methodologies; 4) determine whether or not the subunits of L7/L12 undergo subunit exchange on the ribosome. Data is presented that unequivocally and reproducibly demonstrate, via several different (and some rather novel) methods, that the subunits of L7/L12 undergo a rapid dynamic exchange process in the time-scale of ~100 milliseconds. The phenomenon of L7/L12 subunit exchange is utilized to demonstrate the distances between specific locations within L7/L12 and provide further support for the model presented earlier in Figure 40. Finally, preliminary data is presented which suggests that the subunits of L7/L12 are able to at least in part, undergo rapid subunit exchange on the ribosome and the data seem consistent with the idea that a "weak" and "strong" binding site exist for L7/L12. If the subunits of L7/L12 exchange on the ribosome in the order of ~100 milliseconds, then interpretations of its direct role in protein biosynthesis might be reconsidered past, present, and future.

ELUCIDATION OF L7/L12 SUBUNIT EXCHANGE VIA INTERSUBUNIT GROUND-STATE RHODAMINE DIMER FORMATION, A NOVEL AND POWERFUL METHOD FOR THE DETERMINATION OF PROTEIN SUBUNIT EXCHANGE

The first observations of a peculiar visible absorption spectrum occurring in rather high concentrations of Rhodamine B (structurally like the Rhodamine derivative depicted earlier in Figure 9, pg. 40, except tetraethyl rather than tetramethyl and no iodoacetamide moiety), were reported and discussed by Förster and Köning (1957). They explained the phenomenon as a result of a ground-state dimer formation. Numerous groups (see Gal et al, 1973 and references therein) later reported the same phenomenon and explanation, but several other groups attributed the peculiar absorption spectra of Rhodamine B to a unique molecular form (see Sadkowski and Fleming, 1978 and refernces therein). It was not until the early 1980s, that Arbeloa and Ojeda (1981; 1982) laid the issue to rest: the peculiar rhodamine absorption spectra (shown in Figure 56) is due solely to the formation of rhodamine *dimers* (trimers or higher aggregates apparently don't form) and pH has insignificant effect on the spectrum. They presented a molecular model for the rhodamine dimer (also shown in Figure 56) and claimed that the interaction was largely enthalpic with a dimer to monomer K_D of ~550 μM (ΔG_D = 4.4 kcal/mol). *It will be shown later in this section that this rhodamine dimer formation is purely a ground-state process (i.e., occurs in the absence of electromagnetic excitation; vide infra).*

Rhodamine Dimer Formation Subsequent to 5-TMRIA Binding to L7/L12 Cysteine Mutants: The author intially labeled the cysteine mutants, C-33, C-63, and C-89 of L7/L12 using the same procedures as that described earlier (see Chapter Two in Materials and Methods) in this dissertation. An enormous

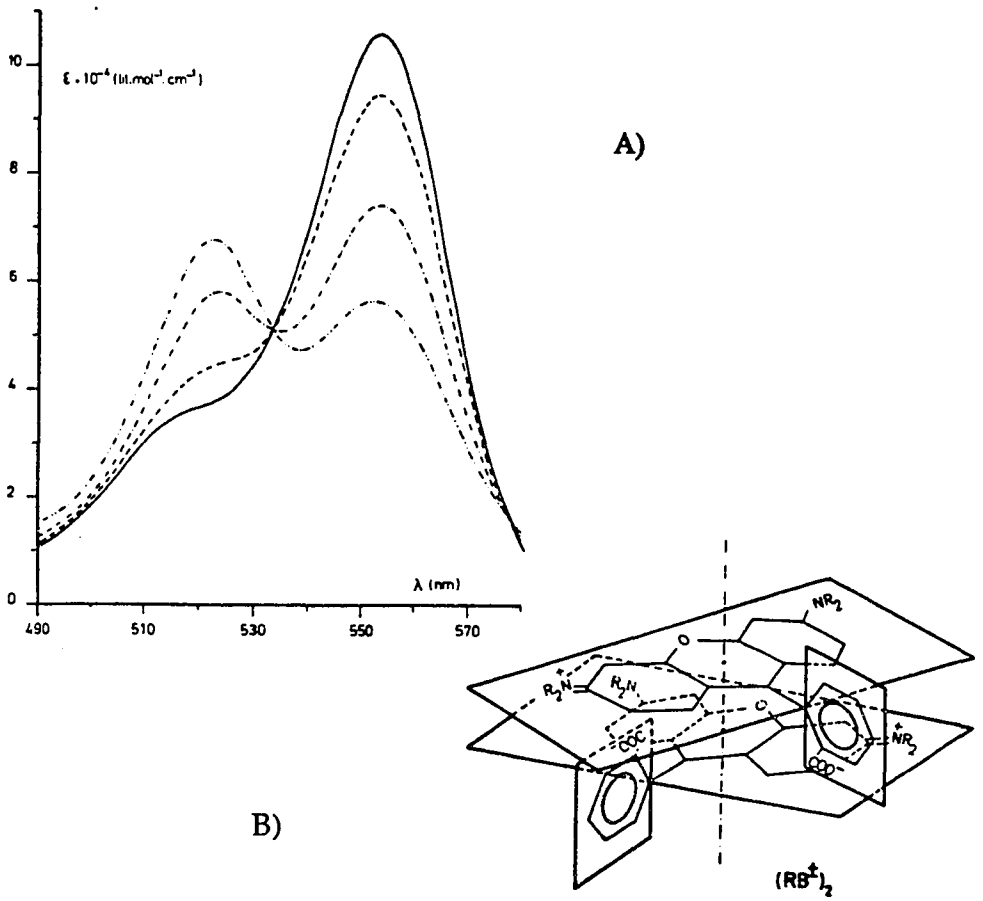

Figure 56: In A), the absorption spectra for 8×10^{-7} M (solid line), 8×10^{-5} M (dashed line), 6×10^{-4} M (dash-dot-dash line), and 3.5×10^{-3} M (dash-double dot-dash line) rhodamine B is shown; in B) the putative molecular interaction and/or geometric structures and orientation of the two rhodamines. Both figures were taken from Arbeloa and Ojeda (1982). Compare to the structure of 5-TMRIA shown earlier in Chapter Two, Figure 9.

amount of precipitation was observed during the labeling reaction, which consisted at that time of ~8 mM 5-TMRIA, 3 mgs/ml L7/L12, and pH 8.0 Tris buffer. Nonetheless, after*three* cycles of microcentrifugation and Biospin-6 purification subsequent to the labeling reaction, no precipitate was visible. The absorption spectrum of each is presented in Figure 57 and one must realize that the ~555 nm absorption maximums evident with 5-TMRIA bound to C-63 or C-89 are normal for the absorption spectra of 5-TMRIA lightly labeled to a protein. At that time the author thought little more of the unique 517 nm peak of 5-TMRIA bound to L7/L12 C-33 (unaware at that time

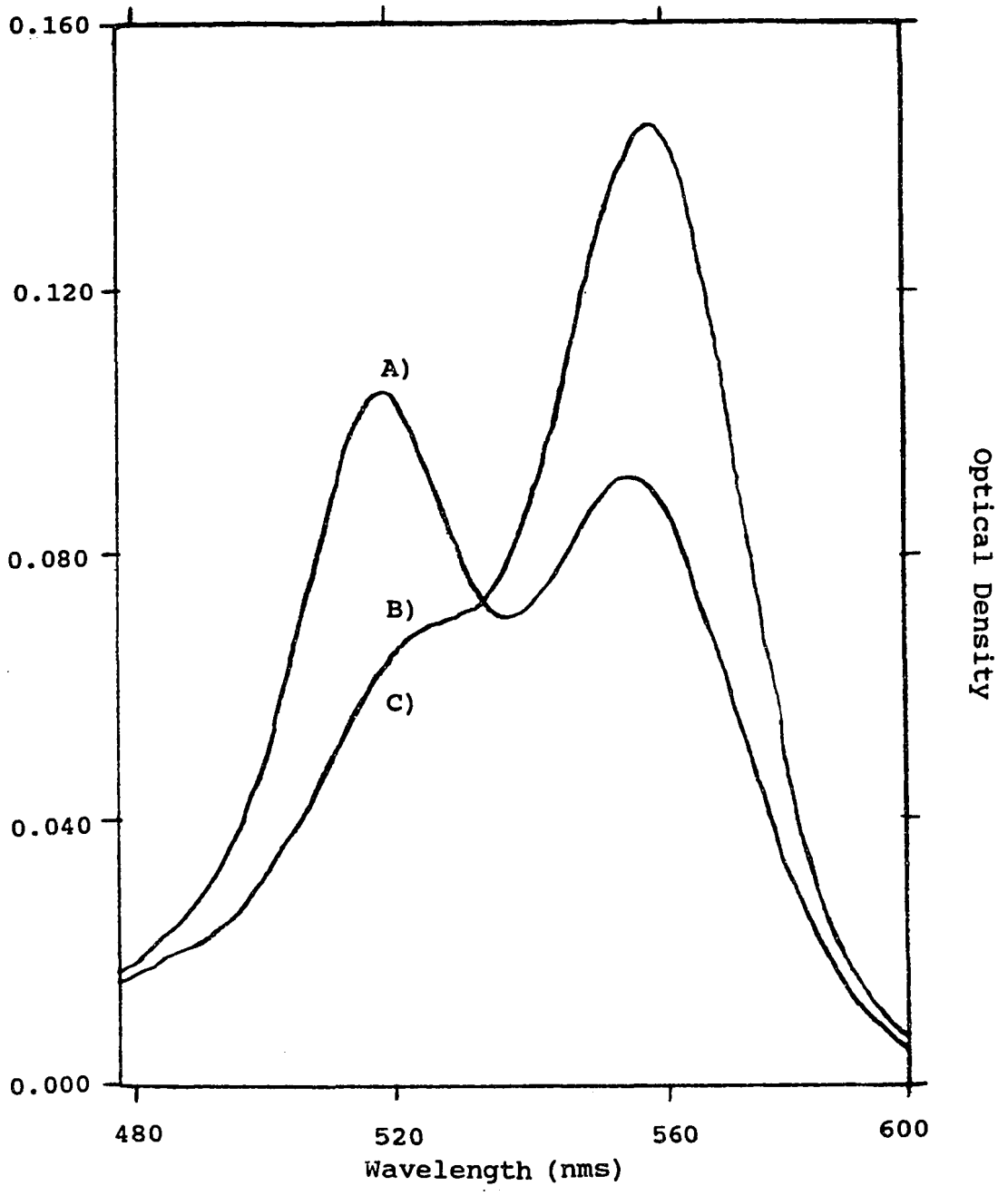

Figure 57: The absorption spectra of 5-TMRIA fully labeled (~two probes/dimer) to dimeric L7/L12 C-33 (A), C-63 (B), and C-89 (C). The results are highly reproducible upon complete removal of free probe. All absorption measurements acquired on either a Perkin-Elmer Lambda 5 or Cary 118 spectrophotometer. Note how the 517/555 nm optical density ratio is about 0.4 for C-63 or C-89, but ~1.25 for C-33. Note how the 517/555 ratio for the rhodamine dimers characterized by Arbeloa and Ruiz (Figure 56) are about 1.25 as well. The 517/555 nm ratio is about 1.1 for Peak1 L7/L12 C33-TMRIA (data not shown).

of the literature mentioned in the previous paragraph). The focus of our attention at that time was on FRET methods. Several months later, after several failed attempts to observe transfer in the C-89 system (between numerous different donor/acceptor pairs), the author began to focus on the L7/L12 C-33 mutant. In preparation for energy transfer experiments between L7/L12 C33-TMRIA and L7/L12 C33-IAF, the peculiar 517 nm peak showed up once again subsequent to removal of unbound probe and hence, the author began to focus more fully on this phenomenon with L7/L12 C33-TMRIA.

Since the possibility of a unique non-covalent binding of 5-TMRIA to L7/L12 arose, the author checked the effects of Gu-HCl on the absorption spectra. Rather unsurprisingly, as seen in Figure 58, the protrusive 517 nm peak began to disappear upon addition of Gu-HCl. The midpoint of the transition was strikingly at 1.1 M (recall from the previous chapter that 1.1 M is exactly the midpoint of the depolarization transition monitored by 5-IAF bound to ~1 μM C33). *Most importantly, the 517 nm peak is readily and perfectly recoverable subsequent to removal of the Gu-HCl with a Biospin-6 column* (also shown in Figure 58). Hence, the author instantly realized that the 517 nm peak represented an intersubunit interaction since any non-covalently attached probe should certainly fall off in 4 M Gu-HCl and be removed with subsequent Biospin or dialysis; furthermore, as described in Chapter 2, labeling was highly site-specific.

Since the rhodamines formed an intersubunit dimer bound to L7/L12 C33-TMRIA, a simple method for observing subunit exchange in proteins was born. Five times excess of unlabeled wild type L7/L12 was added to the L7/L12 C33-TMRIA sample and the 517 peak once again disappeared in a matter of seconds (see Figure 59 for similar experiment)!! The best explanation for this result was that we were observing rapid subunit exchange

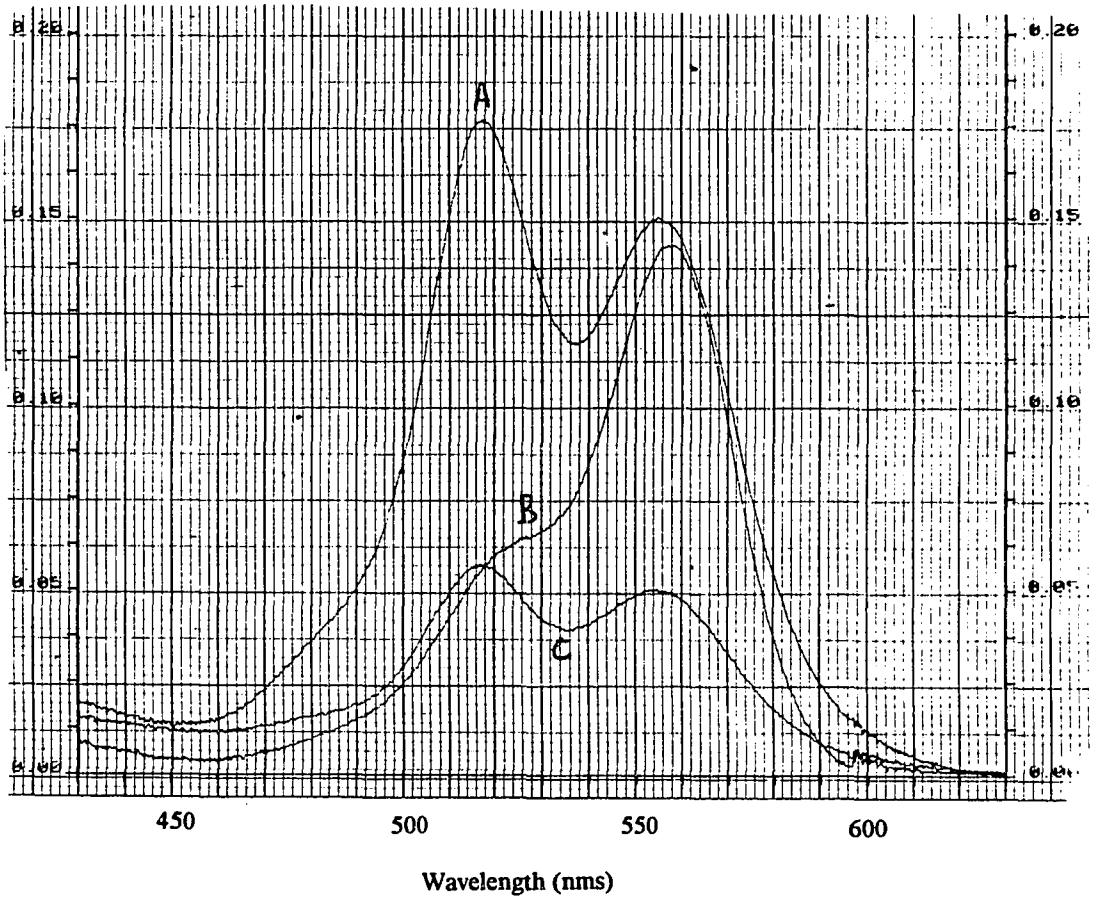

Figure 58: Effects of adding guanidine HCl to dimeric L7/L12 C33-TMRIA as judged from changes in the ratio of the 517 nm/555 nm optical density ratio. Measurements were obtained on the Perkin-Elmer spectrophotometer. Spectra A) represents ~1.4 μM dimeric L7/L12 C33-TMRIA (88% labeled), spectra B) represents the same sample in 4 M Gu-HCl, and spectra C) represents the Gu-HCl treated sample subsequent to Biospin-6 removal of the Gu-HCl. Note how the 517 nm/555 nm optical density ratio is reduced to ~0.4 upon addition of 4M Gu-HCl, identical to the ratio obtained for 5-TMRIA bound to C-63 or C-89.,and how this ratio is fully reversed back to ~1.2 subsequent to removal of the Gu-HCl.

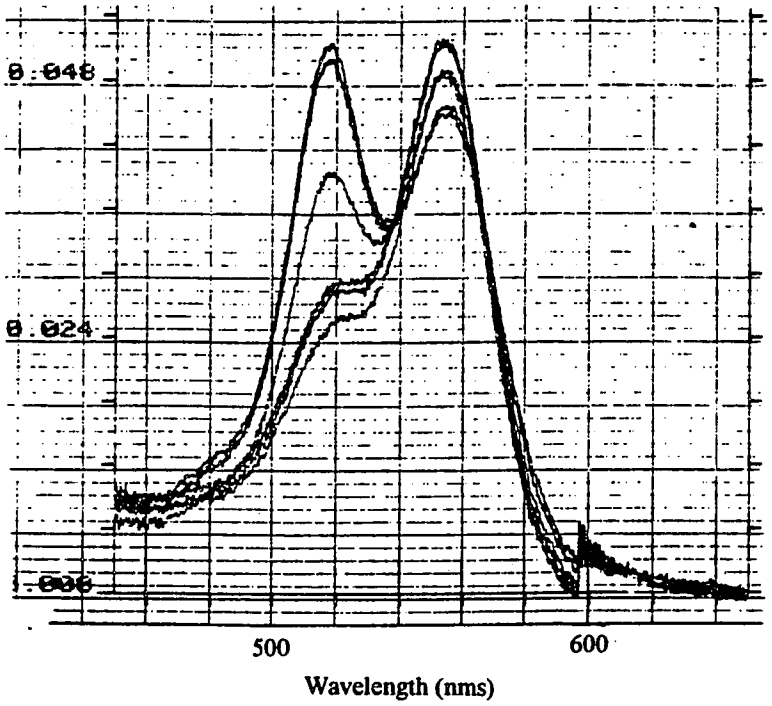

Figure 59: Effects of adding sequentially, increased ratios of unlabeled dimeric wild type L7/L12 to fully labeled dimeric C33-TMRIA. The molar ratios of unlabeled wild type added to C33-TMRIA are represented from the maximum to minimum 517 nm absorbance as follows: 1) 0; 2) 0.1; 3) 1.0; 4) 3.0; 5) 4.0; 6) 10.0. Note: as the 517 nm optical density peak decreases with loss of intersubunit rhodamine dimers, a corresponding increase occurs in the 555 nm optical density; furthermore, ~50% of the rhodamine dimers are lost in the presence of equimolar unlabeled wild type L7/L12 indicative of insignificant free energy changes induced via rhodamine dimerization (see next subsection for calculations of expected dimers of L7/L12 containing two dyes). It is worthy of mention here that in all cases, addition of unlabeled wild type L7/L12 resulted in subunit exchange that occurred in less than a couple of seconds (vide infra for more details). *Furthemore, no differences were observed between L12 C33-TMRIA or L7 C33-TMRIA (data not shown).*

Since one might argue that the intersubunit rhodamine interaction may have been the result of some complex local pH environment induced only in the presence of two rhodamines (i.e. conformational change), we verified that pH had absolutely no effect on the absorption spectra of one micromolar rhodamine B (data not shown). Furthermore, it is unequivocal from Figure 60 below, that this unusual 517 nm peak is the result of a ground-state dimerization, as an excitation spectra of the L7/L12 C33-TMRIA sample results in the normal low 517/555 peak ratio (an excitation spectra differs

from a simple absorption spectra in that the former is the result of an excited-state process, i.e., the intensity of the 582 nm emission maximum is collected at various wavelengths of excitation). Finally, the 517/555 nm optical density ratio for 5-TMRIA is ~1.25, or, exactly the same as that observed by Arbeloa and Ruiz (1982) who claimed that the ratio was strictly caused via rhodamine dimer formation. Hence, the data here demonstrated that the unusual absorption spectra of 5-TMRIA fully labeled on L7/L12 C-33 were the result of intersubunit rhodamine dimer formation and that the subunits of L7/L12 can rapidly exchange.

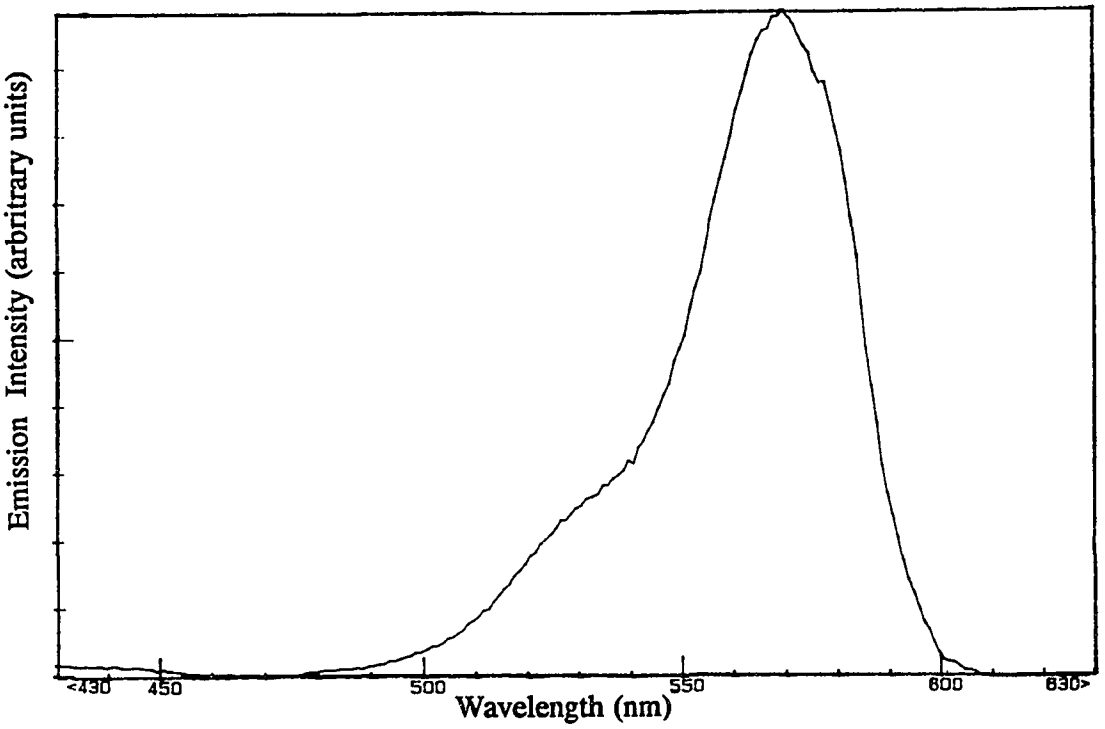

Figure 60: An uncorrected excitation spectra of 5-TMRIA bound to L7/L12 C-33 indicating that the intersubunit rhodamines form a complex in the ground-state rather than the excited-state. Excitation was achieved at each of the values given on the x-axis and emission was collected via an emission monochromator at 582 nm (where maximum emission of 5-TMRIA occurs).

How do we know that the rhodamine dimers are not dissociating upon addition of wild type L7/L12 via an aggregation process? As shown above in Figure 59, addition of equimolar wild type L7/L12 results in 50% of the

possible reduction of the 517 rhodamine dimer peak (see Figure 61). Hence, the free energy of L7/L12 subunit association (~-10.1 kcal/mol) is considerably greater in absolute magnitude than that of the rhodamine dimer association (~4.4 kcal/mol; Arbeloa and Ojeda, 1982) and thus, the thermodynamic equilibrium of L7/L12 subunits seems rather unaltered by the presence of rhodamine dimers. We see in Figure 61, via SE-HPLC with a diode-array

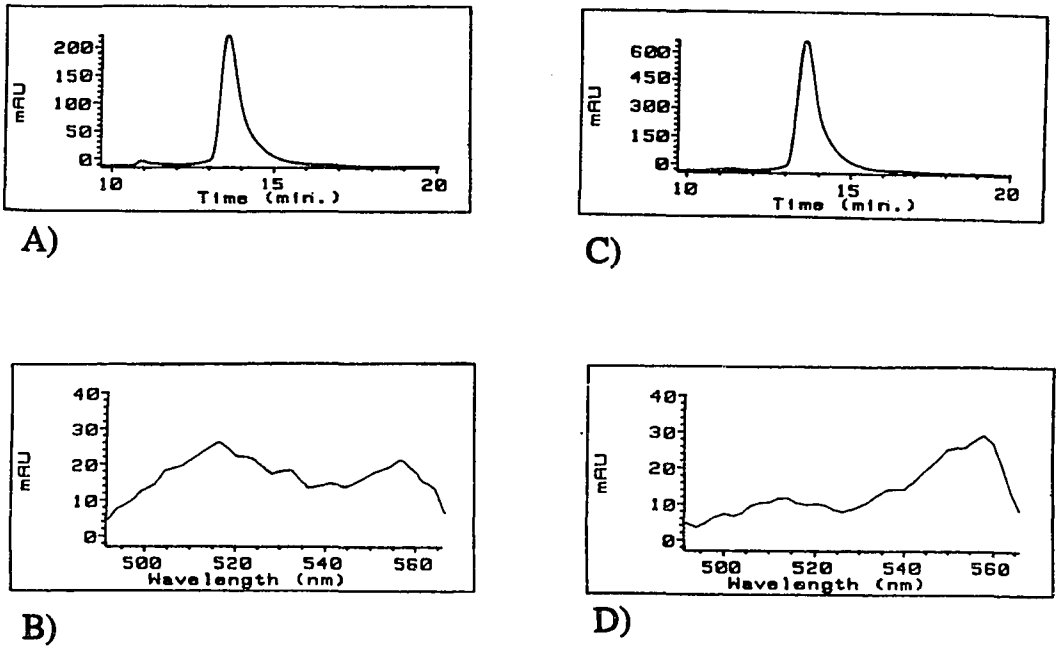

Figure 61: SE-HPLC evidence for the subunit exchange between dimeric wild type L7/L12 and dimeric L7/L12 C33-TMRIA. In A), we see a chromatogram of dimeric (Peak2, although trace of Peak1 still present) L7/L12 C33-TMRIA; in B) we see the absorption spectra of the sample in A) at ~13.8 minutes elution; in C) the chromatogram of L7/L12 C33-TMRIA exchanged with 10x excess wild type L7/L12 and in D) its subsequent absorption spectra at ~13.8 minutes elution. Details of the method were shown in the Materials and Methods (Chapter Two). Hence, the data here unequivocally determine that aggregation is not the cause of the decrease in the 517/555 nm optical density ratio upon addition of unlabeled wild type L7/L12.

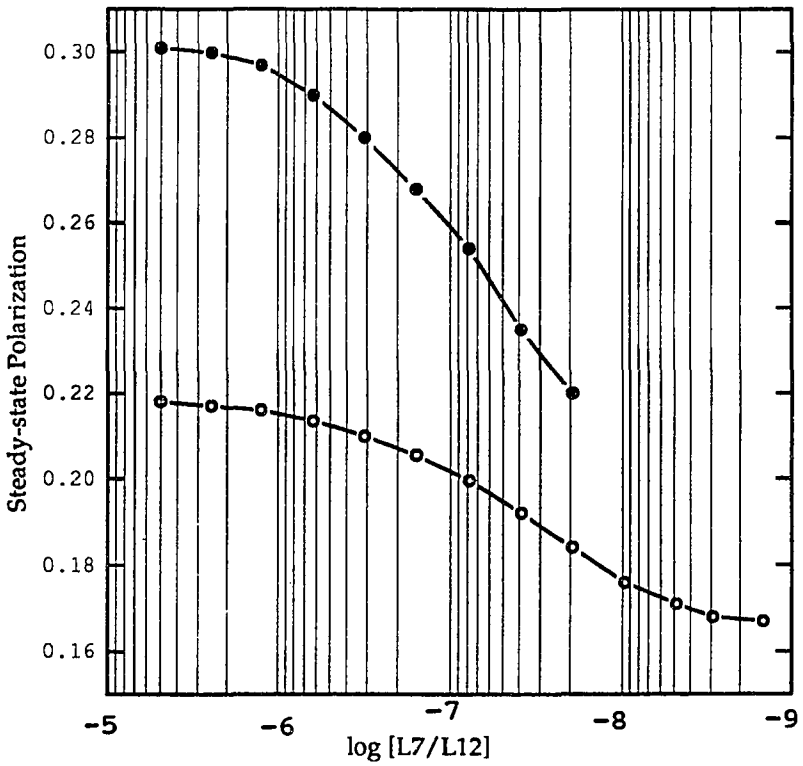

Figure 62: The dimer to monomer dissociation constant of L7/L12 is not altered by the presence of rhodamine dimers, as elucidated by fluorescence depolarization subsequent to dissociation. Hollow circles represent results of diluting fully labeled dimeric L7/L12 C33-TMRIA and filled circles represent results of diluting the same L7/L12 C33-TMRIA exchanged with 10 x unlabeled wild type L7/L12. The higher S.S.P. values of C33-TMRIA/10 unlabeled wild type are the result of loss of homo-FRET (see next section for more details).

detector, that this subunit exchange occurs strictly between dimers of wild type L7/L12 and L7/L12 C33-TMRIA (their is abso-lutely no evidence of any change in the state of aggregation of the mixture of these two forms of dimeric L7/L12). Dilution of the SE-HPLC Peak2 (dimeric) eluate of fully-labeled L7/L12 C33-TMRIA, or a hybrid of this conjugate and a 10x molar excess of unlabeled wild type L7/L12, results in the usual K_D of ~40 nM (see Figure 62). Thus, the data demonstrate that the dimer/monomer equilibrium is unaltered by the presence of intersubunit rhodamine dimers.

Necessity for Cycles of Dissociation and Association (AD cycles) in the Ability of L7/L12 Subunits to Exchange. Additionally, several controls were used to verify that the subunit exchange requires the ability of L7/L12 to both dissociate and reassociate (recall AD cycles):

1) When a 3 x excess of glutaraldehyde crosslinked (~50% crosslinked dimers and most of the rest is a crosslinked higher aggregate as judged from SDS-PAGE; recall Chapter two, Materials and Methods) wild type L7/L12 is added to uncrosslinked and fully-labeled L7/L12 C33-TMRIA, the 517/555 nm optical density ratio (let us simply nominate $OD_{517/555}$) is reduced a mere 0.003 (from 1.27 to 1.24). Furthermore, when a 2x excess of unlabeled/ uncrosslinked wild type L7/L12 is added to this same mixture, the $OD_{517/555}$ is reduced to the stoichiometrically expected value of 0.62. The data could be explained in that one or two percent of the crosslinked sample was not crosslinked (hence, the few percent drop in the $OD_{517/555}$) and more importantly, *that the ability of L7/L12 to dissociate is a requirement for its ability to exchange subunits;*

2) When the cysteines in the N-terminal of dimeric L7/L12 C-33 are covalently oxidized forming an intersubunit disulfide bridge (98% oxidized dimers as judged from SDS-PAGE; recall Chapter Two, Materials and Methods), they become unable to undergo subunit exchange with L7/L12 C-33-TMRIA. More specifically, when a 3x excess of the intersubunit oxidized C-33 is added to C33-TMRIA, the $OD_{517/555}$ drops a mere 0.003. Hence, the data here once again proved that the ability of L7/L12 C-33 to *dissociate* is necessary for subunit exchange to occur;

3) Conversely, one method was utilized to prove that the *ability of L7/L12 to associate is obviously necessary for subunit exchange*: recall from Chapter One (and esp. Chapter Two Materials and Methods), if the three

methionines in the N-terminal domains of wild type L7/L12 are oxidized, the protein appears unable to reassociate into a dimer. Direct experimental evidence for the inability of these methionine oxidized monomers of L7/L12 to reassociate into observable dimers was observed in the present study. The $OD_{517/555}$ of L7/L12 C33-TMRIA is unaltered upon addition of 5x excess of methionine oxidized (as judged from SE-HPLC as described in Chapter Four) wild type L7/L12.

Further evidence in our data for the necessity of AD cycles comes from the fact that, as discussed in the introduction of this chapter, the exchange rate of L7/L12 subunits with L7/L12 C33-TMRIA was independent of the concentration of protein (not necessary to show data here, since in all cases the subunit exchange was completed in ≤one second). The data here were in agreement once again that the rate of dissociation (k_-) is the primary factor involved in subunit exchange (recall Equations 51-53, in the introduction of this chapter) since the rate of association (k_+) is in theory and practice dependent on the protein concentration. *Thus, the process by which L7/L12 subunits exchange must involve cycles of dissociation and reassociation (maybe better to call DA cycles?) rather than a simple collision-induced subunit exchange.*

Finally, the author shall briefly mention here that a rapid spectrophotometric mixing method (instrument of Dr. Seifried) was used to determine that the subunit exchange of L7/L12 was completed in less than two hundred milliseconds (data not shown). It was simply determined that mixing of concentrated L7/L12 C33-TMRIA to a rapidly stirring buffer (via magnetic stirrer underneath the cuvette) resulted in an equilibration completion time of ~200 milliseconds (spectral acquisition time ~40 milliseconds). Similarly, when concentrated/unlabeled wild type L7/L12 was

added to rapidly mixing and fully labeled L7/L12 C33-TMRIA, the completion of the increase in OD_{555} took maybe slightly (maybe 50 milliseconds) longer than the ~200 milliseconds necessary for simple equilibration.

Hence, the L7/L12 subunit exchange data presented here in conjunction with the data presented in the previous chapter indicate that the subunits of L7/L12 undergo cycles of dissociation and reassociation. Since the equilibrium dissociation constant (K_D) of dimeric L7/L12 is ~38 nM its dissociation rate ($<k_+>$) is > 5 sec^{-1}, one can already calculate (from Equations (51-53, pg. 220) and assuming that the rate of subunit exchange and the rate of dissociation are equal in the time-scale of our measurements) that the effective $<k_+>$ must be on the order of greater than 1.3×10^8 $M^{-1}sec^{-1}$. Thus, our experimental data are in excellent agreement with classic theoretical rate constant theory, i.e., recall pg. 220, where we calculated an association rate for monomeric L7/L12 of ~1.5×10^9 $M^{-1}sec^{-1}$ and a dissociation rate (rate of subunit exchange) of between 5 and 50 sec^{-1}. It was also stated that collisions between the more complex proteins are typically less productive (in terms of complex formation) than the more simple molecules, for which the classic rate theory was developed. A more accurate determination could be obtained with a stopped-flow instrument with millisecond resolution.

Investigation of Various other 5-TMRIA Labeled Substitution and Deletion Mutant Forms of L7/L12. Recall the absorption spectra depicted earlier for 5-TMRIA attached to L7/L12 C-33, C-63, or C-89. Additionally, the substitution mutants C-99 and C-12, as well as the deletion mutants Δ35-52 C-89 have been labeled with 5-TMRIA. Since the absorption spectrum of 5-TMRIA labeled to C-99 ultimately looked identical to 5-TMRIA bound to C-89 or C-63, we shall not show it here. *The author shall only reiterate that when 5-TMRIA is bound to cysteines within the C-terminal domain, it does not form*

intersubunit rhodamine dimers. Conversely, as seen again in Figure 63, when 5-TMRIA is bound to an N-terminal amino acid cysteine residue, such as Cys-33 (as shown earlier in Figure 57) or Cys-12, (as shown in Figure 63), the intersubunit rhodamine dimers appear with the high (~1.2-1.3) $OD_{517/555}$. When this conjugate was characterized in Dr. Traut's laboratory, we observed that simple dilution in the protein concentration range of ~5 μM to 0.2 μM, resulted in a conspicous drop in the $OD_{517/555}$, also shown in Figure 63. The results were in good agreement with the L7/L12 C12-IAF data presented in the

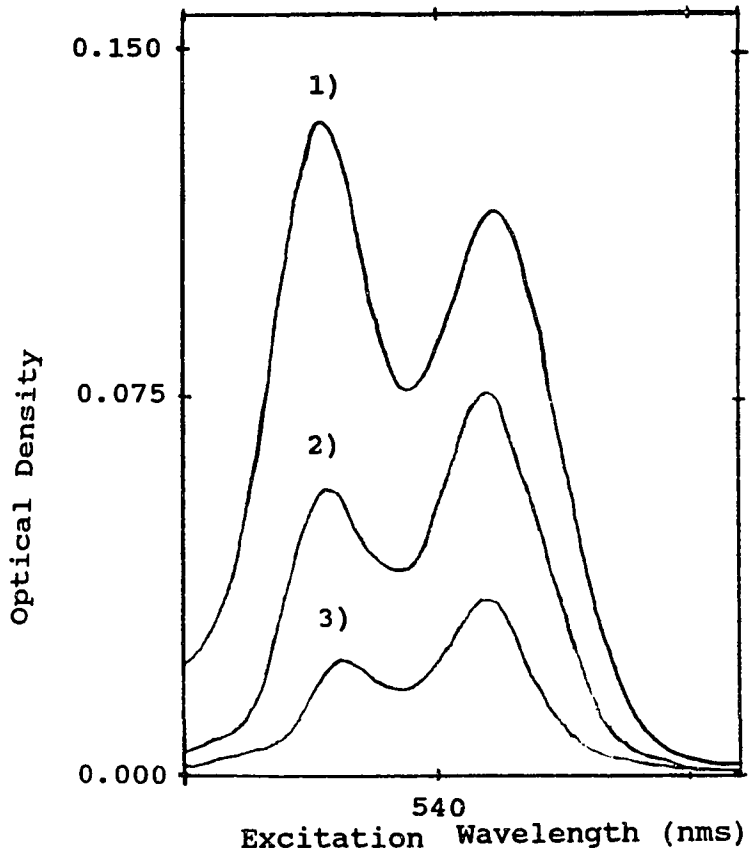

Figure 63: Absorption spectra of 1)1.1 μM; 2) 0.35 μM; or 3) 0.12 μM L7/L12 C12-TMRIA, demonstrating once again that the dimer to monomer K_D of L7/L12 C-12 is ~0.3 μM (as demonstrated earlier, in Figure 49, via fluorescence polarization methodologies). The rate of subunit exchange once again appeared to be very rapid (less than a second, or so). In contrast, no changes in the abosrption spectra of L7/L12 C-33 labeled with 5-TMRIA are observed upon dilution in this range (data not shown).

previous chapter, which also showed that the dimer to monomer K_D of L7/L12 Cys-12 was around 0.3 μM (probably higher simply due to the point mutation in the putative coiled-coil NTF at residue 12). Thus, once again (like at C-33) intersubunit rhodamine dimer formation has no effect on the dimer monomer equilibrium of L7/L12.

Let us now analyze more closely the significance of the data presented so far in this section with respect to L7/L12 dynamics. In all three C-terminal domain cysteine substitution mutants (C-63, C-89, C-99), there were no signs of intersubunit rhodamine dimer formation. In both N-terminal domain cysteine mutants (C-12, C-33) there was definite and complete (as long as L7/L12 is in its dimeric form, the $OD_{517/555}$ is about 1.2-1.3 depending on the extent of labeling) rhodamine dimer formation. Hence, the results indicate: 1) the mobility of the C-terminal domains via the flexible hinge is such that the rhodamines cannot approach close enough to form stable rhodamine dimers; 2) the harsh treatment (6 M constant urea and ~50% DMF; recall Chapter Two, Materials and Methods) sometimes necessary to get efficient labeling of the C-terminal domain cysteine mutants resulted in some sort of permanent unfolded state of at least part of the C-terminal domains such that they could no longer interact; or 3) both possibilities are true. The data presented in the previous two chapters suggest that the second possibility is unlikely, since all data indicated that the C-terminal domains are probably distant from one another on average. Furthermore, the data provided in Table 22 demonstrates absence of significant effect on the activity of various L7/L12 cysteine mutants labeled with 5-TMRIA in the promotion of *in vitro* poly-phenylalanine synthesis.

Several conclusions can be made from Table 22: 1) substitution of cysteine for the native amino acid residue (recall Figure 7, Chapter Two) little

if any effect on the resultant functionality of L7/L12, regardless of whether or not it is in the C- or N-terminal domain; 2) placing a rather bulky fluorescent label at each ot the residues has no effect on L7/L12 functionality; 3) the functionality of L7/L12 is resistant to the harsh, 50%DMF/6M urea labeling conditions used for labeling with 5-TMRIA. In conclusion, the data in Table 22 provided us with further evidence that the lack or presence, respectively,

Table 22: Effects of Labeling Various Cysteine Mutant Forms of L7/L12 with 5-TMRIA on *in vitro* Poly-phenylalanine synthesis.*

Form of L7/L12	phe incorporated/ribosome
wild type	14.5
C-33	12.9
C-89	14.3
C-99	12.6

*The protocol for measuring L7/L12-induced poly-phenylalanine synthesis was described in Chapter Two, Materials and Methods. This function test was performed only once. All three cysteine mutants listed here were labeled in the presence of 50% DMF and 6 M urea to prevent extensive protein loss or probe/protein precipitation. See text for more details.

of rhodamine dimer formation in the C- or N-terminal domains, reflected the conformational state of the native and functional form of L7/L12. The author shall mention again in the last section of this chapter, the binding of 5-TMRIA labeled L7/L12 cysteine mutants to the ribosome.

Hence, the rhodamine dimer formation phenomenon not only demonstrates L7/L12 subunit exchange, but also something about the conformational mobility. In Figure 64, another analytical model for the dynamic structure of L7/L12 is presented. The figure is drawn similar in geometric proportion as that expected in nature. The structure of the 5-TMRIA was depicted earlier in Figure 9, pg. 43. The intersubunit rhodamine dimer interaction is an adaptation of that depicted earlier in Figure 56 (from Arbeloa and Ojeda, 1982). The average distances between each bond in the

cysteine side chain and the protein backbone are roughly estimated as 1.2-1.5 Å. The author suspects that the rotation around the Cα-Cβ side chain bond or the nitrogen-aromatic bond are rather unrestricted (from time-resolved fluorescence data; data for 5-TMRIA is nearly identical to that of 5-IAF presented in previous chapter with the exception of C-63, where the local mobility becomes more restricted--data not shown). From simple geometry of a triangle, the schematic in Figure 64 demonstrates that the distance between the bases of the intersubunit C-33 or C-12 side chains when rhodamine dimers are present might be as much as ~23 Å apart. The reasoning is simple: the distance between the bases of the cysteine side chain to the middle of the xanthene group (center of rhodamine dimer interaction) is about 16Å and the two rhodamines are putatively oriented 90° to one another. *If we consider the N-terminal domains as an unstaggered coiled-coil of 28 amino acid residues and we assume that the cysteine residues are perpendicularly oriented to one another, then the diameter of the coiled-coil is* $\geq 23\text{Å}$. Hence, the rhodamine dimer data presented in the chapter are in excellent agreement with the idea of an ~ 32-35 Å diameter coiled-coil in the N-terminal domain of L7/L12 as opposed to the sedimentation and low-angle x-ray scattering data. Alternatively, the data might be considered in agreement with a staggered dimeric N-terminal domain (of some presently unknown structure or possibly even a staggered coiled-coil), in which the base of the cysteine side chains are ~16.5 Å apart in the long axis of the N-terminal domain. The data here demonstrate that the N-terminal domain of L7/L12 is quite stable and dimeric, whereas, the C-terminal domains are quite mobile and monomeric. Furthermore, the data demonstrates further that the two monomers of dimeric L7/L12 are in parallel alignment.

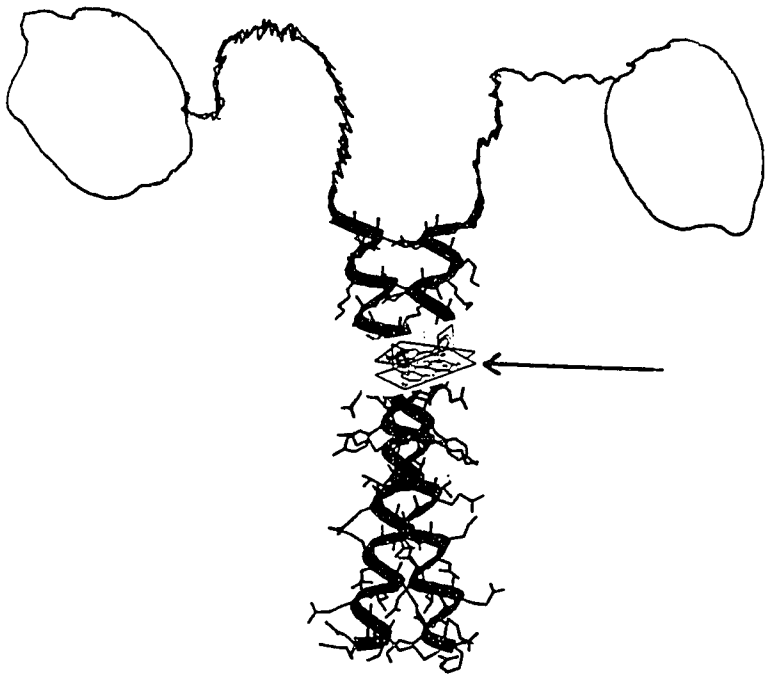

Figure 64: A schematic illustrating the author's interpretation of the interactions of 5-TMRIA bound to dimeric L7/L12. The dimensions of the various domains of L7/L12 are as depicted earlier in Figures 29 and 40. An average overall bent conformation, such as depicted in Figure 40 is seen here. The geometrical proportions of the 5-TMRIA relative to that of the protein, are estimates. The relative orientations of the the rhodamines in the rhodamine dimer are 90°, or, identical to that proposed by Arbeloa and Ojeda, 1982 (recall Figure 56). The unstaggered coiled-coil structure putatively existent in the N-terminal domain was taken from the x-ray structure of the coiled-coil peptide GCN4 (O'Shea et al, 1991).

Finally, the author shall briefly mention that labeling of the L7/L12 Δ35-52 *C-89 hinge deletion* mutant with 5-TMRIA results in the formation of an apparent intersubunit C-terminal domain complex (see Figure 65). *The data indicated that, subsequent to deletion of the hinge, the C-terminal domain movement is suffuciently stabilized enough so that intersubunit rhodamine dimers are now able to form at the residue 89 positions.* Addition of Gu-HCl resulted in gradual reduction of the $OD_{517/555}$ to a normal value of 0.45 in 3 M Gu-HCl (see Figure 65). Subsequent removal of the Gu-HCl

resulted in nearly complete reversal of the $OD_{517/555}$ back to ~1.0 (lower than usual, for C-33 or C12, simply because of only 0.75 5-TMRIAs/subunit of protein). Furthermore, the midpoint of the Gu-HCl denaturation curves as judged from fluorescence depolarization of the 5-TMRIA was also ~0.75 M (also shown in Figure 65). Interestingly, the Gu-HCl denaturation transition curves are *broader* here than that demonstrated earlier (Figure 50) for the Δ35-52 C-89 mutant labeled with 5-IAF (data not shown). Hence, it is possible that the structure *local* to the C-89 residue is unaltered by the presence of the rhodamine dimers; conversely, the quaternary structure, which might dissociate in the higher concentrations of Gu-HCl (recall difference between dimers and monomers of NTF or C-33 in Gu-HCl from previous chapter), is somewhat stabilized by the presence of the rhodamine dimers (thus, leading to the broadening of the transition). Similarly, we also determined that dilution of the hinge-deletion mutant resulted in no changes in the $OD_{517/555}$ (data not shown) giving further support to the suggestion that the dimeric (or other aggregate) state is at least nearly as stable as the hinge-intact mutant. Interestingly, addition of unlabeled Δ35-52 to fully 5-TMRIA labeled Δ35-52 resulted in minuscule changes in the $OD_{517/555}$ (data not shown) and hence, it appeared that either the rhodamine dimers somehow stabilized the "dimer" state of the protein so that it became unable to significantly exchange subunits (in the time-scale of 10-20 minutes), or the dimer state of the hinge deletion mutant form of L7/L12 is simply more stable than the hinge-intact L7/L12. We shall mention again in the next section, that addition of unlabeled Δ35-52 does result in slight increases in S.S.P. of the 5-TMRIA over a time scale of minutes, possibly indicating further evidence for a quaternary structure of higher stability than the hinge-intact proteins. Future investigations on the dependence, if any, of the Gu-HCl denaturation transtion midpoint on the

protein concentration *might* tell us more about the quaternary structure of Δ35-52 C89-TMRIA; the possibility of a heterogeneous state of aggregation for the protein cannot at this time be excluded.

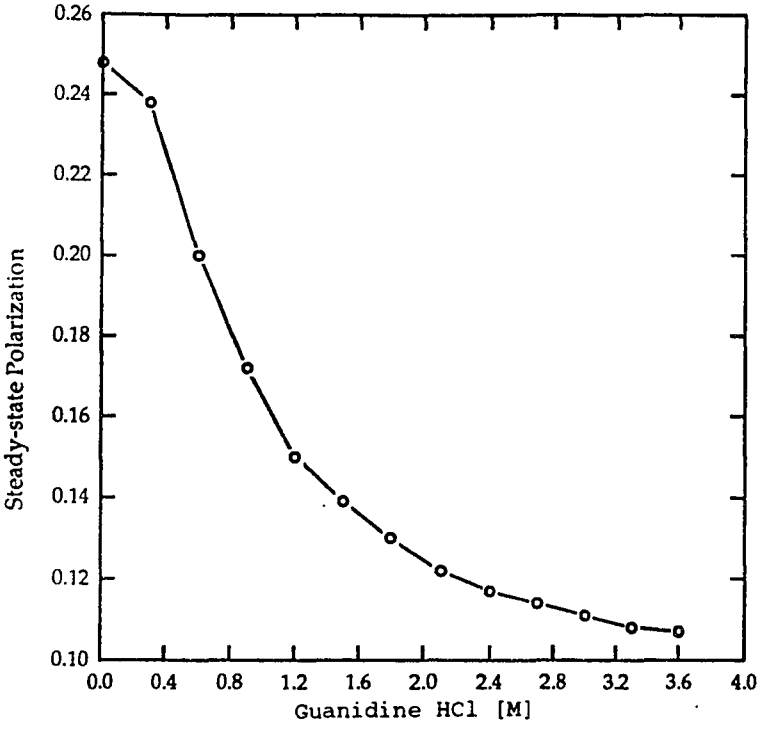

Figure 65: The effects of guanidine HCl addition to L7/L12 Δ35-52 C-89 hinge-deletion mutant labeled with 5-TMRIA (which form intersubunit rhodamine dimers). Compare to Figure 50, presented in the previous chapter for Δ35-52 C-89 labeled with 5-IAF. It is rather easy for one to visualize the feasibility of an intersubunit rhodamine dimer complex for the hinge-deletion mutant at C-89 when one considers Figures 5 (Chapter 1) and 40 (Chapter 4).

VERIFICATION AND CHARACTERIZATION OF L7/L12 SUBUNIT EXCHANGE VIA FLUORESCENCE RESONANCE "HOMO" AND "HETERO" ENERGY TRANSFER

The concept of homo and hetero energy transfer was mentioned in Chapter Four, the difference simply being that the former occurs between identical fluorophores and the latter between different fluorophores. The concepts of fluorescence resonance energy transfer (FRET) were described in fair detail on pages 68-73 in Chapter Three of this dissertation and again on

pages 76-83 and other rather scattered locations throughout the subsequent text.

As mentioned in the introduction, FRET is presently (maybe arguably) the best method available for detecting and characterizing subunit exchange in proteins. Hence, our initial work on L7/L12 in this area utilized this very powerful method to qualitatively and eventually (penultimate results section of this chapter) semi-quantitavely characterize the subunit exchange and conformational dynamics of L7/L12. The advantage in using this method over the novel rhodamine dimer method described in the previous section, is that it would seem less likely that two probes not physically interacting as in the former method, would cause any changes in the free energy of a naturally occurring equilbrium.

Fluorescence Depolarization via Homo-FRET between FITCs Bound to Wild Type or NTF L7/L12. As first described in Chapter Four (Table 3), labeling of wild type L7/L12 in excess of 0.5 FITC begins to result in significant homo-FRET. Recall from Chapter Three that Weber and co-workers (Weber, 1952; Weber, 1953; Weber and Daniel, 1966; Weber and Anderson, 1969; Anderson and Weber, 1969) provided the first theoretical description and experimental data for homo-FRET within a protein. Since the classic paper of Anderson and Weber (1969), in which an ANS derivative (with R_0 merely 10-12Å) was utilized, the apparently esoteric *homo*-FRET method has been nearly ignored or forgotten in the *quantitative* determination of distances within macromolecules. More recently, Weber and numerous co-workers (Erijman and Weber, 1991A/B; 1993; Ruan and Weber, 1993) have used this method of homo-FRET in the determination and characterization of subunit exchange among dimeric or oligomeric proteins (although, distances were not quantitatively determined). In these cases, the investigators utilized

fluorescein isothiocyanate, with its superior extinction coefficient, quantum yield, and absorption/emission overlap integral (recall from pages 76-83 in Chapter Four that the R_0 for FRET between FITCs bound to L7/L12--or probably most proteins--is about 40Å). Since the overlap integral of FITCs bound to L7/L12 is about 40Å, it seemed reasonable that the method of homo-FRET would be at least as effective in determining distances as the much more exoteric hetero-FRET methods (ubiquitous in the literature). In the hetero-FRET method (described in detail in the next subsection), two different donor and acceptor fluorophores, usually IAEDANS and a fluorescein derivative (R_0 usually around 35-50Å) or a coumarin derivative and fluorescein derivative (R_0 usually around 35-50Å), are utilized.

Let us now re-evaluate the method of homo-FRET (for more details, see Weber and Daniel, 1966; Weber and Anderson, 1969; Anderson and Weber, 1969). Recall from page 67 in Chapter Three that the quantitative result of homo-FRET is depolarized emission. The efficiency of the transfer of energy can be calculated from the resultant depolarization by the following equation:

$$N = (1/P - 1/P\infty) / (1/P\infty - 1/3) \qquad (54)$$

where N is the average number of *effective* transfers (one effective transfer is equal to 100% energy transfer, essentially the same as E in Equation 25 on page 69), P is the polarization in the *presence of FRET*, and $P\infty$ is the polarization of the emission in the *absence of FRET*. The R_0 must be calculated separately (such as that described on pages 65 or 79 of this dissertation) and thus, the R_0 can take into account the J or κ^2 terms. One can then use Equation 25 to calculate R.

In the case of wild type L7/L12, homo-FRET occurs between FITCs located primarily on the same subunit (Figure 17), although the data in Figure

17 suggested that maybe a small % of the FRET was intersubunit. The results presented in Chapter Four for NTF-FITC suggested that at most 25% of the FITCs that bind to the wild type even when labeling is done at pH 9.4 (i.e., 1.2 FITCs/wild type L7/L12 subunit), bind to the NTF (where probes are close enough for FRET to occur). Hence, insignifcant FRET should be observed between FITCs located on separate subunits of wild type L7/L12 if the subunit equilbrium was truly unaltered by the FITCs. The author shall simply state that no significant increase in the steady-state fluorescence polarization of FITCs bound to wild type L7/L12 occurs subsequent to subunit exchange; the increase of 0.001 might be attributed to removal of trace free fluorescein. Furthermore, treatment of this protein mixture with 6 M Gu-HCl or 8 M urea and subsequent denaturant removal via extensive dialysis, once again results in insignificant changes in the S.S.P. of FITC.

Recall from page 145 of Chapter Four that some energy transfer (up to 15% of the total emission) may have been apparent between <0.15> FITCs bound per subunit of NTF, as some missing anisotropy was evident in the analysis of the time-resolved fluorescence data. Why would one expect 15% of the total emission a result of FRET when only 0.15 FITCs are bound per subunit of NTF? One can easily calculate (or use a Bernoulli distribution; e.g., see Weber, 1992, pg. 76) that only $0.15^2 = 2.25\%$ of dimers of NTF will possess two FITCs. Similarly, 25.5% of the dimers will possess only one FITC. Obviously, since we do not see the remaining 72.25% (no probe bound), we can simply divide the molar fraction of the two FITCs bound per dimer of NTF, by the total FITC. Hence, 4.5 (<u>two</u> FITCs/per dimer NTF) divided by 30 (total subunits possessing FITC) gives us 15% of the total FITC emission from intersubunit FRET. In Table 23, we see the results of adding 10x unlabeled NTF to <0.15> FITC/(NTF) subunits. The steady-state polarization of the

FITCs bound to the NTF rapidly (less than the time necessary for the polarization measurement of ~a few seconds) increases from 0.172 to 0.180. Hence, it was apparent that some loss of homo-FRET between FITCs had occurred upon subunit exchange.

Why, then, do we observe an increase in S.S.P. of 0.008 in the case of <0.15> FITCs bound to NTF, but only at most 0.001 in the case <0.5> FITCs bound to wild type L7/L12?? As described earlier, ~75% of the FITCs bound to wild type L7/L12 are located in the C-terminal domains and hence, ~75% of the total emission is from FITC bound to the C-terminal domains that would thus, obscure the remaining intersubunit FRET emission from FITC bound to the NTF. From Table 23 and Equation 54 one can calculate 0.05 effective

Table 23: Results of Adding a 10x Excess of Unlabeled NTF or Wild Type L7/L12, respectively, to FITC-labeled NTF or Wild type L7/L12*.

fluorescent sample: molar ratio of probe per subunit	molar excess of unlabeled protein used for subunit exchange prior to S.S.P	increase in S.S.P. as a result of loss of homo-FRET upon mixing
0.2 FITC/WT L7/L12	10X wild type L7/L12	0.001
1.2 FITC/WT L7/L12	" " "	0.001
"+ 4 M Gu-HCl*	" " "	0.001
0.15 FITC/NTF	10X NTF	0.008
"+ 4M Gu-HCl*	" "	0.008

*All experiments repeated three times at 20°C; abbreviations: NTF is the N-terminal fragment; Gu-HCl is guanidine HCl; WT is wild type; S.S.P. is steady-state polarization.

transfers for the <0.15> FITCs attached to NTF. What does this mean? If we say hypothetically, that one FITC is bound per subunit of NTF, and consider an R_0 of ~40Å (recall page 80) for the FITCs, we can calculate from Equation 25 (page 66) an R of 65.3 Å. The percentage of dimers in the NTF sample consisting of <0.15> FITCs per subunit will, at a given time, consist of ~15%

dimers with two FITCs bound. Hence, the efficiency of energy transfer in this case appears to be about 15% that possible when all dimers possess two FITCs undergoing intersubunit FRET. Thus, we can multiply the 0.05 effective transfers by (100/15) and find that the true efficiency is about 33%. From Equation 25 we can calculate an intersubunit distance between the FITCs (bound to the NTF; recall R_0 is ~40Å) of R = 44Å. There is certainly the possibility of error in this calculation as we do not know for sure where the FITC (s) are located in the NTF and we do not know if there is more than one binding site. Furthermore, we have assumed a κ^2 of 2/3, and have not yet needed to rigorously determine it. It is not difficult to imagine the two FITCs facing outward at rather distant edges of the putative coiled-coil (which is already 30-35Å in diameter) would appear at a distance of 44 Å from the center of each xanthene ring (Figure 66). In the next subsection, the author presents an explanation for how the schematic in Figure 66 is truly compatible with the rhodamine dimer schematic earlier in Figure 64.

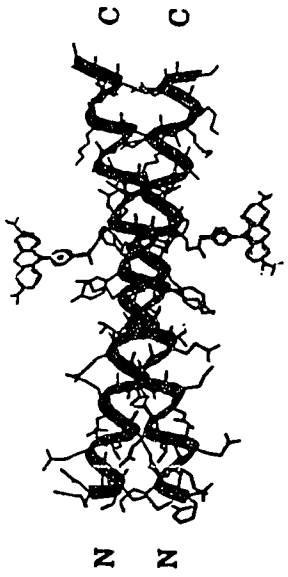

Figure 66: Feasibility of two FITCs facing outward and away from each other bound to a coiled-coil. The structure of the coiled-coil was taken from O'Shea and the FITCs were taken from Figure 9 in Chapter One of this dissertation. The C-terminal domains are not shown here. See next subsection for more details.

Existence or Absence of Homo-FRET between Fluorophores Bound to Various Cysteine Substitution and Deletion Mutants. The necessity for knowing the location of the probes undergoing FRET was demonstrated in the previous subsection. Conversely, in this subsection, we know precisely where the probe is bound. Furthermore, as demonstrated in Chapter Four, the local motion of all probes bound to the various cysteine mutants undergo significant local mobility (~≤50% fractional anisotropy) and thus, an assumption of 2/3 for the κ^2 seems quite reasonable.

In Table 24, we see the results of subunit exchange on the steady-state fluorescence polarization of 5-IAF bound to various cysteine mutant forms of dimeric L7/L12. All data were acquired at 20°C and the effects were all concentration independent, essentially indicating once again that subunit exchange was occurring via AD cycles rather than collision-induction. The concept of intersubunit homo-FRET is best described in Figure 67 between 5-IAFs labeled at the C-33 position.

Since all data presented in Table 24 are the result of samples fully-labeled with 5-IAF, we could easily calculate R's using the method described in the previous subsection. Furthermore, the R_0 was calculated if necessary using the method described on pages 65 and 79 of this dissertation. The quantum yields and extinction coefficients were determined as described on pages 64-67. The overlap integral, J, was calculated from the overlap (nearly same as FITC) of the absorption and emission spectra (for 5-IAF derivatives, the actual overlap of the spectra are all the same, only the quantum yield or extinction coefficient change slightly).

The data presented in Table 24 are in excellent agreement with the rhodamine dimer data presented in the previous section. If the probes are

located in the C-terminal domains, no homo-FRET was observed with one interesting exception: C-99. The data in Table 24 indicate that the two C-99

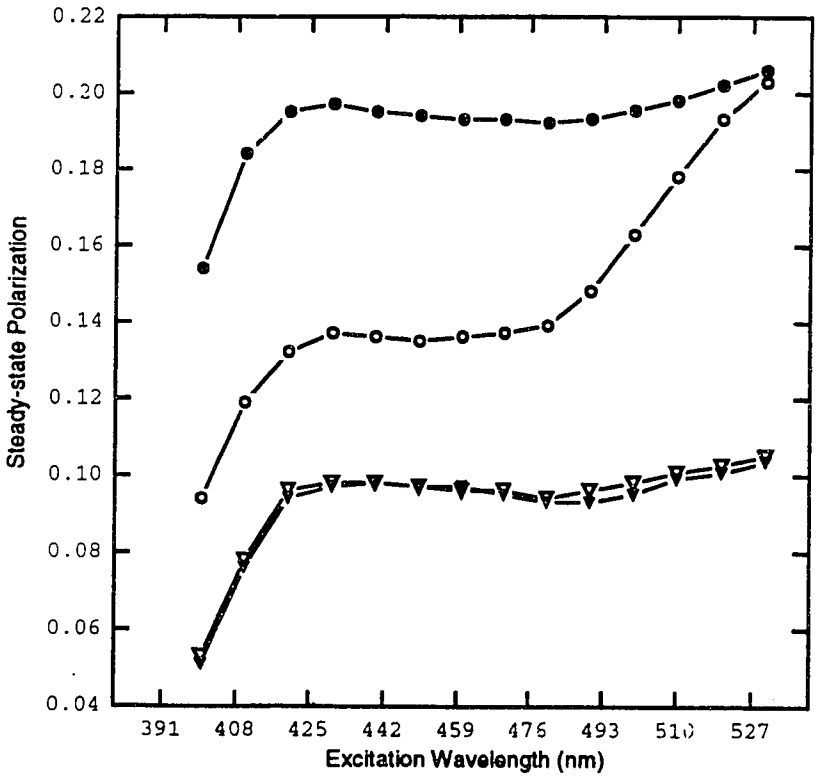

Figure 67: Intersubunit FRET between 5-IAFs bound to residue C-33, elucidation via the Weber red-edge effect (Weber and Shinitzky, 1970; recall Figure 17). Filled circles represent the excitation polarization spectra for 5-IAF fully labeled to L7/L12 C33 subsequent to subunit exchange with 10x excess unlabeled wild type L7/L12; hollow circles represent the excitation polarization spectra for 5-IAF fully labeled to L7/L12 C33; filled and hollow triangles respectively, represent 5-IAF fully labeled to L7/L12 C-33 with 4 M GuHCl or methionine's oxidized. Hence, we see here unequivocally, that the depolarizing intersubunit homo-FRET is lost subsequent to dissociation or subunit exchange with 10 x unlabled wild type L7/L12. Furthermore, the polarization of 5-IAF fully labeled to L7/L12 C33 is regained at the red-edge of the fluorescein absorption spectrum (recall Figure 19, Chapter 4) as expected from the Weber red-edge effect. All dimeric protein concentrations were 2 μM and temperature kept constant at 20°C. Excitation was with 488 nm light and emission was usually collected with 085 cut-on filters. When using 085 filters, background/scattering is subtracted when excitation is greater than 520 nms.

Table 24: Monitoring Subunit Exchange and Intersubunit Distances via Homo-FRET between 5-IAFs Bound to Separate Subunits of Various Cysteine Mutants of Dimeric L7/L12*.

mutant fully labeled with 5-IAF:	P	P_∞	N	$<R_0>$	$<R>$
C-12	0.126	0.185	0.46	40 Å	41 Å
C-33	0.135	0.192	0.38	40 Å	43 Å
C-63	0.104	0.104	0.00	41 Å	>90 Å
C-89	0.190	0.191	0.00	41 Å	≥90 Å
C-99	0.094	0.104	0.18	40 Å	52 Å
CTF C-89*	0.160	0.160	0.00	41 Å	——
poly-pro C-89	0.186	0.190	0.02	41 Å	75 Å
Δ35-52 C-89	0.107	0.145	0.35	39 Å	44 Å

*The terms P and P_∞ were discussed in Equation 54 as the polarizations respectively, with and without FRET; excitation was at 470 nm where no loss of FRET has occurred (recall Weber red-edge effect--Weber and Shinitzky, 1970). N is the effective transfers of the emission (Equation 54). R and R_0 were discussed in the text. In cases of the fully labeled hinge intact cysteine mutants (*as well as CTF C-89*), a 10 x excess of unlabeled wild type L7/L12 was added to reach P_∞; in the case of fully labeled Δ35-52 C-89, a 10 x excess of unlabeled Δ35-52 was added to reach P_∞. All experiments were repeated at least 3 x except the poly-proline mutant.

residues, located at the N-terminal base of the C-terminal domains, appear to be within ~55 Å of each other. Hence, the data were in excellent agreement with the model depicted earlier in Chapter Four (Figure 40; also, see Chapter 1, Figure 5). Conversely, the C-89 or C-63 residues were greater than 90 Å apart. Hence, the data here are in good agreement with a parallel quaternary structure for L7/L12 similar to that in Figure 40 and the tips of the two C-terminal domains are distant. Furthermore, like the rhodamine dimer data, the homo-FRET data for Δ35-52 C-89 indicated that the two, intersubunit C-terminal domains come in rather close contact subsequent to deletion of the hinge. Interestingly, exchange of the hinge-deletion mutant subunits takes 10-100x greater than that of the hinge-intact L7/L12 (data not shown). Finally,

substitution of poly-proline for the native alanine rich hinge region of L7/L12 results in a protein in which the C-terminal domains, on average, appear closer to one another presumably due to lesser mobility; hence, the data are in good aggreement with the time-resolved fluorescence data mentioned in the previous chapter.

What does the data in Table 24 tell us about the N-terminal domains? The data indicate that when the probes are located in the dimeric N-terminal domains, they are able to readily undergo FRET. Furthermore, it is not difficult to imagine that the midpoint of the xanthene rings are facing outward on opposite sides of the coiled-coil (as depicted earlier in Figure 66) and thus be ~40 Å apart. The data, therefore, were not necessarily in disagreement with the rhodamine dimer data, which indicated that the base of the cysteine side chains were about 23 Å apart. It is not difficult to imagine that the free energy of rhodamine dimer association is such that they can associate on the surface of the putative coiled-coil, whereas, the fluorescein derivatives "repel" one another away from the coiled-coil.

The P of fully labeled C33-TMRIA is 0.220 and its P_∞ is 0.305. The efficiency of transfer was thus, only 0.43 and since we know that the two 5-TMRIAs undergoing FRET are complexed R should be nearly 0 Å unless one or both of the following are true: 1) the K^2 term must be significantly altered via rhodamine dimer complexing; 2) the quantum yield or extinction coefficient is drastically altered in the rhodamine dimer complex. Thus, the R_0 and R terms in Table 24 should only be taken as approximate estimates, as we have not yet calculated the K^2 terms. If we assume that the rhodamines in the dimer complex are oriented 90° relative to one another (as depicted earlier in Figure 56), then we might assume a K^2 term of near 0 (recall page 66, equation 28; a K^2 of 4.0 is optimal, i.e., when the two fluorophores are

perfectly aligned--although in this case, less depolarization would occur with homo-FRET). This would obviously result in a reduction of the R_0 and might explain the less than optimal transfer efficiency. The time-resolved fluoresence data for this rhodamine dimer at the C-33 position indicated unusually large amounts of local motion and considerable missing anisotropy (data not shown). Similar to the C33-IAF, the large fractional anisotropy amplitude and the missing anisotropy, respectively, decrease and increase upon subunit exchange. The data could be explained in that the large local motion component of the 5-TMRIAs involved in rhodamine dimers, is largely due to to the rapid FRET, and does not necessarily indicate that large local mobility still persists when the rhodamines are complexed (which might lead to a higher value of K^2). In the case of 5-IAF bound to each of the cysteine mutants, where fluorophore dimer complex is not formed (5-IAF is *capable* of forming complexes, Förster, 1957, but does not in any case listed in Table 24 as judged by its absorption spectra as well as the FRET data) and the local motion is extensive, an assumed K^2 value of 2/3 is justifiable. Finally, we have not rigorously attempted to calculate the extinction coefficient or quantum yield for the rhodamine dimer. Although, if one looks at Figure 58 one can see that the extinction coefficient in the overlap region is only about 50% that of a rhodamine monomer; hence, the R_0 is already diminished by ~10 Å. Furthermore, for the record, the lifetime of the 5-TMRIA becomes bi-exponential when the rhodamine dimer is formed indicating possibly a change in quantum yield.

Finally, the author shall mention here that the data presented in Table 24 reveal further excellent proof for the absence of significant C-terminal domain interaction. Mixing of 10x unlabeled wild type L7/L12 with the CTF C89-IAF results in absolutely no change in the S.S.P. in contrast to what one

might expect if the C-terminal domains form a complex. On a similar note, the author shall mention here that addition of 10 x molar excess NTF to C33-TMRIA resulted in the usual instant loss of the rhodamine dimer absorption peak (data not shown) as expected via the fact that the N-terminal domains do form a complex. Conversely, addition of CTF to C33-TMRIA results in no loss of the rhodamine dimers.

The Use of Hetero-FRET in the Elucidation of Intersubunit Distances Within Different L7/L12 Cysteine Mutants. In this subsection, data is presented using the hetero-FRET method. The hetero-FRET method has the advantage over the homo-FRET method in that one can measure more easily intersubunit distances between probes located in different sites (vide infra). The author begain initial hetero-FRET studies with the donor and acceptor fluorophore pair of respectively, 1,5-IAEDANS and 5-IAF. The primary reason for using IAEDANS rather than the coumarin derivative is that the IAEDANS has a much longer lifetime (~13 ns instead of ~4 ns), and is therefore easier to monitor via the donor lifetime method of hetero-FRET (recall pages 65-69 of Chapter One).

The overlap between the emission spectra of L7/L12 C33-IAEDANS and the corrected emission spectra of L7/L12 C33-IAF are shown in Figure 68. Furthermore, the extinction coefficent and quantum yield of IAEDANS and 5-IAF bound to L7/L12 C-33 were determined as described on pages 65-69 of Chapter One of this dissertation. From the overlap integral in Figure 68 and the measured extinction coefficents and quantum yields, we could estimate an R_0 of ~40 Å for critical transfer of energy from IAEDANS to 5-IAF when both are bound to C-33 (since the spectral overlap, extinction coefficients and quantum yields were the ~same for 5-IAF or IAEDANS bound to C-63 or C-89, we can assume that roughly the same R_0 exists between the probes as when

bound to the C-33 position). With the excellent R_0 for IAEDANS energy transfer to 5-IAF, a set of unique experiments were performed as seen in Table 25. A comparison is made in Figure 69 between the measurement of R via the steady-state method and the time-resolved method. In Table 25, results are from the time-resolved method of FRET, whereas, in Figure 69, we see that the reduction of steady-state emission of the donor fluorescence of IAEDANS bound to C-33 in the presence of FRET is quite comparable to the reduction of its lifetime. As mentioned previously, the author considers the time-resolved method superior to the steady-state method for elucidation of energy transfer efficiencies (recall pages 68-73). The average efficiency of energy transfer (recall E from Equation 24, in Chapter Three) is defined as:

$$E = 1 - [<\tau_{DA}> - <\tau_D>(1-f_a)f_d \; / \; <\tau_D>] \qquad (55)$$

where $<\tau_{DA}>$ and $<\tau_D>$ are respectively, the lifetimes of the donor probe in the presence or absence of the acceptor, whereas, f_d is the molar fraction of donors and f_a is the molar fraction of acceptors.

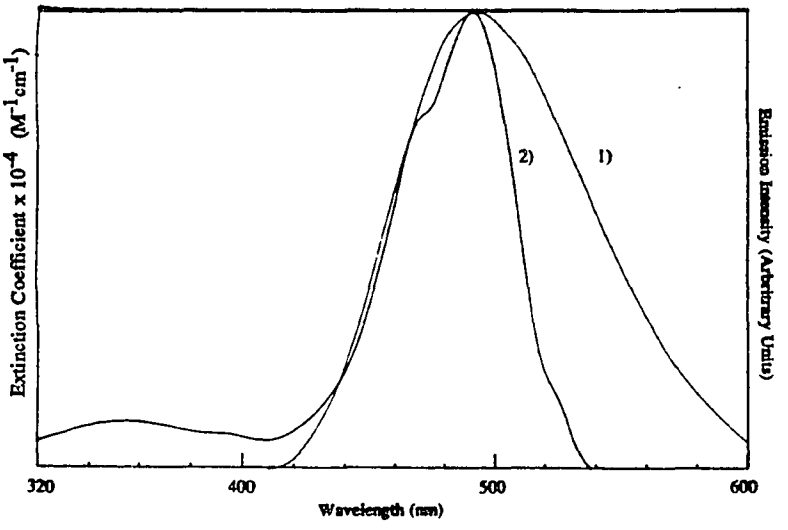

Figure 68: The overlap of the corrected emission spectra (1) of IAEDANS bound to L7/L12 C-33 and the absorption spectra (2) of 5-IAF bound to L7/L12 C-33 are depicted. The emission spectra of 1,5 IAEDANS was acquired via 351 nm excitation.

The data in Table 25 and Figure 69 are once again in excellent agreement with the dynamic polarization data presented in Chapter Four, the rhodamine dimer data in the previous section, and the homo-FRET data presented in Table 24: 1) it seems unequivocal that the C-33 residues are on rather opposite sides of the N-terminal domain, and it is not doubtful that the probes are facing away from each other; 2) all data sets are in agreement that

Table 25: Approximate Distances Between the Various Cysteine Residues of the Dimeric L7/L12 Cysteine Mutants as Judged from Intersubunit Hetero-FRET between 1,5-IAEDANS and 5-IAF.*

fully-labeled sample	molar excess of acceptor added	$\langle\tau_D\rangle$	$\langle\tau_{DA}\rangle$	%E	~ R
C33-IAEDANS	----------	13.5	--------	--------	--------
"	3 x excess of free fluorescein	--------	13.4	--------	--------
"	equimolar C33-IAF	13.5	11.2	0.42	43 Å
"	9 x excess of C33-IAF	"	9.4	0.56	39 Å
"	3 x excess of C89-IAF	"	11.8	0.30	47 Å
"	3 x excess of C63-IAF	"	11.9	0.28	48 Å
C63-IAEDANS	----------	12.6	--------	--------	--------
"	3 x excess of C63-IAF	"	12.4	--------	≥ 85 Å
"	3 x excess of C89-IAF	"	12.4	--------	≥ 85 Å
C89-IAEDANS	----------	12.4	--------	--------	--------
"	3 x excess of C89-IAF	12.3	--------	--------	≥ 85 Å

* Excitation was accomplished with 351 nm laser light; since 5-IAF is excited as well with 351 nm light, the IAEDANS emission was separated from fluorescein emission (which begins at ~470 nm if one recalls Figure 19) via a 459.6 nm interference filter (with ~5 nm half-width). All measurments were acquired only once at 20°C, except equimolar C33-IAEDANS/C33-IAF, which was acquired 3 x and hence, the value given here is the average. The lifetimes are given in units of ns. $\langle\tau_D\rangle$ and $\langle\tau_{DA}\rangle$ are respectively, the fluorescent lifetimes of IAEDANS in the absence or presence of the acceptor fluorophore, 5-IAF. %E is the efficiency of energy transfer as described earlier in Equation 24, except the emission intensities are substituted by the essentially comparable lifetimes. R is the average distance between the fluorophores as calculated from Equations 24-27 and assuming an R_0 of ~40 Å.

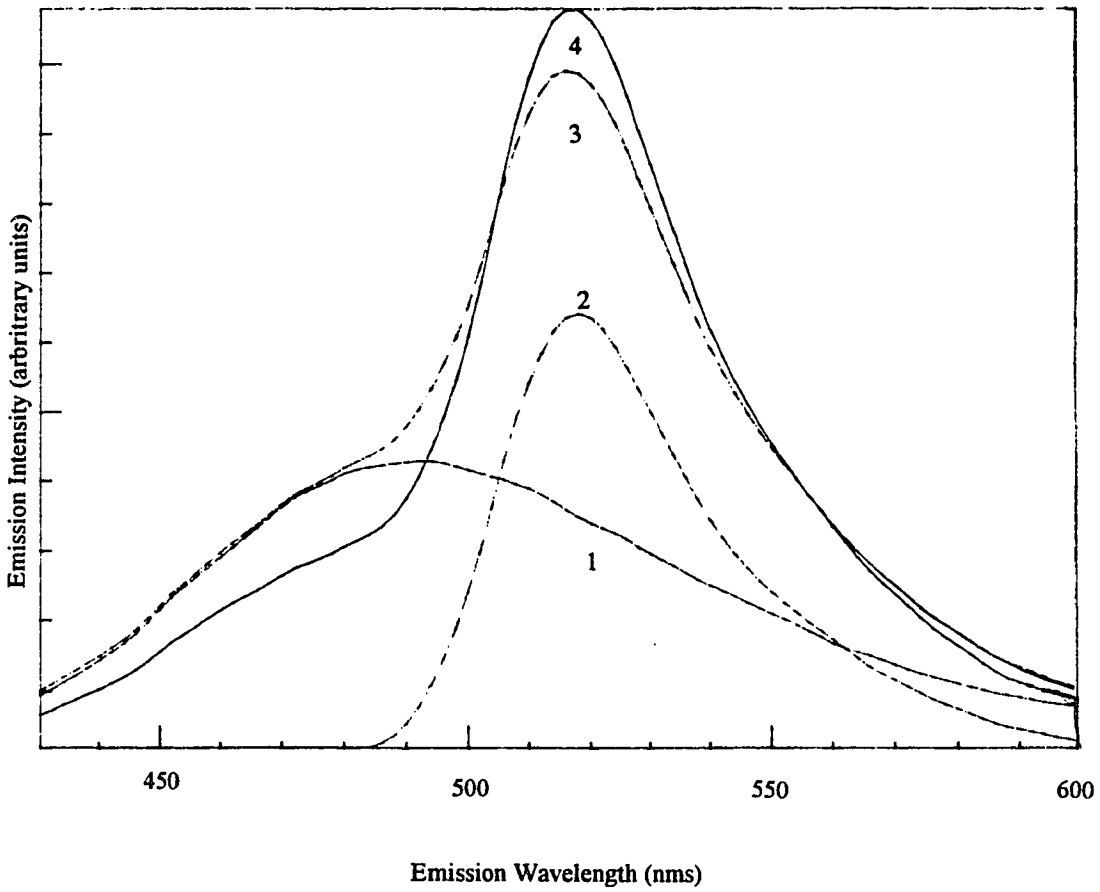

Figure 69: Comparison of steady-state emission intensities method to the time-resolved method data presented in Table 25. Here we see the emission intensity of C33-IAEDANS in the absence of FRET upon 351 nm excitation (1), the emission spectra of equimolar C33-IAF upon excitation (2), spectra one and two simply added (3), and (4) the combined emission spectra of each in the presence of hetero-FRET. Note how the donor emission intensity is decreased about 25% in the presence of FRET, similar to its lifetime shown in Table 25.

residues C-63 and C-89 are quite distant from each other in the case of free L7/L12; 3) subsequent to deletion of the flexible hinge, the C-terminal domains are on average much closer (recall rhodamine dimers form and

significant homo-FRET occurs between fluorophores bound to residue C-89; 4) the homo-FRET data on C-99 indicate that the N-terminal *base* of the C-terminal domains are reasonably close on average (~55 Å), in agreement with the average conformational model depicted earlier in Figure 40 (also see Figure 5); 5) the N-terminal domains are rather structurally stable in the dimer state and in conjunction with the rhodamine dimer data, are close enough such that it is quite feasible that they form a coiled-coil with diameter of the usual 30-35 Å. Hence, the 10 Å axial diameter (recall Figure 4 in Chapter One) axis existing in the literature is not in agreement with the data presented in this dissertation; finally, 6) the very striking finding in Table 25 was that fluorophores labeled at residues C-63 or C-89 were able to undergo FRET with fluorophores bound at residue C-33!! Hence, the data here provided excellent evidence for the model depicted earlier in Figure 40--the distal C-terminal tips of the C-terminal domains on average, are not so distant from the N-terminal domains as previous models suggested (recall Figures 4 and 29). An average consensus model from all data presented in this dissertation for the dimeric structure of L7/L12 is presented in the next chapter.

IMMUNOAFFINITY CHROMATOGRAPHY: A NON-SPECTROSCOPIC METHOD FOR VERIFYING L7/L12 SUBUNIT EXCHANGE

In this section, the author briefly presents data using a non-spectroscopic method to verify the validity of the spectroscopic methods. There are two arguments that one might have for data already presented in this chapter: 1) subunit exchange only occurs between the N-terminal cysteine mutants. This argument seems absurd at this time seeing the author has repeatedly demonstrated that unlabeled and unaltered wild type L7/L12 readily undergoes subunit exchange with the mutants; 2) the fluorophores in

the C-terminal domain are aligned such that they cannot efficiently undergo significant FRET. This argument as well seems absurd since the author demonstrated in Chapter Four that fluorophores labeled at C-63 or C-99 exhibit unusually large amounts of local motion, which would lead to the estimated K^2 value of 2/3. Nonetheless, let us proceed to demonstrate rather non-spectroscopically that the subunits of all forms of L7/L12 readily undergo subunit exchange.

Dr. Ed Voss, Jr., at the University of Illinois, Urbana, has produced several different immunoglobins that are highly specific for fluorescein derivatives. We have used both the single chain antifluorescein antibody (described in Voss et al, 1993) and the polyclonal antifluorescein antibody (described in Voss, 1984) to study the quenching of L7/L12-bound fluorescein fluorescence, which in both cases is about 98 % depending on the exact location of the probe (data not shown). Dr. Voss and colleagues have found that both antibodies bind fluorescein with an association constant of nearly $10^{10}\,M^{-1}$ (Voss, 1984; Voss et al, 1993). Furthermore, Dr. Voss and colleagues (personal commun-ication) have found that that the polyclonal antifluorescein IgG can be conjugated to cyanogen-bromide activated Sepharose 4B (protocol given previously in Materials and Methods, Chapter Two) with the high affinity for fluorescein maintained; the complex of Sepharose 4B and polyclonal anti-fluorescein IgG can be effectively called an immunoadsorbent. Finally, Dr. Voss has found that the anti-fluorescein antibodies do not bind to rhodamine, regardless of their similarity in structure. In Table 26, data is presented for the binding, if any, of various samples of unlabeled L7/L12 and L7/L12 labeled with rhodamine or fluorescein. The data presented in Table 26 once again, non-spectroscopically and unequivocally, determine that the subunits of L7/L12 can exchange.

Furthermore, in the case of L7/L12 C-89 or wild type L7/L12-FITC, the absence of homo-FRET was solely due to the fact that fluorophores bound to the C-terminal domain of L7/L12 are unable to undergo FRET as the C-terminal domains are quite distant to each other. No one can now argue that the absence of FRET loss subsequent to mixing was the result of lack of subunit exchange.

Table 26: The Binding of Various Unlabeled or Labeled Samples of L7/L12 to the Anti-fluorescein Immunoadsorbent.*

Sample added to immunoadsorbent	% of FITC fluorescence lost to the immunoadsorbent	% of 5-TMRIA fluorescence lost to the immunoadsorbent
1) 0.3 μM of dimeric wild type L7/L12 labeled with 1.2 FITCs	95%	
2) 0.3 μM dimeric L7/L12 C-33 fully labeled with 5-TMRIA	—	10%
3) 0.3 μM dimeric L7/L12 C-33 fully labeled with 5-TMRIA and exchanged with equimolar L7/L12 labeled with 1.2 FITCs	—	55%
4) 0.3 μM dimeric L7/L12 C-89 fully labeled with 5-TMRIA	—	12%
5) 0.3 μM dimeric L7/L12 C-89 fully labeled with 5-TMRIA and exchanged with equimolar L7/L12 labeled with 1.2 FITC's	—	58%

*The procedures are as described in Materials and Methods; this particular experiment was done only once; similar results were obtained in another experiment, except up to 25 % of the rhodamine samples were lost to the immonoadsorbent probably reflecting some unmasked reactive groups on the immunoadsorbent.

DO THE SUBUNITS OF L7/L12 UNDERGO EXCHANGE WHEN BOUND TO THE RIBOSOME AS WELL??

PRELIMINARY DATA

The issue of L7/L12 subunit exchange on the ribosome has been confronted via fluorescence spectroscopy methods (Zantema et al, 1982; Thielen et al, 1984). This group determined that the subunits of L7/L12 bound to its weak ribosome binding site are unable to undergo subunit exchange with subunits located in the strong binding site. Hence, their data were simply in agreement with the idea that a strong and weak binding site for each of the two dimers of L7/L12 exists on the ribosome. Their data did not, however, determine whether or not subunit exchange occurs between weak sites or strong sites, which thermodynamically seems more feasible to the author. In one other study (Lee et al, 1981), the investigator's data did not leave out the possibility of subunit exchange on the ribosome; although, they concluded it was unlikely because the dimers of L7/L12 are "highly stable".

Preliminary investigations for the exchange of L7/L12 subunits on the ribosome were obtained in our laboratory as follows:

1) We determined that L7/L12 C33 labeled with IAEDANS is able to bind to the ribosome, as its S.S.P. rises from 0.049 to 0.151 upon binding to ribosome cores (prepared as described in Chapter Two).

2) After subunits of L7/L12 C-33 were added in 10 x excess to the ribosome cores (all L7/L12 supposedly removed), non-reconstituted protein was removed via SE-HPLC and the resultant ribosomes with L7/L12 C33-IAE (which eluted in the void volume as described in Chapter Four) were found to possess an S.S.P. of 0.151 as mentioned above. Although we did not quantitate the number of IAEDANS bound to the ribosome (low extinction

coefficient of IAEDANS), it seemed likely that most binding sites were filled as a 10 x excess of (L7/L12)/ribosome core was added.

3) In another separate sample, it was observed that reconstitution with fully-labeled L7/L12 C33-TMRIA resulted in nearly complete loss of the uncorrected rhodamine dimer absorption spectrum (see Figure 70). Hence, the data indicated that either a large conformation change occurs in the region near to the C-33 or else, the subunits of L7/L12 C33-TMRIA were exchanging with subunits that were not fully removed from the ribosome (as described in Materials and Methods). Stoichiometrically, it is unlikely that such a drastic change in the rhodamine dimer absorption spectrum would occur if only say, ≤40% of native L7/L12 remained. Subsequent SE-HPLC of 10 x molar excess fully labeled L7/L12 added to the ribosome cores showed that about 10% of the C33-TMRIA had bound to the ribosome as expected if no native L7/L12 was presented prior to reconstitution. *Furthermore, the S.S.P. of the 5-TMRIA bound to L7/L12 C-33 had only increased from 0.215 to 0.233 verifying that the loss of rhodamine dimers could be solely attributed to a conformational change in the region of the C-33's and not from subunit exchange.* More specifically, if the rhodamine dimers are lost ($OD_{517/555}$ goes from 1.2 to <0.5 like when subunit exchange occurs) and the homo-FRET is not significantly lost (recall when *subunit exchange* occurs, the S.S.P. increases to 0.305!!), then the change in the rhodamine absorption spectra is not due to subunit exchange with unremoved and unlabeled L7/L12;

4) A rather startling result occurred when a 5 x excess of L7/L12 C33-IAE is added to the ribosome-reconstituted L7/L12 C33-TMRIA: the S.S.P. rapidly (although seemingly slower than when protein is free in solution) increases from 0.235 to 0.275!! Furthermore, when a sample of ribosomes reconstituted with L7/L12 C33-TMRIA was added to a sample of ribosomes

reconstituted with L7/L12 C33-IAEDANS, the S.S.P. of the TMRIA once again increases rapidly to 0.272. Hence, that data here appeared to indicate that subunit exchange was occurring on the ribosome. The S.S.P. value of

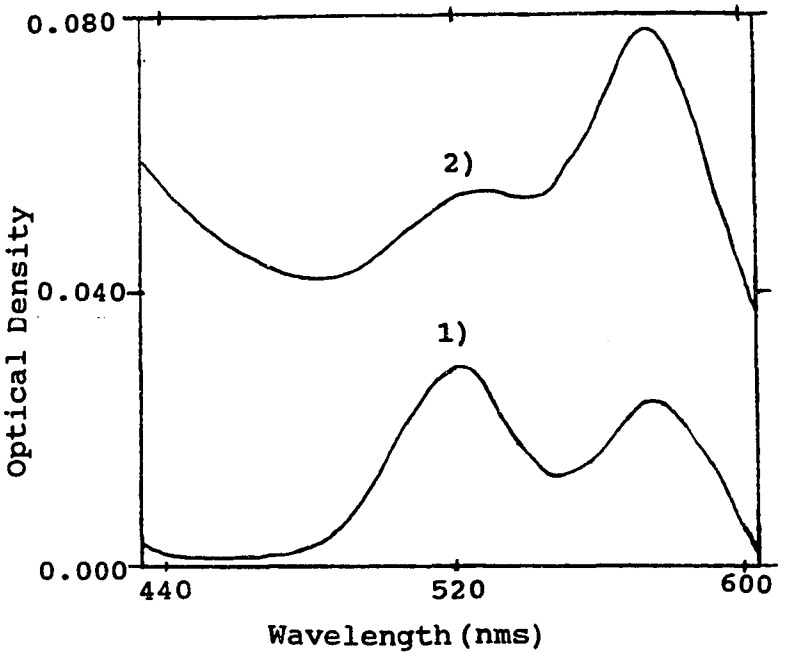

Figure 70: Uncorrected absorption spectra for L7/L12 C33-TMRIA free (1) and reconstituted into the 70 S ribosome (2) demonstrating a conformational change that results in subsequent loss of rhodamine dimers (although, as described in the text, the 5-TMRIAs are still quite near, as homo-FRET is still quite prevalent).

value of 0.275 is slightly lower than that expected for fully reconstituted and subunit exchanged L7/L12 C33-TMRIA (measured to be 0.312 (recall for simple exchange in solution, S.S.P. rises to 0.305). Hence, the data were in excellent agreement with the possibility of subunit exchange occurring on the ribosome between at least part of the dimers of L7/L12 bound to the ribosome. It is tempting at this time to attribute this partial exchange to that between dimers of L7/L12 located at the weak binding site on the ribosome (recall Chapter One);

5) Finally, as a control, L7/L12 C33-TMRIA was added to native ribosomes of Escherichia coli possessing putatively (although, not checked

yet) a fully-intact share of two L7/L12 dimers per ribosome. The logic was simple: does the recombinant form of L7/L12 exchange subunits with native L7/L12?? Interestingly, addition of equimolar L7/L12 C33-TMRIA resulted in an increase in S.S.P. to 0.248. The SE-HPLC data indicated that ~30 or 40 % of the 5-TMRIA bound to L7/L12 eluted as part of the ribosome. The S.S.P. of this native ribosome/(L7/L12) C33-TMRIA mixture was 0.278 and that of the L7/L12 C33-TMRIA was now 0.238. Once again, the data were in excellent agreement with the possibility of recombinant L7/L12 undergoing subunit exchange with at least part of the native and ribosome-bound L7/L12. Future investigations of this phenomenon might prove quite fruitful in the elucidation of the functional role and dynamics of L7/L12 on the ribosome (see next Chapter).

CONCLUSIONS TO CHAPTER SIX

In this chapter several rather novel discoveries were presented. The results presented in the previous chapter included a semi-quantitative determination of the subunit equilibrium of dimeric L7/L12; more specifically, a dimer to monomer dissociation constant 38 nM was reported. At the beginning of this chapter the author described the simple theoretical equilibrium calculations that predicted a subunit exchange between dimers of L7/L12 on the order of 100 milliseconds. The calculation (Equations 51-53) included an estimated rate of association (k_+) based on previous translational diffusion data (e.g., Wong and Paradies, 1974) and Stokes radii (recall Table 2, Chapter Four) estimates for monomeric L7/L12. Hence, from the experimentally determined dimer/monomer K_D (present study) andk_+ of L7/L12, one can calculate from Equations 51-53 a rate of subunit exchange (k_-) of less than 57 sec^{-1}. In this chapter the author unequivocally demonstrates with experimentation that the subunit of L7/L12 exchange to complete

equilbrium in less than one second. Numerous methods were in excellent agreement:

1) The very unique absorption spectra of 5-TMRIA bound to the N-terminal domains indicated directly an intersubunit interaction; this interaction was disrupted completely with either 3 M guanidine HCl (Gu-HCl) or 10 excess of unlabeled wild type L7/L12. The rhodamine dimers were fully recoverable subsequent to removal of Gu-HCl; conversely, the author believes the only way to recover rhodamine dimers from a hybrid mixture of unlabeled wild type L7/L12 and 5-TMRIA labeled L7/L12 would be via some rigorous affinity chromatography methods (i.e., something that is highly specific for rhodamine) that work in the presence of urea or guanidine HCl. Similarly, the author demonstrated via SE-HPLC that the rhodamine dimers are formed between the subunits of *dimeric* L7/L12 and unequivocally do not effect the dimer/monomer equilibrium of L7/L12. Interestingly, Peak1 L7/L12 forms rhodamine dimers, but the $OD_{517/555}$ of 5-TMRIA fully labeled to micromolar L7/L12 is ~1.10 instead of 1.28 (like for fully labeled dimeric L7/L12); the data indicated that some "strain" occurs in this N-terminal region of Peak1. The other exciting finding with the 5-TMRIA probe is when bound to C-terminal cysteines, no rhodamine dimers are formed; the data demonstrated that the C-terminal domains are quite mobile within L7/L12 and hence, unable to form stable rhodamine dimers. When the hinge is deleted, the C-terminal domains become stable enough such that 5-TMRIA bound to all of the C-89 residues can form intersubunit rhodamine dimers. Finally, the author has demonstrated, via quick mixing single wavelength absorption techniques that this exchange is completed in times significantly less than one second. A schematic of this intersubunit rhodamine dimer interaction is given in Figure 64.

2) Another major method used in the present study to elucidate and characterize the subunit exchange of L7/L12 is that of fluorescence resonance energy transfer (FRET). The author utilized the method of homo-FRET to unequivocally determine that subunit exchange occurs with dimeric L7/L12 (Figure 67). Furthermore, the author has found that these changes in steady-state polarization subsequent to mixing fully 5-IAF (or 5-TMRIA; in fact some homo-FRET is observed between IAEDANS' labeled at C-33--S.S.P. rises 0.01 upon exchange) labeled L7/L12 C-33 with unlabeled wild type L7/L12 occur in less than a couple of seconds (the time necessary for measurement). Hence, the data were in perfect agreement with the rhodamine dimer data. Similar to the 5-TMRIA data, homo-FRET does not occur between 5-IAFs labeled in the C-terminal domains of L7/L12 (Table 24). Thus, both sets of data (rhodamine dimers, homo-FRET) are in excellent agreement with *hetero* FRET (Table 25, Figure 69) data. Hetero-FRET occurs effectively between intersubunit 5-IAFs located in the N-terminal domain. In fact, the distance calculations made via the homo-FRET and hetero-FRET methods were in excellent agreement indicating that Weber's homo-FRET equation (54) was equally valid as the more common hetero-FRET equations (Chapter Three). The one striking addition to the story made from the hetero-FRET data was that 5-IAFs bound to C-terminal C-63 or C-89 residues transferred resonance energy to 5-IAFs bound to the N-terminal C-33 residue. Once again (like in Chapter Four) the data here are in superb agreement with Figure 40 (see also Figures 64 and 66).

3) A novel, rather non-spectroscopic method for the elucidation of subunit exchange was also presented. The author utilized the polyclonal anti-fluorescein antibody supplied from Dr. Ed Voss, Jr., as well as his method for conjugating the polyclonal antibody to cyanogen bromide activated

Sepharose-4B. It was then found that wild type L7/L12 labeled with FITC binds with 95 % efficiency to the immunoadsorbent; conversely, insignificant amounts (10%) of 5-TMRIA labeled L7/L12 cysteine mutants were able to bind the immunoadsorbent (Table 26). When 5-TMRIA labeled L7/L12 is simply mixed with FITC labeled L7/L12, approximately 50-60% of the 5-TMRIA was found to be bound or lost to the immunoadsorbent indicating that essentially subunit exchange had reached a nearly perfect equilibrium. This method might provide an effective tool in studying not only subunit exchange in proteins, but also protein purification (as the Voss laboratory has done), etc.

4) Finally, preliminary data was presented in this chapter suggesting that up to 50% of the subunits of L7/L12 bound to the ribosome are able to undergo rapid subunit exchange. The results presented here are rather preliminary and experiments are designed for the near future to elucidate more quantitatively the events on the ribosome. It is also of interest that the rhodamine dimer of L7/L12 dissociates subsequent to binding to the ribosome (experiment has been repeated four times already)--this would indicate a free energy change in the conformation of L7/L12 in this region (where the flexible hinge and N-terminal domain meet) of 3-4 kcal/mole (dissociation of rhodamine dimers).

As mentioned in the introduction, not so many papers have been written on the subunit exchange of dimeric or oligomeric proteins. Equations 50-53 were adapted from classic rate theory for rather simple molecules in comparison to proteins. Hence, it is quite likely that subunit exchange of proteins may be somewhat more complex than that described by classic rate theory and as Weber describes, the efficiency of subunit exchange in proteins is usually around 10% of that calculated from the K_D and $k+$. Thus, the $k-$ of L7/L12 might be more likely greater than 17 milliseconds. In the near future

we expect to directly measure the rate of subunit exchange with a rapid stopped-flow instrument. It shall be very interesting to determine the precise effects of temperature, denaturants, organic solvents, salt, and pH on the rate of subunit exchange. Furthermore, it should be interesting to see how accurate the classical rate constant theory is with a more complex protein, such as the various substitution or deletion mutant forms of L7/L12 that can form rhodamine dimers when labeled with 5-TMRIA. More precise comparisons might be made between the stability of these proteins in comparison to wild type forms of L7/L12 (i.e., the effects of site-specific substitutions or deletions on subsequent protein stability).

CHAPTER 7:
SUMMARY AND PROSPECTUS

L7/L12 is one of the most thoroughly studied of all ribosomal proteins. The present author has discussed the discrepancies in the literature considering the quaternary structure and segmental flexibility of dimeric L7/L12 (Figure 4, Chapter One; Table 2, Chapter Four). Such discrepancies included the following: 1) what is the average axial ratio of dimeric L7/L12?; 2) is dimeric L7/L12 highly flexible as numerous crosslinking, one low-angle x-ray scattering, or several electron microscopy studies suggest, or is it a rigid rod like sedimentation velocity, translational diffusion, intrinsic viscosity, and a couple of x-ray scattering studies have indicated?; 3) are the two monomers associated antiparallel or parallel relative to one another?; 4) are the two monomers associated in a staggered or unstaggered manner?; 5) are the two C-terminal domains of dimeric L7/L12 associated as a complex as x-ray crystallography studies indicate or do they rotate independently as zero-length crosslinking and proton NMR studies have suggested?; 6) is L7/L12 a "stable" dimer or is it a tetramer or monomer ?; 7) is it possible that the subunits of L7/L12 can undergo significantly rapid exchange on or off the ribosome? The answers to these questions were at least partially elucidated in this dissertation. In this chapter the author shall summarize some of the primary points discovered and briefly their possible relation to protein biosynthesis *in vivo*. The present author briefly presents prospective experiments.

CHAPTER FOUR

In Chapter Four of this dissertation, experimental data using various state of the art fluorescence techniques and SE-HPLC indicate that the conformation of L7/L12 is in fact rather unusual. The initial data presented in Chapter Four, with various probes bound to wild type L7/L12, indicated that our samples were actually heterogeneous in aggregation or rotational states. More specifically, the longer the excited-state lifetime of the probe, the longer the global rotational relaxation time monitored. Furthermore, the various χ^2 confidence curves reported in the early part of Chapter Four indicated that the shorter the excited-state lifetime of the fluorophore used, the more the error with increasing rotational relaxation times (i.e., fluorescein derivative, see Figure 27, pg. 112). The data were explained in that the emission of light is simply detected with less accuracy at times significantly greater than a few times that of the average excited-state lifetime of the probe. The author confirmed what had already been communicated several months earlier (from the Traut laboratory): an unusual, apparently high molecular weight form of L7/L12 was present in our samples, in addition to the "native" dimeric form of L7/L12. Subsequent to removal of this Peak1 "aggregate" of L7/L12, it became apparent that the very long global rotational relaxation times (>~40 ns) monitored with the longer lifetime probes (~10-150 ns) in previous studies, were simply the result of contamination with an aggregated form of L7/L12. In conjunction with the structure/stability results presented in Chapter Five, the data in Chapter Four agree that Peak1 L7/L12 is an aggregated form of L7/L12, probably greater than that of a tetramer. Nonetheless, it is apparent that this Peak1 form of L7/L12 still has some independent C-terminal domain mobility, primarily that of the individual C-terminal domains (as probes bound to the C-terminal domains of L7/L12

always monitor some of the segmental global rotational relaxation time--vide infra).

Extensive time-resolved fluorescence studies of dimeric SE-HPLC purified forms of fluorescently labeled L7/L12 were reported later in Chapter Four. Numerous conclusions were made from these studies including a highly reproducible rotational relaxation time of ~70% that expected for a sphere observed fairly independent of the fluorescence lifetime of the probe. The author demonstrated with contemporary fluorescence and rotational diffusion theory that the data must only indicate that the two independent C-terminal domains and the one complexed (dimeric) N-terminal domain each rotate independently with rather unrestricted mobility. Our results were quite dependent on the site-specific mutagenesis methods performed at the Traut laboratory. By substituting cysteine for alanine or serine at putative structureless loop regions within L7/L12, we could subsequently place sulfhydryl-specific fluorescent probes in the C- or N-terminal domains of L7/L12 and monitor flexible motions of each of these domains. In Figure 40, the author presented a new model describing L7/L12 as a dimeric protein with considerable independent C- and N-terminal domain mobility as opposed to all previous studies, which proposed that the two C-terminal domains of L7/L12 are complexed as well as the N-terminal domains. Ambiguously, the results presented in Chapter Four are hardly in disagreement with all previous studies (using a multitude of techniques) of L7/L12; rather, we propose here a more fine-tuned analysis of free L7/L12 conformational dynamics. The model depicted in Figure 40 for a flexible L7/L12 does <u>not</u> indicate that the axial ratio of L7/L12 is incapable of reaching maximum extension of up to ~160 Å (nearly the diameter of the entire ribosome). If one assumes that the N-terminal domains of L7/L12 are fixed to

the ribosome (i.e., rigid, unable to rotate), then it is rather difficult to imagine that the C-terminal domains could rotate in towards the middle of the ribosome with such extension (L5, peptidyl transferase domain; recall Figure 6, page 14). The crosslinking data (of Zecherle et al, 1992B; Oleinikov et al, 1993 A/B; and Traut et al, 1993) all indicate that the C-terminal domains of L7/L12 can flex downward beyond the N-terminal edge of the N-terminal domain, to interact intimately with L10. Hence, the data in Chapter Four of this dissertation are in excellent agreement with these recent crosslinking studies. Finally, the present author believes that L7/L12 could only span the diameter of the 50S ribosome subunit (i.e., to the peptidyl transferase region) if considerable flexibility exists within the putative frayed most N-terminal six amino acids. The author believes that in the near future it would be a wise investment to use site-directed mutagenesis and time-resolved fluorescence to characterize this far N-terminal region of L7/L12. The significance of these results is discussed again below.

Other conclusions made in Chapter Four included: 1) the rigidity and slight elongation of the N-terminal domains (when probes are bound to the putative coiled-coil region); 2) the rigidity and even apparent elongation of the hinge-deletion mutant (axial ratio at least 4:1); and 3) the rather spherical nature of C-terminal domains. Hence, the data here are not in such disagreement with the previous models of L7/L12 (i.e., Figure 4, Chapter One; model revised in Figure 40 of this dissertation).

CHAPTER FIVE

Only one quantitative study has been published on the subunit equilibrium thermodynamics of L7/L12 (Kar and Aune, 1981) prior to the results presented in this dissertation. Kar and Aune claimed that L7/L12 is ~90% monomeric at concentrations of ~one μM (tetramer/dimer/monomer

equilibrium association constant of 4.5 x 10^4 M). The concentration of L7/L12 inside an *E. coli* bacterium can be simply estimated as follows: 1) the wet volume of an *E. coli* ribosome is approximately 5 x 10^{-12} L; 2) the ribosomes (~2 x 10^4 copies per cell) makeup roughly 45 % of the dry weight of an*E. coli cell* (Leihninger et al, 1993, pg. 969); 3) assume L7/L12 exists as four copies (each 12 kD) per ribosome and thus, exists as roughly 1/50th the weight of the ribosome (~2600 kD; assuming that all L7/L12 is bound to the ribosome in the cell); *4) hence, ~ 0.1 picograms of L7/L12 exists per 5 picoliter cell and the cellular concentration of L7/L12 in its dimeric form is roughly 0.5 μM.* At 0.5 μM concentrations of L7/L12, the 5 x 10^4 K_a value for a tetramer/ dimer/ monomer equilibrium given by Kar and Aune would indicate that L7/L12 is ~95 % monomeric. Hence, Kar and Aune's analytical centrifugation studies indicate that the dimer of L7/L12 is quite unstable when removed from the ribosome. Finally, the biological significance of their results is doubted as monomeric L7/L12 does not bind the ribosome and it would take about 10 kcal/mol to induce dimerization of two monomers on the ribosome under the assumed biological conditions (vide infra). Numerous studies had qualitatively proclaimed the dimeric state of L7/L12 as "highly stable" presumably due to the original urea and PAGE studies of Möller et al, (1972). Numerous other crosslinking, chromatography, PAGE, sedimentation, low-angle x-ray scattering, and diffusion studies (i.e., Table 2, Chapter Four) have indicated that L7/L12 is dimeric at concentrations of greater than ~0.5 μM. Furthermore, recall from Caldwell et al (1978), monomeric L7/L12 does not bind to the ribosome. Even more ambiguously, the possibility of a tetrameric form of L7/L12 has been proposed (Georgalis et al, 1989).

Our SE-HPLC studies and subsequent time-resolved fluorescence studies indicated that ~50% of the *recombinant* L7/L12 is part of a larger

aggregate form of L7/L12 (larger than a tetramer). Makarov and co-workers (personal communication) have apparently attributed this larger aggregate (as elucidated from the present study) to an unfolded/aggregated form of L7/L12 resulting from the overexpression as it does not appear in samples purified from native ribosomes. Finally, the present author has found that this Peak1 L7/L12 is not in equilibrium with the dimeric (Peak2) form of L7/L12. Hence, in the present study, the author experimentally and reproducibly discovered an equilibrium dimer to monomer dissociation constant of ~38 nM for L7/L12. A K_D value of 38 nM agrees well with the idea of L7/L12 existing in solution as a dimer with rather average stability at biologically significant concentrations (~99% dimeric at 0.5 μM protein concentrations). *It was also confirmed in the present study (via SE-HPLC or fluorescence techniques/subunit exchange methods) that L7/L12 is solely dimeric up to 100 μM concentrations (data not shown).* In conclusion, we have not yet determined whether or not the dimer/monomer equilbrium is altered when bound to the ribosome; the results presented in Chapter Six bear on this issue.

The author demonstrated in Chapter Five that the probes or the mutations at position 33 in the N-terminal domain or at position 89 in the C-terminal domain have no effect on the natural stability of dimeric L7/L12; more specifically, the dimer to monomer K_D is exactly the same for fully labeled L7/L12 C33-IAF as it is for the same protein exchanged with 10 x excess of unlabeled wild type L7/L12. Furthermore, wild type L7/L12 exchanges to perfect equilbrium with fully labeled L7/L12 C33-IAF in less than one second (Chapter 6). Incidentally, the author has found that the reduced and unlabeled forms of the C-33 mutant exchanges with similar relative rapidity (data not shown) providing further evidence for the validity of our K_D determination. Finally, it was also demonstrated in Chapter Six that the

probes or mutations have insignificant effect on the function of L7/L12, lending further support that we were observing the true dimer/monomer K_D of native L7/L12.

Several other interesting conclusions from Chapter 5 should be mentioned again here. The two C-terminal domains of L7/L12 are not in a complex as previous x-ray crystallographers had suggested. The SE-HPLC studies verified that CTF C-89 must be monomeric at micromolar concentrations (or, at least a very unstable dimer that dissociates readily on the SE-HPLC column). Maybe more importantly, absolutely no transition was observed subsequent to dilution of the CTF C-89 from 10 μM to 10 nM (vide infra for more evidence of independent C-terminal domain motion). Conversely, a conspicuous dimer to monomer transition is observed with the NTF tails leading to K_D of ~0.3 μM. Hence, the data indicated two important findings: 1) dimerization of L7/L12 appears solely attributed to the N-terminal domains (with putative coiled-coil); 2) the stability of the N-terminal association is attenuated by nearly one order of magnitude subsequent to deletion of the hinge and C-terminal domains; and 3), very little structural changes are apparent in comparison to the C-33 region subsequent to dissociation--this conclusion was made from a combination of Gu-HCl and dilution studies. *In conjunction with the time-resolved fluorescence studies presented in Chapter Four, the data here indicate that the region local to the FITC within the structured part of the NTF is not at the interface of the two interacting monomers (in contrast to the C33-IAF or C12-IAF).*

It was also apparent in our studies that mutation from alanine at position 12 to cysteine resulted in destabilization of the subunit interaction in this putative coiled-coil region. Hence, the data indicated that alanine plays some sort of role in the structure and energetics necessary for dimerization.

In the near future it will be interesting to elucidate just what this N-terminal domain structure is--the Traut laboratory is preparing to use some other methods in the near future to determinine whether or not this is a coiled-coil structure. Further evidence for a coiled-coil NTF was presented in Chapter 6 (vide infra).

CHAPTER SIX

In Chapter 6, the author unequivocally determined that the subunits of dimeric (even Peak1, although less rapidly) L7/L12 undergo exchange to equilibrium completion in less than one second. The data were predicted in the introduction from classic rate theory equations. Several methods were utilized to verify this event within L7/L12 (both SE-HPLC peaks one and two, but not three). A rather novel method utilizing intersubunit rhodamine dimer interactions verified and initially quantified some characteristics of the subunit exchange. More specifically, the 517 nm absorption band of 5-TMRIA is enhanced more than three times when two rhodamines are complexed. Subsequent to addition of Gu-HCl or 10 x excess*unlabeled wild type L7/L12* this 517 nm peak is reduced back to normal (~40% of the absorption at 555 nm). Removal of the Gu-HCl results in complete recovery of the intersubunit rhodamine dimers indicating that their was no non-covalently attached 5-TMRIA (also verified by the fact that 5-TMRIA does not bind wild type L7/L12). Furthermore, it was verified that the 517 nm peak is strictly the result of a ground-state interaction as an excitation spectra of 5-TMRIA fully labeled to L7/L12 C33 results in no unusual 517 nm peak (Figure 60, Chapter Six). It was also verified that the rhodamine dimerization added (or subtracted) any observable changes in the subunit association free energy of dimeric L7/L12 (Figures 61 and 62).

Several other conclusions could be made from the rhodamine dimer data. Rhodamine dimers only occur between probes bound to the N-terminal domains of L7/L12 as rhodamine dimers were observed when 5-TMRIA is labeled at cysteines 12 or 33. No rhodamine dimers are observed when 5-TMRIA is bound to cysteines 63, 89, or 99, all located in the C-terminal domains. Further analysis of the rhodamine dimer data presented in this study and the data of Arebeloa and Ojeda (1982), indicate that the base of the two cysteines involved with rhodamine dimers (i.e., C-12/C-12 or C-33/C-33) must be ~23 Å apart. Hence, the data are once again consistent with a coiled-coil N-terminal domain for L7/L12 and highly flexible and independent C-terminal domains (see Figure 64). Another unique finding was that the two C-terminal domains become stable enough subsequent to deletion of the flexible hinge such that rhodamine dimers can form between 5-TMRIAs bound to the C-89 positions. Hence the data here and in Chapter Four, indicate that the free energy of C-terminal domain rotation with hinge-intact L7/L12 is greater in absolute value than the free energy of rhodamine dimer association (3-4 kcal/mol). The author described later in Chapter Six that a similar change in free energy occurs in the region local to the intersubunit L7/L12 C-33 residues subsequent to binding to the ribosome. It is very likely that this result represents a major structural change in the region local to the C-33 (recall from Chapter Five that a similar large conformational change occurs in this region upon dissociation and thus, it is tempting to attribute these changes to a "spreading" of the structureless hinge region). It will be exciting in the near future to see if the rhodamine dimers are lost at the C-12 position upon ribosome binding.

The use of homo-FRET and hetero-FRET were in excellent agreement with the rhodamine dimer data (Tables 24 and 25). It seems that the probes

used in this technique (5-IAF or 1,5-IAEDANS) were pointing away from the coiled-coil (Figure 66), rather than pointing inward as was the case of the rhodamine dimers. More specifically, both energy transfer techniques suggested that the probes bound to the N-terminal domain residues C-12 or C-33 were roughly 40 Å apart. This slight discrepancy is explained in that the association free energy of the rhodamine dimers is simply sufficient such that the two probes associate along the outside surface of a coiled-coil (see Figure 64). It is not difficult to imagine that two fluoresceins, with their negative surface charge, are located far away from each other (Figure 66). In the homo-FRET method, absolutely no depolarizing FRET is observed when the 5-IAFs are located in the C-terminal domains, with one exception: position C-99. Some homo-FRET is observed between 5-IAFs located at position C-99; hence, the data were in excellent agreement with Figure 40 (also, see Figure 5), which suggested that the bases of the two C-terminal domains were closer to each other than the tips of the two C-terminal domains. Similarly, the probes bound to C-89 of the hinge-deletion mutant do not appear so near to one another as is the case of the rhodamine dimers; more specifically, the probes now appear to be ~40 Å apart. It is possible that the κ^2 term accounting for the orientation of the probes relative to one another was significantly less than 2/3; a very similar phenomenon was verified with rhodamines attached to the C-33 residues, in which it is apparent that the two rhodamines in the dimer complex are oriented close to 90° relative to one another leading to lower than expected values for R.

Finally, the hetero-FRET data presented us with one more piece of information about the dynamics of L7/L12: FRET occurs between probes bound in the C-terminal domain (residues C-89 and C-63) and probes bound to the N-terminal domain residue C-33. The data were once again in good

agreement with the model proposed in Figure 40--that the two C-terminal domains are rather close (~55 Å) to the N-terminal domain on average (~15 ns time-scale of IAEDANS), whereas, the outer tips of the two C-terminal domains are rather distant to one another (>90 Å).

In closing, the author has presented a refined and more quantitative consensus model for the structure and dynamic of dimeric L7/L12 free in solution based on the results of previous studies and with the results presented in this dissertation (e.g., Figure 40). At the end of Chapter Six, data is presented that suggests significant amounts of L7/L12 subunits exchange while bound to the ribosome. The possibility of a "weak" or "strong" ribosome binding site seemed plausible. Characterization of this phenomenon is the subject of studies in the very near future in our laboratory. If the subunits of L7/L12 can exchange on and off the ribosome, then it is certainly feasible that other ribosomal proteins in fact exchange on and off the ribosome. If the ribosomal proteins are in a dynamic exchange equilibrium on the ribosome, on a similar time-scale for protein biosynthesis events to occur, then it may have significant impact on the interpretations of their role in protein biosynthesis. For example, in the case of L7/L12, an alternative theory for its ability to interact with regions distant on the ribosome might be that one or both dimers can dissociate from L10 on the ribosome and reassociate at a distant site (it takes at least five seconds for *E. coli* to make a fully functional 100 amino acid protein--Alberts et al, 1989). The recent data of Traut and colleagues (Oleinikov et al, 1993B; Traut et al, 1993) partially argues against the significance of the theory that subunits of L7/L12 exchange on the ribosome as crosslinked dimers of L7/L12 are still fully functional in *in vitro* poly-phenylalanine synthesis. Of course, it could be possible that *dimers* of L7/L12 can rapidly dissociate from L10 on the

ribosome and interact with another region. More specifically, dimeric L7/L12 might associate weakly with the L1 ridge (~150 Å away from the base of the L7/L12 stalk) or the peptidyl transferase region (~90Å away from the base of the L7/L12 stalk) as the distance between dimers of L7/L12 in a micromolar solution is ~400 Å (method of Chandrasekhar, 1943); since subunit exchange of L7/L12 occurs in less than 200 milliseconds free in solution, and it takes greater than 5 seconds to fully synthesize an average protein in *E. coli,* it is worth investigating more closely the dynamic equilibria of L7/L12 bound to the ribosome (although, caution must be exercised here in that it only takes less than 200 milliseconds per amino acid elongation cycle). Finally, as to flex and extend to the peptidyl transferase domain of the ribosome (please look once again at Figure 6, page 14, Chapter One). If free mobility of L7/L12 occurs via its N-terminal six amino acids in*addition* to its flexible hinge (conformational changes of less than several nanoseconds as examined in this dissertation), then it is possible that L7/L12 could interact with a number of regions on the ribosome at times compatible with most (if not all) of the various steps of protein biosynthesis.

REFERENCES

Abrahamson, J., Laue, T., Miller, D., and Johnson, A. (1985) Biochemistry 24, 692-700.

Ackers, G. K. (1975) in The Proteins, 3d ed., vol. 1, ed. H. Neurath and R.L. Hill (New York: Academic Press), p. 1.

Alberts, B., Bray, D., Lewis, J., Raff, M., Roberts, K., and Watson, J. D., eds. (1989) In: Molecular Biology of the Cell, 2nd ed. Garland Publishing, New York, p. 211.

Alcala, J. R., Gratton, E., and Jameson, D. M. (1985) Anal. Instrum. 14, 25-250.

Alcala, J., Gratton, E., and Prendergast, F. (1987) Biophys. J. 51, 925-936.

Allen, G. (1981) Sequencing of Proteins and Peptides, Elsevier/North Holland, Oxford, pp. 58-59.

Anderson S. and Weber, G. (1969) Biochemistry 8, 371-377.

Aqvist, J., van Gunstern, W.T., Leijonmarck, M., and Tapia, O. (1985) J. Mol. Biol. 183, 461-477.

Arbeloa, I. L. and Ojeda, P. R. (1981) Chem. Phys. Lett. 79, 347-350.

Arbeloa, I. L. and Ojeda, P. R. (1982) Chem. Phys. Lett. 87, 556-560.

Arellano, A., Canales, M., Jullian, C., and Brunet, J. (1988) Biochem. Biophys. Res. Comm. 150 (2), 633-639.

Ausubel, F. M., Brent, R., Kingston, R. E., Moore, D. D., Seidman, J. G., Smith J.A., Struhl, K. (1992) Current Protocols in Molecular Biology. Greene Publishing Associates and Wiley-Interscience, New York, Volume 2, 16.0.5-16.7.6.

Barta, A., Steiner, G., Brosius, J., Noller, H. F., and Kuechler, E. (1984) Proc. Natl. Acad. Sci., USA 81, 3607-3611.

Beauclark, A., Cundliffe, E., and Dijk, J. (1984) J. Biol. Chem. 259, 6559-6569.

Beechem, J., Knutson, J., and Brand, L. (1986) Biochem. Soc. Trans. 14, 832-835.

Beechem, J. and Gratton, E. (1988) Spectroscopy in Biochemistry, Proceedings of S.P.I.E., column 909.

Beechem, J., Gratton, E., Ameloot, M., Knutson, J., Brand, L. (1991) Fluorescence Spectroscopy, Vol. 2 "Principles and Techniques", Plenum Press, pp 1-66.

Belford, G. G., Belford, R. L., and Weber, G. (1972) Proc. Natl. Acad. Sci., USA, 69, 1392-1393.

Benecky, M., Kolvenbach, C., Wine, R., DiOrio, J., and Mosesson, M. (1990) Biochemistry 29, 3082-3091.

Boublik, M., Brot, N., and Weissbach, H. (1973) Biopolymers 12, 2083-2092.

Boublik, M. and Hellmann, W. (1976) J. Mol. Biol., 107, 479-490.

Boublik, M., Visenton, L., Weissbach, H., and Brot, N. (1979) Arch. Bioch. Biop. 198, 53-59.

Brunet, J. E., Vargas, V., Gratton, G., and Jameson, D. M. (1993) Biophysical J. in press.

Bucci, E. and Steiner, R. F. (1988) Biophys. Chem. 30, 199-124.

Burghardt, T. P. and Thompson, N. L. (1985) Biochemistry 24, 3731-3735.

Burma, D. P., Srivastava, S., Srivastava, A. K., Mahanti, S., Dash, D. (1986) In: Structure, Function, and Genetics of Ribosomes. Hardesty, B. and Kramer, G., eds., Springer-Verlag Press, New York, pp. 438-453.

Burten-Bastians, P. (1992) Fluorescence Relaxation Spectroscopy: Light on Dynamical Structures of Flavoproteins.

Bushuev, V., Sepetov, M., and Gudkov A. (1984) FEBS Lett. 178, 101-104.

Bushuev, V., Gudkov, A., Liljas, A., and Sepetov, M. (1989) J. Biol. Chem. 264, 4498-4505.

Caldwell, P., Luk, D., Weissbach, H., and Brot, N. (1978) Proc. Natl. Acad. Sci, USA 75, 5349-5352.

Cantor, C. R. and Schimmel, P. R. (1980) Biophysical Chemistry, Part 2: Techniques for the Study of Biological Structure and Function. Freeman, W.H. and Co, San Fransisco, CA. pp 433-439.

Careri, G., Fasella, P., and Gratton, E. (1975) CRC Critical Reviews in Biochemistry, August, p. 141-164.

Careri, G., Fasella, P., and Gratton, E. (1979) Ann. Rev. Biophys. Bioeng. 8, 69.

Cario and Franck, (1922) Z. Physik. 17, 202.

Casiano, C. (1992) Doctoral Dissertation, University of California, at Davis.

Chandrasekhar, S. (1943) Rev. Mod. Phys. 15, 1-89.

Chen, R. and Scott, C. (1985) Anal. Lett. 18 (A4), 393-421.

Cheng, X. H., Wu, Z. C., and Fenselau, C. (1993) J. Amer. Chem. Soc. 115, 11-20.

Cheung, H., Gonsoulin, F., and Garland, F. (1983) J. Biol. Chem. 258, 5775-5786.

Cheung, H. C., Gryczynski, I., Malak, H., Wiczk, W., Johnson, M. L., and Lakowicz, J. R. (1991) Biophys. Chem. 40, 1-7.

Chou, P. Y. and Fasman, G. D. (1974) Biochemistry 13, 211-222.

Chryssomallis, G., Torgerson, P., Drickamer, H., and Weber, G. (1981) Biochemistry 20, 3955-3959.

Cohn, E. L. and Edsall, J. T. (1943) in Proteins, Amino Acids, and Peptides as Ions and Dipolar Ions, Reinhold, New York.

Cowgill, C., Nichols, B., Kenny, J., Butler, P., Bradbury, E. and Traut, R. (1984) J. Biol. Chem. 259, 15257-15263.

Dale, R. E. and Eisenger, J. (1974) Biopolymers 12, 1573-1605.

Dale, R. E., Eisinger, J., and Blumberg, W. E (1979) Biophysical J. 26, 161-194.

der Haar, D. (1967) The Old Quantum Theory, Pergamon, Oxford.

Dijk, J., Littlechild, J., and Garrett, R. (1977) FEBS Lett. 77, 295-300.

Dijk, J., Garrett, R, and Muller, R. (1979) Nucleic Acids Research 6, 2717-2729.

Donner, D., Villems, R., Liljas, A., and Kurland, C. (1978) Proc. Natl. Acad. Sci., USA 75, 3192-3195.

Duchinsky, F. (1933) Z. Phys. 81, 7-22.

Eccleston, J. F., Gratton, E., and Jameson, D. M. (1987) Biochemistry 26, 3902-3907.

Einstein, A. (1917) Phys. Z. 18, 121.

Erijman, L. and Weber, G. (1991A) Biochemistry 30, 1595-1599.

Erijman, L. and Weber, G. (1991B) Photochemistry and Photobiology 57, 411-415.

Erijman, L., Lorimer, G., and Weber, G. (1993) Biochemistry 32, 5187-5195.

Fairclough, R. and Cantor, C. (1978) Methods Enzymol. 48, 347-379.

Förster, Th. (1946) Naturwiss. 33, 166.

Förster, Th. (1948) Ann. Phys. (Liepzig) 2, 55-75.

Förster, Th. (1951) Fluoreszenz organischer Verbindungen (Vandenhoeck and Ruprecht, Gottingen), p.85.

Förster, Th. and König, E. (1957) Ber. Bunsenges. Physik. Chem. 61, 344-350.

Förster, Th. (1967) Comp. Biochem. 22, 61-80.

Franck, J. and Condon, E. U. (1926) Trans. Faraday Soc. 21, 536.

Frauenfelder, H., Sligar, S., and Wolynes, P. (1991) Science 254, 1598-1603.

Gal, M. E., Kelly, G. R., and Kurucsev, T. (1973) J. Chem. Soc. Faraday 69, 395.

Gavish, B., Gratton, E., and Hardy, J. C. (1983) Proc. Natl. Acad. Sci., USA 80, 750-754.

Georgalis, Y., Dijk, J., Labischinski, H., and Wills, P. (1989) J. Biol. Chem. 264, 9210-9214.

Girshovich, A., Kurtskhalia, T. V., Ovchinnikov, Y. A., and Vasiliev, V. D. (1981) FEBS Lett. 130, 54.

Globals Unlimited Technical Reference (1993) Lab. for Fluor. Dynam., Urbana, Ill.

Goldberg, G., Caldwell, P., Weissbach, H., Brot, N. (1979) Proc. Natl. Acad. Sci., USA, 76,1716-1720.

Gratton, E. and Limkeman, M. (1983) Biophys. J., 44, 315-324.

Gratton, E., Jameson, D., and Hall, R. (1984a) Ann. Rev. Biophys. Bioeng., 13, 105-124.

Gratton, E., Jameson, D., Rosato, N., and Weber, G. (1984b) Rev. Sci. Instrum. 55, 486-494.

Gratton, E., Alcala, R., Marriott, G., and Prendergast, F. (1986A) in Progress and Challenges in Natural and Synthetic Polymer Research, Kawabata, C. and Bishop, A., eds. Ohmshu Press, Tokyo.

Gratton, E., Alcala, J. R., and Marriott, G. (1986B) Biochem. Soc. Trans. 14, 835-838.

Gratton, E., Silva, N., Mei, G., Rosato, N., Savini, I., and Finazzi-Agro, A. (1992) Intern. J. Quant. Chem 42, 1479-1489.

Gratton, E. (1993) personal communication.

Greenfield, N. J. and Hitchcock-DeGregori, S. E. (1993) Protein Science, 2, 1263-1273.

Gryczynski, I., Cherek, H., and Lakowicz, J. (1988) Biophys. Chem. 30, 271-277.

Gudkov, A. (1977) Mol. Biol. 11, 1202-1205.

Gudkov, A. and Behlke, (1978) Eur J. Biochem 90, 309-312.

Gudkov, A., Khechinashvili, N., and Bushuev, V. (1978A) Eur J. Biochem. 90, 313-318.

Gudkov, A., Tumanova, L., Veryaminov, L., Khechinashvilli, N. (1978B) FEBS Lett. 93, 215-218.

Gudkov, A., Tumanova, L., Gongadze, G., and Bushuev, V. (1980) FEBS Lett. 109, 34-38.

Gudkov, A. T., Gongadze, G. M., Bushuev, B. N., and Okon, M. S. (1982) FEBS Lett. 138, 229-232.

Gudkov, A. and Gongadze, G. (1984) FEBS Lett. 176, 32-36.

Gudkov, A. and Bubunenko, M. (1989) Biochimie 71, 779-785.

Gudkov, A., Bubunenko, M., and Gryaznova, O. (1991) Biochimie 73, 1387-1389.

Gutel, R. R., Weiser, B., Woese, C. R., and Noller, H. F. (1985) Prog. Nucleic Acid Res. Mol. Biol. 32, 155-216.

Haas, E., Katchalski-Katzir, E., and Steinberg, I. (1978) Biochemistry 17, 5064-5070.

Hamel, E., Koka, M., and Nakamoto, T. (1972) J. Biol. Chem. 247, 805-814.

Hamman, B. D., Jameson, D. M., Oleinikov, A. V., and Traut, R. R. (1993) Biophys. J. 64, A53.

Hanson, D. C., Yguerabide, J., and Schumaker, V. N. (1981) Biochemistry 20, 6842-6852.

Hanson, D. C., Yguerabide, J., and Schumaker, V. (1985) Mol. Immunol. 22, 237-244.

Hardy, S. J. S. (1975) Mol. Gen. Genet. 140, 253-274.

Harvey, R. C. and Cheung, H. C. (1977) Biochemistry 16, 5181.

Hazlett, T. L., Johnson, A. E., and Jameson, D. (1989) Biochemistry 28, 4109-4117.

Hermann, R., Rudolph, R. and Jaenicke, R. (1982) Hoppe Seyler's Z. Physiol. Chem. 363, 1259-1265.

Holtzer, M., Breiner, T., and Holtzer, A. (1984) Biopolymers 23, 1811-1833.

Hudson, E. and Weber, G. (1973) Biochemistry 12, 4154-4161.

Isono, S., and Isono, K. (1981) Mol. Gen. Genet. 183, 473-477.

Jaenicke, R. and Rudolph, R. (1989) Folding Proteins. In Protein Structure. A Practical Approach (edited by T.E. Creighton), pp.191-223. IRL Press, Oxford, England.

Jaenicke, R. (1991) Biochemistry 30, 3147-3161.

James, E., Wu, P. G., Stites. W., and Brand, L. (1992) Biochemistry 31, 10217-10225.

Jameson, D. M. and Gratton, E. (1983) New Directions in Molecular Luminescence, American Society for Testing and Materials, pp 67-81.

Jameson, D. M., Gratton, E., and Hall, R. (1984) App. Spectroscopy Rev. 20 (1), 55-106.

Jameson, D. M. (1984) Fluorescein Hapten: An Immunological Probe, Voss, E., Jr., Ed., Library of Congress, Washington, D.C., CRC Press, Inc., Chapter 3.

Jameson, D. M., Gratton, E., and Eccleston, J. (1987) Biochemistry 26, 3894-3901.

Jameson, D. M. and Reinhart, G. (1989) Fluorescent Biomolecules: Methodologies and Applications, Plenum Press, New York.

Jameson, D. M. and Hazlett, T. (1991) Biophysical and Biochemical Aspects of Fluorescence Spectroscopy, Chapter 4, Plenum Press, New York.

Jameson, D. M. and Sawyer, W. H. (1993) Methods. Enzymol., in press.

Jameson, D. M. (1993) unpublished results.

Jelenc and Kurland (1979) Proc. Natl. Acad. Sci. U.S.A., 76, 3174-3178.

Johnson, F. H., Eyring, H. and Stover, B. J., eds. (1974) Theory of Rate Processes in Biology and Medicine, John Wiley and Sons, Inc., New York.

Johnson, A. E., Miller, D. L., and Cantor, C. R. (1978) Proc. Natl. Acad. Sci. USA 75, 3075-3079.

Johnson, A. E., Adkins, H. J., Matthews, E. A., and Cantor, C. R. (1982) J. Mol. Biol. 156, 113-140.

Josephs, R. and Harrington, W. (1969) Proc. Natl. Acad. Sci. U.S.A. 58, 1587-1594.

Kar, E. and Aune, K. (1981) Biochemistry 20, 4638-4646.

Karplus, M. and McCammon, J. A. (1981) CRC Critic. Rev. Bioc. 9, 293-349.

Kaziro, Y. (1978) Biochim. Biophys. Acta. 505, 95-127.

Kenny, J. W., Lambert, J. M., and Traut, R. R. (1979) Methods Enzymol. 59, 534-550.

King, J. (1989) Chem. Eng. News, April, 31-54.

King, L. and Weber, G. (1986a) Biochemistry 25, 3632-3637.

King, L. and Weber, G. (1986b) Biochemistry 25, 3637-3640.

Kirsebom, L. A. and Isaksson, L. A. (1985) Proc. Natl. Acad. Sci. 82, 717-721.

Kirsebom, L. A., Amons, R., and Isaksson, L. A. (1986) Eur. J. Biochem. 156, 669-675.

Knopp, J. and Weber, G. (1969) J. Biol. Chem. 244, 6309-6315.

Kuntz, I. D. (1971) J. Amer. Chem. Soc. 93, 514-518.

Kuntz, I. D. and Kauzmann, W. (1974) in Advances in Protein Chemistry, vol. 28, eds. C.B. Anfinsen, J.T. Edsall, and F.M. Richards (New York: Academic Press), p. 239.

Kuruki, Y., Inoue, N., and Kaziro, Y. (1970) Biochem. Biophys. Acta 224, 487.

Lakowicz, J. R., Cherek, H., Maliwah, B. P., and Gratton, E. (1985) Biochemistry 24, 376-383.

Lakowicz, J. R., Cherek, H., Gryczinski, I., Joshi, N., Johnson, M. L. (1987) Biophys. Chem. 51, 755-762.

Lakowicz, J. R., Gryczinski, I., Cheung, H., Wang, C.-K., and Johnson, M .L. (1988) Bioplymers 27, 821-830.

Lakowicz, J. R., ed. (1991) Topics in Fluorescence Spectroscopy, Plenum Press, New York, volumes 1-3.

Langer, J., Jurnak, F., and Lake, J. (1984) Biochemistry 23, 6171-6178.

Lau, S. Y. M., Taneja, A. K., and Hodges, R. S. (1984) J. Biol. Chem., 259, 13253-13261.

Lee, C. C., Cantor, C, and Wittmann-Liebold, B. (1981a) J. Biol. Chem. 256, 41-48.

Lee, C. C, Wells, B, Fairclough, R., and Cantor, C. (1981b) J. Biol. Chem. 256, 49-53.

Leihninger, A. L., Nelson, D. L., and Cox, M. M. (1993) Principles of Biochemistry, 2nd ed., Worth Publishers, Inc., New York.

Leijonmarck, M., Ericksson, S., and Liljas, A. (1980) Nature, 286, 824-826.

Leijonmarck, M. and Liljas, A. (1987) J. Mol. Biol. 195, 555-580.

Liljas, A. (1982) Progr. Biophys. Mol. Biol. 40, 161-228.

Liljas, A. and Gudkov, A. (1987) Biochimie 69, 1043-1047.

Liljas, A. (1991) Int. Rev. of Cytology 124, 105-110.

Lin, S.-H., Harzelrig, J. B., and Cheung, H. (1993) Biophys. J. 65, 1433-1444.

Linderstrom-Lang, K. U. and Schellman, J. A. (1959) Enzyme 1, 443.

Liu, B. M., Cheung, H. C., and Mestecky, J. (1981) Biochemistry 1997-2003.

Louden, R. (1983) The Quantum Theory of Light, Clarendon Press, Oxford.

Luer, C. and Wong, K.-P. (1979) Biochemistry 18, 2019-2027.

Luer, C. and Wong, K.-P. (1980) Biochemistry 19,178-183.

Maassen, J., Schop, E., and Möller, W. (1981) Biochemistry 20, 1020-1025.

Maassen, A., Thielen, T. and Moller, W. (1983) Eur. J. Biochem. 134, 327-330.

Makarov, E., Oleinikov, A., Zecherle, N., and Traut, R.R. (1993) Biochimie, in press.

Mantulin, W. and Pownall, H. (1985) Biochim. Biophys. Acta. 836, 215-221.

Matheson, A.T., Möller, W., Amons, R., and Yaguchi, M. (1980) In: Ribosomes, Structure, Function, and Genetics. Chambliss, G., ed. University Park Press, Baltimore, pp. 297-332.

Mendelson, R.A. and Cheung, P. (1978) Biochemistry 17, 2139.

Mo, J., Holtzer, M. and Holtzer, A. (1991) Proc. Natl. Acad. Sci., USA 88, pp 916-920.

Molecular Probes Catalogue (1993) Molecular Probes, Inc., Eugene, Oregon.

Möller, W. and Castleman, H. (1967) Nature 215, 1293-1297.

Möller, W., Castleman, H., and Terhorst, C. P. (1970) FEBS Lett. 8192-8196.

Möller, W., Groene, A., Terhorst, C., and Amons, R. (1972) Eur. J. Biochem. 25, 5-14.

Möller, W., Schrier, P., Maasen, J., Zantema, A., Schop, E., Reinalda, H., Cremers, A., and Mellema, J. (1983) J. Mol. Biol. 163, 553-573.

Möller, W. and Maasen, J. (1986) Protein Structure, Function, and Genetics of Ribosomes, Hardesty, B. and Kramer, G., eds., Springer-Verlag Press, New York, pp. 309-325.

Möller, W. (1990) The Ribosome: Structure, Function, & Evolution, Hill, W., Dahlberg, A., Garrett, R., Moore, P., Schlessinger, D., and Warner, J., eds., American Society for Microbiology, Washington, D.C., pp. 380-389.

Nag, B., Tewari, D., and Traut, R. (1987) Biochemistry 26, 461-465.

Neumann, N. P. (1967) Meth. Enzymol. 11, 485-488.

Nierhaus, K. H., Rheinberger, H.-J., Geigenmuller, U., Gnirke, A., Saruyama, H., Schilling, S., Wurmbach, P. (1986) In: Structure, Function, and Genetics of Ribosomes. Hardesty, B. and Kramer, G., eds., Springer-Verlag Press, New York, pp. 454-471.

Noller, H. F. and Woese, C. R. (1981) Science 212, 403-411.

Noller, H., Hoffarth, V., and Zimniak, L. (1992) Science 256, 1416-1419.

Oi, V. T., Vuong, T. M., Hardy, R., Reidler, J., Dangl, J., Herzenberg, L. A., and Stryer, L. (1984) Nature, 307, 136.

Oleinikov, A., Perroud, B., Wang, B., and Traut, R. R. (1993A) J. Biol. Chem. 268, 917-922.

Oleinikov, A., Jokhadze, G., and Traut, R. (1993B) Proc. Natl. Acad. Sci., U.S.A. in press.

Oleinikov, A. (1993C) personal communication.

Olsen, H. M., Sommer, A., Tewari, D., Traut, R., and Glitz, D. (1986) J. Biol. Chem. 261, 6924-6932.

O'Shea, E., Klemm, J., Kim, P., and Alber, T. (1991) Science 254, 539-544.

Österberg, R., Sjoberg, B., Liljas, A., and Pettersson, I. (1976) FEBS Lett. 66, 48-51.

Paladini, A., and Weber, G. (1981a) Rev. Sci. Instrum. 52(3), 1981.

Paladini, A., and Weber, G. (1981b) Biochemistry, 20, 2587-2593.

Paladini, A., Silva, J., and Weber, G. (1987) Anal. Biochem. 161, 358-364.

Panda, D., Roy, S., and Battacharyya, B. (1992) Biochemistry 31, 9709-9716.

Perrin, F. (1926) J. Phys. 7, 390-401.

Perrin, J. (1927) C.R. hebd. Seances Acad. Sci. 184, 1097.

Perrin, F. (1929) Ann. Phys. Ser. X 12, 169-275.

Perrin, F. (1932) Ann. Chim. Physique 17, 283.

Perrin, F. (1934) J. Phys. Radium 5, 487-511.

Perrin, F. (1936) J. Phys. Radium VII.7, 1-11.

Petterson, I., Hardy, S., and Liljas, A. (1976) FEBS Lett. 64, 135-138.

Prince, J. B., Gutell, R. R., and Garrett, R. A. (1983) Trends Biochem. Sci. 9, 359-363.

Ptitsyn, O. and Semisotnov, G. (1991) in Conformations and Forces in Protein Folding. Nall, B. and Dill, K., eds. American Assoc. Adv. Sci., Washington, D.C., Chapter 3.

Rawitch, A., Hudson, E., and Weber, G. (1969) J. Biol. Chem. 244, 6543-6547.

Reinhardt, G. and Lardy, H. (1980) Biochemistry 19, 1484-1490.

Rietveld, A. (1993) personal communication.

Rice, P. and Steitz, T. (1989) Nucleic Acids Res. 17, 3757-3762.

Richardson, J. S. and Richardson, D. C. (1990) in Prediction of Protein Structure and the Principles of Protein Conformation. Fasman, G.D., ed., Plenum Publishing, New York, N.Y., pp. 1-98.

Rosen, C.-G. and Weber, G. (1969) Biochemistry 8, 3915-3922.

Ruan, K. and Weber, G. (1988) Biochemistry 27, 3295-3301.

Ruan, K. and Weber, G. (1989) Biochemistry 28, 2144-2153.

Ruan, K. and Weber, G. (1993) Biochemistry 32, 6295-6301.

Saad, A. D., Pardee, and Fischman, D. A. (1986) Proc. Natl. Acad. Sci., USA 83, 9483-9487.

Sadkowski, P. J. and Fleming, G. R. (1978) Chem. Phys. Lett., 57, 526-530.

Sambrook, J., Fritsch, E. F., and Maniatis, T. (1989) Molecular Cloning, Cold Spring Harbor Lab. Press, New York.

San Jose, C, Kurland, C., and Stoffler, G. (1976) FEBS Lett. 71, 133-137.

Schop, E. and Maassen, J. (1982) Eur. J. Biochem. 128, 371-379.

Schrier, Maassen, and Möller, W. (1973) Biochem. Biophys. Res. Comm. 53, 90-100.

Silva, J., Miles, E., and Weber, G. (1986) Biochemistry 25, 5780-5786.

Silva, J., Villas-Boas, M., Bonafe, C., Meirelles, N. (1989) J. Biol. Chem. 264, 15863-15868.

Silva, J., Silveira, C., Correia Jr., A., and Pontes, L. (1992) J. Mol. Biol. 223, 545-555.

Silva, J., Luan, P., Glaser, M., Voss, E., and Weber, G. (1992) J. Virology, April.

Sommer, A., Stoffler-Meilicke, M., Noah, M., Stoffler, G. (1985) FEBS Lett. 163, 94-98.

Small, E. W. and Isenberg, I. (1977) Biopolymers 16, 1907-1928.

Spencer, R. and Weber, G. (1969) Ann. New York Acad. Sci. 158, 361-376.

Steiner, R. F. and Norris, L. (1987) Biopolymers 26, 1189-1204.

Stöffler, G., Hasenbank, R., Bodely, J. W., and Highland, J. H. (1974) J. Mol. Biol. 86, 171-174.

Strycharz, W. A., Nomura, M., and Lake, J. A. (1978) J. Mol. Biol. 126, 123-140.

Stryer, L. (1978) Annu. Rev. Biochem. 47, 819-846.

Subramanian, A. R. (1975) J. Mol. Biol. 95, 1-8.

Tao, T. (1969) Biopolymers 8, 609-632.

Tao, T., Nelson, J. H., and Cantor, C. R. (1970) Biochemistry 9, 3514.

Tate, W. P., Kastner, B., Edgar, C. D., McCaughan, K. K., Timms, K. M., Trotman, C. N. A., Stöffler-Meilicke, M., Stöffler, G., Nag, B., and Traut, R. R. (1990) Eur. J. Biochem. 187, 5473-5481.

Tawada, K., Wahl, P., and Auchet, J-C. (1978) Eur. J. Biochem. 88, 411-419.

Terhorst, C., Wittmann-Liebold, B., and Möller, W. (1972) Eur. J. Biochem. 25, 13-22.

Terhorst, C., Möller, W., Laursen, R. and Wittmann-Liebold, B. (1973) Eur. J. Biochem. 34, 138-152.

Tewari, D., Sommer, S., and Traut, R. (1986) J. Biol. Chem. 258, 14592-14598.

Thielen, A, Maassen, J, Kriek, J, and Möller, W. (1984) Biochemistry 23, 3317-3322.

Thompson, K. S., Vinson, C. R., and Freire, E. (1993) Biochemistry, 32, 5491-5496.

Timasheff, S. N. (1993) Annu. Rev. Biophys. Biomol. Struct. 22, 67-97.

Timm, D. and Neet, K. (1992) Protein Science 1, 236-244.

Tischendorf, G. W., Zeichardt, H., and Stöffler, G. (1975) Proc. Natl. Acad. Sci., USA 72, 4820-4824.

Tokimatsu, H., Strycharz, W. A., and Dahlberg, A. E. (1981) J. Mol. Biol. 152, 397-412.

Traut, R., Lambert, J., and Kenney, J. (1983) J. Biol. Chem. 258, 14592-14597.

Traut, R. R., Tewari, D., Sommer, Gavino, G., Olson, H., Glitz, D. (1986) Structure, Function, and Genetics of Ribosomes, Hardesty, B. and Kramer, eds., Springer-Verlag Press, New York, 289-309.

Traut, R. R., Oleinikov, A. V., Makarov, E., Jokhadze, G., Perroud, B., and Wang, B. (1993) Structure and Function of *Escherichia coli* Ribosomal Protein L7/L12: Effect of Cross-Links and Deletions. in The Translational Apparatus (eds. Nierhaus, K. H. et al) Plenum Press, New York, in press.

Traut, R. R. (1993) Personal communication.

Tsurugi, K. and Mitsui, K. (1991) Biochem. Biophys. Res. Comm. 174, 1318-1323.

Valeur, B. (1991) Molecular Luminescence Spectroscopy-Methods and Applications: part 3, Wiley-Interscience, New York, in press.

van Agthoven, A., Maasen, J., Schrier, P, and Möller, W. (1975) Biochem. Biophys. Res. Comm. 64, 1184-1191.

van Der Meer, B. W., Raymer, M., Wagoner, S., Hackney, R., Beechem, J., Gratton, E. (1992) Time-Resolved Laser Spectroscopy in Biochemistry, 3, SPIE, 220-229.

vanderMeulen, D. L., Nealon, D. G., Gratton, E., and Jameson, D. M. (1990) Biophys. Chem. 36, 177-184.

Voss, E., Jr (1984) Fluorescein Hapten: An Immunological Probe, CRC press., Inc, Washington, D.C.

Voss, E., Jr. (1990) Comments on Mol. Cell. Biophys. 6, 197-221.

Wahl, P. (1975) in Biochemical Fluorescence, eds. R.F. Chen and H. Edelhoch, Plenum Press, New York, vol. 1.

Wahl, P. and Weber, G. (1967) J. Mol. Biol. 30, 371-381.

Waley, S. (1973) Biochemical J. 135, 165-172.

Wang, C.-K. and Cheung, H. (1986) J. Mol. Biol. 191, 509-521.

Wang, C.-K., Liao, R., and Cheung, H. (1993) J. Biol. Chem. 268, 14671.

Watson, B. S., Hazlett, T. L., Eccleston, J. F., Jameson, D. M., and Johnson, A. E. (1992) Biophys. J. 61, A489.

Waxman, E., Laws, W., Laue, T., Nemerson, Y., and Ross, J. B. (1993) Biochemistry 32, 3005-3012.

Weber, G. (1952) Biochemical J. 51, 145-167.

Weber, G. (1953) Adv. Prot. Chem. 8, 415-459.

Weber, G. (1954) Trans. Faraday Soc. 50, 552-555.

Weber, G. and Teale (1957) Trans. Faraday Soc. 63, 646-655.

Weber, G. and Daniel, E. (1966) Biochemistry, 5, 1900-1907.

Weber, G. and Anderson, S. (1969) Biochemistry, 8, 361-370.

Weber, G. and Shinitzky, M. (1970) Proc. Natl. Acad. Sci., USA. 65, 823-830.

Weber, G. and Teale, (1970) J. Amer. Chem. Soc. 92, 687.

Weber, G. (1975) Adv. Protein Chem. 29, 1.

Weber, G. (1977) J. Chem. Phys. 66, 4081-4091.

Weber, G. (1981) J. Phys. Chem. 85, 949-952.

Weber, G., and Drickamer, H. (1983) Quart. Rev. of Biophys. 16, 89-112.

Weber, G. (1984) Proc. Natl. Acad. Sci., USA 81, 7098-7102.

Weber, G. (1986) Biochemistry 25, 3626-3631.

Weber, G. (1989A) J. Phys. Chem. 93, 6069-6073.

Weber, G. (1989B) J. Mol. Liq. 42, 255-268.

Weber, G. (1992A) Protein Interactions, Routledge, Chapman, and Hall, Inc., pp. 216-234.

Weber, G. (1992B) High Pressure in Chemistry, Biochemistry, and Material Science. Winter, R. and Jonas, J., eds, Kulwer, Netherlands.

Weber, G. (1993) personal communication

Wegener, W.A. (1982) Biopolymers 21, 1049-1080.

Wendt, H., Berger, C., Leder, L., and Bosshard, H. R. (1993) Protein Science 2 (Suppl. 1), 137.

Wong, K.-P. and Paradies, H. (1974) Bioc. Biop. Res. Comm. 61, 178-184.

Wu, C. and Stryer, L. (1972) Proc. Natl. Acad. Sci., USA 69, 1104-1110.

Wu, C. and Brand, L. (1992) Biochemistry 31, 7939-7947.

Xu, G.-J. and Weber G. (1982) Proc. Natl. Acad. Sci., USA 79, 5268-5271.

Yguerabide, J., Epstein, H. F., and Stryer, L. (1970) J. Mol. Biol., 51, 573-590.

Zantema, A., Maassen, J., Kriek, J., and Möller, W. (1982a) Biochemistry 21, 3069-3076.

Zantema, A, Maassen, J., Kriek, J., and Möller, W. (1982b) Biochemistry 21, 3077-3082.

Zecherle, G. (1990) Doctoral Dissertation, Univ. of California, Davis.

Zecherle, G., Oleinikov, A., and Traut, R. (1992) J. Biol. Chem. 267, 5889-5896.

Zecherle, G., Oleinikov, A., and Traut, R. (1992) Biochemistry 31, 9526-9532.

Zhou, N. E., Kay, C. M., and Hodges, R. S. (1992) Biochemistry 31, 5739-5746.

Zhou, N., Kay, C., and Hodges. (1993) Biochemistry 32, 3178-3187.

Zhu, B.-Y., Zhou, N., Kay, C., and Hodges, R. (1993) Protein Science 2, 383-394.